Electric Technology U.S.S.R.

ЭЛЕКТРИЧЕСТВО

Volume 1, May, 1958

Selected papers from *Elektrichestvo* Nos. 1-4, 1957

Published by

PERGAMON PRESS NEW YORK LONDON PARIS LOS ANGELES

for Pergamon Institute, New York and London, a non-profit-making foundation

ELECTRIC TECHNOLOGY, U.S.S.R.

PERGAMON INSTITUTE

A NON-PROFIT FOUNDATION FOR THE FURTHERANCE
AND DISSEMINATION OF SCIENTIFIC KNOWLEDGE

Joint Presidents of the Board of Governors:

Dr. Detlev W. Bronk

Sir Robert Robinson, O.M., F.R.S.

Executive Director: Captain I. R. Maxwell

4 & 5 Fitzroy Square, London W.1
122 East 55th Street, New York 22, N.Y.

Pergamon Institute urgently requires translators for science and engineering material to assist with this programme of translation from Russian and other Slavonic languages.

Scientists and engineers who have a knowledge of Russian, and who are willing to assist with this work, should apply to the Administrative Secretary of the Institute. They should write to either New York or London for rates of payment and other details.

Four volumes per annum. Approximately 700 pages per annum.
Annual Subscription Rate £20 ($56).
Single volumes may be purchased for £6 ($17).

Orders should be sent to the distributors at either of the following addresses

4 & 5 Fitzroy Square, London W.1

122 East 55th Street, New York 22, N.Y.

PUBLISHED BY

PERGAMON PRESS LTD.

LONDON · NEW YORK · PARIS · LOS ANGELES

FOREWORD

It is becoming appreciated that the scale and intensity of engineering effort and engineering education in the Soviet Union ensure that this group of countries will make major contributions to future engineering progress. Electrical engineering in particular has claimed a certain priority of effort since Lenin proclaimed electrification to be a necessary basis for socialist construction. In certain aspects of electrical engineering the U.S.S.R. is already in the front rank. It is pioneering, for example, in d.c. power transmission, with concomitant developments of rectifier and invertor equipment and supervisory controls. The U.S.S.R. now has the highest voltage a.c. line in the world. The development of water-power resources on a large scale implies developments in alternators, switchgear and transmission systems. Noteworthy contributions are being made to the theory of automatic control and remote control, based in part on past Russian achievements in non-linear mechanics. The level of theoretical and mathematical work is high.

The keen desire of engineers in other countries to keep contact with progress in electrical engineering in the U.S.S.R. has been frustrated by the language barrier. A decision has now been made by the Pergamon Institute, a non-profit-making foundation, to publish an English translation of the Russian journal "Elektrichestvo". This is the leading broad publication in the field of electrical engineering in U.S.S.R. It covers technical and economic aspects of power supply systems, the design and application of electrical machines, switchgear and measuring instruments, and it also carries articles on broader topics such as automatic control and the analysis of fields and networks. In general the topics of radio and communication are excluded.

"Elektrichestvo" is a journal of long history and high standards. It was one of the first three electrical engineering journals to be published anywhere in the world. It will no doubt continue to be the central and leading journal covering the main fields of electrical engineering except aspects special to communications. The English edition will make Soviet progress in a broad field of electrical engineering accessible for the first time to English-speaking engineers.

L.V. BEWLEY
I.R. MAXWELL
A. TUSTIN

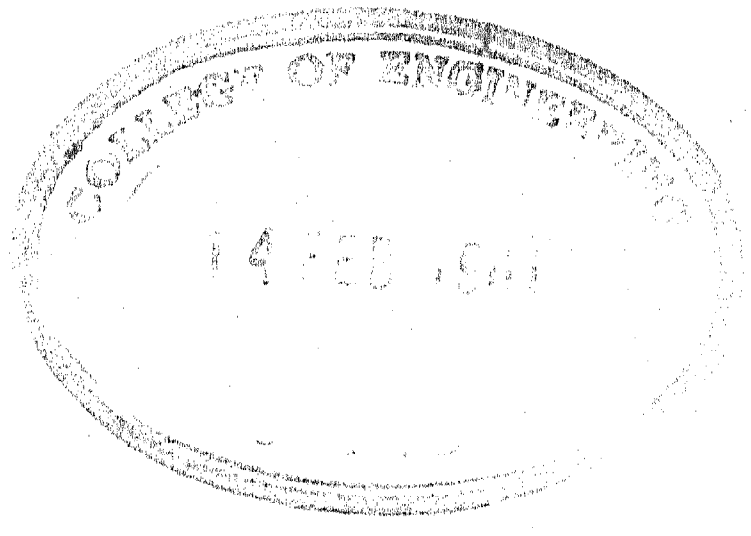

IMPORTANT EDITORIAL NOTICE

To assist readers, reprints of any article appearing in Electric Technology U.S.S.R. can be obtained on application at a price of $2 (10s) per reprint, to cover the overhead costs involved in production. The Reprint No. of each article (which appears on the foot of the first page of the article) must be quoted on every order. Orders should be accompanied by the correct remittance.

All orders of reprints of Russian articles should be addressed to the Administrative Secretary of The Pergamon Institute at either 122 East 55th Street, New York 22, or 4, Fitzroy Square, London, W.1., which ever is more convenient.

FUNDAMENTALS OF AN INTERCONNECTED POWER GRID FOR THE EUROPEAN PART OF THE SOVIET UNION*

V. I. VEITS

"Krzhizhanov", Power Institute of the Academy of Sciences of the U.S.S.R.

(Received 12 September 1956)

The Sixth Five-Year-Plan initiates a new stage in the development of Soviet power production grid interconnexion of power systems.

When the Kuibyshev and Stalingrad power stations and the transmission systems connecting these Volga giants with the central systems and with the Central Black-earth Region, the South and the Urals have been commissioned during the present Five-Year-Plan the first section of the European U.S.S.R. grid will have been completed.

During this period the creation of a Siberian Grid (from Irkutsk to Novosibirsk) will be initiated. The Bratsk and Krasnoyarsk hydro-electric stations which are under construction will dominate the development of the Siberian Grid similarly to Kuibyshev and Stalingrad in the case of the European U.S.S.R. grid. Large transmission lines will connect Bratsk with the Krasnoyarsk and Irkutsk Cheremkhovsk systems, and Krasnoyarsk with the West Siberian systems. Later, the central Siberian grid will be linked with the European U.S.S.R. grid, thus producing an integrated Soviet grid system. The Caucasian and north-west systems will then be connected and a number of Kazakhstan systems will be connected to the European and Siberian grids. Central-Asian and Far-Eastern power systems will be developed. Nuclear power stations will become more important which will affect the development of the U.S.S.R. grid systems in many ways.

The grid ensures the most efficient use of the various sources and provides maximum flexibility and economy. It is now no longer correct

Elektrichestvo No. 1, 1–8 (1957). [Reprint Order No. EL. 1]

to plan power stations and high-voltage systems without considering their part in the future grid.

Areas of the European U.S.S.R. grid

The first stage of the European U.S.S.R. grid covers the following areas: (Fig.1) The Central, Volga, Central Black-earth Region, South,

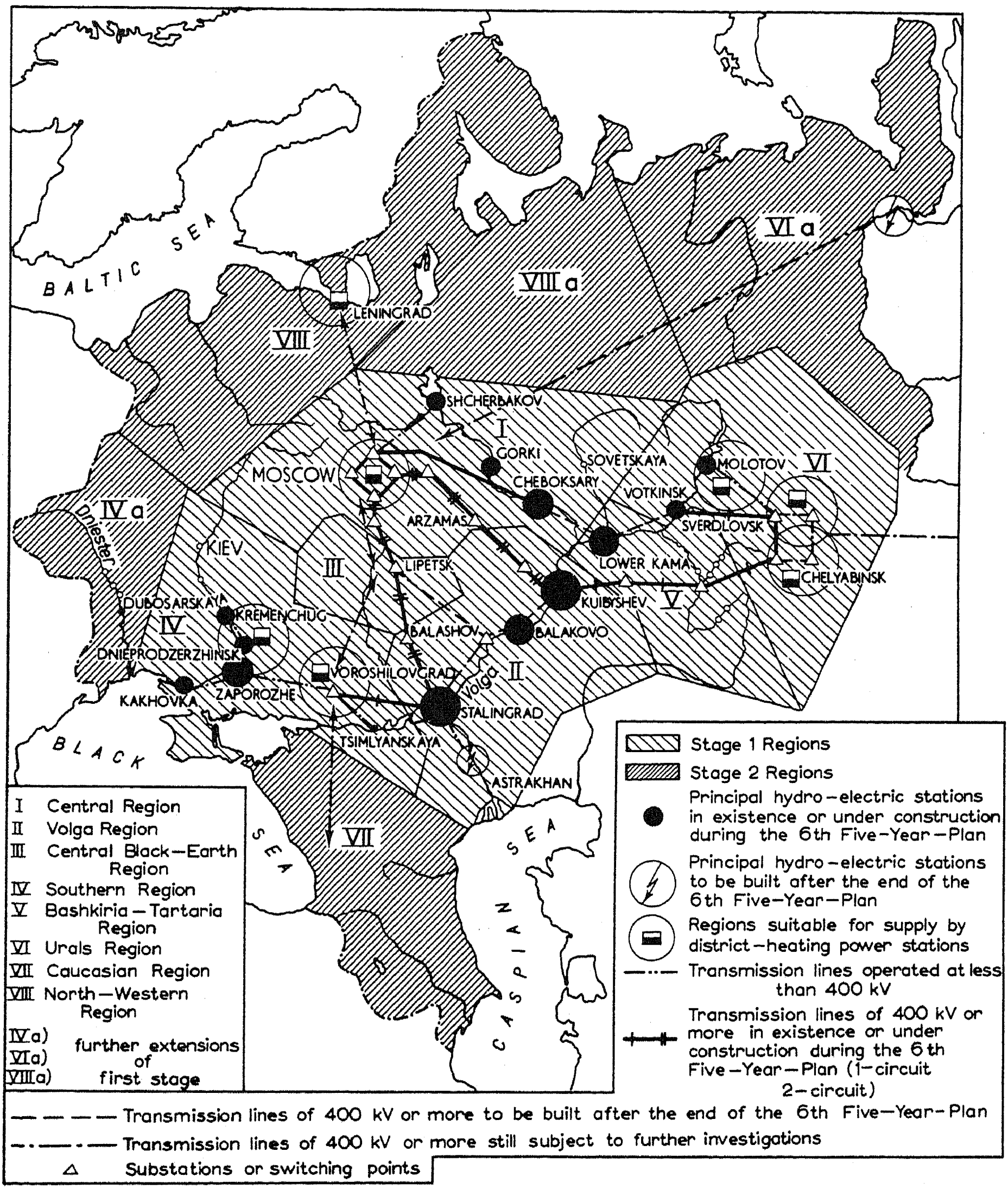

Fig. 1.

Bashkiria and Tataria, and Urals areas. The total area is over 2.7 x 10^6 km^2: population 110 million. The maximum east-west distance is over 2700 km, and the maximum south–north 1500 km. In the first section of the European U.S.S.R. grid the present annual output is about 106 x 10^9 kWh or 63 per cent of the total for the country. This is about 40000 kWh per km^2 and 1000 kWh per head.

The future levels and regional characteristics of the energy balance in the U.S.S.R.

The basic layout of the European grid is considered for two different energy levels: 500 and 1000 x 10^9 kWh. The 500 x 10^9 kWh level relates to the output of a substantial part of the Volga, Kama and Dnieper hydroelectric stations and the 1000 x 10^9 kWh to the completed All-Union grid.

500 x 10^9 kWh might be reached in the second half of the next (Seventh) Five-Year-Plan, and 1000 x 10^9 kWh early in the Ninth Plan. In the first stage the output of the first European grid section (without the northwest and Caucasian links) will increase from 106 in 1955 to 240 x 10^9 kWh and in the second stage to 410 x 10^9 kWh, according to our estimates.

On account of the considerable absolute rate of increase of the energy balance in the European grid this rate of increase will be slightly less than the average increase of the All-Union power production. This is due to more rapid expansion of output in areas east of the Urals. Thus the output in the Siberian grid area will increase by a factor 20 when stage 2 is reached, and by 8 – 15 times in other Asian parts of the Soviet Union. The relative output of the European regions (including the Urals) will decrease from 79 per cent to about 52 per cent and that of the Asian regions will increase from 21 per cent to about 48 per cent.

Yet even the European grid will comprise areas with two different rates of development: the older industrial areas in the Central, Urals and southern areas, where the rate of development is smaller than that of the Union as a whole, and the new industrial regions of Bashkiria, Tataria, Central Black-earth Region and Volga, with their rich natural resources and high population density. Here the output will increase faster than that of the Soviet Union as a whole, and their relative output will not decrease, but increase (from 7 – 10 per cent).

The above levels have only been used as a guide. The basic assumptions and the results have been checked with respect to possible deviations from the initially assumed pattern in the levels, rates of development, and general energy balance structures of the individual regions.

Regional characteristics of the energy balance and estimates of future load diagrams

Decrease in the relative industrial load is typical of the European grid. Agriculture, transport and domestic consumers will use more power and the industrial load will decrease from 81 per cent of the total in 1955 to 70 per cent whereas rural power consumption will increase from 2.5 to 6.1 per cent, transport from 3.3 to 8.6 per cent and domestic use from 13.2 to 15.1 per cent.

The load structure varies in the different regions. These variations affect the daily and annual load curves of the regions and of the grid considerably, and thus affect the maximum demand and grid layout.

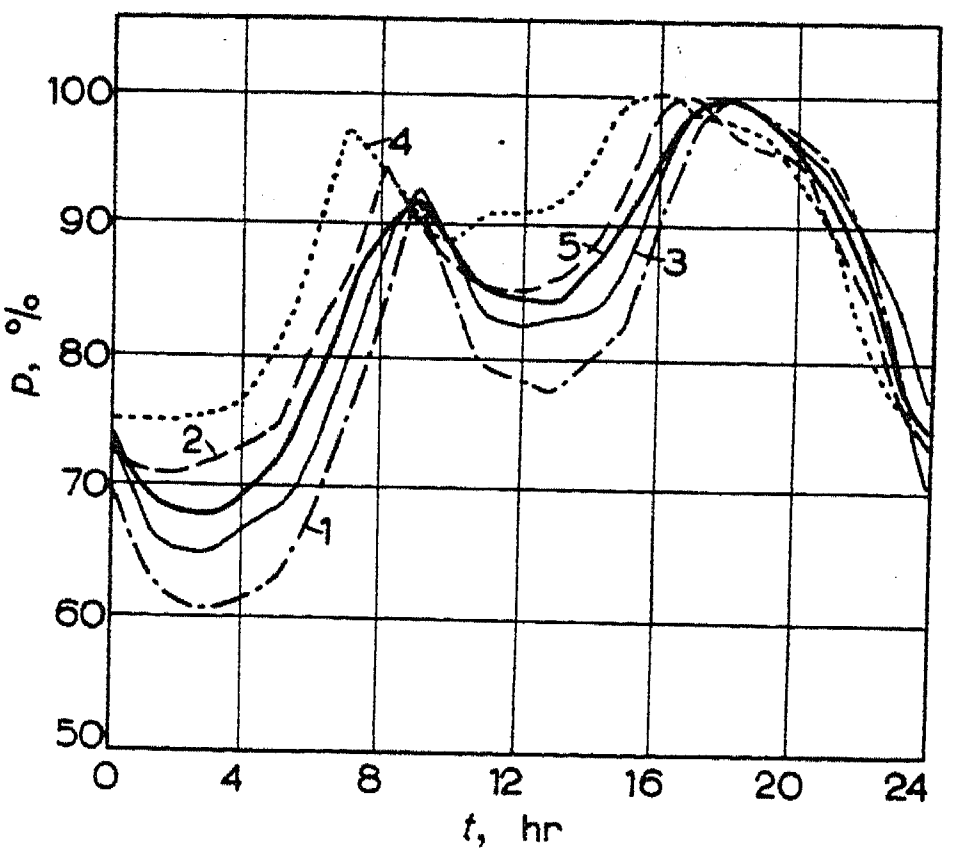

Fig. 2.

Fig. 2 shows the winter load curves for the European grid in the second stage, and the table gives the following:

$\gamma_d^{(w)}$ (load factor of a December day)

$\alpha_d^{(w)}$ (the ratio of minimum off-peak power to the evening peak)

h_m (hours of maximum demand per annum)

Regions	$\gamma_d^{(w)}$	$\alpha_d^{(w)}$	h_m
European grid	0.848	0.679	6300
Central	0.806	0.605	5900
South	0.834	0.653	6200
Volga	0.855	0.710	6400
Central Black-earth Region	0.798	0.592	5600
Tataria and Bashkiria	0.876	0.745	6600
Urals	0.884	0.750	6700

will decrease slightly (by about 1 or 2 per cent) when a 7 hr day is introduced. It would be more complicated to estimate the effect of a 6 hr working day on the load curve; no accurate prediction can be made, since period shift work increases the maximum demand in some industries and decreases it for others.

An upper limit is $h_m = 6300$; this corresponds to higher $\gamma_d^{(w)}$ and $\alpha_d^{(w)}$ in the second stage. Actually h_m may be expected to be 200 – 300 hr less, which must be allowed for in designing the grid structure. By the second stage the diversity effect* for a winter day is about 500 MW.

The structure of the European grid

The maximum demand on the European grid will be about 38 GW (1 GW = 1000 MW) in the first stage and about 65 GW in the second stage. Assuming a minimum spare capacity requirement for frequency, emergency and maintenance purposes†, the total installed capacity of the European grid will be about 42 GW in the first stage and about 72 GW in the second. Fig.3 shows the relative contribution to the total capacity from different types of power station.

The hydro-electric stations form one of the main factors affecting the grid design and determining the intersystem tie line loads.

---

* The difference between the arithmetic sum of the regional maximum demands and the grid maximum demand.

† Problems relating to the magnitude, constitution and distribution of power reserves will not be discussed here.

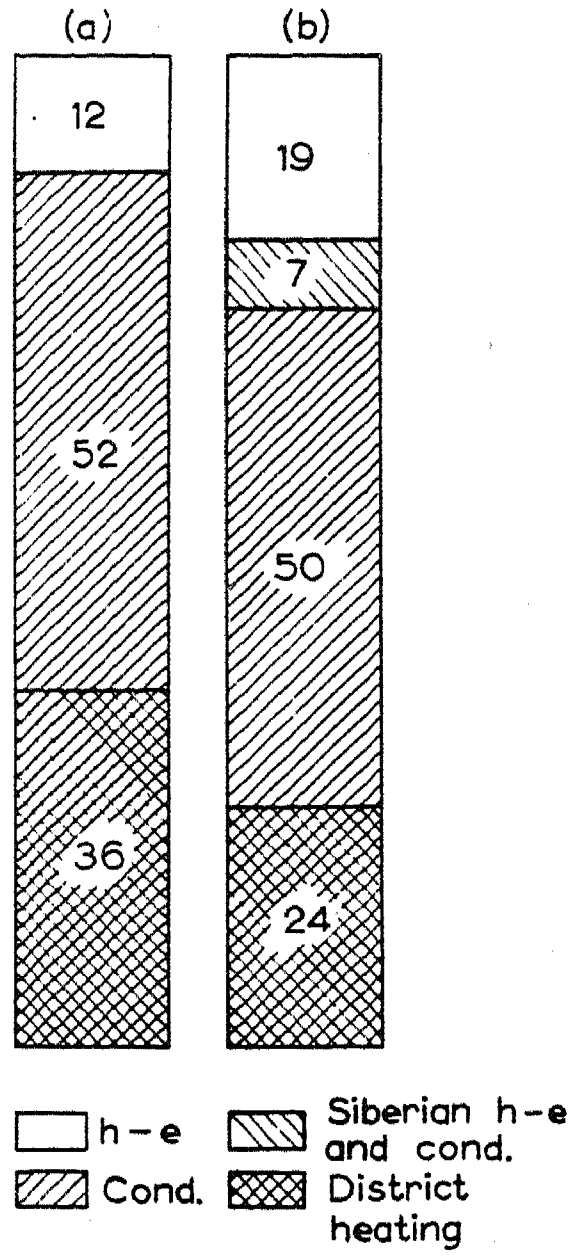

Fig. 3.

The total hydro-electric energy in the first stage of the European grid is planned to be about 66 x 10^9 kWh in a year of average flow.*

The total output in an average year would then be:

11.7 x 10^9 kWh from existing stations,

30 x 10^9 kWh from stations under construction

24 x 10^9 kWh from hydro-electric stations in the design stage.

The hydro-electric schemes in the European grid will produce 16 per cent of the annual output and comprise 19 per cent of the installed capacity in the second stage.

---

* This refers to existing stations and those under construction in various design stages on the Volga and Kama and their tributaries, and on the Dnieper, Don and Dniester. The Volga developments include the lowest barrage at Astrakhan giving 6 x 10^9 kWh. The output of the hydro-electric stations on the Dniester will be about 1.1 x 10^9 kWh. The lower Ob scheme and the so-called "Northern Supply" (direction of the northern river waters into the Volga) are not included.

The part played by the hydro-electric station in covering the load is of great importance in determining the MW-capacity and hence its overall economic effect.

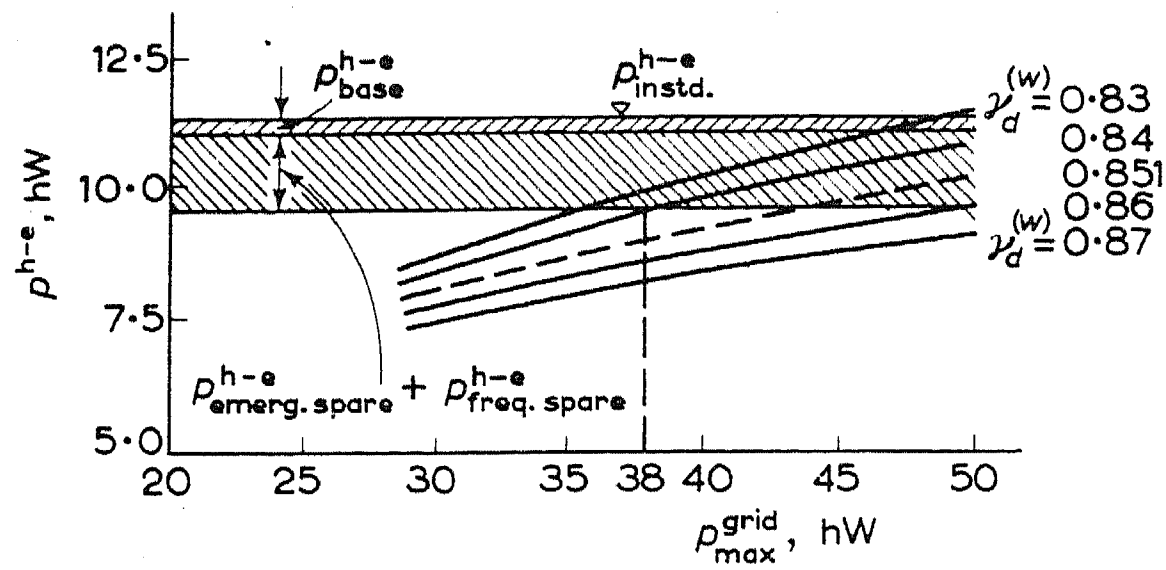

Fig. 4.

Fig.4 shows the effect of changes in the theoretical maximum demand and in the load curve shape for the European U.S.S.R. grid, all other conditions on the total working maximum* of the hydro-electric stations remaining unchanged.

The maximum grid demands are plotted horizontally. The basic figure for the first estimated level is 38 GW, the range of variation being 30 – 50 GW. The hydro-electric capacity is taken as ordinate. $\gamma_d^{(w)}$ ranges from 0.83 – 0.87, the basic value being = 0.851 and $\alpha_d^{(w)} = 0.668$, the guaranteed hydro-electric output and installed capacity being 4 and 11.3 GW respectively. Below the 11.3 GW level are marked the imposed basic load of the hydro-electric stations (0.3 GW) and the minimum spare (frequency and emergency) capacity (1.5 GW) which may be allocated to the hydro-electric stations. The difference between installed and available capacity due to head variations is less than 0.1 GW.

Fig.4 shows that at the first level, which will be reached by about 1963–64, the total hydro-electric output utilizable without duplication by thermal power stations already constitutes about 9.3 – 9.8 GW† in

---

* The total output of the hydro-electrical stations taking part in the basic and peak-load parts of the load curve.

† The first and second figures refer to the allocation of frequency and emergency spare capacity to the hydro-electric stations, i.e. 1 and 1.5 GW respectively. It should be borne in mind that not all the total planned hydro-electric capacity (11.3 GW) will be in service during that period; some stations will still be under construction.

the first alternative considered (dotted line). If $\gamma_d^{(w)}$ should not be 0.851, but only 0.84, the hydro-electric capacity utilised for the total grid maximum demand would be 9.8 – 10.3 GW. When the maximum grid demand increased by 1/3, with $\gamma_d^{(w)} = 0.851$ to 0.841,* it will be possible to utilize 11.8 – 12.5 GW of hydro-electric capacity without duplication, i.e., 0.5 – 1.2 GW more than the planned installed hydro-electric capacity.

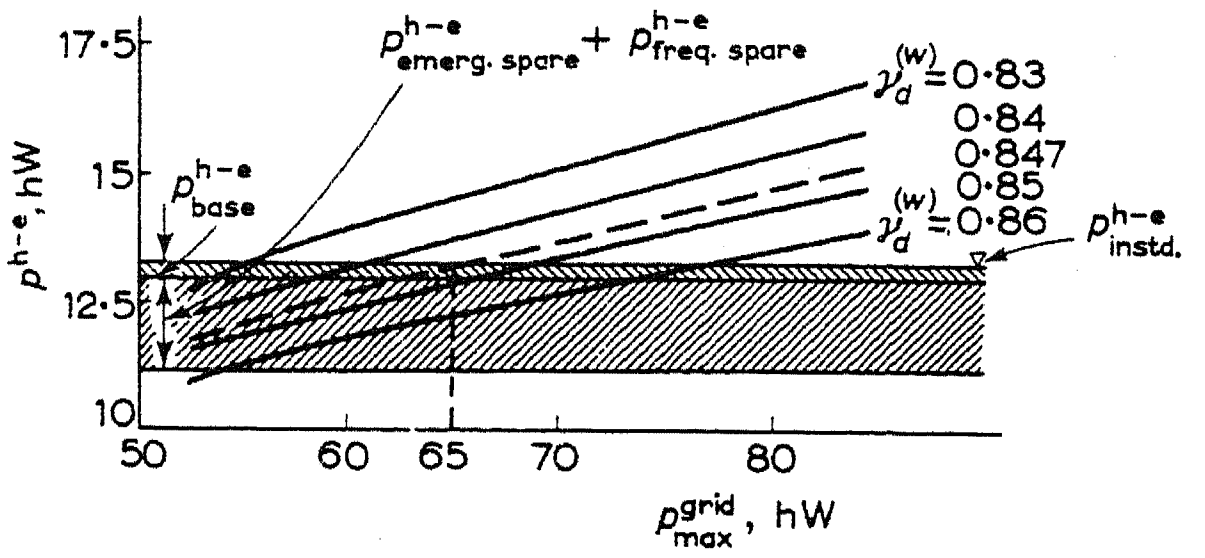

Fig. 5.

The effect of the maximum demand and of the shape of the load curve on the working maximum of the hydro-electric stations appears greater in the diagram Fig.5, where the second estimated level has been considered and where new possible hydro-electric developments (Astrakhan and others) have been taken into account. The total hydro-electric station capacity (13.3 GW) by the time the second estimated level is reached (maximum grid demand 65 GW, $\gamma_d^{(w)} = 0.847$, minimum essential spare capacity at the hydro-electric stations 2 GW) can be increased by more than 2 GW as compared with the data of the present plan.

We have graphs showing how the installed capacity of the hydro-electric stations of the European grid would vary with deviations of the development of the individual regions from the basic alternative, e.g. the actual rates of maximum demand increase may be lower in the Volga and Central Black-earth regions and higher in the Urals and the South, etc.

The total installed capacity of the above hydro-electric schemes in the European grid is too low. In the investigations and planning work of 1951 and the following years it was found necessary to increase the capacity of the Kuibyshev and Stalingrad power stations beyond their original ratings, i.e. by 1.7 – 2 GW.

At present the capacity installed at these stations is being increased by 700 MW. Further possible increases in the installed capacity must be

---

* Frequency and emergency spare capacity of thermal power stations 1.5 GW.

provided for by performing the appropriate engineering and other works; equipment can be installed later. The capacity installed at Saratov, Lower Kama, Chebokarsk and Astrakhan should be reconsidered in relation to their future part in the development of the European grid.

Of course Figs. 4 and 5 only deal with matters of principle as regards the need to increase the total hydro-electric capacity in the European grid by 2 – 2.5 GW over the present design figure. The individual schemes must be subject to cost analysis. Provision must be made at the design stage for the subsequent installation of additional equipment, otherwise the most efficient and complete use of resources in regions of restricted water supply would be prevented.

These proposals become more important when the link-up between the European and north-west and the Caucasus systems is allowed for, since a tie line will link the European grid with that of Siberia and the "Northern Supply" will become available. These will increase the hydro-electric capacity in the European grid and thus facilitate extension of their working and installed capacities.

The hydro-electric capacities can be assessed for the time when the links connecting the Central, Central Black-earth, Bashkiria, Tataria, Urals and Southern regions are commissioned.

In the second stage thermal stations will supply 75 – 80 per cent of the European grid power, the first including and the second excluding the Siberian hydro-electric stations.

In the second stage the district heating power stations in the European grid will have a capacity of about 17 GW. Their contribution towards covering the maximum demand will depend on their industrial heating load curves.

District heating stations will have dual-purpose turbogenerator sets of increased rating and be larger,* and together with new bleeder-turbine designs with higher efficiencies under various load conditions, application of the "boiler-turbine" unit system, creation of heat supply systems with parallel heat infeed, introduction of efficient heat distribution systems, complex automation and remote control of district-heating power stations.

---

* Unit ratings rising from 12 – 25 MW to 50 – 100 MW, higher input pressures and temperatures will be used. By replacing steam at 90 atm and 500°C by steam at 200 atm and 600°C the heat output per Mcal will be increased by 30 – 50 per cent for 2 atm and 10 atm gauge pressure at the bleed points for heating and industrial steam, respectively.

The regional thermal condensation stations play the largest part in the European grid. Their capacity will be increased to 36 – 41 GW in the second stage.* The major increase (18 out of 27 GW) will occur between the first and the second stages when the water resources in the European grid regions will already be largely utilized. Condensation stations will contribute from 52 to 50 to 57 per cent.*

The grid will facilitate the introduction of stations with sets of 200 – 300 MW and later 500 MW unit rating, with ultra high-pressure steam input and boiler-turbine units.

The siting of the new condensation stations – whether at the fuel source or at the load centres – is of primary importance. The grid will introduce new factors which will greatly influence the solutions adopted. Also the grid layout and design will depend to a great extent on the location of the condensing plant.

Reversible operation in intersystem ties might make it more economic to locate the condensation plant in low-cost fuel areas and substitute electric power transmission for fuel transport by rail.

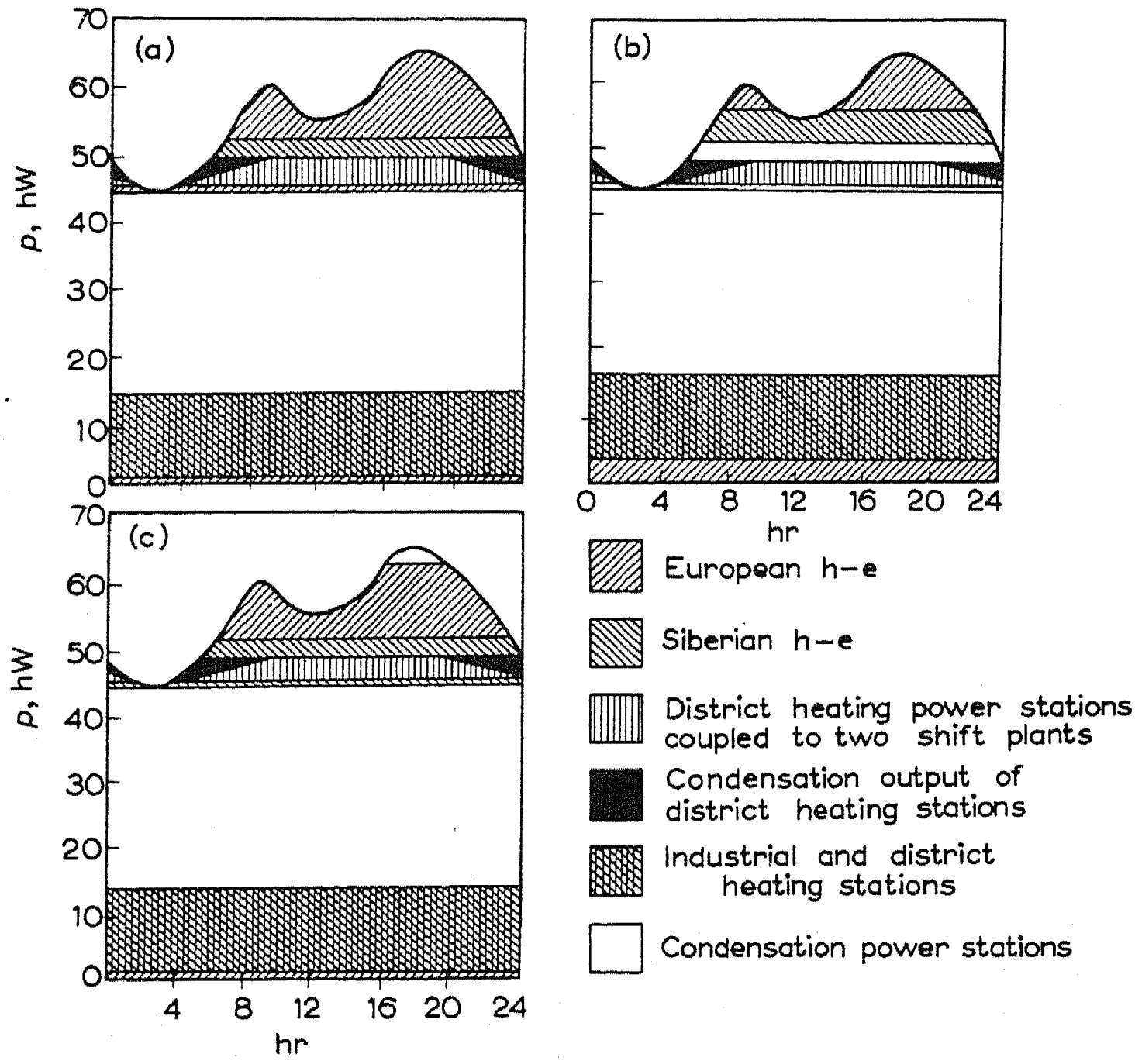

Fig. 6.

---

* The second figure excludes the Siberian hydro-electric stations.

In some regions stations will be developed in which the fuel will be used for power generation as well as for industrial or technological purposes and will drive gas-turbines, particularly in stations related to underground gasification schemes.

Fig.6 shows three alternative basic plans for covering the winter load curve in a year of low hydro-electric output, corresponding to the second stage in the European grid. The upper part in Fig.6(a) is occupied by the hydro-electric stations on the European rivers, replacing as much power as possible from condensation plant. In this case the total installed capacity (13.2 GW) helps to cover the load curve. Since part of the essential spare capacity may economically be allocated to hydro-electric stations their total capacity should be increased by more than 2 GW. If the hydro-electric station capacities are restricted as in the present plan the total spare capacity must be concentrated in the thermal stations.*

In Fig.6(b) the hydro-electric stations provide 2 GW of reserve capacity, and 11.3 GW covering the winter grid load in a year of low water. This assumes here that 8.3 GW is used for peak load and 3 GW for base load, part of the condensation plant being transferred to peak load, involving lower efficiency.

Fig.6(c) differs from the previous in that 11 GW (i.e. almost all of the hydro-electric power except 300 MW of its inherent base load) is placed just below the peak, but 2.5 GW at the peak is supplied from lower-efficiency steam condensation plant.†

The most favourable conditions for the different types of station in the different seasons and in years of different water availability must be chosen from technical and economic calculations with necessarily complicated conditions of the total energy balance of the grid.

General layout of the European grid

Fig.1 shows the basic layout of the European grid at the second stage. Some new intersystem ties not included in the Sixth Five-Year-Plan are:

---

* This alternative would involve wasting some water, the power loss being 1.4×10^6 kWh. Some 400 MW of hydro-electric power in addition to the 300 MW above must be transferrred from peak to base to avoid this loss. Correspondingly condensation plant would have to be transferred from base to peak, to compensate.

† The Siberian water power contribution to the European grid has also been considered.

Besides the first large 400 kV Moscow-Kuibyshev Hydro - Tatneft - Ufa Zlatoust trunk line (included in the Sixth Five-Year Plan), a second 400 kV trunk line, viz. Moscow - Chebokarsk Hydro - Lower Kama Hydro - Botkinsk Hydro - Sverdlovsk, is under consideration. The design of the Chebokarsk - Moscow line is linked to that of the Chebokarsk hydro-electric station. The Botkinsk hydro-electric scheme will be connected with Sverdlovsk. It would be incorrect to plan the individual links in these trunk lines in isolation, and the entire trunk line must be designed as one of the main features of the integrated high-voltage grid. The second 400 kV trunk line with its three auxiliary hydro-electric stations (Chebokarsk, Lower Kama and Botkinsk) is 1700 km long. The transmission conditions will vary during construction. In the first stage the flow will be from West to East via two branches: Lower Kama Hydro - Botkinsk Hydro - Sverdlovsk; and Lower Kama Hydro - Tatneft - Ufa - Zlatoust. In the second stage power from the Lower Kama hydro-electric scheme and some from the Lower Yenesei stations will flow along the same line from east to west. The capacity of the second 400 kV trunk line and branches must be determined from the second stage requirements.

The overall plan will ensure that the 400 kV Kuibyshev - Saratov line and the equipment operate at full efficiency. The line should be extended to Stalingrad if the Astrakhan scheme is proceeded with. If not, the extension will not be economic. A 400 kV transmission is being further investigated.

The good industrial and agricultural prospects of the Central Black-earth Region justify the 400 kV Saratov - Central Black-earth Region (Lipetsk substation) transmission system. Use of the hydro-electric station at Saratov to supply the Central Black-earth Region would replace more condensation plant than any other alternative.

The chart also shows a Donbass - Central Black-earth Region - Moscow transmission line. This line will supply the Central Black-earth and Central Regions from stations situated in the Don Basin operating on low-grade residues from coal enrichment processes, or on coal of calorific values below 4000 – 5000 kcal/kg.

The technical and economic aspects of this system will be determined when several supply problems have been resolved, viz. the fuel production of individual regions and the energy available for exchanges with the European grid, etc. Other energy sources competitive with power transmission, must be investigated, particularly nuclear stations.

The basic intersystem grid lines (including those between the 400 kV substations in Moscow and the Urals) comprise about 8700 km of single-circuit line.*

The operating conditions for individual lines will vary with the water supply and during different stages of development. Of the many problems involved only reverse power flow in individual ties will be briefly reviewed since this may be very important for economy in operation.

The essential character of one such operation is illustrated by the Stalingrad - Donbass transmission line.

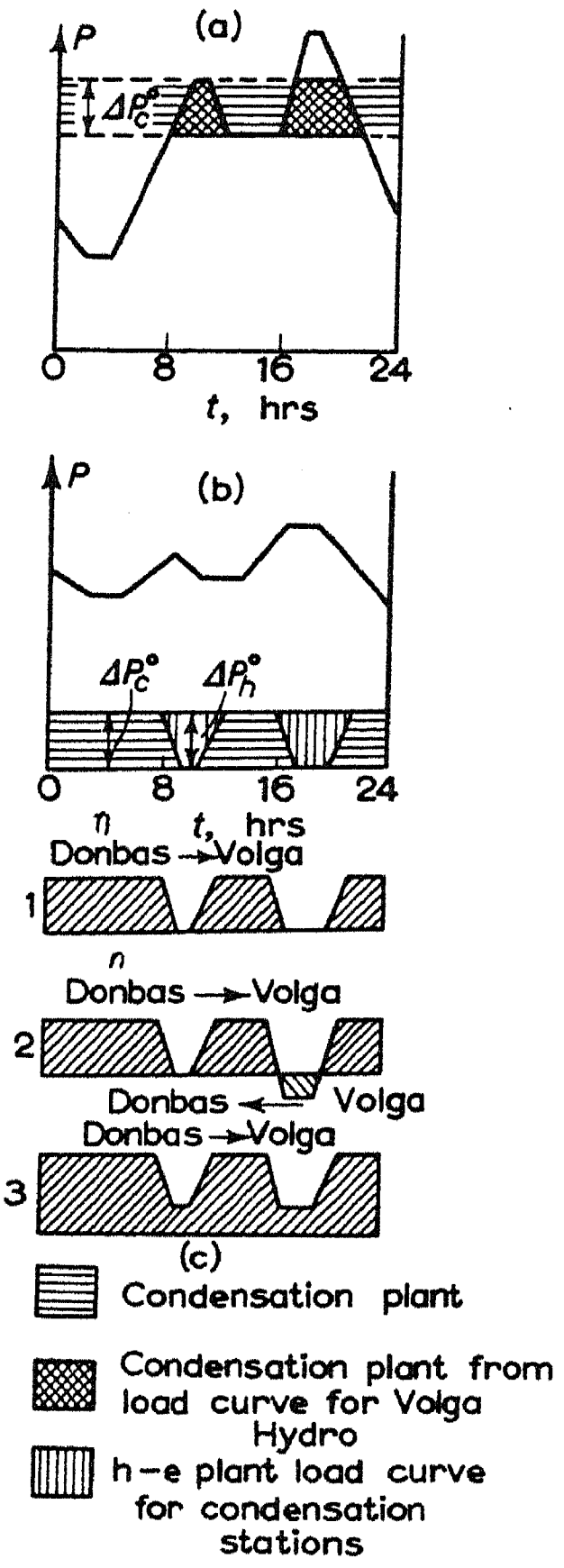

Fig. 7.

---

* The Donbass- Central Black-earth Region - Moscow and Saratov Stalingrad Hydro Astrakhan Hydro lines are not included. The capacities of the lines connecting the Urals with the Central region may have to be increased if power is received in the European grid from the Yenesei hydro-electric scheme.

Fig. 7 shows that two distinct operating conditions alternate because the Stalingrad hydro-electric station supplies power Δp_h^0 to the load curve, the peak of which is determined by the Southern system. During off-peak periods the Donbass supplies Δp_c^0.* Thus the condensation plant in the South has a constant output, the Stalingrad hydro-electric station supplying the peak load at some hours, energy being sent to the Volga at other times.

The operating conditions in the Stalingrad - Donbass tie depend on the structure of the Volga and Southern systems, on the individual station characteristics, on the magnitude and shape of the load peak in the Southern system and the Southern system load allocated to the Stalingrad station, on the Donbass condensation plant capacity, on the contribution to the Volga area load, etc. A winter day flow curve (Fig. 7) may be two-way or unidirectional ($\Delta p_c^0 \gtrless \Delta^0 p_h$).

Severe breakdowns in the Southern system may require power to be drawn from the Volga region. Then part or all of the normal Donbass - Volga flow will not be available, and power will have to flow westwards.† The operating conditions in other European grid links will also change during emergencies.

Reversed flow operation has the following advantages: an increase of the coefficient of transformation of the guaranteed power of the hydro-electric stations and, consequently, the possibility of an increase of its installed capacity and output which, in turn, guarantees the economy of the power output of the condensation power stations, fuel economy and reduction of the production cost of the energy, reduction of power and energy losses by intersystem transmission, cost reduction of intersystem transmission in connection with the reduction of the theoretical power flow and reduction of the required transmission capacity.

There are additional ways of increasing the maximum demand covered by the hydro-electric stations and the grid flexibility while retaining the same transmission capacity.

---

* Condensation plant must be installed between the first and second stages in addition to hydro-electric and district-heating stations to accord with long-term plans. This condensation plant will, as usual, supply the Volga region base load. The new condensation plant should be in the Donbass, where coal-enrichment residues are available, and not in the Volga region, for economic reasons.

† This justifies allocating some spare capacity (up to about 300 MW, 2 – 3 sets) at the Stalingrad hydro-electric station to the Southern lines.

Reversed flow operation is of advantage when regions with different times of maximum demand, different load curve shapes and different load structures are interconnected. It facilitates a new approach to the condensing station siting problem.

Another type of reversed flow operation is obtained by using the hydro-electric stations to supply peak loads in the grid when the regional load curves and time zones differ.

Economic efficiency in the European grid

Some approximate round figures for the efficiency of the European grid may be given.

The capital cost of the intersystem lines is about 5.8×10^9 roubles,* and the running cost about 340 million roubles p.a.

The total capital cost of the European grid will be 9.6×10^9 roubles, and running costs 625 million roubles p.a.

The grid will reduce the requirement for condensing stations by 4.8 GW.†

The fuel saved by the additional hydro-electric output (6×10^9 kWh) due to increase in hydro-electric station capacity and the smaller auxiliary consumption is about 2.3 million tons of coal p.a.

The capital saved on generating equipment is 6.7×10^9 roubles and the operating cost is reduced by about 1×10^9 roubles p.a. The additional capital outlay of about 3×10^9 roubles will be saved in less than 8 years by reduced operating costs (375 million roubles p.a.).

These estimates are conservative. The actual effect will be considerably larger. For example, the figures do not allow for concentration of thermal power stations in individual regions which will occur, nor for the savings from the increased guaranteed power from the interconnected Volga, Kama and Dnieper systems. The spare capacity reductions

---

* The Kuibyshev Hydro - Saratov Hydro and Donbass - Central Black-earth Region - Moscow lines are not included.

† About 3.9 GW will be supplied by additional plant at hydro-electric stations; the spare capacity required will be reduced by 0.9 GW when the difference in the auxiliaries at hydro-electric and thermal stations is allowed for.

assumed have been estimated to be 1.5 - 2 times smaller than those predicted by probability formulae.* The same applies to the sum of the individual load curves. The savings produced by coupling the hydro-electric units to the Urals and Southern area before the industrial loads in the Volga and adjacent regions have reached the planned levels (due to water wastage) have not been allowed for. Allowance of these additional factors would shorten the time taken to amortize the cost.

One unfavourable effect not allowed for in the above estimates is the "freezing" of some capital during construction until all the lines can be fully utilized.

The above figures refer to the European grid as a whole. Individual lines vary in economy. For example, the Kuibyshev - Urals and Stalingrad Donbass lines will take less than 4 years to pay off but the Kuibyshev - Moscow and Stalingrad - Moscow lines will take about 10 years.

The problems of the economic efficiency of the European grid will form the subject of further investigations on the methodological side as well as where the accuracy of the fundamental relations and basic data is concerned. Existing possibilities of further improvement of the economy of the European grid must be explored and utilized.

Connexion of the Caucasian and north western systems with the European grid

The basic problems of developing the Caucasian and North Western Regional grids, and of connecting them to the European grid, have not yet been fully studied.

In a year of medium water supply the hydro-electric potential of the Caucasus has been estimated to be about 180×10^9 kWh. Caucasian rivers have flows which vary in different years and between seasons. Storage lakes are costly and can only partly even out the annual flow. Hydrograph records for the Volga and Dnieper differ considerably from those for the Caucasian mountain rivers which have their largest flows in July and August, due to melting snow.

The Caucasian water power resources would be most efficiently used by linking the Caucasian system with the European grid, particularly with the Southern part. In good years this would reduce the demand on thermal

* The coefficient of availability was assumed as 0.9999; the average maintenance of a unit as 1 per cent, the individual generating units were assumed of 100 MW capacity.

condensation stations in the south and elsewhere. In bad years the flow would be from the southern system to the Caucasus. The Caucasian hydro-electric systems consist of relatively small units, which must be allowed for.

The line connecting the Caucasus with the European grid is about 1000 km long and about 1 GW capacity.

It was originally proposed to connect the north western system to the European grid by a 220 kV line from Leningrad to Moscow, from which the October railway was to be supplied. Such a low-power link (150 – 200 MW) between systems of many million kW capacity is unsatisfactory. It is necessary to envisage other alternatives which would economically justify the creation of a strong power link between the north western Region and the European grid. In particular, it is necessary to consider a line connecting the Lower Ob hydro-electric scheme with Leningrad via the upper Volga region. Such a line would be about 2500 km long and of about 2.5 – 3 GW capacity.

Only a few problems relating to a European grid which have been studied in detail by the Institute of Power Engineering of the U.S.S.R. Academy of Sciences have been dealt with here. In particular the methods of calculating power demand and supply and the economic factors determining basic parameters of the grid have not been touched upon. The Siberian grid, its connection with the European grid, and the future contributions of nuclear power stations will form the subject of separate papers.

INVESTIGATION OF VARIABLE-SPEED A.C. MACHINES*

I. I. TRESHCHEV

Introduction

Modern electrical engineering developments are associated with the continuous increase of machine ratings and operating speeds. Transients then assume an ever greater importance, and are indeed decisive in some practical cases. Cases are known in which a synchronous three-phase generator on dead short-circuit has slowed considerably within a relatively short time. This retardation is due to the braking torque set up by the short circuit, and as the flywheel masses will be different in every concrete case the retardations will differ. The torque speed function must be known in order to determine conditions under which normal operation is rapidly restored.

The maximum short circuit torque must be known in order to determine the mechanical strengths of generator and foundations. But the maximum torque depends on the generator speed changes under these conditions.

The effect of the rate of change of slip on induction motor characteristics is usually neglected in the theory. The power lost on changing the magnetic energy is not considered in the energy balance. Every slip is assumed to have a corresponding well-defined torque independent of the slip variation rate. However, the static mechanical characteristic applies only to the steady state. Even at normal induction motor accelerations the actual torque deviates considerably from its static value. For example, for a type A92–4 motor with a run-up time $t = 2.6\ T_m = 1$ sec, the maximum torque difference will be about 50 per cent of the rated value for small slips.

When the load seizes or jams the retardation is very rapid. If the slip variation rate is considered the effective maximum torque may exceed the maximum steady-state torque by a factor of almost 2, and the rated torque by a factor of almost 5, which must be allowed for in specifying the mechanical strengths of motor and load. A difference

* *Elektrichestvo* 2, 49–55, 1957 (Reprint Order No. EL2)

between these characteristics will also exist when speed control is by frequency variation. The effect of slip variation rate on the motor characteristic is of particular importance in repeated short-time and high-speed processes in connexion with the current general tendency to increased operating speeds. A criterion defining the maximum error in such cases has already been suggested [1].

The short-circuit torque of a synchronous machine can be calculated only if the quadrature components of the currents and flux linkages are known; this complicates matters even if the speed is constant and operational methods are used. On the other hand the short-circuit currents are given approximately by simple formulae which are in satisfactory agreement with experiment.

Great theoretical difficulties also arise when an induction motor is operated at variable speeds.

It will be shown that the power associated with the magnetic energy during a short-circuit may be determined with satisfactory accuracy if the symmetrical current components are known along one axis. These data, together with the energy balance, give the short-circuit torque simply and with the desired accuracy with due allowance for speed changes. Recurrence formulae for the torque of a synchronous machine and the stored magnetic energy will be derived from the energy balance, from which the behaviour under variable speed conditions can be predicted.

Fundamental relationships

The co-ordinate system is assumed at rest relative to the rotor. The voltage equilibrium equations for the stator and (on the usual assumptions) take the form [1],

$$\left.\begin{aligned} u_d &= i_d r_s + \frac{d\psi_d}{dt} - \omega\psi_q ; \\ u_q &= i_q r_s + \frac{d\psi_q}{dt} + \omega\psi_d ; \\ u_0 &= i_0 r_s + \frac{d\psi_0}{dt} . \end{aligned}\right\} \qquad (1)$$

On a per unit basis and for the rotor we get

$$\left.\begin{aligned} u_{rd} &= i_{rd} r_r + \frac{d\psi_{rd}}{dt} \\ u_{rq} &= i_{rq} r_r + \frac{d\psi_{rq}}{dt} \end{aligned}\right\} \qquad (2)$$

where:

u_d, u_{rd}, i_d, i_{rd}, ψ_d, ψ_{rd}, are the components of voltages, currents and flux linkages along the d-axis; u_q, u_{rq}, i_q, i_{rq}, ψ_q, ψ_{rq}, being the components of the voltages, currents and flux linkages along the q-axis;

u_0, i_0, ψ_0 the same for the zero-components;

r_s, r_r the resistances of stator and rotor, respectively;

and ω is the rotor angular velocity.

For simplicity the zero-components will be omitted because they are unrelated to the other components and can easily be considered if necessary. For a normal induction motor $u_{rd} = u_{rq} = 0$ in equation (2), and for a normal synchronous generator without damper these equations degenerate into one along the direct axis for the field winding.

If the generator has a damper in the direct axis, the two equations will relate quantities referring to this axis, viz. one for the field winding and the second for the damper winding. The number of equations in (2) will increase with the number of rotor windings.

Equations (1) and (2) are equivalent to reducing the machine to two transformers with windings about the d and q axes mutually related by the rotational e.m.f. These transformers rotate together with the co-ordinate system, at the rotor speed (Fig.1).

If we multiply the left hand and right hand sides of (1) and (2) by i_d, i_q, i_{rd} and i_{rq} respectively, and add these parts we get

$$p = p_T + \frac{dW_m}{dt} + \omega M \qquad (3)$$

where p is the total electrical power supplied to the machine or by it; p_T the copper losses in the stator and rotor; $\omega M = \omega(\psi_d i_q - \psi_q i_d)$

is the mechanical power supplied to the rotor or derived from it; dW_m/dt, the power expended on varying the magnetic energy. Also

$$\frac{dW_m}{dt} = \frac{d\psi_d}{dt} i_d + \frac{d\psi_q}{dt} i_q + \frac{d\psi_{rd}}{dt} i_{rd} + \frac{d\psi_{rq}}{dt} i_{rq} . \qquad (4)$$

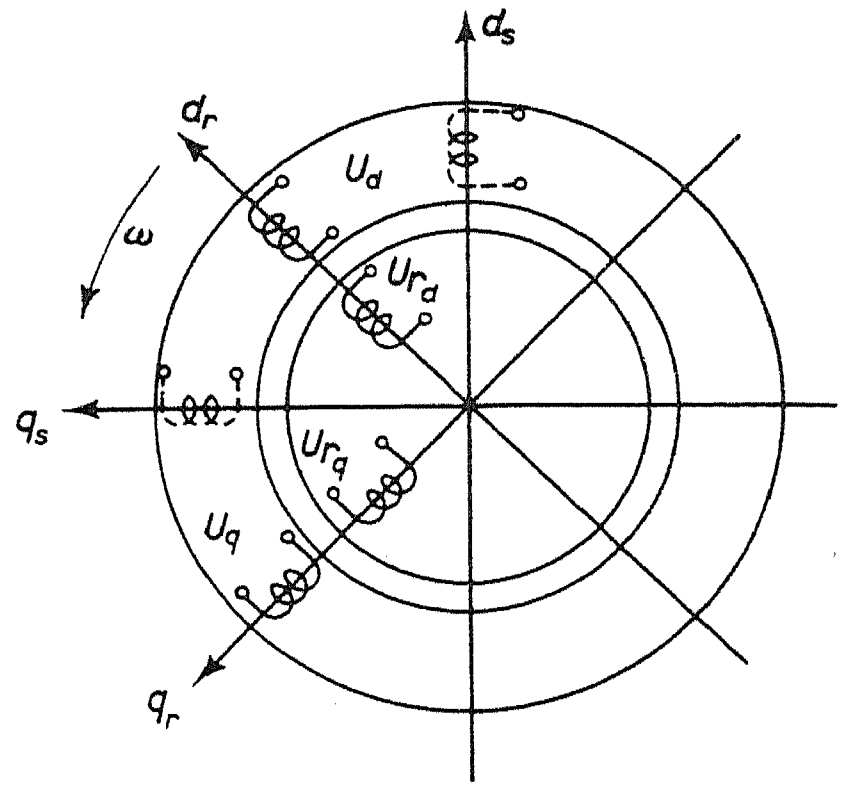

Fig. 1. Reduction of a three-phase machine to two double-wound transformers.

Equation (3) expresses the power balance. It is easy to show that if $dW_m/dt = 0$, no transient electromagnetic processes take place in the machine. Consequently, this term in the over-all power balance (3) determines the effect of transient electromagnetic processes on the behaviour.

If we introduce generalized complex terms for the flux linkages, $\bar{\psi}_s$, $\bar{\psi}_r$, and currents, $\bar{i}_s$, $\bar{i}_r$, of stator and rotor, respectively, (4) takes the form:*

$$\frac{dW_m}{dt} = \left(\frac{d\bar{\psi}_s}{dt} \bar{i}_s^* + \frac{d\bar{\psi}_r}{dt} \bar{i}_r^* \right)_{Re} . \qquad (5)$$

where, $\bar{i}_s^*$, $\bar{i}_r^*$ are the complex conjugates of $\bar{i}_s$, $\bar{i}_r$.

The magnetic energy stored in the machine is

$$W_m = -\frac{1}{2} (\bar{\psi}_s \bar{i}_s^* + \bar{\psi}_r \bar{i}_r^*)_{Re} . \qquad (6)$$

Differentiating (6) and incorporating (5), we find

---

* Subscript *Re* indicates the real part.

$$\frac{dW_m}{dt} = \left(\bar{\psi}_s \frac{d\bar{i}_s^*}{dt} + \bar{\psi}_r \frac{d\bar{i}_r^*}{dt}\right)_{Re} . \tag{7}$$

Equation (7) offers considerable advantages in approximate work. Equations (5) and (7) are also valid if we use the complex conjugates of the flux linkages instead of those of the currents. Operational methods are usually used nowadays with a.c. machines. This is possible if we assume the rotational speed constant and that the currents vary exponentially. The stator and rotor current vectors $\bar{i}_s$ and $\bar{i}_r$, rotate at variable speeds, and their amplitudes are also variable, i.e.

$$\left.\begin{aligned} \bar{i}_s &= i_{sm} e^{j(\int \omega_s dt + \theta_{s0})} ; \\ \bar{i}_r &= i_{rm} e^{j(\int \omega_r dt + \theta_{r0})} . \end{aligned}\right\} \tag{8}$$

where i_{sm}, i_{rm}, ω_s, ω_r, are the variables.

Substituting (8) into (7) and considering that for a symmetrical machine $[j\bar{\psi}_s \bar{i}_s^*]_{Re} = -[j\bar{\psi}_r \bar{i}_r^*]_{Re}$ we find

$$\frac{dW_m}{dt} = \frac{1}{i_{sm}} \frac{di_{sm}}{dt} [\bar{\psi}_s \bar{i}_s^*]_{Re} + \frac{1}{i_{rm}} \frac{di_{rm}}{dt} [\bar{\psi}_r \bar{i}_r^*]_{Re} -$$

$$- (\omega_s - \omega_r) [j\bar{\psi}_s \bar{i}_s^*]_{Re} . \tag{9}$$

If the currents decay exponentially then

$$\frac{1}{i_{sm}} \frac{di_{sm}}{dt} = -\alpha_s, \quad \frac{1}{i_{rm}} \frac{di_{rm}}{dt} = -\alpha_r ,$$

where α_s and α_r are the stator and rotor damping factors respectively.

When the current and flux linkage vectors lie along one axis, for example the *d*-axis, or almost so (symmetrical components in a three-phase short-circuit), the first two terms in (9) may be determined with a high degree of accuracy if we consider only the components along the *d*-axis, since we then get

$$[\bar{\psi}_s \bar{i}_s^*]_{Re} = \psi_d i_d + \psi_q i_q \approx \psi_d i_d ,$$

because when ψ_q and i_q are small $\psi_q i_q$ is a second-order infinitesimal. To determine the last term in (9) the in-phase and quadrature components must be accurately known because

$$[j\bar{\psi}_s \bar{i}^*_s]_{Re} = \psi_d i_q - \psi_q i_d .$$

Herein lies the main difficulty. However, we see from (9) that this term vanishes when $\omega_s = \omega_r$. But if the current vectors rotate at different angular velocities (e.g. if the aperiodic component is considered), the last term in (9) will not vanish. But we need to know the current amplitudes and initial phases only approximately, because the relative phases of the current vectors vary continuously.

This property of dW_m/dt occurs only when variations in the total magnetic energy of the machine are considered. It is no longer true if variations in the magnetic energy of stator or rotor alone are considered.

If the machine is not symmetrical, strictly speaking, (9) no longer applies. However, in most practical cases the error associated with the asymmetry is small. Consequently, the property of dW_m/dt discussed above will occur in asymmetric machines, i.e. synchronous generators with or without damping windings.

For a three-phase dead short-circuit at the terminals of an induction motor, if copper losses are neglected and there is no shaft load the dynamic equation and (3) give

$$W_{m1} - W_{m0} \approx J \frac{\omega_0^2 - \omega_1^2}{2} .$$

The change in magnetic energy is equal to the change in kinetic energy. Applications of the above relations will now be dealt with.

The torque of a synchronous generator on three-phase dead short-circuit

In this case we must put $p = u_f u_f$ in (3).

Consequently

$$M = \frac{1}{\omega}\left(\frac{dW_m}{dt} + p_T - u_f u_i\right) \qquad (10)$$

We stated above that dW_m/dt and the copper losses are practically completely determined by the currents in stator and rotor. The short-circuit currents can also be satisfactorily calculated from simple formulae based on the assumption that the symmetrical component vectors lie in the direct axis (2,3).

Using these formulae together with equation (4), dW_m/dt is found for a generator without damper winding by assuming that T'_d and T_a (in radians) are relatively large (Appendix)

$$\frac{dW_m}{dt} \approx \omega E_0^2 e^{-t/(T_a)} \sin\beta_\omega \left[\frac{1}{x_d} + \left(\frac{1}{x'_d} - \frac{1}{x_d}\right) e^{-t/(T'_d)}\right] - \omega \frac{E_0^2}{2} e^{-2t/(T_a)} \sin 2\beta_\omega \left(\frac{1}{x'_d} - \frac{1}{x_q}\right). \quad (11)$$

The main copper loss may be calculated by Lyuter's method (3) by considering the losses to currents set up in the rotor by the aperiodic stator current component. For a generator with damper winding this method, with the same simplifications, gives:

$$\frac{dW_m}{dt} \approx \omega E_0^2 e^{-t/(T_a)} \sin\beta_\omega \left[\frac{1}{x_d} + \left(\frac{1}{x'_d} - \frac{1}{x_d}\right) e^{-t/(T_d)} + \left(\frac{1}{x''_d} - \frac{1}{x'_d}\right) e^{-t/(T''_d)}\right] - \omega \frac{E_0^2}{2} e^{-2t/(T_a)} \sin 2\beta_\omega \left(\frac{1}{x''_d} - \frac{1}{x''_q}\right). \quad (12)$$

Equations (10 – 12) show that when the generator speed is sharply reduced copper loss effects increase, this causing an additional rise in braking torque.

Where the angular velocity is constant at the synchronous value ω_{syn} i.e. $\omega = \omega_{syn} = 1$ and also if we simplify for T''_d, T'_d and T_a very large the torque formulae coincide with those obtained by Lyuter's method [3]. The more exact treatment used here will only apply to low-rated machines with small time-constants and running at synchronous speed.

Fig. 2 shows the torque curve for a three-phase dead short-circuit in a W999 synchronous generator (28.2 kVA; 220/380 V; 74/43 A) during no-load operation for $E_0 = 1.$ and $\alpha = 1500$ rev/min.

The instantaneous copper losses are considered. The braking torque rises very rapidly and reaches almost 10 times its initial value. This causes the generator to lock suddenly which from (10) in turn causes a further increase in the maximum torque as indicated in Fig.2.

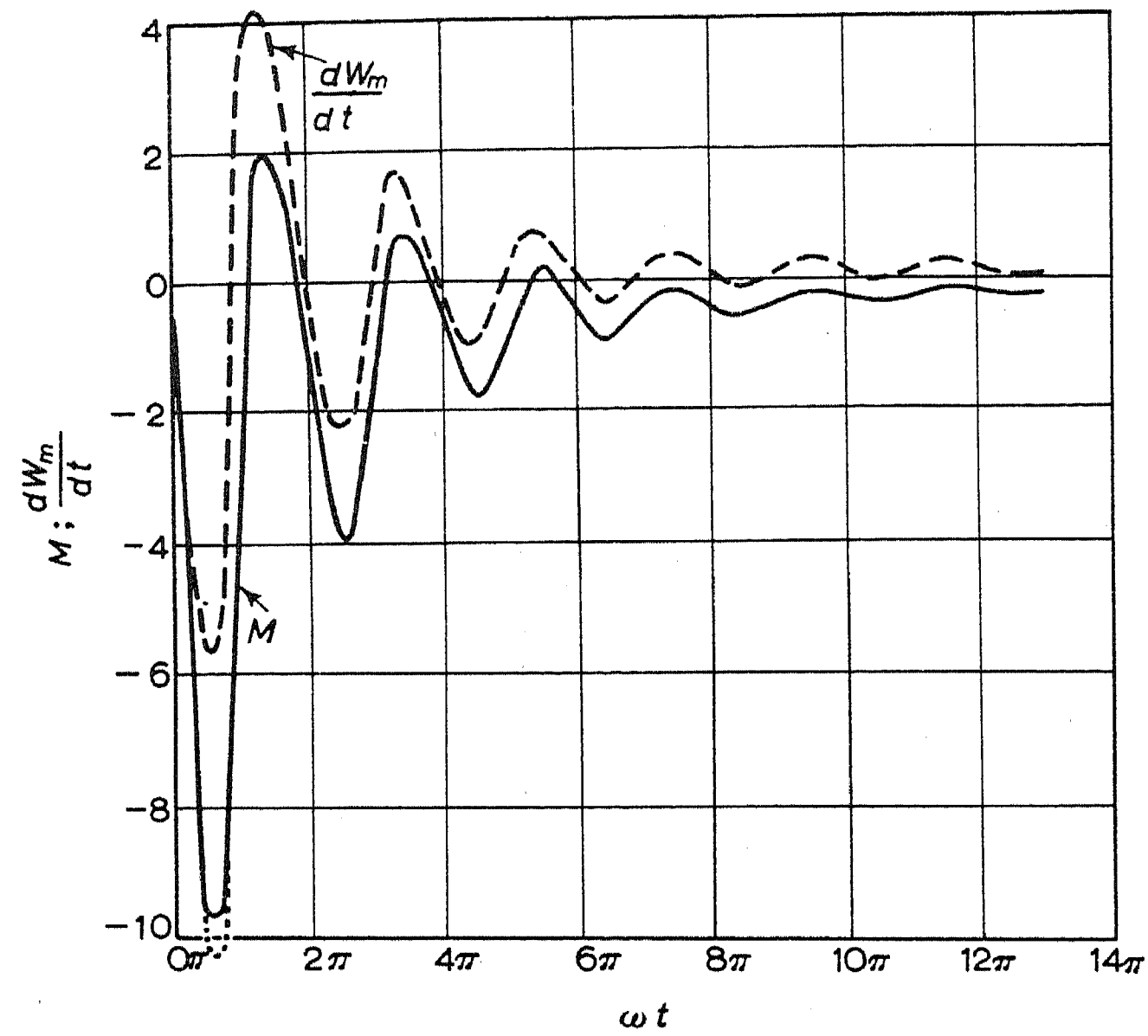

Fig. 2. Torque variation and dW_m/dt curves for a three-phase dead short-circuit across a W999 synchronous generator (28.2 kVA; 220/380 V;) 74.3/43 A; 1500 rev/min under no-load conditions at $E_0 = 1$.

... — is the effect of speed change on M_{max} when $\Delta n = -10$ per cent.

Variable-speed operation of an induction motor

The voltage balance equations for the generator, referred to axes rotating at synchronous speed, take the symbolic form

$$\left.\begin{aligned} \bar{u} &= \bar{i}_s r_s + j\bar{\psi}_s + \frac{d\psi_s}{dt}; \\ 0 &= \bar{i}_r r_r + js\bar{\psi}_r + \frac{d\bar{\psi}_r}{dt}. \end{aligned}\right\} \qquad (13)$$

where $\bar{i}_s$ and $\bar{\psi}_s$ are the complex stator currents and flux linkages

$\bar{i}_r$ and $\bar{\psi}_r$ are the same for the rotor;

r_s and r_r are the resistances of stator and rotor, respectively.

Equation (13) can be solved by numerical integration if we assume $r_s = 0$ when s is variable [4]. But even then special functions have to be used and, if the slip-time relation is linear, series which are not always rapidly convergent. The grapho-analytical method [5] also has some severe drawbacks. This problem, of considerable practical importance, is difficult to solve.

The stator and rotor currents will be written in the following form so that the energy relations can be used:

$$\left.\begin{aligned} \bar{i}_s &= \bar{i}_{se} + \bar{i}_{sv} \; ; \\ \bar{i}_r &= \bar{i}_{re} + \bar{i}_{rv} \; , \end{aligned}\right\} \qquad (14)$$

where i_{se} and i_{re} are the complex stator and rotor currents which approach, and at small rates of change of s are equal to the steady-state currents i_{sss} and i_{rss} ; i_{sv} and i_{rv} are the complex transient equalizing currents of stator and rotor.

If we assume a normal linear relation between currents and flux linkages we get

$$\left.\begin{aligned} \bar{\psi}_s &= \bar{\psi}_{se} + \bar{\psi}_{sv} \; ; \\ \bar{\psi}_r &= \bar{\psi}_{re} + \bar{\psi}_{rv} \; . \end{aligned}\right\} \qquad (15)$$

The magnetic energy changes associated with the flux linkage changes $d\bar{\psi}_{se}/dt$, $d\bar{\psi}_{re}/dt$, are normally small. Then (13), using (14) and (15) splits up into the following four equations.

$$\left.\begin{aligned} \bar{u} &= \bar{i}_{se} r_s + j\bar{\psi}_{se} + \frac{d\bar{\psi}_{se}}{dt} \; ; \\ \bar{i}_{re} r_r + js\bar{\psi}_{re} + \frac{d\bar{\psi}_{re}}{dt} &= 0 \; ; \end{aligned}\right\} \qquad (16)$$

$$\left.\begin{aligned} \bar{i}_{sv} r_s + j\bar{\psi}_{sv} + \frac{d\bar{\psi}_{sv}}{dt} &= 0 \ ; \\ \bar{i}_{rv} r_r + js\bar{\psi}_{rv} + \frac{d\bar{\psi}_{rv}}{dt} &= 0 \ . \end{aligned}\right\} \qquad (17)$$

A solution of (17) containing no constant term gives expressions in the form of elementary functions. Equation (16) is solved from the energy balance by successive approximation for the effect of magnetic energy changes on the motor currents. When the currents and flux linkages have been determined we get recurrence formulae for the torque and stored magnetic energy, from which the behaviour of a variable speed induction motor can be predicted (Appendix):

$$M_n = M_e + e^{-\alpha(t)}[\cos \beta_r (M_{n-1} - M_e) - \sin \beta_r (W_{n-1} - W_e)] - i_{sn}^2 r_s \ ; \qquad (18)$$

$$W_n = W_e + e^{-\alpha(t)}[\cos \beta_r (W_{n-1} - W_e) + \sin \beta_r (M_{n-1} - M_e)]. \qquad (19)$$

where, M_n, W_n and i_{sn} are the torque, stored magnetic energy and stator current for the n–th range of variation of s;

$$M_e = \frac{M_{ss}}{1 + \epsilon} \ ; \qquad (20)$$

$$\epsilon \approx \frac{M_{ss}}{u^2} \cdot \frac{ds}{dt} \cdot \frac{(x_1 + c_1 x_2')}{\omega} \left(\frac{c_1}{s} + \frac{r_s}{r_r} \right); \qquad (21)$$

is the steady-state torque:

$$\beta_r \approx \beta + \alpha_r' \alpha_s' (t - \beta) \ ;$$

$$\beta = \int s dt;$$

$$\alpha(t) \approx \alpha_r' t + \alpha_s' s \beta \ .$$

ds/dt is small for ordinary induction motors under normal operating conditions and so, from (21), $\epsilon = 0$.

Then

$$\left.\begin{aligned} M_e &\approx M_{ss}; \\ W_e &\approx W_{ss} \end{aligned}\right\}. \qquad (22)$$

the torque and magnetic energy stored in the stator are determined by the static characteristics. (18) and (19) may be similarly simplified.

Calculations using (18) and (19) are hardly more difficult than predicting the behaviour from steady-state characteristics, particularly if the stator copper losses are neglected and (22) used.

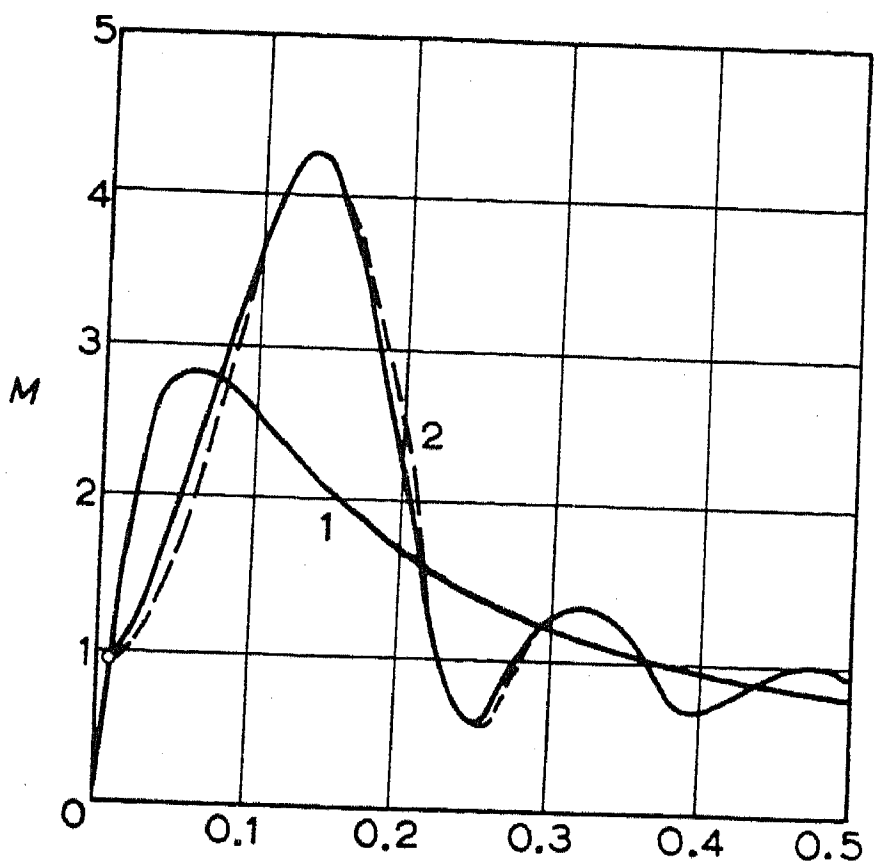

Fig. 3. Induction motor torque curves on braking at constant acceleration ($2a = 1/48\pi$)

1 - steady-state characteristic;

2 - characteristic including electromechanical transients.

To test (18) and (19), Fig. 3 shows torque curves for an induction motor during braking at constant acceleration $2a = 1/48\pi$, the parameters being: $x_s = x_r = 3.07$; $x_m = 2.99$; $r_s = r_r = 0.01$. The figure also shows the result predicted by using a computer [6] (broken curve). Table 1 gives the theoretical results. Where stator resistance is allowed for and M_e and W_e are used instead of M_{ss} and W_{ss} the agreement is satisfactory.

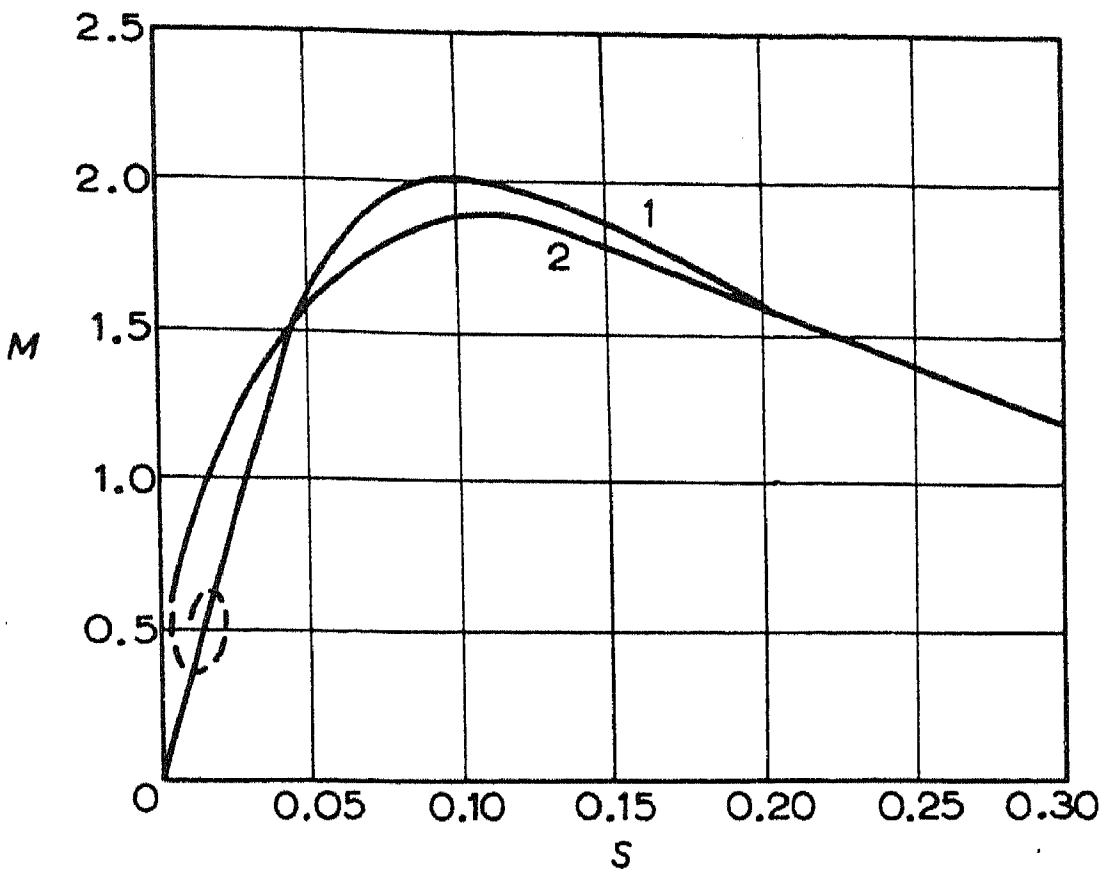

Fig. 4. Torque of a A92–4 induction motor on starting with an acceleration $2a = -1$ sec^{-2},

1 – steady-state characteristic

2 – characteristic including speed variation effects.

Fig. 4 shows the torque curve for a type A92–4 induction motor (100 kW, 1460 r.p.m.) run-up time $t = 2.6\ T_m = 1$ sec and $2a = -1$ sec^{-2} (a typical practical value). Table 2 gives the numerical values. The figure shows that the effect on the motor speed changes on the characteristic is fairly considerable around s_{max} and in the working range.

By considering the aperiodic current and flux linkage components in a similar way, we may predict the conditions during a three-phase dead short-circuit across the terminals of an induction motor.

Conclusions

The transient torque can be determined comparatively simply to the required accuracy by using the energy relations if approximate expressions are available for the currents, particularly the reactive short-circuit currents. This enables us to solve a number of practical problems.

Equations (18) and (19) can be used in simple calculations on induction motors operated at variable speeds where electromechanical transients are involved. These transients may solve many particularly important problems.

A similar study of power surges in synchronous machines and other such detailed processes not considered here may yield equally important results.

Appendix I

The stator currents i_d and i_q as well as the field current i_f during a three-phase dead short-circuit across a generator without damping winding may be expressed approximately by the following formulae [2,3]:

$$\left.\begin{aligned} i_d &\approx E_0\left[\frac{1}{x_d} + \left(\frac{1}{x'_d} - \frac{1}{x_d}\right)e^{-t/(T'_d)}\right] - \\ &\qquad - \frac{E_0}{x'_d}\, e^{-t/(T_a)} \cos \beta_\omega \ ; \\ i_q &\approx \frac{E_0}{x_q}\, e^{-t/(T_a)} \sin \beta_\omega \ ; \\ i_f &\approx i_{f0} + i_{f0}\,\frac{x_d - x'_d}{x'_d}\left(e^{-t/(T'_d)} - e^{-t/(T_a)} \cos \beta_\omega\right), \end{aligned}\right\} \quad (\mathrm{I},1)$$

where $\beta_\omega = \int \omega\, dt$.

where E_0 is the no-load e.m.f.

The flux linkages of stator ψ_d and ψ_q and rotor ψ_f will be

$$\left.\begin{aligned} \psi_d &= -E_0 e^{-t/(T_a)} \cos \beta_\omega \ ; \\ \psi_q &= E_0 e^{-t/(T_a)} \sin \beta_\omega \ ; \\ \psi_f &= E_0 x_{af}\left[\frac{1 - e^{-t/(T'_d)}}{x_d} - \frac{1}{x_d - x'_d}\right] . \end{aligned}\right\} \quad (\mathrm{I},2)$$

The magnetic energy variation dW_m/dt, from (4) taking into account (I,2), is

$$\frac{dW_m}{dt} \approx E_0 e^{-t/(T_a)} \left[\left(\omega \sin \beta_\omega + \frac{\cos \beta_\omega}{T_a} \right) i_d + \right.$$

$$\left. + \left(\omega \cos \beta_\omega - \frac{\sin \beta_\omega}{T_a} \right) i_q \right] -$$

$$- \frac{E_0^2 e^{-t/(T_d')}}{T_d' x_d} \left[1 + \frac{x_d - x_d'}{x_d'} \left(e^{-t/(T_d')} - e^{-t/(T_a)} \cos \beta_\omega \right) \right] . \qquad (I,3)$$

T_d' and T_a are some tens or hundreds of radians for normal machines. For simplicity therefore we may neglect terms containing T_d' and T_a in the denominator. After substituting the currents from (I,1) into (I,2) we get (11) for dW_m/dt.

Appendix II

The flux linkages of the stator ψ_{sv} and rotor ψ_{rv} are:

$$\left.\begin{aligned} \bar{\psi}_{sv} &= x_s \bar{i}_{sv} + x_m \bar{i}_{rv} \ ; \\ \bar{\psi}_{rv} &= x_r \bar{i}_{rv} + x_m \bar{i}_{sv} \ . \end{aligned}\right\} \qquad (II,1)$$

where x_s and x_r are the total stator and rotor reactances; x_m is the magnetizing reactance. From (17), (II,1) and (II,7) we get

$$\frac{d\bar{i}_{sv}}{dt} = - \frac{\alpha_s' \alpha_r + j\alpha_s' s + j(\alpha_r' + js)}{j\alpha_s' \alpha_r - \alpha_s' s + \alpha_s' + j} \bar{i}_{sv} \ , \qquad (II,2)$$

where α_s', α_r' and α_r are the damping factors of stator and rotor Since α_s' and $\alpha_r \approx 0$ (II,2) may be written in the form;

$$\frac{d\bar{i}_{sv}}{dt} \approx - j \frac{j + \alpha_s'}{j + \alpha_s'(1 - s)} s \bar{i}_{sv} - \frac{\alpha_r'}{1 - j\alpha_s'(1 - s)} \bar{i}_{sv} \ .$$

As $\alpha_s'(1 - s)$ has relatively little effect and neglecting second-order infinitesimals, integration gives an approximate expression for the effect of stator resistance.

$$\bar{i}_{sv} \approx Ce^{-j\beta_r} e^{-\alpha(t)} , \qquad (II,3)$$

where

$$\beta_r = \beta + \alpha_r'\alpha_s'(t - \beta) ;$$

$$\beta = \int s\, dt ;$$

$$\alpha(t) = \alpha_r' t + \alpha_s' s\, \beta .$$

substituting (II,3) into (14), we find

$$\bar{i}_s = \bar{i}_{se} + Ce^{-j\beta_r} e^{-\alpha(t)} \qquad (II,4)$$

When $t = 0$, $\beta_r = 0$, $\alpha(t) = 0$. From (II,4) we find:

$$C = \bar{i}_{s0ss} - \bar{i}_{se} .$$

Consequently

$$\bar{i}_s = \bar{i}_{se} + (\bar{i}_{s0ss} - \bar{i}_{se}) e^{-j\beta_r} e^{-\alpha(t)} . \qquad (II,5)$$

The smaller di_{se}/ds x ds/dt the better (II,5) satisfies the original differential equations. In the working range when ds/dt is comparatively large (II,5) will therefore yield sufficiently accurate results from relatively small ranges of slip variation. For this reason we will transform (II,5) into the following recurrence formula

$$\bar{i}_{sn} = \bar{i}_{se} + (\bar{i}_{sn-1} - \bar{i}_{se}) e^{-j\beta_r} e^{-\alpha(t)} , \qquad (II,6)$$

where $\bar{i}_{sn}$ and $\bar{i}_{s(n-1)}$ are the complex stator currents for the nth and $(n-1)$th ranges of slip variation.

We then find i_{se} for the given slip, and β_r and $\alpha(t)$ are read every time. (II,6) agrees with a similar formula obtained by another method in (5) when $\beta_r \approx \beta$, $\alpha(t) \approx \alpha_r' \Delta t$ and $i_{se} \approx i_{s\,ss}$.

The complex stator flux linkage ψ_s, when approximate allowance is made for the stator resistance, becomes

$$\bar{\psi}_s \approx \frac{\bar{u}}{j} + j\bar{i}_s r_s \,. \qquad \text{(II,7)}$$

M_n and W_n are given by

$$\left.\begin{aligned} M_n &= [j\bar{\psi}_{sn}\bar{i}^*_{sn}]_{Re} \,; \\ W_n &= [\psi_{sn} i^*_{sn}]_{Re} \,. \end{aligned}\right\} \qquad \text{(II,8)}$$

Substituting (II,6) and (II,7) into (II,8) we get (18) and (19).

To determine i_{se}, M_e and W_e we start from (16) and use (3). As dW_e/dt is small we assume to a first approximation that the current and flux linkage variations follow the steady-state characteristics. If we simplify the equivalent circuit of the induction motor by eliminating the magnetizing circuit, we get

$$\frac{dW_e}{dt} \approx M_{ss}\epsilon \,,$$

where

$$\epsilon \approx \frac{M_{ss}}{u^2}\,\frac{ds}{dt}\,\frac{x_1 + c_1 x'_2}{\omega}\left(\frac{c_1}{s} + \frac{r_s}{r_r}\right).$$

Successive improvement of the term for the effect of magnetic energy variation on the motor currents, and repeated calculation of the energy relations from (3) yield a formula for the torque, viz.

$$M_e = M_{ss}(1 - \epsilon + \epsilon^2 - \epsilon^3 + \ldots) \,. \qquad \text{(II,9)}$$

The terms in brackets are in geometrical progression; this gives (20). The magnetic energy stored in the stator is

$$W_e \approx \frac{u^2}{c_1 x_m} + \frac{u^2\sqrt{x_m^2 + \epsilon(r_m^2 + x_m^2)}}{c_1(1 + \epsilon)(r_m^2 + x_m^2)} \,,$$

where

$$r_m = r_s + c_1 \frac{r_r}{s} ; \qquad x_m = x_1 + c_1 x_2' .$$

REFERENCES

1. A.V. Ivanov - Smolwnskii; Effect of the rate of slip variation on the torque of an induction motor. *Elektrichestvo* No.6 (1950).
2. M.P. Kostenko; *Electric Machines (Special Part)*. Gosenergoizdat (1949).
3. R.A. Luyter; Prediction of induction motor short-circuit torques. *Elektrosila* No.7 (1950).
4. E. Ia. Kazovskii; Transients in induction motors on load cut-in and cut-out. *Vestnik Elekt. Prom,* No.2 (1949).
5. V.A. Shubenko and I.S. Pinchuk; A graphical method of predicting transients in induction motors. *Elektrichestvo* No.2 (1950).
6. F.I. Maggines and M.R. Shultz; Characteristics of induction motors. *Trans. Amer. Inst.Elect. Engrs.* **63**, 641, (1944).

THE USE OF AMPLIDYNES AND TRANSISTOR AMPLIFIERS FOR INDUSTRIAL DRIVES*

V.A. NAIDIS

Machine Tool Experimental Research Institute

Controlled feed mechanisms driven by d.c. motors supplied by quadrature field controlled amplidynes are now widely used on heavy horizontal and vertical lathes, boring and milling machines.

The motor speed ranges on heavy machine tools feed drives must be large (1:100 upwards) speeds constant to better than ±10 per cent and the automatic control system must be sufficiently fast. The latter arises from the need for the drive to be uniform and stable notwithstanding the varying motor loading from heavy slow moving tool rests, head and tail stocks, etc.

Most heavy electric units use velocity feedback in which the difference between the set and d.c. tachometer voltages is fed to the amplidyne control winding either directly or through an intermediate amplifier.

In 1950 ESRIMCL (Machine Tool Experimental Research Institute) developed the first electric machine tool feed using electronic amplification; this was installed on an experimental vertical lathe type P.521. Such units have been widely used in a series of boring machines produced by "Sverdlov" machine-tool works in Leningrad. Considerable control-circuit gain is required as the speed range is up to 1:1800 and this demands intermediate amplification in the feedback circuit.

Intermediate amplification is also advantageous with much smaller speed ranges (1:100 or less) if the amplifier is sufficiently simple, reliable and of small size.

* *Elektrichestvo* No.3, 5–10 (1957). [Reprint Order No. EL.3]

If the tachometer's output is fed directly to the amplidyne input the amplidyne control winding must be of low resistance to give sufficient gain. The fairly high amplidyne control winding currents required demand tachogenerators and reference sources of rather larger capacity and size. For example, in units made to the designs of the "Elektroprivod" K.D.B. for large lathes, vertical lathes and other machine tools PN-2.5 type d.c. generators built into the feed gearbox are used as tachometers being themselves gear-driven. The voltage references are too large to be fitted on rack panels. Bulky anti-hunt transformers types TS 72-60 and TS 144-110 are used.

Intermediate feedback circuit amplifiers greatly reduce the size, weight and price of tachometer, regulator, etc. Smaller d.c. or a.c. tachometers integral with the motors can be used as well as small speed (references) with or without contactors which can be controlled from several places, e.g. from rack panels, as well as small anti-hunt R-C -circuits.

Intermediate feedback circuit and amplifiers improve the speed stability against load variation, reduce the effect of magnetization in the amplidyne winding, heating, exciter voltages etc. At constant overall gain, the gain of the time-lag element (amplidyne) can be reduced because the gain of the quick response element (intermediate amplifier) is higher, and this produces an improvement in the transient response.

Disadvantages of intermediate electronic amplifiers in units with speed ranges of 1:100 are limited valve life, filament preheating time, etc.

A number of organizations "Elektroprivod", Central Design Bureau, the Leningrad Electrotechnical Institute, together with the "Sverdlov" machine tool factory ESRIMCL, etc. have worked on intermediate magnetic amplifiers powered at 500 and 50 c/s. A 500 c/s magnetic amplifier can replace an electronic amplifier completely, but a frequency changer is required. A magnetic amplifier supplied from 50 c/s mains cannot be made to give a short enough response time. Stability becomes difficult to obtain because there is now an extra time constant. It was quite sufficient in the intermediate amplifier control system to introduce an amplidyne feedback to the intermediate amplifier input via an R-C-circuit A magnetic amplifier control system also requires a series of derivative feedbacks between the amplifier stages and overall derivative feedback.

Transistor amplifiers

The production (1956) of a 1 W output Germanium transistor (type P.3) by the electronic industry resulted in the development of a transistor amplifier for machine tool control systems. Transistor amplifiers comparable with electronic amplifiers on gain and response time have advantages such as longer life, fewer service faults and smaller size. Transistor amplifiers have lives 10-15 times greater than vacuum valves. Transistors have no heaters and hence no warm-up time. The higher efficiency as compared with the electronic amplifier reduces the size of the supply transformer, rectifier and voltage stabilizer. The complete transistor amplifier is therefore only about half the size of an equivalent electronic amplifier.

The comparatively low input impedances of transistors might appear to be a disadvantage since this restricts the tachometer and reference source resistances and increases the derivative circuit capacitances, but these disadvantages can be avoided by using suitable circuits. The lower input impedance of a transistor amplifier enables one to isolate the input without fear of producing interference and noise. The need to earth the input of an electronic amplifier is disadvantageous especially when the amplifier and the rest of the drive circuit are connected electrically. Current production transistors still show large scatters in parameters; moreover many with high initial collector currents must be rejected as unsuitable for use in d.c. amplifiers.

The main disadvantage of transistors is, however, their sensitivity to ambient temperature variations. For example, in a simple two-stage amplifier with P3A transistor the output current changes by factors of 1.3 – 2 according to the working point used when the ambient temperature varies by 30°C. This causes difficulties in using transistor amplifiers in modern feed controls. Various methods of transistor amplifier temperature compensation are given in foreign journals. Either *p–n–p* and *n–p–n* triodes are used in alternate stages or else the parameters are stabilized by means of nonlinear resistances sensitive to ambient temperature. The first method cannot be used here because Soviet industry does not produce the barrier layer *n–p–n* type transistor. Parameter temperature-compensation circuits have been tested satisfactorily. Their disadvantages lie in the need to adjust the circuit, and the compensation is upset when one parameter changes. Considerably better results are obtained when the temperature compensation is obtained via special interstage circuits.

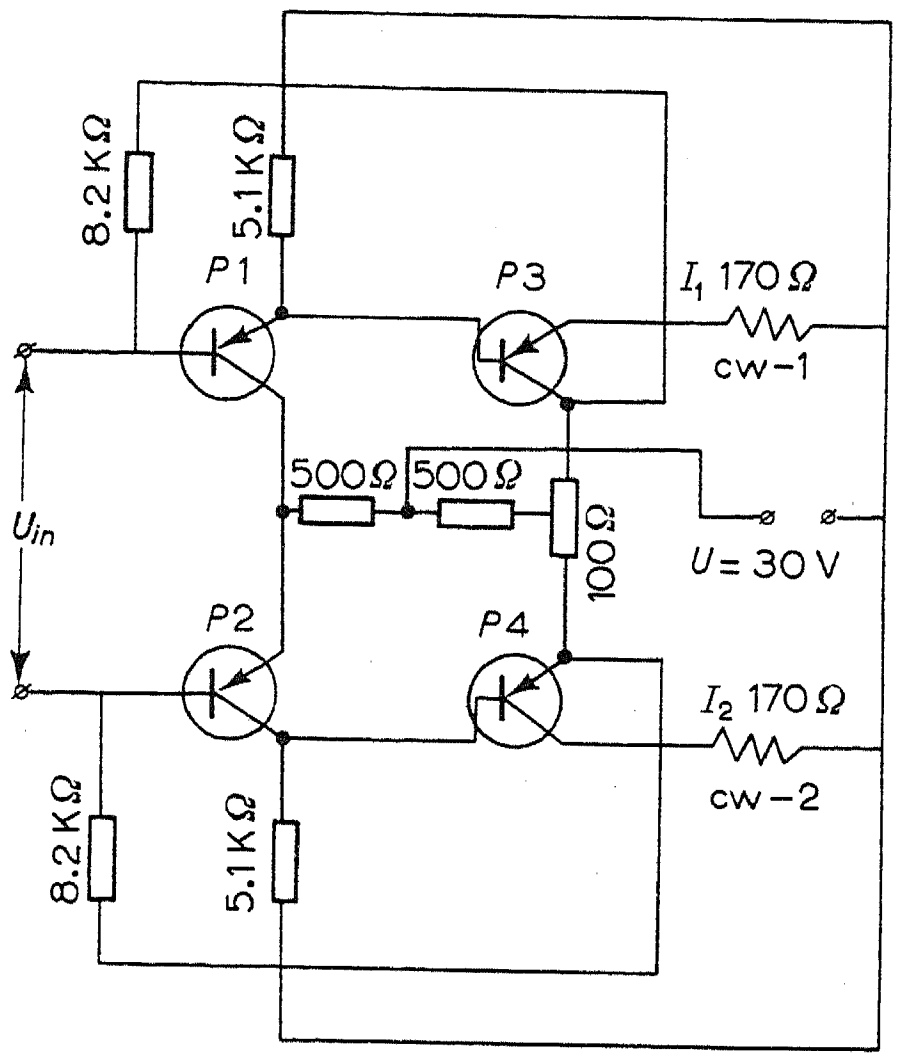

Fig. 1. Outline circuit of a two-stage balanced transient amplifier.
cw 1, *cw* 2 amplidyne control windings.
*P*1 – *P*4 transistors type P3A.

Fig. 1 shows the basic circuit of a two-stage balanced amplifier with P3A transistors which can be used for reversible drives. Temperature compensation is obtained as follows. The collector current increases

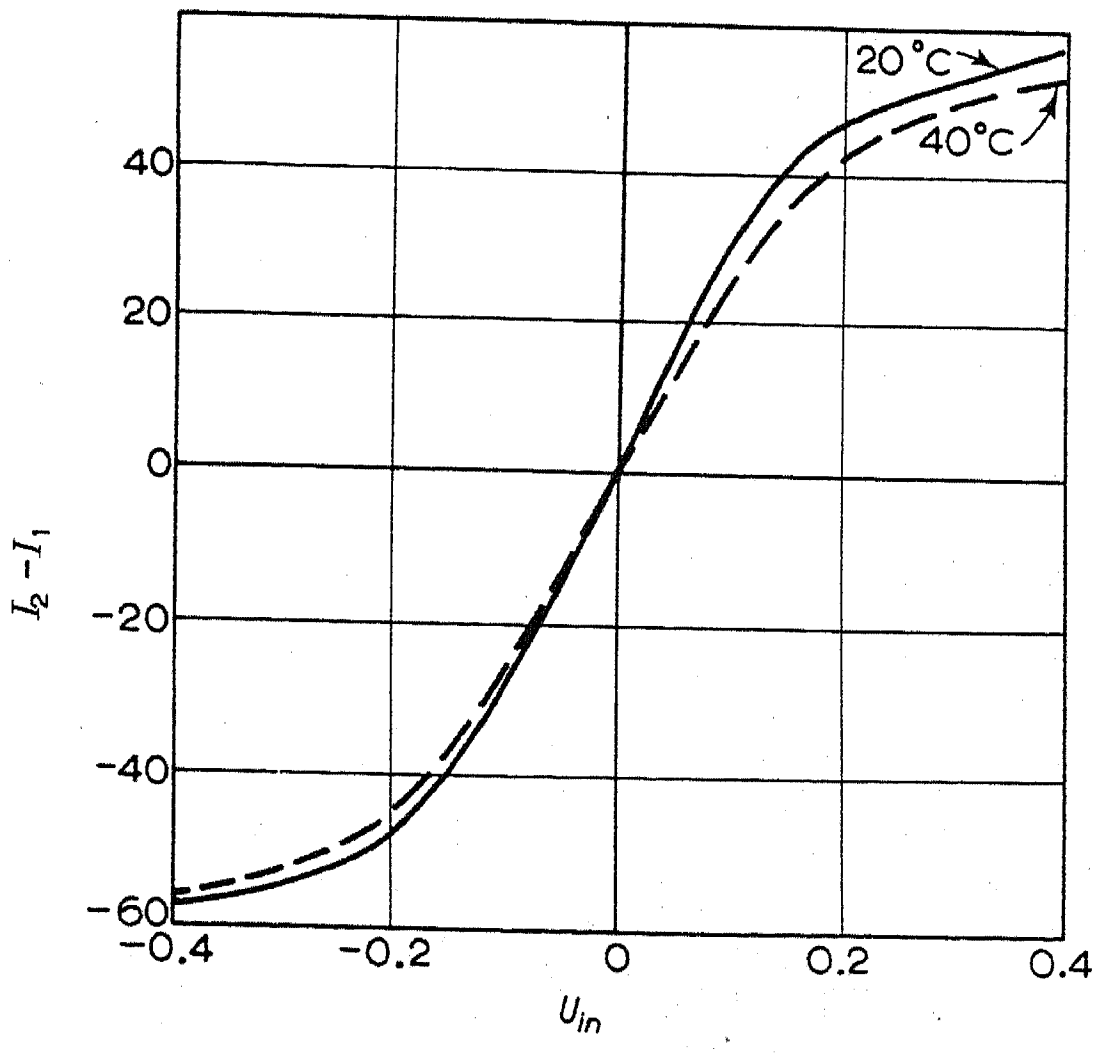

Fig. 2.

with ambient temperature. The collector current increase in stage one causes a decrease in positive emitter-base current in stage two i.e the load current falls. Suitable choice of the resistance controlling the collector-emitter voltage and suitable gain of the first stage and the use of negative feedback gave a characteristic $I_2 - I_1 = f(U_{input})$ almost independent of ambient temperature (Fig.2).

Units using the tachometers

Fig.3 shows the basic circuit of a feed drive for heavy horizontal and vertical lathes developed by the ESRIMCL. In these machines one d.c. motor provides feed movement in two directions at 90°. The feed direction is controlled by four electromagnetic clutches also used for copying work. A simple non-reversing circuit can then be used. The

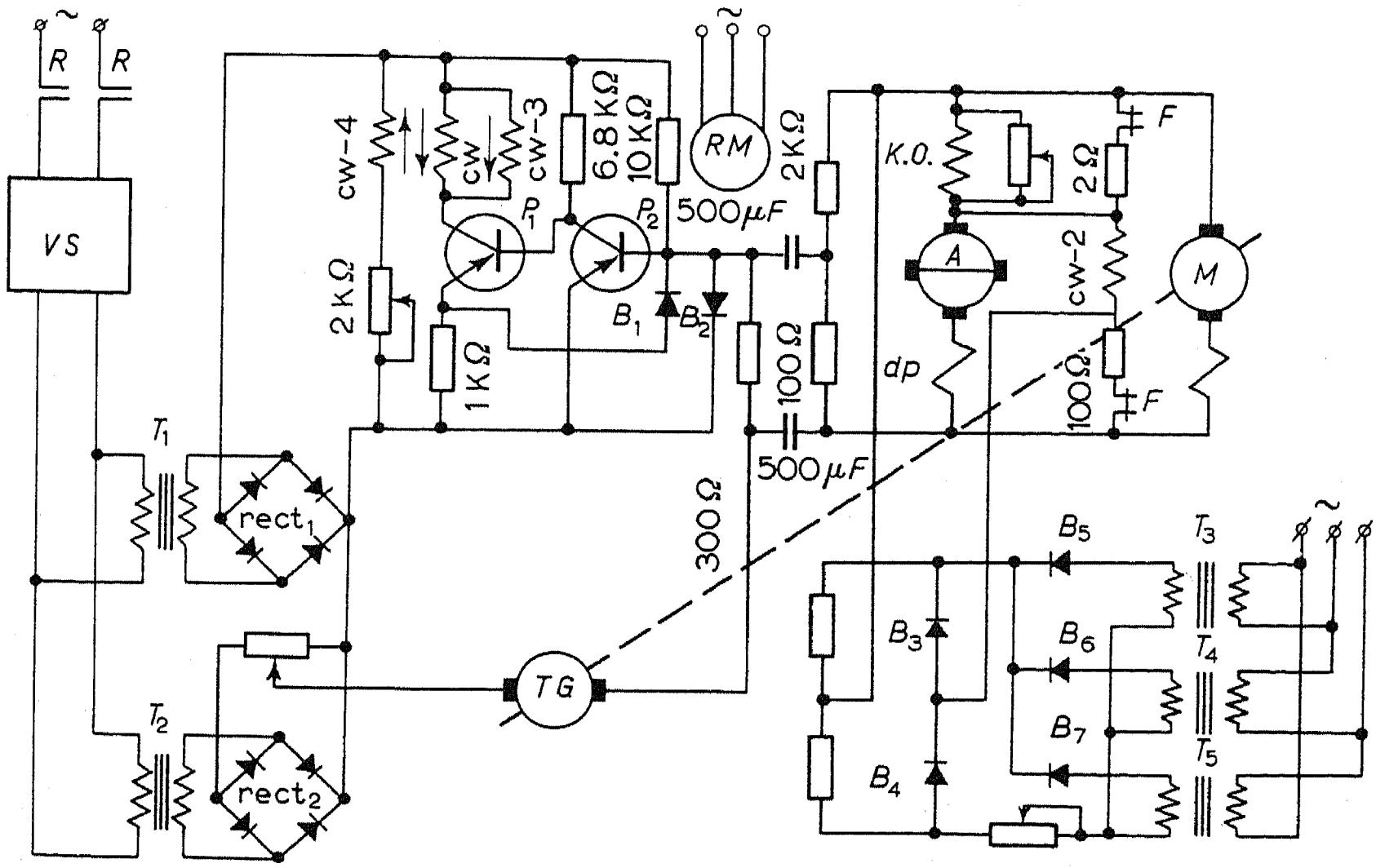

Fig.3 Outline circuit of the feed drives of horizontal and vertical lathes using d.c. tachometers.

IM induction motor, *A* amplidyne type EMU-25, 2.5 kW, 230 V, 2850 rev/min, *M* motor PN-28.5, 4.2 kW, 220 V 22 A, (I_{don} = 13 A at n = 0), *TG* tachogenerator TMG 30P, 250 V, 4000 rev/min, T_1 – T_5 transformers, *VS* voltage stabilizer, *P*1 transistor P3A, *P*2 transistor P1A, B_1, B_2 DG TS 27 diodes.

speed ranges required may be as high as 5000 – 10000. But electro-mechanical control plus gearbox-controlled steps of 1:100 would be more suitable.

A signal proportional to speed is provided by a small permanent-magnet d.c. tachometer *TG*, attached to the motor *M*. The difference between the set voltage and the velocity feedback signal is applied to the transistor amplifier input. The amplifier has r.c. feedback.

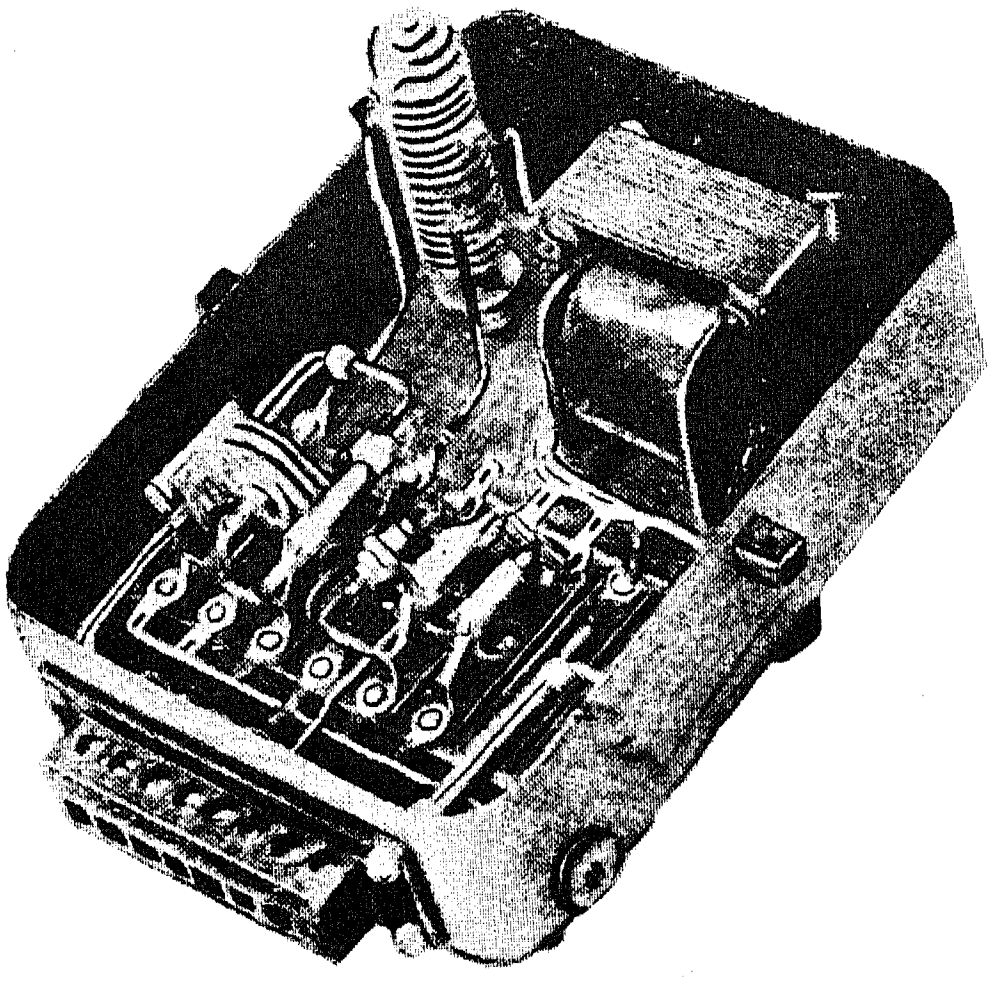

Fig.4 General view of the intermediate transistor amplifier (circuit diagram of Fig.3).

A photograph of the two-stage transistor amplifier shown in Fig.4 forms one of the arms in the circuit of Fig.1. At zero input and positive emitter-base in the first stage the collector current of the input stage is a maximum. The output stage load current is then a minimum (Fig.5). The working point I_w at the minimum motor speed I_w, is determined by the control winding flux *cw* 4, and the residual flux in the amplidyne. By varying the resistance in the circuit of *cw* 4 it is possible to adjust this current to ensure maximum amplification at minimum motor speed and to reduce the effects of ambient temperature variations. The input is shunted by germanium diodes B_1 and B_2 to protect the amplifier against large input voltages during transients. B_1 has a voltage limiter protecting against the effects of the forward resistance of the diode in the steady-state conditions.

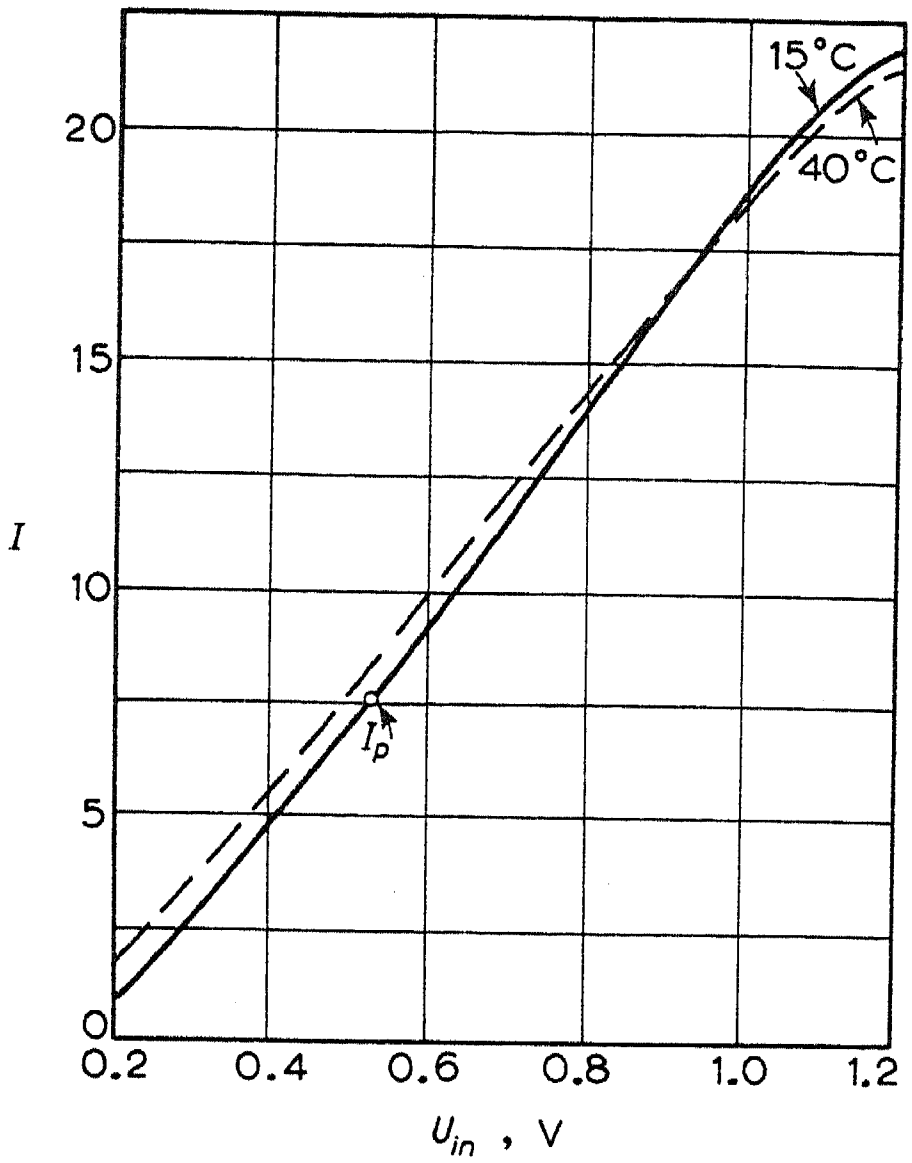

Fig. 5.

The current limitation is not different from that usual in amplidyne circuits of electric drives. The negative voltage feedback in the amplidyne effects braking and demagnetization on switching off and the compensation winding is shunted by a small resistance.

The unit was tested on the test bed and on a vertical lathe over a motor speed range of 1:100 (25 – 2500 rev/min). The set speed was constant within ±10 per cent for load variations from zero to rated load, the exciter voltage variations from 0.85 to 1.1 U_n, ambient temperature change from 10 to 40°C, and amplidyne remanent voltages of –20 to +20 V; temperature rise of the machine during 8 hour continuous operation at rated load, variation of the transistor amplifier supply voltage from 0.85 to 1.1 U_n, of the antihunt circuit leakage resistance by up to 1000 Ω, and successive replacement of both transitors.

Transient tests are equally important in heavy machine tools, especially sudden load change tests. It was stated above that during low-speed saddle feed movements without cutting work being done the load varies periodically. When the load suddenly changes the motor speed varies because of the natural regulation in the drive, recovering after a time dependent on the control system response time.

The initial motor speed change, the tool movement during the transient and the recovery time are all important with machine tools. At present there is no rule covering the permissible values of these quantities. The permissible overshoot under transient conditions should not, however, be more than 0.2 of the minimum feed rate expressed in mm per faceplate revolution.

For heavy horizontal and vertical lathes the minimum feed rate per revolution is supposed to be not less than 0.05 - 0.1 mm/rev and therefore the saddle movement must not be more than 0.01 - 0.02 mm. The reduction ratio from motor to saddle must be taken into account when calculating the permissible armature rotation. In heavy lathes the minimum feed-drive motor speed corresponds to a feed-rate of 0.1 - 10 mm/min depending on the lathe type and size. In the most unfavourable case, viz. 10 mm/min at a minimum motor speed of about 25 rev/min the permissible angular travel is 10 - 20°.

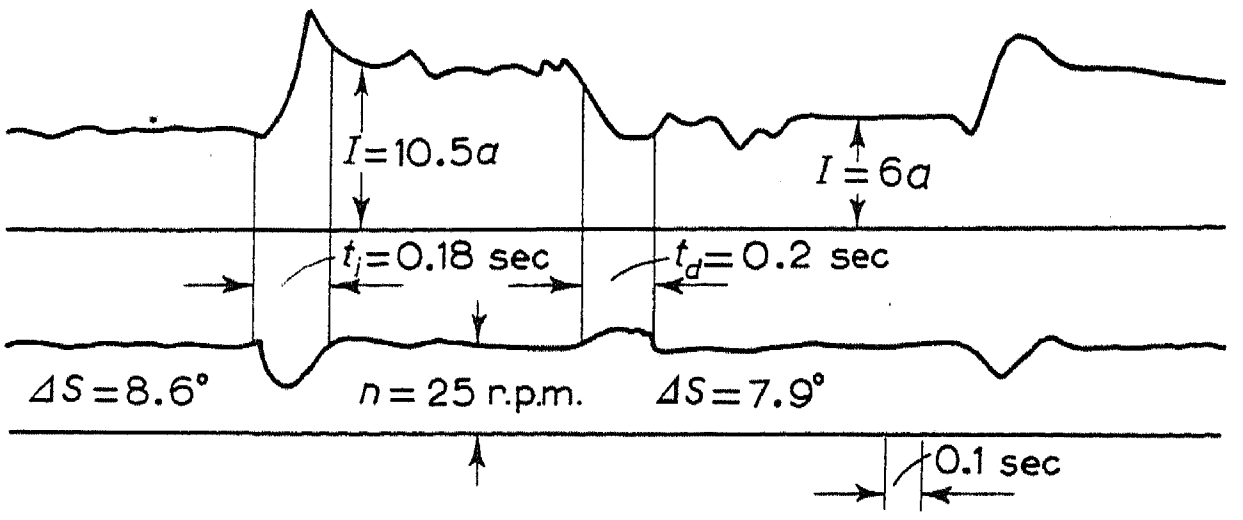

Fig. 6.

Fig. 6 shows an oscillogram for sudden load changes at 25 rev/min (range 1:100). The load change was 75 per cent which is 2 - 3 times more severe than the values usual under actual lathe working conditions. The oscillogram shows that the motor overshoot Δs, did not exceed 10 per cent, i.e. the fundamental requirement was satisfied.

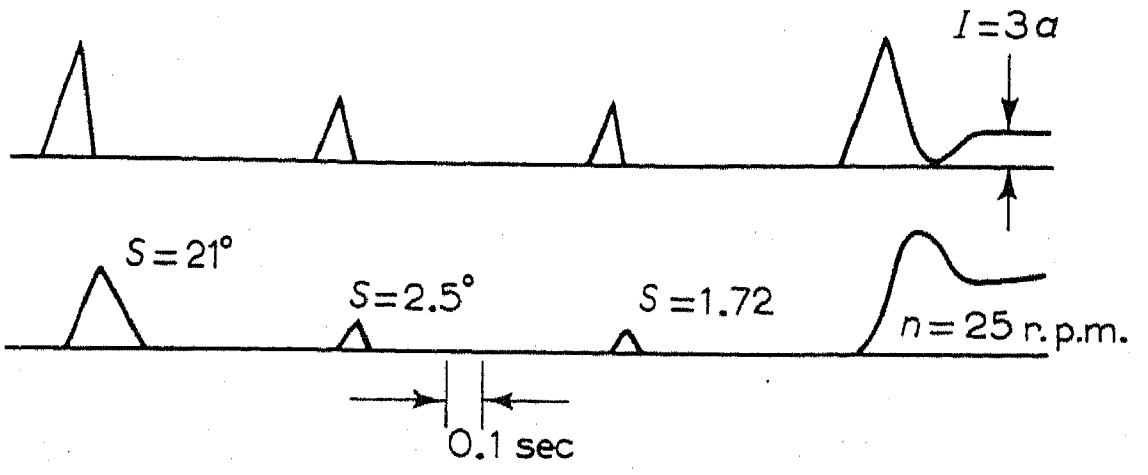

Fig. 7.

When the overshoot as a function of transient time was recorded for a minimum motor speed of 25 rev/min the angular travel (S) was between 2 and 20^{o} which corresponds to saddle movements of not more than 2 – 20 μ (Fig. 7) in heavy horizontal and vertical lathes, even under the most unfavourable conditions.

Starting and braking at maximum motor speed are less important with these machine tools since electromechanical clutches are usually used.

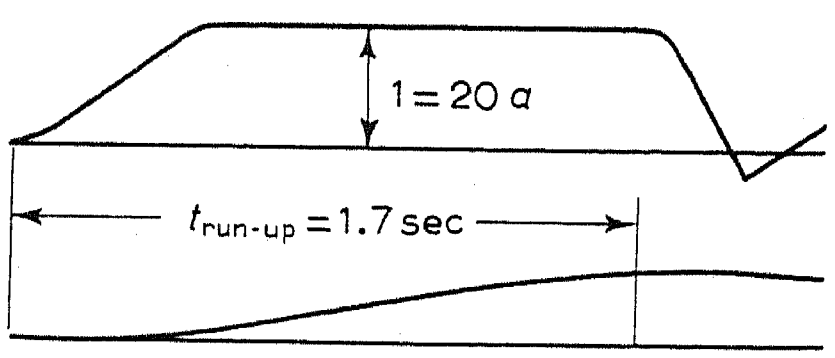

Fig. 8

Fig. 8 shows an oscillogram for a motor starting under load and running up to a 2500 rev/min. The long run-up time is due to the current being limited to the rated amplidyne current. The transient response time could be reduced considerably by increasing the amplidyne rating to 4.5 kW and the maximum current to 40 A.

Electric feed using an a.c. tachometer

The following advantages follow from replacing d.c. tachometers by a.c. ones: Absence of brushes and slot or commutator ripple on the output, and the possibility of using contactless selsyn regulators, the output being compared directly with the tachometer voltage.

Induction type a.c. tachometers with cup type rotors give outputs of constant frequency (50 c/s) this being their main advantage over synchronous a.c. tachometers, but induction-type tachometers with low induced e.m.f.s are very difficult to make.

The first experimental induction-type a.c. cup type rotor TG-56 tachometer has now been produced at The Moscow Electromechanical Engineering works to ESRIMCL specifications. The induced e.m.f. does not exceed 15 mV in these prototype tachometers the alternating component being 2 – 5 mV for a 60 V rating at 4000 rev/min.

ESRIMCL developed an electric feed unit with a.c. tachometer and transistor amplifier in which control of the feed from a number of

separate locations is particularly required with heavy vertical lathes, where the control must be both from a central panel and from the tool-

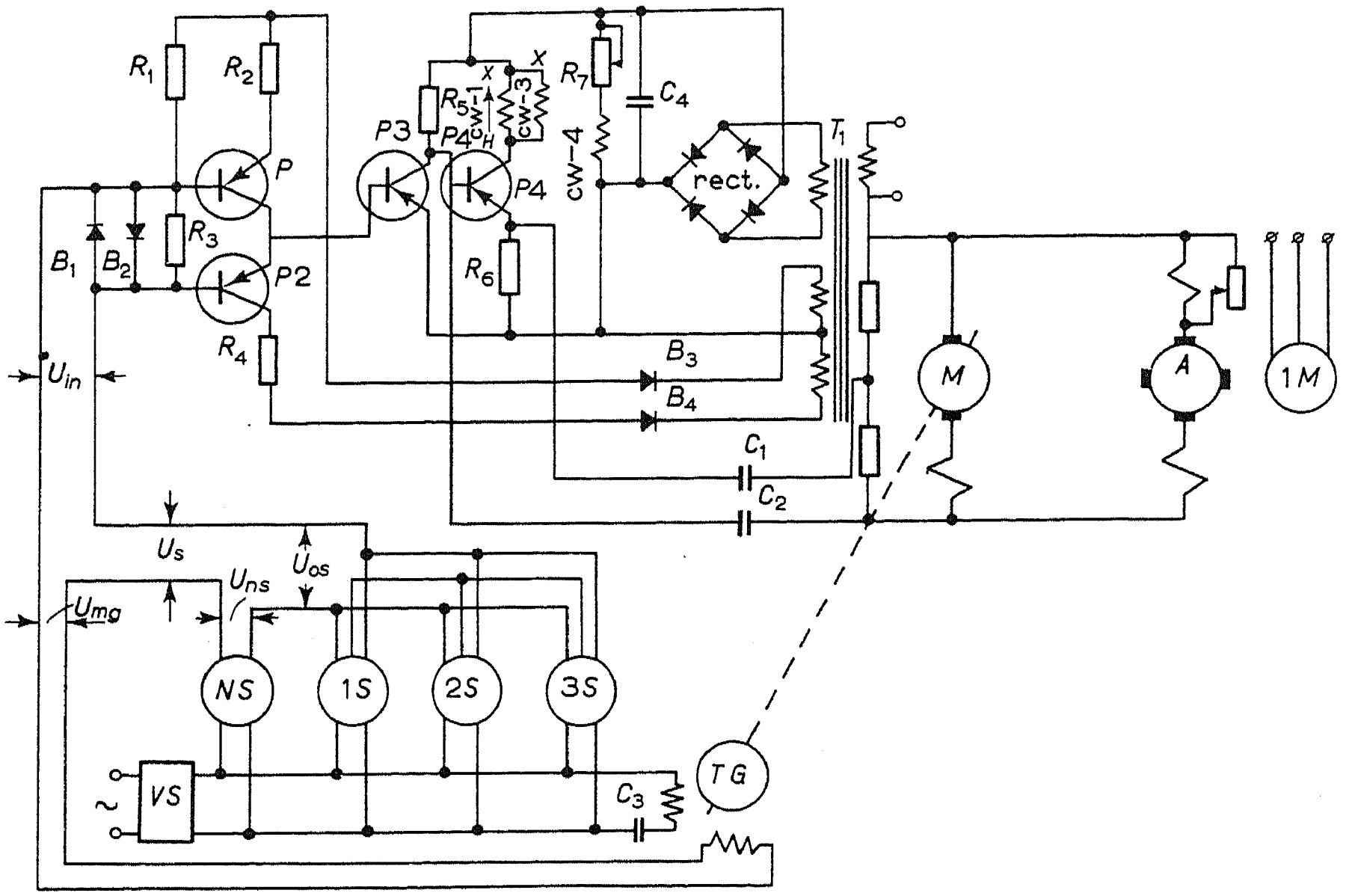

Fig.9 Outline circuit of heavy and turret lathe feed drives using a.c. tachometers.

M d.c. motor, *A* amplidyne, *IM* induction motor, *TG* tachometer, 1*S* – 3*S* selsyns, *NS* non-movable selsyn, *VS* voltage stabilizer, *P*1 – *P*4 transistors, $B_1 - B_4$ semiconductor diodes, *cw* 1 – *cw* 4, amplidyne control windings.

post control panels. Fig.9 shows the basic circuit without the current limitation, demagnetization and braking feedsback.

Selsyn receivers at appropriate check points transmit the required speed variations. 1*S* – 3*S* Selsyns serve as indicators, their secondary windings giving the required reference voltage.

The voltage U_{ns} from the stationary Selsyn NS on the control panel is subtracted from the output voltage U_{os} from the 1*S* – 3*S* Selsyns (Fig.10a).

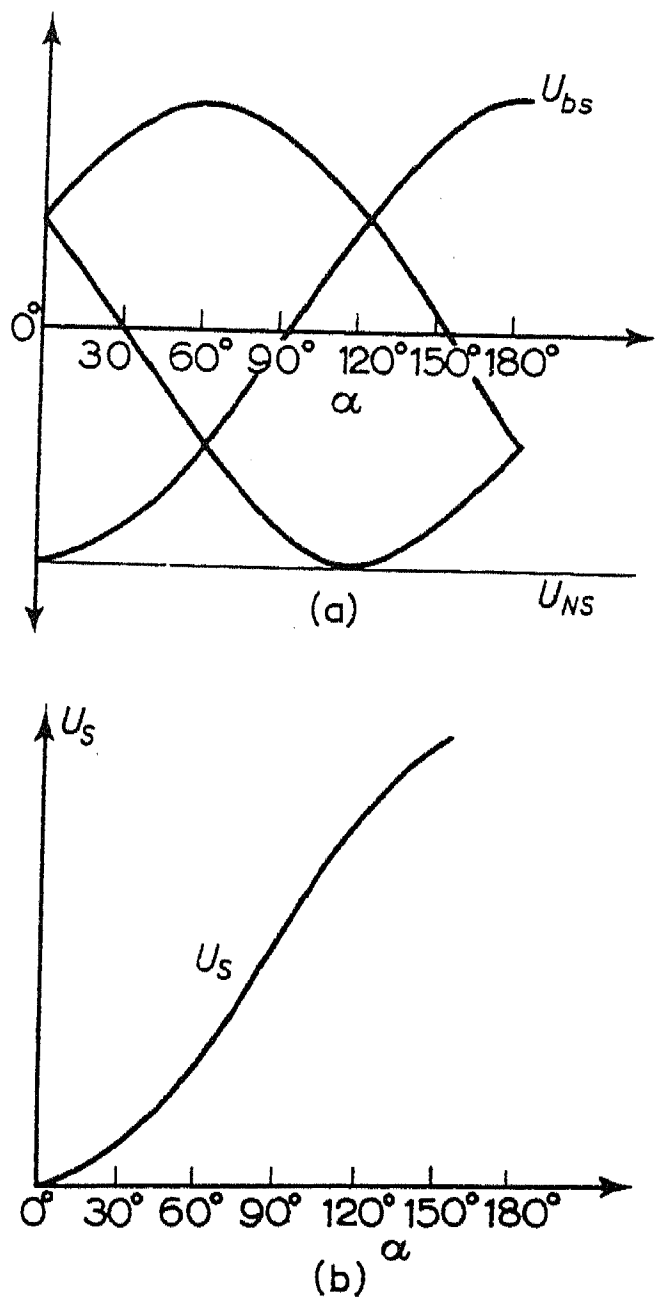

Fig. 10.

The $U_s = U_{os} - U_{ns}$ curve (Fig.10b) gives a convenient scale for the speed recording selsyns (these scales cover unequal ranges). The capacitor C_3 connected to the tachometer primary causes a phase difference of 180° between the speed voltage feedback U_{tg} and U_s. $U_i = U_s - U_{tg}$ is fed to the transistor amplifier input. This differs from the amplifier shown in Fig.3 only in having a preliminary phase-sensitive stage with P1A transistors (P1 and P2). The diodes B_3 and B_4 prevent reverse currents through the transistors.

The a.c. tachometer drives were tested over a speed range of 1:100 the test programme being the same as with the d.c. tachometers. The results were very similar.

Conclusions

Intermediate amplifiers should be used even in automatic speed control systems for heavy machine tool feed drives using small speed ranges (1:100 and less) which could be controlled without them. The intermediate amplifier reduces the sizes, weights and prices of the regulators, tachos and damping circuits required and improves the drive characteristics.

SHORT-CIRCUIT TRANSIENTS ON LONG LINES

R. I. KARAEV*

Molotov Power Engineering Institute, Moscow

When long lines are affected by short-circuits, wave phenomena occur which cannot be obtained in circuits with lumped parameters. Although several papers on this problem have appeared [1,2] only the methods of solution have been described. The solutions are obtained by numerical methods which sometimes lead to tedious calculations involving complex numbers. The classical orthogonal function method (Sturm-Liouville's problem) which is comprehensively treated in works on mathematical physics [3] has not yet been applied to this problem. Sturm-Liouville's treatment assumes self-adjoint boundary conditions at the ends of a system with distributed parameters (open-circuit or short-circuit conditions, or time-independent ones). This condition is not fulfilled in transmission line circuits, especially compensated ones, in which the functions are not orthogonal in the narrow sense as formulated in Sturm-Liouville's problem. But when the system is considered as a whole, the functions will, nevertheless, be orthogonal in loss-free systems. The method described here is based on the orthogonality condition and yields a general solution for every concrete case. Such a solution facilitates analysis of the way individual parameters affect the phenomena without involving laborious calculations. The structure of the solution obtained is connected with the normal co-ordinates (natural oscillations) of the system which is advantageous when protective relay operating conditions are to be predicted.

Only the fault component of the short-circuit current is computed in this method since the normal load conditions can easily be determined. Transient phenomena in a three-phase circuit are considered using $\alpha\beta 0$ components. This is superior to the symmetrical component method under these conditions [2,5]. Thus the problem is reduced to the formulation of the additional sinusoidal e.m.f. in the individual single-phase

* Candidate in Technical Sciences, Molotov Power Engineering Institute, Moscow

component circuits when the initial condition is zero, the circuits being connected in accordance with the varying fault symmetry or asymmetry.

The circuit then has linear parameters, since the voltages in the various parts of the circuit do not increase during the short-circuit, even when the neutral is not effectively earthed. Iron-cored transformers and reactors also continue to operate on the linear parts of their characteristics. This simplifies the problem considerably.

Only the currents and voltages during the first 3 – 5 cycles are of interest at 50 c/s, since after that time the transients on the line have practically decayed. The operating time of the main protective equipment of a long line usually falls within this interval, and during these first 3 – 5 cycles the negative-sequence impedances in turbo-generators and in machines with damping cages, which are usually large hydro electric generators, differ from the positive-sequence values by not more than 20–25 per cent [4]. Moreover, with long transmission lines the generator reactances are of secondary importance, and in practice it is therefore possible to ignore this difference since it would not reduce the accuracy appreciably.

The method may be demonstrated by computing for a single-phase short-circuit at the end of an uncompensated long line supplied at both ends (Fig. 1).

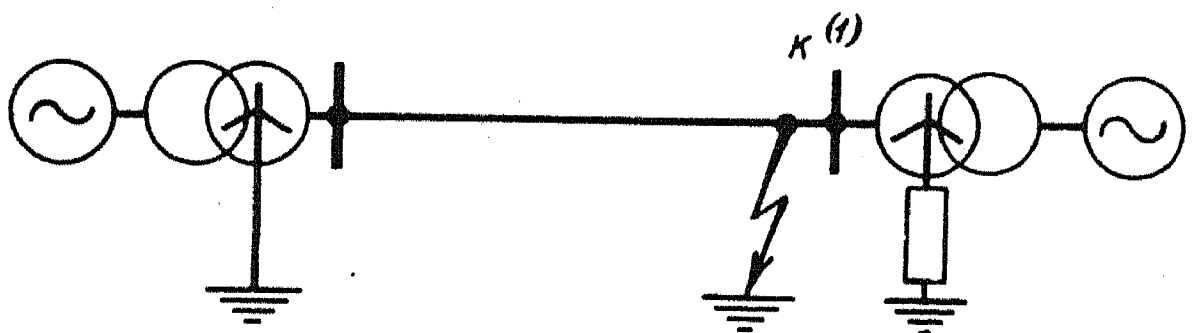

Fig. 1

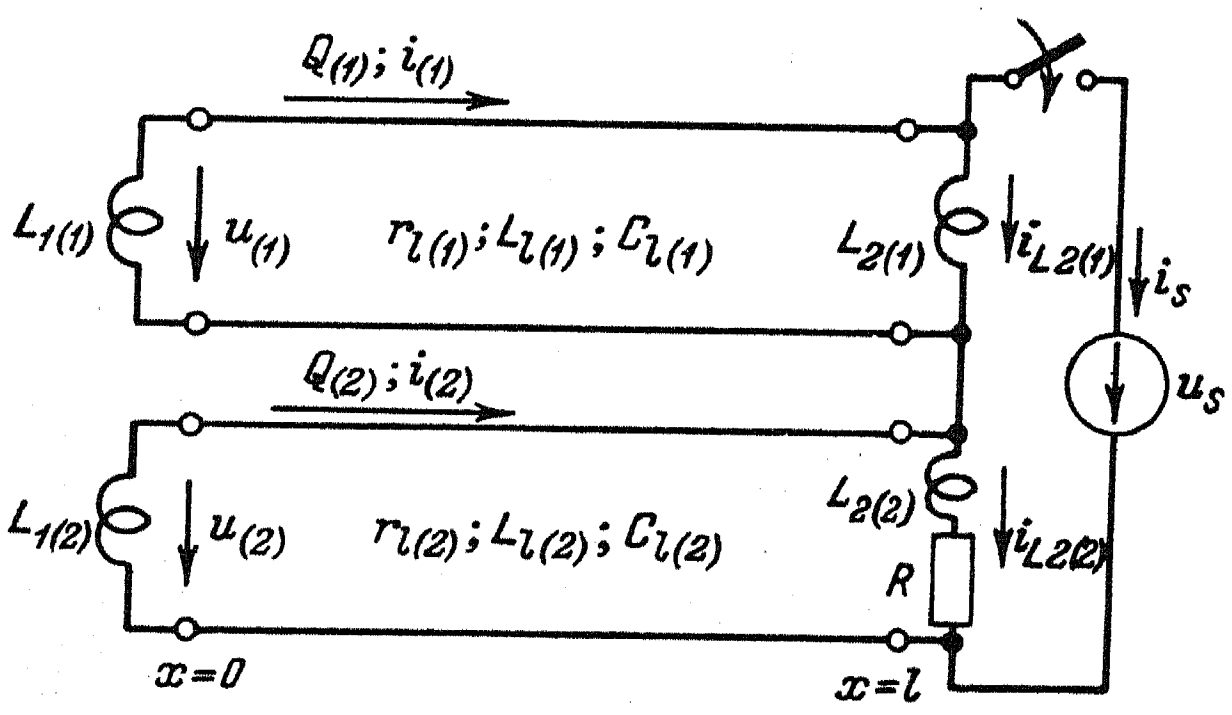

Fig. 2

The equivalent circuits used are shown in Fig.2 the upper representin the α-component, the bottom one the zero-component, the impedances being halved [2]. At first we consider circuits consisting of reactive elements only, but the method will subsequently be extended to include active resistances.

From electromechanical analogies [6] we take the unknown to be the charge $Q(x,t)$, which has passed through a point x on the line at a time t.

Q must satisfy

$$\frac{\partial^2 Q(x,t)}{\partial t^2} = \frac{1}{L_l C_l} \frac{\partial^2 Q(x,t)}{\partial x^2}$$

and is related to the voltages and currents at the point by:

$$u(x,t) = -\frac{1}{C_l} \frac{\partial Q(x,t)}{\partial x} \tag{1}$$

$$i(x,t) = \frac{\partial Q(x,t)}{\partial t} . \tag{2}$$

Separating the variables, we obtain the solution in the form:*

$$Q_{f(m)} = \sum_{k=1}^{\infty} p_{kf} \left[A_{k(m)} \sin \frac{\omega_k}{v_{(m)}} x + B_{k(m)} \cos \frac{\omega_k}{v_{(m)}} x \right] + p_{0f} X_{0(m)} \tag{3}$$

where

$$p_{kf} = n_k \sin \omega_k t + m_k \cos \omega_k t ;$$

$$p_{0f} = n_{0t} + m_0$$

---

* In what follows the subscript (1) indicates quantities relating to the α-component, (2) those relating to the zero-component, and (m) quantities relating to both components; (k) denotes quantities relating to the k-th root of the characteristic equation

the ω_k are the angular frequencies of the natural oscillations;

the $v(m)$ are the electromagnetic wave propagation velocities.

The boundary conditions for the circuit shown in Fig.2 are as follows (quantities corresponding to the root $k = 0$ will be considered later):

$$\left| \frac{1}{C_{l(m)}} \frac{\partial Q_{f(m)}}{\partial x} = L_{1(m)} \frac{\partial^2 Q_{f(m)}}{\partial t^2} \right|_{x=0} \tag{4}$$

$$\left| \frac{1}{C_{l(1)}} \frac{\partial Q_{f(1)}}{\partial x} = -\frac{1}{C_{l(2)}} \frac{\partial Q_{f(2)}}{\partial x} \right|_{x=l} \tag{5}$$

$$\left| \frac{1}{C_{l(1)} L_{2(1)}} \frac{\partial Q_{f(1)}}{\partial x} + \frac{\partial^2 Q_{f(1)}}{\partial t^2} = \frac{1}{C_{l(2)} L_{2(2)}} \frac{\partial Q_{f(2)}}{\partial x} + \right.$$

$$\left. + \frac{\partial^2 Q_{f(2)}}{\partial t^2} \right|_{x=l} \tag{6}$$

Using equation (4) and assuming that

$$p''_{kf} = -\omega_k^2 p_{kf}$$

we get

$$B_{k(m)} = -A_{k(m)} \frac{Z_{s(m)}}{\omega_k L_{1(m)}} = A_{k(m)} \cot \theta_{1k(m)} \tag{7}$$

where

$$\theta_{1k(m)} = \tan^{-1} \frac{\omega_k L_{1(m)}}{Z_{s(m)}} \quad ;$$

$Z_{s(m)}$ is the surge impedance of the line.

Substituting the $B_{k(m)}$ in equation (3), we find that

$$Q_{f(m)} = -\sum_{k=1}^{\infty} p_{kf} \frac{A_{k(m)} \cos\left((\omega_k / v_{(m)})\, x + \theta_{1k(m)}\right)}{\sin \theta_{1k(m)}} + p_{0f} X_{0(m)} \,.$$

The boundary condition (5) leads to the relation

$$A_{k(2)}Z_{s(2)}\frac{\sin\ (\omega_k\tau_{(2)}+\theta_{1k(2)})}{\sin\ \theta_{1k(2)}}\ =$$

$$=\ -A_{k(1)}Z_{s(1)}\frac{\sin\ (\omega_k\tau_{(1)}+\theta_{1k(1)})}{\sin\ \theta_{1k(1)}}$$

and (6) gives the characteristic equation as:

$$\frac{\omega_k}{Z_{s(1)}}\left[\cot\ (\omega_k\tau_{(1)}+\theta_{1k(1)})+\frac{Z_{s(1)}}{\omega_k L_{2(1)}}\right]+$$

$$+\frac{\omega_k}{Z_{s(2)}}\left[\cot\ (\omega_k\tau_{(2)}+\theta_{1k(2)})+\frac{Z_{s(2)}}{\omega_k L_{2(2)}}\right]\ =\ 0\ , \qquad (8)$$

the roots of which are the natural frequencies of the system. Equation (8) is solved by iteration; the solution is not given here.

Passing from the free components to the actual values of the quantities, we write them in the following way:

$$Q_{(1)}\ =\ \sum_{k=1}^{\infty} q_k\frac{\cos\ (\omega_k/v_{(1)}\ x+\theta_{1k(1)})}{Z_{s(1)}\ \sin\ (\omega_k\tau_{(1)}+\theta_{1k(1)})}+p_0X_{0(1)} \qquad (9)$$

$$Q_{(2)}\ =\ -\sum_{k=1}^{\infty} q_k\frac{\cos(\omega_k/v_{(2)}\ x+\theta_{1k(2)})}{Z_{s(2)}\ \sin\ (\omega_k\tau_{(2)}+\theta_{1k(2)})}+p_0X_{0(2)} \qquad (10)$$

where

$$q_k\ =\ -p_kA_{k(1)}Z_{s(1)}\frac{\sin\ (\omega_k\tau_{(1)}+\theta_{1k(1)})}{\sin\ \theta_{1k(1)}}\ .$$

Lagrange's equation is used to determine the generalized co-ordinate $q_k(k \geqslant 1)$ (7)

$$\frac{d}{dt}\left(\frac{\partial T}{\partial q_k'}\right)+\frac{\partial V}{\partial q_k}+\frac{\partial F}{\partial q_k'}\ =\ f_k \qquad (11)$$

where T is the magnetic field (kinetic) energy of the system as a whole, (Fig.2);

V is the electric field (potential) energy,

F is the electromagnetic energy loss function (in a lossless system $F = 0$)

f_k is a generalized force.

The well-known theorem in algebra, that two homogeneous quadratic functions can be reduced by linear transformations to a sum of squares, can be used to give V and T for a lossless system in a form having no cross-products of co-ordinates (or velocities) but squares only [8, p.201].

With lossless long distance lines the above transformation of V and T is not required if these are considered for the system as a whole, i.e. they will not involve cross-products (of q_k and q_k'). This is also a property of orthogonal functions in general with consideration of the loads which also extends to the direct current component (corresponding to $k = 0$).

It is not necessary to calculate both T and V when considering harmonics since in a lossless system V is obtained by multiplying the corresponding terms in T by ω^2 [8, p.205].

It is simpler to calculate V for Fig.2, this being:-

$$V_{l(m)} = \int_0^l \frac{C_{l(m)} u^2_{(m)}}{2}\, dx = \frac{1}{2C_{l(m)}} \int_0^l \left(\frac{\partial Q_{(m)}}{\partial x}\right)^2 dx =$$

$$= \frac{1}{2} \sum_{k=1}^{\infty} q_k^2\, \omega_k^2\, a_{k(m)}$$

where

$$a_{k(m)} = \frac{\partial V_{l(m)}}{\partial q_k} \frac{1}{\omega_k^2\, q_k} =$$

$$= \frac{2\omega_k \tau_{(m)} - \sin 2(\omega_k \tau_{(m)} + \theta_{1k(m)}) + \sin 2\theta_{1k(m)}}{4\omega_k Z_{s(m)} \sin^2(\omega_k \tau_{(m)} + \theta_{1k(m)})}\,.$$

Adding the energies for both components, we find that V for the system as a whole is

$$V = V_{l(1)} + V_{l(2)} = \frac{1}{2}\sum_{k=1}^{\infty} q_k^2 \omega_k^2 a_k$$

where

$$a_k = a_{k(1)} + a_{k(2)}.$$

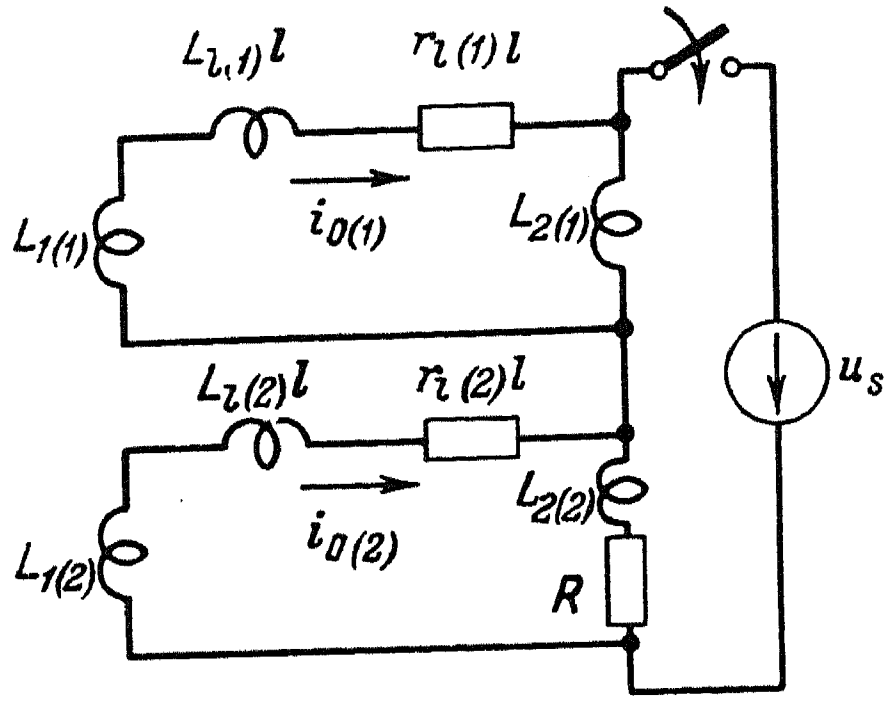

Fig. 3

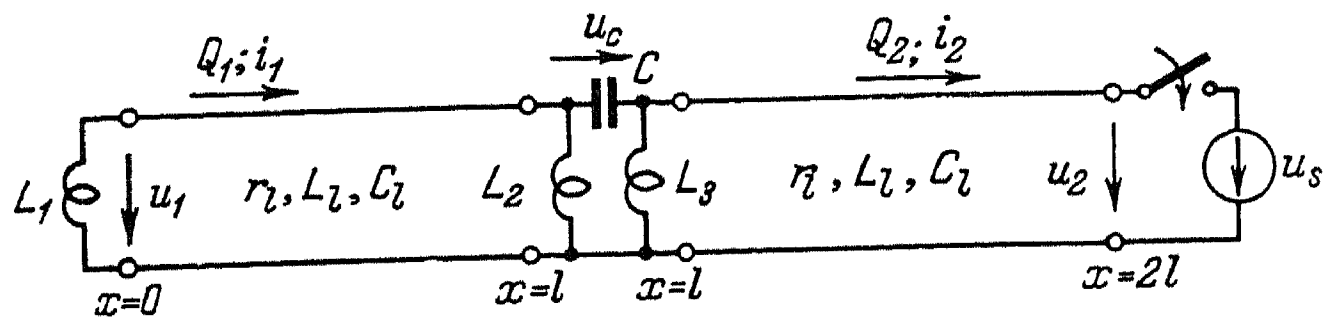

Fig. 4

If the line is capacity-compensated (Fig. 4) the energy stored in the capacitances would have to be added.

Substituting V and T in equation (11) we get

$$a_k(q_k'' + \omega_k'' q_k) = f_k \qquad (12)$$

To find f_k we must determine the energy the generator supplies when q_k changes by Δq_k:

$$f_k = \frac{u_s \Delta Q_{ks}}{\Delta q_k}.$$

where

$$u_s = U_{max} \sin(\omega t + \psi) = \text{the switched e.m.f.}$$

Since

$$\int q_k dt = -\frac{q_k'}{\omega_k^2}$$

we obtain

$$i_{L2k(1)} = \frac{1}{L_{2(1)}} \int u_{k(1)} dt \Big|_{x=l} =$$

$$= -\frac{1}{C_{l(1)} L_{2(1)}} \int \frac{\partial Q_{k(1)}}{\partial x} dt \Big|_{x=l} = -\frac{q_k'}{\omega_k L_{2(1)}} . \quad (13)$$

From equations (9) and (13), the charge passing through the source is

$$\Delta Q_{ks} = \frac{\Delta q_k}{Z_{s(1)}} \left[\cot(\omega_k \tau_{(1)} + \theta_{1k(1)}) + \frac{Z_{s(1)}}{\omega_k L_{2(1)}} \right] .$$

And finally the expression for the generalized force is:

$$f_k = \left[\cot(\omega_k \tau_{(1)} + \theta_{1k(1)}) + \frac{Z_{s(1)}}{\omega_k L_{2(1)}} \right] \frac{U_{max}}{Z_{s(1)}} \sin(\omega t + \psi).$$

The integral of (12)[9, equations 5-96] is:

$$q_k = \frac{U_{max} \left[\cot(\omega_k \tau_{(1)} + \theta_{1k(1)}) + (Z_{s(1)}/\omega_k L_{2(1)}) \right]_x}{Z_{s(1)} (\omega_k^2 - \omega^2) a_k}$$

$$\left[\sin(\omega t + \psi) - \sin\psi \cos\omega_k t - \frac{\omega}{\omega_k} \cos\psi \sin\omega_k t \right] . \quad (14)$$

Substituting this in equations (9) and (10) and further in (1) and (2) the formulae are obtained for currents and voltages corresponding to the characteristic equations in (8) for $k \geqslant 1$.

In a lossless system the d.c. components of the free current and potential energy correspond to the root $k = 0$, and are zero. Fig.3, with open-circuited capacitances, also gives this result.

The Lagrange equation (in a lossy circuit) is then written as

$$\frac{d}{dt}\left(\frac{\partial T}{\partial q_0'}\right) + \frac{\partial F}{\partial q_0'} = f_0 \,. \tag{15}$$

From the line current components corresponding to $k = 0$,

$$i_{0(m)} = p_0' X_{0(m)} \,,$$

the current component in the supply is

$$i_{s0} = p_0' X_{0(m)} \frac{L_{1(m)} + L_{l(m)} l + L_{2(m)}}{L_{2(m)}} \,.$$

Assuming that this affects the α- and zero-components in the same way, the generalized co-ordinate is

$$q_0 = p_0 X_0 \frac{L_{1(m)} L_{l(m)} l + L_{2(m)}}{L_{2(m)}} \,.$$

So the generalized force is

$$f_0 = u_s = U_{\max} \sin(\omega t + \psi) \,.$$

The magnetic energy component corresponding to $k = 0$ is

$$T_0 = \frac{a_0}{2} (q_0')^2$$

where

$$a_0 = L_{0(1)} + L_{0(2)}$$

and

$$L_{(m)} = \frac{(L_{1(m)} + L_{l(m)} l)\, L_{2(m)}}{L_{1(m)} + L_{l(m)} l + L_{2(m)}} \,.$$

The solution to (15) for a lossless circuit ($F = 0$) is

$$q_0' = \frac{U_{max}[\cos \psi - \cos (\omega t + \psi)]}{\omega a_0} \tag{16}$$

Circuits with losses will now be considered.

The resistances in the equivalent circuits for single-phase and two-phase earth faults are

$$r_{lk} = (r_{ek} + r_c)/2$$

where $r_{ek} = 1.5\pi \cdot 10^{-4} w_k$ ohms/km [10], is the earth impedance per unit length (depending on frequency)

r_c = the conductor impedance per unit length

The line zero sequence inductance is only slightly frequency-dependent, and this effect will not be considered in what follows.

Unlike T and V, cross-products are retained in F and these influence the results somewhat. Assuming that the current distribution depends basically on the reactive elements, the dissipation function $F_{l(m)}$ for the line is:

$$F_{l(m)} = \int_0^l \frac{r_{l(m)}}{2} \left(\frac{\partial Q_{(m)}}{\partial t} \right)^2 dx =$$

$$= \int_0^l \frac{r_{l(m)}}{2} \left[\sum_{k=1}^{\infty} (\pm q_k') \frac{\cos [(\omega_k / v_{(m)})x + \theta_{1k(m)}]}{Z_{s(m)} \sin(\omega_k \tau_{(m)} + \theta_{1k(m)})} + \right.$$

$$\left. + q_0' \frac{L_{2(m)}}{L_{1(m)} + L_{l(m)} l + L_{2(m)}} \right]^2 dx =$$

$$= \sum_{k=1}^{\infty} \left[\frac{b_{k(m)}}{2} (q_k')^2 + \sum_{\substack{n=0 \\ n \neq k}}^{\infty} b_{kn(m)} q_k' q_n' \right]^*$$

---

* In this formula the positive sign corresponds to $m = 1$ and the negative sign to $-m = 2$.

where

$$b_{k(m)} = \frac{r_{lk(m)}}{L_{l(m)}} \times$$

$$\frac{2\omega_k\tau_{(m)} + \sin 2(\omega_k\tau_{(m)} + \theta_{1k(m)}) - \sin 2\theta_{1k(m)}}{4\omega_k Z_{s(m)} \sin^2(\omega_k\tau_{(m)} + \theta_{1k(m)})} \quad (k \geqslant 1);$$

$$b_{kn(m)} = \frac{r_{lkn(m)}}{L_{l(m)}} \times$$

$$\times \frac{[1/(\omega_k + \omega_n)]\{\sin[(\omega_k + \omega_n)\tau_{(m)} + \theta_{1k(m)} + \theta_{1n(m)}] - \sin(\theta_{1k(m)} + \theta_{1n(m)})\}}{4 Z_{s(m)} \sin(\omega_k\tau_{(m)} + \theta_{1k(m)}) \sin(\omega_n\tau_{(m)} + \theta_{1n(m)})} +$$

$$+ \frac{[1/(\omega_k - \omega_n)]\{\sin[(\omega_k - \omega_n)\tau_{(m)} + \theta_{1k(m)} - \theta_{1n(m)}] - \sin(\theta_{1k(m)} - \theta_{1n(m)})\}}{4 Z_{s(m)} \sin(\omega_k\tau_{(m)} + \theta_{1k(m)}) \sin(\omega_n\tau_{(m)} + \theta_{1n(m)})} \quad (k \geqslant 1);$$

$$b_{0(m)} = \frac{r_{l0(m)} l L_{2(m)}^2}{(L_{1(m)} + L_{l(m)} l + L_{2(m)})^2} \quad (k = 0)$$

$$b_{0n(m)} = \pm \frac{r_{ln(m)}}{L_{l(m)}} \times$$

$$\times \frac{[\sin(\omega_n\tau_{(m)} + \theta_{1n(m)}) - \sin\theta_{1n(m)}]\, L_{2(m)}}{2\omega_n \sin(\omega_n\tau_{(m)} + \theta_{1n(m)})(L_{1(m)} + L_{l(m)} l + L_{2(m)})}^{*} \quad (k = 0).$$

The quantity $r_{lkn(m)}$ appearing in the dissipation coefficient is given by

$$r_{lkn(m)} = \frac{r_{lk(m)} + r_{ln(m)}}{2}.$$

The current through R (Fig.2) is

$$i_{(R)} = \frac{1}{C_{l(2)} L_{2(2)}} \int \frac{\partial Q_{(2)}}{\partial x}\, dt \Bigg|_{x=l} = \sum_{k=1}^{\infty} \frac{q'_k}{\omega_k L_{2(2)}} - \frac{q'_0 L_{0(2)}}{L_{2(2)}}$$

---

* In this formula the positive sign corresponds to $m = 1$ and the negative sign to $-m = 2$.

The dissipation function for R is:

$$F_{(R)} = \frac{Ri^2_{(R)}}{2} = \sum_{k=0}^{\infty}\left[\frac{b_{k(R)}}{2}(q'_k)^2 + \sum_{\substack{n=0\\ n\neq k}}^{\infty} b_{kn(R)}\, q'_k\, q'_n\right]$$

where

$$b_{k(R)} = \frac{R}{\omega_k^2 L^2_{2(2)}}; \qquad b_{kn(R)} = \frac{R}{2\omega_k \omega_n L^2_{2(2)}};$$

$$b_{0(R)} = \frac{RL^2_{0(2)}}{L^2_{2(2)}}; \qquad b_{0n(R)} = \frac{-RL_{0(2)}}{2\omega_n L^2_{2(2)}}$$

The dissipation coefficient for the circuit as a whole becomes

$$b_k = b_{k(1)} + b_{k(2)} + b_{k(R)}$$

b_{kn} b_0 and b_{0n} are calculated similarly by summing the individual components. For the generalized co-ordinates we substitute V, T and F in equation (11) and obtain a system of $(k + 1)$ differential equations:

$$a_k q''_k + \omega_k^2 a_k q_k + b_k q'_k + \sum_{\substack{n=0\\ n\neq k}}^{\infty} b_{kn} q'_n = f_k \quad (k \geqslant 0)\,. \tag{17}$$

By successive approximation [11] we first eliminate the term $\Sigma b_{kn} q'_n$ (which is small compared with the others) from the left hand side. Then equation (17) separates into independent equations:

$$a_k q''_{kI} + \omega_k^2 a_k q_{kI} + b_k q'_{kI} = f_k \tag{18}$$

the solutions being (9, 5–94):

$$q_{kI} = q_{k\max}\left\{-\cos(\omega t + \psi - \phi_k) + \right.$$

$$+ e^{-\delta'_k t}\left[\frac{\delta_k}{\omega_{kr}}\cos(\psi - \phi_k)\,\sin\omega_{kr}t - \right.$$

$$\left.\left. - \frac{\omega}{\omega_{kr}}\sin(\psi - \phi_k)\,\sin\omega_{kr}t + \cos\,(\psi - \phi_k)\,\cos\omega_{kr}t\right]\right\}, \tag{19}$$

where

$$q_{k\max} = \frac{U_{\max} \sin \phi_k \left[\cot(\omega_k \tau_{(1)} + \theta_{1k(1)}) + (Z_{s(1)}/\omega_k L_{2(1)})\right]}{Z_{s(1)}(\omega^2 - \omega_k^2) a_k} \qquad (k \geqslant 1);$$

$$\tan \phi_k = \frac{\omega_2 - \omega_k^2}{2\delta_k \omega}; \qquad \delta_k = \frac{b_k}{2a_k}; \qquad \omega_{kr} = \sqrt{\omega_k^2 - \delta_k^2}.$$

Further, q'_{kI} is

$$q'_{kI} = q_{k\max}\,\omega \left\{ \sin(\omega t + \psi - \phi_k) - e^{-\delta_k t} \left[\sin(\psi - \phi_k) \cos \omega_{kr} t + \right.\right.$$

$$\left.\left. + \frac{\omega_{kr}}{\omega} \cos(\psi - \phi_k) \sin \omega_{kr} t - \frac{\delta_k}{\omega_{kr}} \sin(\psi - \phi_k) \sin \omega_{kr} t \right] \right\} \quad (k \geqslant 1). \qquad (20)$$

When $k = 0$ we have

$$q'_{0I} = q_{0\max}\,\omega \left[\sin(\omega t + \psi - \phi_0) - e^{-\delta_0 t} \sin(\psi - \phi_0) \right] \qquad (21)$$

where

$$q_{0\max} = \frac{U_{\max} \sin \phi_0}{a_0 \omega^2};$$

$$\delta_0 = \frac{b_0}{a_0}; \qquad \tan \phi_0 = \frac{\omega}{\delta_0}.$$

To find the second approximation, q_{kII}, it is necessary to substitute $q_k = q_{kI} + q_{kII}$ in the main terms and only the first approximation $q_n = q_{nI}$ is necessary in the summation $\Sigma b_{kn} q'_n$. Substituting these values and solving (18) we obtain

$$a_k(q''_{kII} + \omega_k^2 q_{kII}) + b_k q'_{kII} = -\sum_{n=0}^{\infty} b_{kn} q'_{nI} \quad (k \geqslant 0).$$

Applying Duhamel's formula [9, equations 5–116]

$$q_{kII} = \int_0^t \frac{e^{-\delta_k(t-\lambda)} \sin \omega_{kr}(t-\lambda)}{a_k \omega_{kr}} \left[-\sum_{\substack{n=0 \\ n \neq k}}^{\infty} b_{kn} q'_{nI}(\lambda) \right] d\lambda.$$

q'_{nI} can be obtained from [20,21] by substituting subscript-n for subscript k.

Since q_{kII} is only a correction to q_{kI}, we assume in the following calculations that $\delta_k \ll \omega_k$.

Then:

$$q_{kII} = \sum_{\substack{n=0 \\ n\neq k}}^{\infty} \frac{b_{kn} q_{n\max} \omega}{a_k \omega_{kr}}$$

$$\left[\frac{-\omega_{kr} \sin(\omega t + \psi - \phi_n) + \omega e^{-\delta_k t} \sin(\omega_{kr} t + \psi - \phi_n)}{\omega_{kr}^2 - \omega^2} + \right.$$

$$+ \frac{\omega_{kr} \sin(\psi - \phi_n)(e^{-\delta_n t} \cos \omega_{nr} t - e^{-\delta_k t} \cos \omega_{kr} t)}{\omega_{kr}^2 - \omega_{nr}^2} +$$

$$\left. + \frac{(\omega_n/\omega) \cos(\psi - \phi_n)(\omega_{kr} e^{-\delta_n t} \sin \omega_{nr} t - \omega_{nr} e^{-\delta_k t} \sin \omega_{kr} t)}{\omega_{kr}^2 - \omega_{nr}^2} \right] (k \geqslant 0) \quad (22)$$

$$q'_{kII} = \sum_{\substack{n=0 \\ n\neq k}}^{\infty} \frac{b_{kn} q_{n\max}}{a_k} \left\{ \frac{\omega^2}{\omega_{kr}^2 - \omega^2} \left[- \cos(\omega t + \psi - \phi_n) + \right. \right.$$

$$\left. + e^{-\delta_n t} \cos(\omega_{kr} t + \psi - \phi_n) \right] -$$

$$- \frac{\omega \sin(\psi - \phi_n)(\omega_{nr} e^{-\delta_n t} \sin \omega_{nr} t - \omega_{kr} e^{-\delta_k t} \sin \omega_{kr} t) -}{\omega_{kr}^2 - \omega_{nr}^2}$$

$$\left. \frac{- \omega_{nr}^2 \cos(\psi - \phi_n)(e^{-\delta_n t} \cos \omega_{nr} t - e^{-\delta_k t} \cos \omega_{kr} t)}{\omega_{kr}^2 - \omega_{nr}^2} \right\} (k \geqslant 0) . \quad (23)$$

q_{kI} (first approximation) gives the reactive current components with adequate accuracy. q_{kII} (second approximation) differs in phase from the first by $\pi/2$ and gives the ohmic current components satisfactorily. These approximations always suffice since in the majority of practical calculations the first approximation is sufficiently accurate, and (22) and (23) need only be used to check the error involved.

The active resistances affect the current distribution mainly via the component corresponding to $k = 0$. Therefore the zero-components of the currents and voltages should be calculated direct from the circuits in very complicated systems with open-circuit capacitances and high active resistances, without applying Lagrange's equation, (15), in order to avoid errors.

Using the generalized co-ordinates and their derivatives, together with equations (9) and (10), the required currents and voltages are found to be:

$$i_{(1)} = \sum_{k=1}^{\infty} q'_k \frac{\cos\left((\omega_k / v_{(1)})x + \theta_{1k(1)}\right)}{Z_{s(1)} \sin(\omega_k \tau_{(1)} + \theta_{1k(1)})} + \\ + \frac{q'_0 L_{2(1)}}{L_{1(1)} + L_{l(1)} l + L_{2(1)}}; \quad (24)$$

$$u_{(1)} = \sum_{k=1}^{\infty} q_k \frac{\omega_k \sin\left((\omega_k / v_{(1)})x + \theta_{1k(1)}\right)}{\sin(\omega_k \tau_{(1)} + \theta_{1k(1)})} - \\ - \frac{q''_0 L_{2(1)}(L_{1(1)} + L_{l(1)} x) + q'_0 L_{2(1)} r_{l(1)} x}{L_{1(1)} + L_{l(1)} l + L_{2(1)}}. \quad (25)$$

$i_{(2)}$ and $u_{(2)}$ are written by analogy by interchanging subscripts (1) and (2) and reversing the sign. The components corresponding to $k = 0$ do not alter in sign.

The known relationships in the $\alpha\beta 0$ system [2] can be used to calculate the phase currents and voltages in the three-phase system. The forced and free components were calculated simultaneously above. Obviously, they can also be found individually by the symbolic method [9].

---

* See (9) and (10).

The formulae for a three-phase fault on a compensated line are given in the Appendix by way of an example. More complicated systems can also be treated by this method.

Appendix

Formulae for use with three-phase faults at the ends of compensated lines (Fig. 4)

Characteristic equation:

$$\frac{1}{\cot(\omega_k \tau + \theta_{1k}) + Z_s/\omega_k L_2} + \frac{1}{\cot \omega_k \tau + Z_s/\omega_k L_3} = \frac{1}{\omega_k C Z_s}$$

Currents and voltages

$$i_1 = \sum_{k=1}^{\infty} q_k' N_k \cos(\omega_k x/v + \theta_{1k}) ;$$

$$i_2 = \sum_{k=1}^{\infty} q_k' \cos(2\omega_k \tau - \omega_k x/v) + i_0 ;$$

$$u_1 = \sum_{k=1}^{\infty} q_k N_k \omega_k Z_s \sin(\omega_k x/v + \theta_{1k}) ;$$

$$u_2 = -\sum_{k=1}^{\infty} q_k \omega_k Z_s \sin(2\omega_k \tau - \omega_k x/v) + u_0 ;$$

$$u_c = \frac{1}{C} \sum_{k=1}^{\infty} q_k \frac{\sin(\omega_k \tau + \theta_{3k})}{\sin \theta_{3k}} + L_3 \frac{di_0}{dt}$$

where

$$i_0 = \frac{U_{max} \sin \phi_0 [\sin(\omega t + \psi - \phi_0) - e^{-\delta_0 t} \sin(\psi - \phi_0)]}{\omega(L_3 + L_l l)} ;$$

$$u_0 = -[L_3 + L_l(x - l)] \frac{di_0}{dt} + r_l(x - l) i_0 ;$$

$$N_k = \frac{\sin(\omega_k\tau + \theta_{3k}) \sin\theta_{2k}}{\sin\theta_{3k} \sin(\omega_k\tau + \theta_{1k} + \theta_{2k})} \quad (k \geqslant 1)$$

$$\delta_0 = \frac{r_l l}{L_3 + L_l l} .$$

The amplitudes of the generalized co-ordinates are

$$q_{k\max} = \frac{U_{\max} \sin\phi_k}{(\omega^2 - \omega_k^2)a_k} \quad (k \geqslant 1) .$$

The coefficients in the differential equations for the generalized co-ordinates are:

$$a_k = \frac{Z_s}{4\omega_k}\left\{N_k^2[2\omega_k\tau - \sin 2(\omega_k\tau + \theta_{1k}) + \sin 2\theta_{1k}] + \right.$$

$$\left. + 2\omega_k\tau - \sin 2\omega_k\tau + \frac{4\sin^2(\omega_k\tau + \theta_{3k})}{\omega_k C Z_s \sin^2\theta_{3k}}\right\} \quad (k \geqslant 1) ;$$

$$b_k = \frac{r_l}{L_l}\frac{Z_s}{4\omega_k}\left\{N_k^2[2\omega_k\tau + \sin 2(\omega_k\tau + \theta_{1k}) - \sin 2\theta_{1k}] + \right.$$

$$\left. + 2\omega_k\tau + \sin 2\omega_k\tau\right\} \quad (k \geqslant 1) .$$

q_{kI}, q'_{kI}, δ_k, ϕ_k, ϕ_0, ω_{kr} are given by the above formulae.

REFERENCES

1. E.A. Meerovich; Calculation of transient phenomena in complicated electrical systems. *Izv.Akad. Nauk SSSR., otd. tekh. nauk* No. 10 (1950).
2. R.I. Karaev; Transient phenomena in long three-phase lines. *Electrichestvo* No.10 (1954).
3. R. Courant and D. Hilbert; *Methods of Mathematical Physics. Gos. izd. tekh. i teor. lit.* (1951).
4. S.A. Ul'yanov; *Short-Circuits in Electrical Systems.* Gosenergoizdat (1952).

5. E. Gross and L. Rabins; Transient performance of three-phase power systems. *J. Franklin Inst.* (May 1951).
6. K. Teodorchik; Two electromechanical Analogue systems based on Lagrange's equation. *Zh. tekh. fiz.* 8, No.18 (1938).
7. Lord Rayleigh (J.V. Strutt); *Theory of sound.* Gosenergoizdat (1955).
8. E.T. Whittaker; Analytical dynamics. *ONTI NKTP SSSR* (1937).
9. A.V. Neshutil and S.V. Strakhov; *Fundamentals of Electrical Engineering* Part II. Gosenergoizdat (1955).
10. R. Rudenberg; *Transient Performance of Electrical Power Systems NL* (1950).
11. A.N. Krylov; Lectures on approximate calculations. *Gos. izd. tekh. i teor. lit.* (1950).

RATES OF RISE OF RESTRIKING VOLTAGE ACROSS CIRCUIT-BREAKER CONTACTS IN LARGE POWER SYSTEMS *

M.M. BELOUSOV **

Lenin All-Union Electrical Engineering Institute

The rate of rise of the restriking voltage across the contacts of a circuit-breaker clearing a short-circuit is determined by the circuit parameters (neglecting post-arc conductivity). Most determinations of restriking voltage characteristics from theory or experiment comprise values corresponding to various points in existing systems and which are expressed statistically, (by their frequency or by the rate of rise of restriking voltage) and the restriking rate requirements are specified to correspond [1–3].

The design of new circuit breakers must not be governed by present-day operating conditions but should envisage conditions which will probably obtain in 5–10 years time.

The growth of system power is not only due to increase in the number of elements (generators, transformers, transmission lines) but also to increase in their power ratings and to the tendency towards higher operating voltages.

The increase in transformer ratings results in a greater short-circuit MVA at the terminals. To preserve the original operating conditions for a circuit-breaker clearing a fault on the transformer busbars, the increase in the short-circuit MVA would have to be accompanied by a reduction in the restriking voltage frequency. But the frequency does not decrease, and actually becomes slightly higher.

When the system voltage is increased, the number of transmission lines connected to the station busbars is usually reduced. This produces a higher resultant characteristic impedance of all lines connected to these busbars, and also increases the likelihood that a

* *Elektrichestvo* 4, 21–24, 1957 (Reprint Order No. EL5)

** *Candidate in Technical Sciences*

fault occurring at the beginning of one line may be cleared when no other line (or only one) is connected in parallel. In both cases the rate of restriking voltage rise (s) may become high.

Analogue studies of an isolated station with powerful generators (4) indicated values higher than those present in actual systems. It will be shown later that these results are insufficient as criteria of the values in large power systems.

Let us consider, for example, the S value for a 220 kV circuit breaker interrupting a fault at the point K–1, Fig.1. We will assume

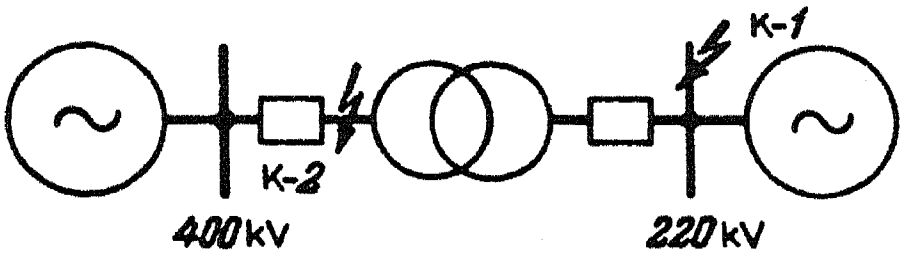

Fig. 1

that the transformer rating is 360 MVA, u_k = 14 per cent, a winding capacitance of 10,000 pF and an external circuit capacitance (busbars and circuit breaker) of 600 pF. Referring one half of the winding capacitance to the line terminal and assuming the h.f. inductance to be 90 per cent of that at 50 c/s, the natural frequency of the restriking voltage becomes

$$f = \frac{1}{2\pi\sqrt{L_t C}} = 9.04 \text{ kc/s}$$

where L_t = transformer inductance

C = capacitance to earth of the transformer line terminal.

Another method is to assume the "high frequency" inductance to be the same as at 50 c/s and to consider only one third of the winding capacitance. Then f = 10.2 kc/s. In what follows the average value of 9.6 kc/s is used. It is obvious that when a short-circuit behind the transformer (K–2) is interrupted we should get the same fundamental frequency if the reactances of the other sources referred to the 220 kV busbars were smaller than the transformer reactance.

The above frequency is much higher than those at which 220 kV circuit-breakers are tested at present; the short-circuit MVA interrupted in Fig 1.can also be considerable (in the example about 2000 MVA).

In determining the S values let us consider only a three-phase fault not involving earth. The amplitude of the 50 c/s recovery voltage is then $1.5U_{ph}\sqrt{2}$.

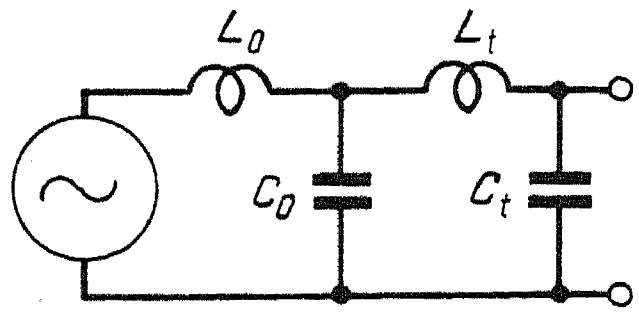

Fig. 2. L_0 is the referred inductance of the system; C_0 is the equivalent parallel capacitance across the left-hand winding of the transformer; L_t the transformer inductance, and C_t the capacitance from live to neutral of the transformer secondary.

If a fault occurs at K-1 the circuit of Fig.1 can be considered as a double-frequency circuit (Fig.2). S is then determined by the h.f. component, of amplitude proportional to L_t:

$$s = 4f \text{ x } 1.15 \text{ x } 1.5U_{ph}\sqrt{2}\,\frac{L_t}{L_0 + L_t}$$

$$= 4 \text{ x } 9600 \text{ x } 1.15 \text{ x } 1.5 \text{ x } \frac{220}{\sqrt{3}} \text{ x } \sqrt{2} \text{ x } 0.835 \text{ x } 10^6$$

$$= 9.9 \text{ kV}/\mu\text{sec}$$

(Allowance has been made for a possible increase of 15 per cent in the system voltage.)

An amplitude factor of 1.57, which allows for the damping is introduce when this formula is used for determining the maximum S. The experimenta value of this factor is about 1.6 [1].

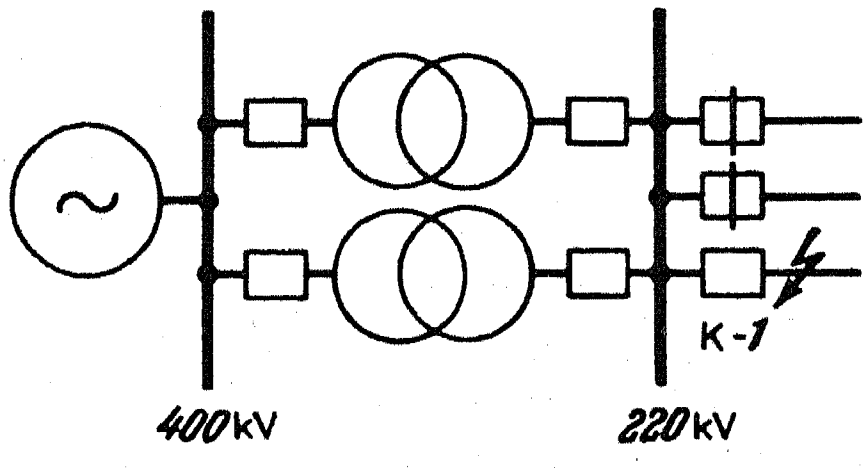

Fig. 3.

Consider the circuit of Fig.3. In this case we assume the short-circuit MVA at the 400 kV busbars to be 15,000 MVA with all the 220 kV lines in circuit and that at the 220 kV busbars to be 10,000 MVA. The transformer parameters are the same as those of Fig.1. Then if all the 220 kV lines are disconnected, the short-circuit MVA interrupted on clearing the fault at K-1 is 364 MVA and $L_t/(L_0 + L_t) = 0.71$. Assuming further that the total capacitances of the busbars and 220 kV switchgear is 6000 pF, the h.f. component frequency becomes

$$f = \frac{1}{2 \text{ x } 3.14\sqrt{0.9(0.06/2)\left[2(10000/2) + 6000\right]}}\,10^{-3} = 7.65 \text{ kc/s}$$

and hence

$$S = 4 \text{ x } 7650 \text{ x } 1.15 \text{ x } 1.5\,\frac{220}{\sqrt{2}}\,\sqrt{2} \text{ x } 0.71 \text{ x } 10^{-6} = 6.72 \text{ kV}/\mu\text{sec}$$

Let us next determine S at the full short-circuit MVA (10,000 MVA) under the least favourable conditions, i.e. when a large short-circuit MVA obtains at a given point (due mainly to generator proximity) and the number of outgoing lines on the busbars is least.

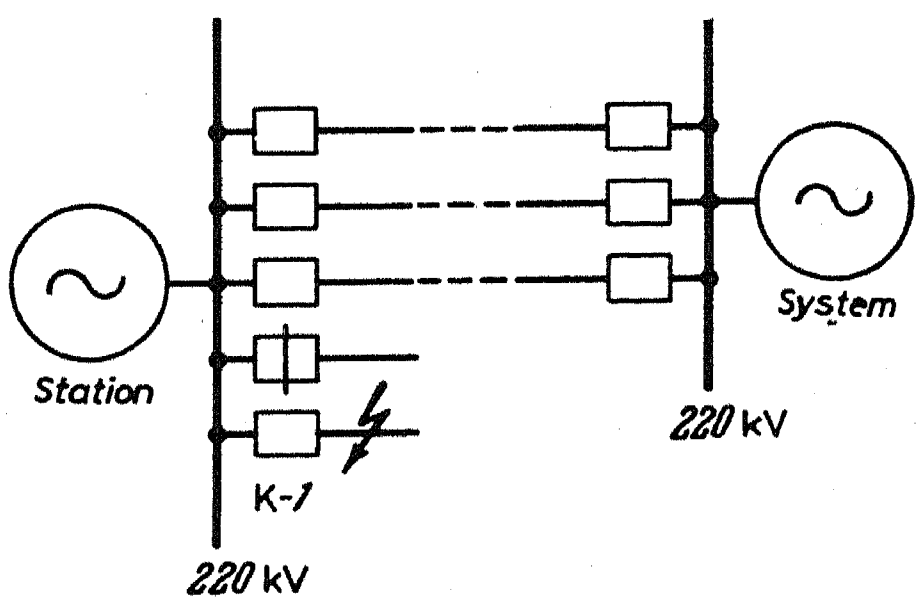

Fig. 4.

Consider a station with five outgoing lines (Fig.4). Three lines connect the station to a large power system, the other two are either spur lines, or may be interconnected with stations which affect the short-circuit currents at K-1 to a negligible extent; one of these lines has been switched off earlier.

Conditions are then most severe when clearing a fault on the spur which had been left in circuit.

For simplicity assume the three lines of the same length (100 km) and that the distant busbars are of infinite capacity. This does not

introduce any serious errors since the line reactances are high by comparison with the referred reactances of the large power system.

Calculating according to the method of [1], we get the restriking voltage curve shown in Fig.5. The restriking voltage is expressed as a relative quantity in this figure, and also in Figs. 6 and 7, the amplitude of the 50 c/s recovery voltage being taken as unity.

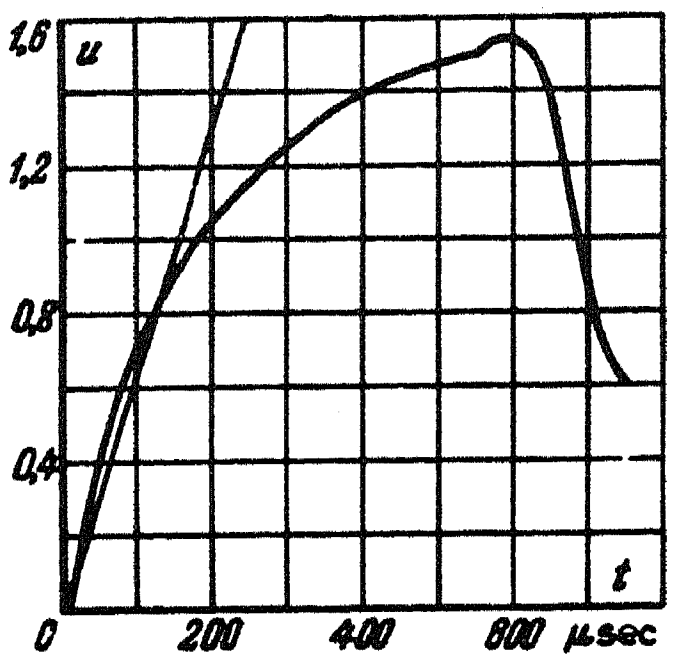

Fig.5.

With this shape of restriking voltage curve it would be incorrect to determine S from the slope of the tangent at the origin. The mean rate of rise to the maximum would also be incorrect, since this would be too low.

We shall take the rate of rise to be the average rate for the interval from the origin to the point corresponding to 80 per cent of the 50 c/s recovery voltage amplitude. The point corresponding to 100 per cent of the 50 c/s recovery voltage amplitude should not be used, since this would give values much too low with nearly-aperiodic curves, and zero rate of rise in the limiting case of complete aperiodicity.

The value of S and the amplitude factor as determined from Fig.5 are 2.05 kV/μsec and 1.53 respectively.

If the number of lines is increased in Fig.4, S will be lowered, e.g. if the number of lines is raised from three to five, S drops from 2.05 kV/μsec to 1.38 kV/μsec.

These relatively high S values are typical for stations and sub-stations working in a large power system where large breaking MVA's are involved. The S values for isolated stations with many lines are considerably lower, even if the stations are of large capacity.

With an isolated station with the same equipment parameters as in the above example, and with five outgoing lines (apart from the line on which a fault is being cleared) we would get the curve shown in Fig.6 and an S of 0.38 kV/μsec when 4000 MVA is interrupted.

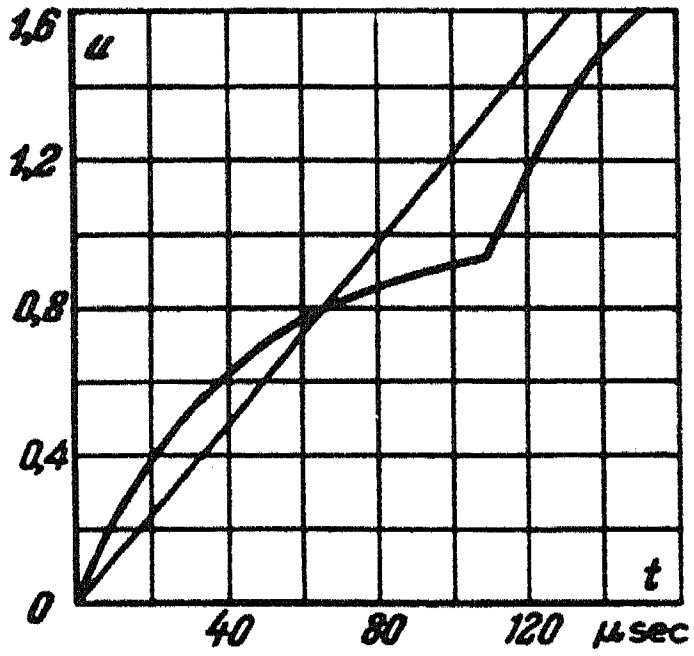

Fig. 6.

Thus it appears that the breaker operating conditions in an isolated station are much easier than in a large power system, and it is therefore incorrect to determine restriking rate requirements for new circuit-breakers from results on an isolated station or its model.

The author has carried out similar calculations for a 110 kV breaker. It was assumed that at full MVA four 30 km lines remained connecting the station busbars to the large power system. The reactance of the 110 kV system was not assumed as zero, as in the 220 kV system example, since the line reactances are considerably lower in this case. The referred reactance of the 110 kV system was taken as 2.01 ohms, which corresponds to a short-circuit MVA of 6000.

No calculations were made for the conditions of Fig.3 for the 110 kV system since at this voltage such a circuit would in practice only be used with relatively small transformers.

The results for the 110 and 220 kV systems are given in the Table 1 below.

Table 1.

Rates of rise of restriking voltage in 110 and 220 kV systems

Circuit diagram	110 kV system			220 kV system		
	MVA interrupted	Rate of rise of restriking voltage, kV/μsec (S)	Frequency, kc/s	MVA interrupted	Rate of rise of restriking voltage, kV/μsec	Frequency, kc/s
Fig. 1	2140	8.65	16.4	2140	9.9	9.6
Fig. 3	–	–	–	3640	6.72	7.65
Fig. 4	6000	1.69	2.73	10,000	2.05	1.65

$$f = \frac{s \times 10^3}{4U} \text{ kc/s}$$

where S = rate of rise of restriking voltage, kV/μsec

U = amplitude of the 50 c/s recovery voltage, kV.

Since the calculations involve a number of assumptions and simplifications they cannot, of course, be expected to be very accurate. Nevertheless, the results can form a basis for selecting restriking voltage requirements for large circuit-breakers of the 110 – 220 kV class.

The present practice of standardizing restriking voltage frequency at 100 and 50 per cent of the ultimate breaking capacity of the circuit breaker should be regarded as unsuitable. Since the restriking voltage parameters depend not on the circuit-breaker but on the power system, they should be chosen in relation to the absolute magnitude of the short-circuit MVA, irrespective of the circuit breaker capacity. Each h.v. circuit breaker intended for operation in a large power system, irrespective of its nominal breaking capacity, should be type-tested at 2000 – 2500 MVA under the conditions represented in Fig. 1, since these very conditions produce the highest S values, as well as at its nominal breaking MVA.

Since the foregoing concerns only breakers without contact shunts, let us now examine the effect of shunting. In transmission line circuits (e.g.Fig.4), the circuit breaker contacts are shunted by the characteristic line impedances. Therefore for a shunt to control the restriking voltage its impedance should be comparable with the effective characteristic line impedance. This means that the shunt resistance should not exceed a few hundred ohms (or sometimes maybe only a few tens of ohms). A subsidiary switch or arc-quenched interrupter has then to be fitted into the main body of the circuit-breaker to interrupt the final shunt current.

In Fig.1 the shunt resistance should also be comparable with the characteristic impedance of the circuit. Assuming that the restriking voltage frequency is to be reduced (by using an ohmic shunt) by at least 25 per cent, we get

$$f_1 = \frac{1}{2\pi}\sqrt{\frac{1}{LC} - \left(\frac{1}{2rc}\right)^2} = \frac{0.75}{2\pi\sqrt{LC}}$$

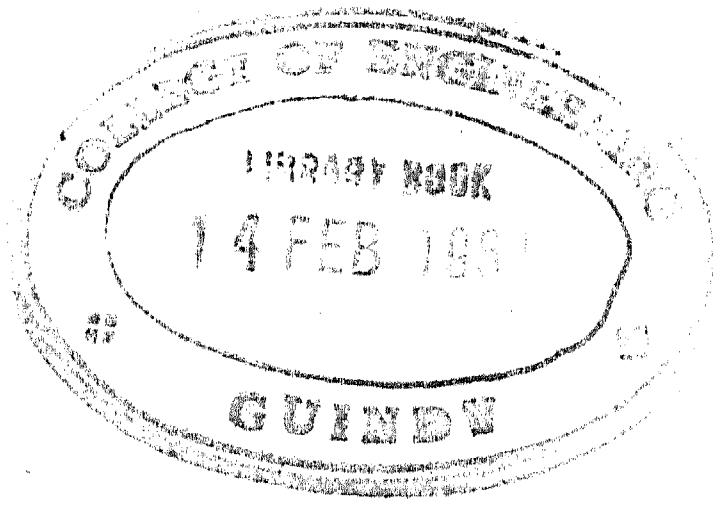

whence

$$r_{sh} \approx 0.755\sqrt{\frac{L}{C}}$$

In particular, with the transformer parameters assumed for Fig.1 r_{sh} becomes 1300 and 2900 Ω for the 110 and 220 kV circuit-breakers respectively.

If the circuit-breaker in Fig.1 has a non-linear shunt having the characteristic $u = ki_{sh}^{\alpha}$ the following equations apply:

$$L\frac{di}{dt} + u = U; \qquad i = C\frac{du}{dt} + \left(\frac{u}{k}\right)^{\alpha^{-1}}$$

After differentiating and rearranging, we get an equation which is not integrable in the general form, viz.

$$\frac{d^2u}{dt^2} = \frac{U}{LC} - \frac{u^{(\alpha^{-1}-1)}}{C\alpha k^{\alpha^{-1}}}$$

Taking a numerical example (transformer 110 kV, 180 MVA, non-linear shunt with $k = 8 \times 10^4$ and $\alpha = 0.25$), we get the curve shown in Fig.7 by numerical integration and iteration. This figure also shows the undamped curve (2) obtained with the same transformer parameters for comparison. In the example the shunt characteristic was so chosen that

the shunt should also be of acceptable size and have a final current which could be interrupted by a simple break in air. It can be seen from Fig.7 that the shunt does not lower S, but only decreases the amplitude and accelerates damping.

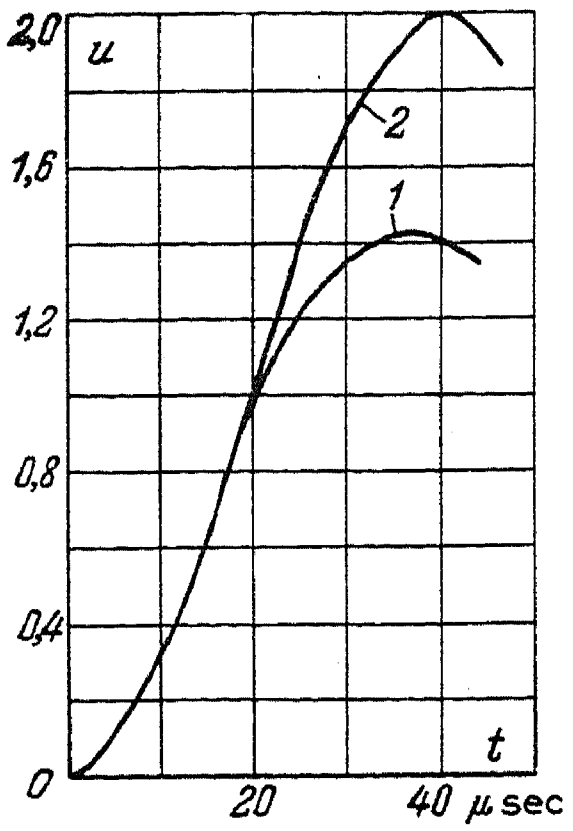

Fig. 7

Thus, shunting the contacts of a h.v. circuit-breaker operating in a large power system can reduce S only if the shunt resistance is sufficiently low. In this case, however, an arc-quenching device is necessary to interrupt the final current, which considerably complicates the design and increases the cost of the circuit-breaker.

Therefore the breaker design in practice should be one which can cope with high S values without resort to contact shunting; light shunting may be used for voltage grading across the gap. The gap should possess a high rate of dielectric strength recovery. It is probably that on interrupting transformer magnetising currents such a breaker would set up high surge voltages.

The surge voltages can be reduced to a permissible level by using a light non-linear shunt having an acceptable size and a small final current which is easy to inetrrupt. However, in all probability, a more suitable solution would be to install valve type surge diverters directly on the transformers (and not on the station busbars).

CONCLUSION

As power systems expand and capacities of generators and transformers increase, the rates of rise of restriking voltage are bound to go up.

New designs for large h.v. circuit-breakers should be based on high rates of rise of restriking voltage. The calculations presented in the present communication may be used to derive standards for the rates of rise of restriking voltage used in circuit-breaker tests.

REFERENCES

1. P. Hammarlund; *Restriking Voltage across the Contacts of a Circuit Breaker*. Gosenergoizdat (1956).
2. Johansen; *CIGRE* Paper no.104, (1952).
3. G.V. Butkevich; Some problems in the design of modern circuit-breakers. *Elektrichestvo* No.2 (1955).
4. Johnson, Schulz and Skeats; *Trans. Amer. Inst. Elect. Engrs.* **111**, 1339 (1953).

SELECTION OF ANTIHUNT TRANSFORMERS FOR AMPLIDYNE ELECTRIC DRIVES*

S.S. ROIZEN †

Tiazhpromelektroproekt

Motor + generator electric drives using amplidynes employ antihunt transformers to secure stability and the required transient characteristics. The transient duration and hence the system quality are determined to a large extent by correct transformer parameter choice in the design stage and correct setting when commissioning the drive.

The solution might appear to be simply to provide the design and erection engineers with the catalogue data, but experience has shown that calculations based on catalogue data for the machines and antihunt transformers give results which do not agree with tests.

The calculated overall maximum gains are usually much higher than the actual ones. For example, the calculated overall gain (K) for a 20 kW system with an EMU-12 A amplidyne and TS–72/60 transformer, was 65, but instability actually sets in at $K = 20$. Allowing for the self and mutual inductances of the amplidyne control windings and the transformer leakage reactance does not produce any considerable difference in the result.

When the system is RC stabilized, the calculated and experimental results are in good agreement. Hence the errors in the transformer calculation are not due to the method but to the transformer data used.

Consider an antihunt circuit including an amplidyne (Fig.1). The following equations can be set up for this circuit:

$$U_{1t} = i_{1t} r_{1t} + w_{1t} p\phi_t \qquad (1)$$

$$w_{2t} p\phi_t = i_{2t}(r_{2t} + r_2) \qquad (2)$$

* *Elektrichestvo* 4, 57–59, 1957 (Reprint Order No. EL6)

† *Candidate in Technical Sciences, Tiazhpromelektroproekt*

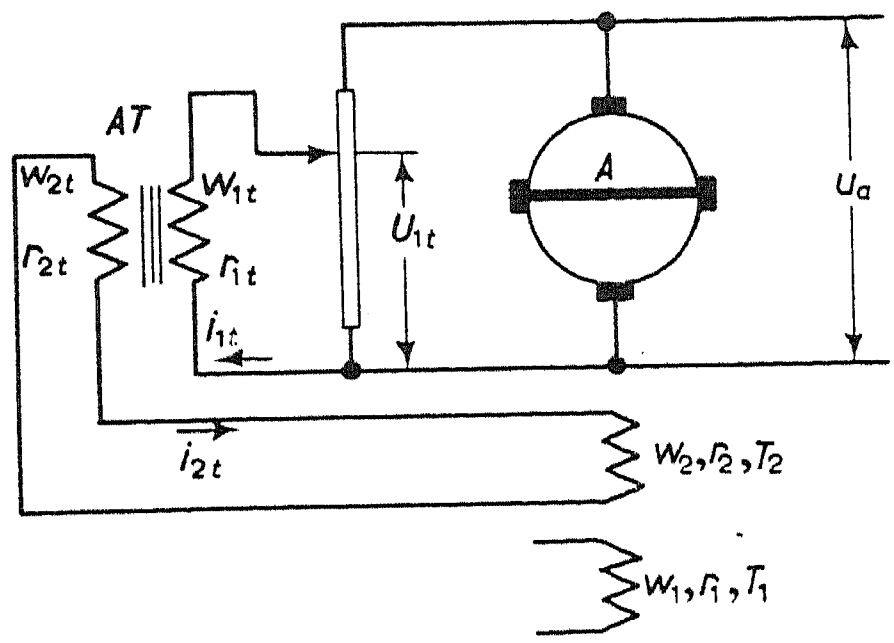

Fig. 1. Circuit diagram of the amplidyne–antihunt transformer unit.

A = amplidyne, AT = antihunt transformer.

$$(i_{1t}w_{1t} - i_{2t}w_{2t}) = \alpha_t\phi_t \qquad (3)$$

where ϕ_t is the magnetic flux in the transformer core. The transformer core is usually assumed unsaturated; α_t is also assumed constant. We make the following substitutions:

$$m = \frac{U_{1t}}{U_a}; \qquad T_{1t} = \frac{w_{1t}^2\alpha_t}{r_{1t}}; \qquad T_{2t} = \frac{w_{2t}^2\alpha_t}{r_{2t} + r_2}$$

$$T_s = T_{1t} + T_{2t}; \qquad K_s = m\frac{w_{2t}}{w_{1t}} \cdot \frac{w_2}{R_2} \cdot \frac{T_{1t}}{T_s}$$

$$R_2 = r_{2t} + r_2$$

Solving equations (1) – (3) simultaneously, we obtain the antihunt transformer operator

$$K_s(p) = \frac{i_{2t}w_2(p)}{U_a(p)} = \frac{K_sT_sp}{(T_sp + 1)} \qquad (4)$$

The variable feedback amplidyne operator is given by

$$K(p) = \frac{U_a(p)}{F_r(p)} = \frac{K_a(p)}{1 + K_a(p)K_s(p)} \qquad (5)$$

where

$$K_a(p) = \frac{K_a}{T_ap + 1}$$

is the amplidyne operator which acts as a simple inertial link, if we assume only one time constant for the cross-field circuit

T_a is the cross-field circuit time-constant,

$K_a = \frac{\Delta U_a}{\Delta F_r}$ the amplidyne transfer coefficient,

F_r is the resultant m.m.f. of the amplidyne.

Substituting the expressions for $K_s(p)$ and $K_a(p)$ into (5) we get

$$K(p) = \frac{K_a(T_s p + 1)}{(T_a p + 1)(T_s p + 1) + K_a K_s T_s} \tag{6}$$

The characteristic vector of the amplidyne plus antihunt transformer can be obtained by replacing p by $j\omega$ and introducing the amplidyne feedback winding parameters;

$$K_{fb} = \frac{F_{fb}}{U_{fb}} = \frac{i_{fb}\omega_{fb}}{i_{fb}R_{fb}} = \frac{\omega_{fb}}{R_{fb}}$$

Some simple transformations and the substitution

$$T_A = T_a + T_s + K_a K_s T_s$$

gave us the characteristic vector of the amplidyne-antihunt transformer unit, viz.

$$W_a(j\omega) = \frac{U_a(j\omega)}{U_{fb}(j\omega)} = \frac{K_a K_{fb}(T_s j\omega + 1)}{T_A j\omega + (1 - T_a T_s \omega^2)} \tag{7}$$

If T_a is neglected the expression becomes much simpler. Then

$$W_a(j\omega) = \frac{K_a K_{fb}(T_s j\omega + 1)}{T_A j\omega + 1} \tag{8}$$

The vector can also be obtained from Morozov's method of following for the self and mutual inductances of the amplidyne control windings. It then takes the form:

$$W_a(j\omega) = \frac{K_a K_{fb}(T_s j\omega + 1)}{j(T'_A\omega - a\omega^3) + (1 - b\omega^2)} \tag{9}$$

where

$$T'_A = T_s + T_a + T_1 + T_2 + K_a K_s T_s = T_A + T_1 + T_2;$$

$$a = T_s T_a T_1 + T_a T_{1t} T_2;$$

$$b = T_a(T_s + T_1 + T_2) + T_s T_1 + T_{1t} T_2;$$

T_1 and T_2 are the time constants of the corresponding amplidyne windings.

Usually

$$(T_1 + T_2) \ll T_s + T_a + K_a K_s T_s$$

and therefore

$$T'_A \approx T_A$$

When deciding which of these three expressions should be used in practice it should be remembered that medium and large power amplidyne industrial units the amplidyne pass band has a cut-off at $\omega = 8 - 10$ sec^{-1}. This explains why the short amplidyne time constants have little effect on the transients, since normally $T_A\omega \gg a\omega^3$ and $1 \gg b\omega^2$ when $\omega = 8 - 10$ sec^{-1}.

Fig.2 shows the log frequency characteristics plotted from tests made on a 20.5 kW unit using an EMU-12A amplidyne, and TS-72/60 antihunt transformer. The transformer settings were chosen to give 30 per cent over-shoot and fast damping. Fig.2 shows that the cut-off frequency is 6 sec^{-1}. The maximum frequency is even smaller with larger units where the generator field winding time constants (T_g) are greater than 0.5 sec.

Only when T_g and the electromechanical time constant of the motor (T_m) are smaller ($T_g < 0.5$ sec, $T_m < 0.05$ sec), does the cut-off frequency increase to 10 sec^{-1}; these values are not typical of large industrial units and will not be considered.

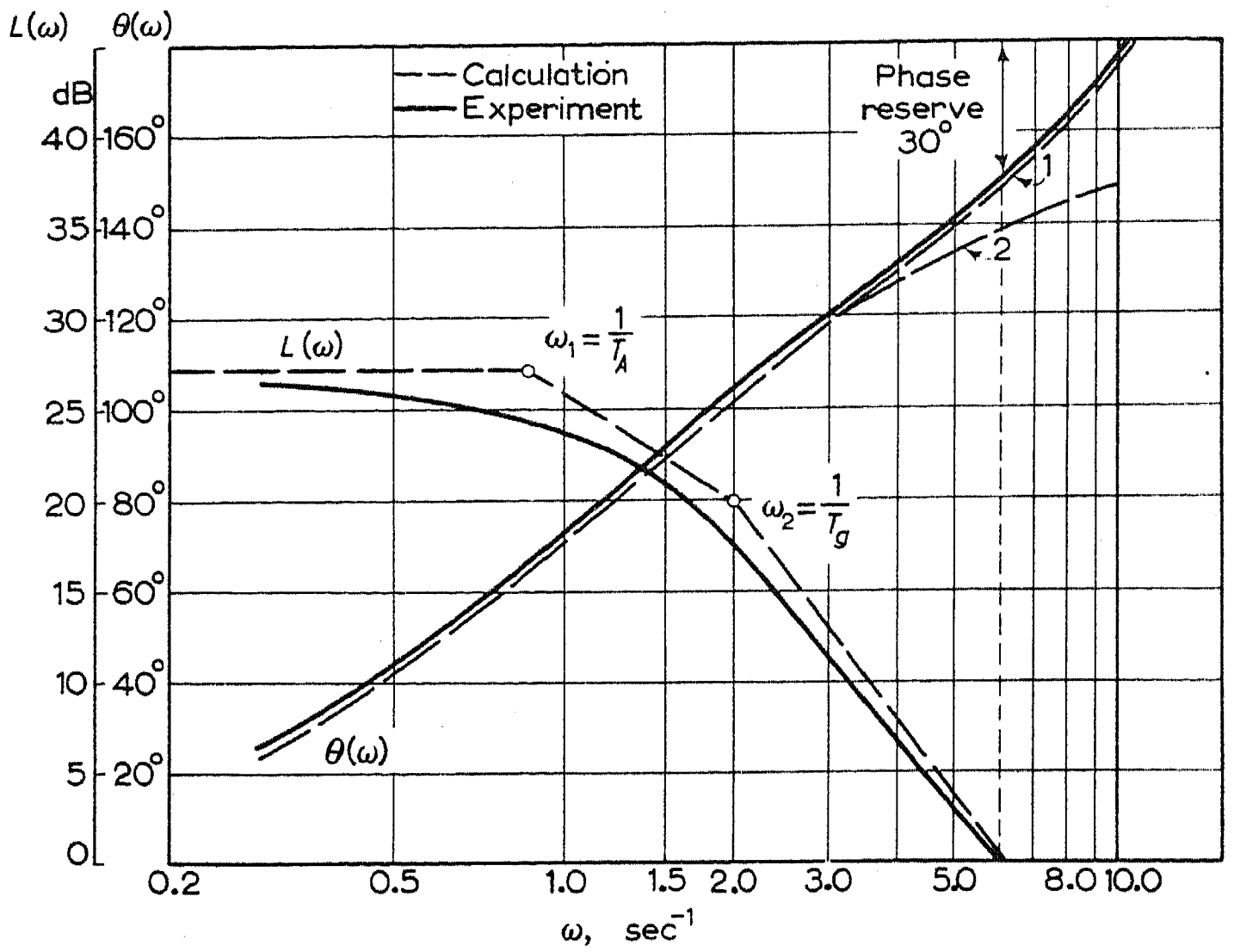

Fig. 2. Frequency characteristics of the motor-generator plus amplidyne system.

1 - Allowing for the armature time constant, T_r;

2 - Without allowance for T_r.

Frequency characteristics have been recorded on various combinations of three types of amplidyne with two types of transformer to prove that small time constants have practically no effect on transient response when the cut-off frequency is not more than 8 – 10 sec^{-1}. Fig. 3 shows the characteristics obtained with an EMU-12A amplidyne and TA-72/60 transformer. These curves (and also (7) and (9)) show that the transient performance of a system with $\omega_c < 8 - 10$ sec^{-1} is completely defined as T_s, T_A and K_a, and that the characteristic vector is given by (10).

T_A and T_s can be easily determined from the asymptotic characteristics via the conjugate frequencies ω_1 and ω_2:

$$T_A = \frac{1}{\omega_1}; \qquad T_s = \frac{1}{\omega_2}$$

T_A and T_s thus obtained are equivalent values if the transformer saturation is taken into account. The most accurate predictions of transient performance calculations are therefore to be expected when the T_A and T_s values used have been determined in the operating voltage range of the unit.

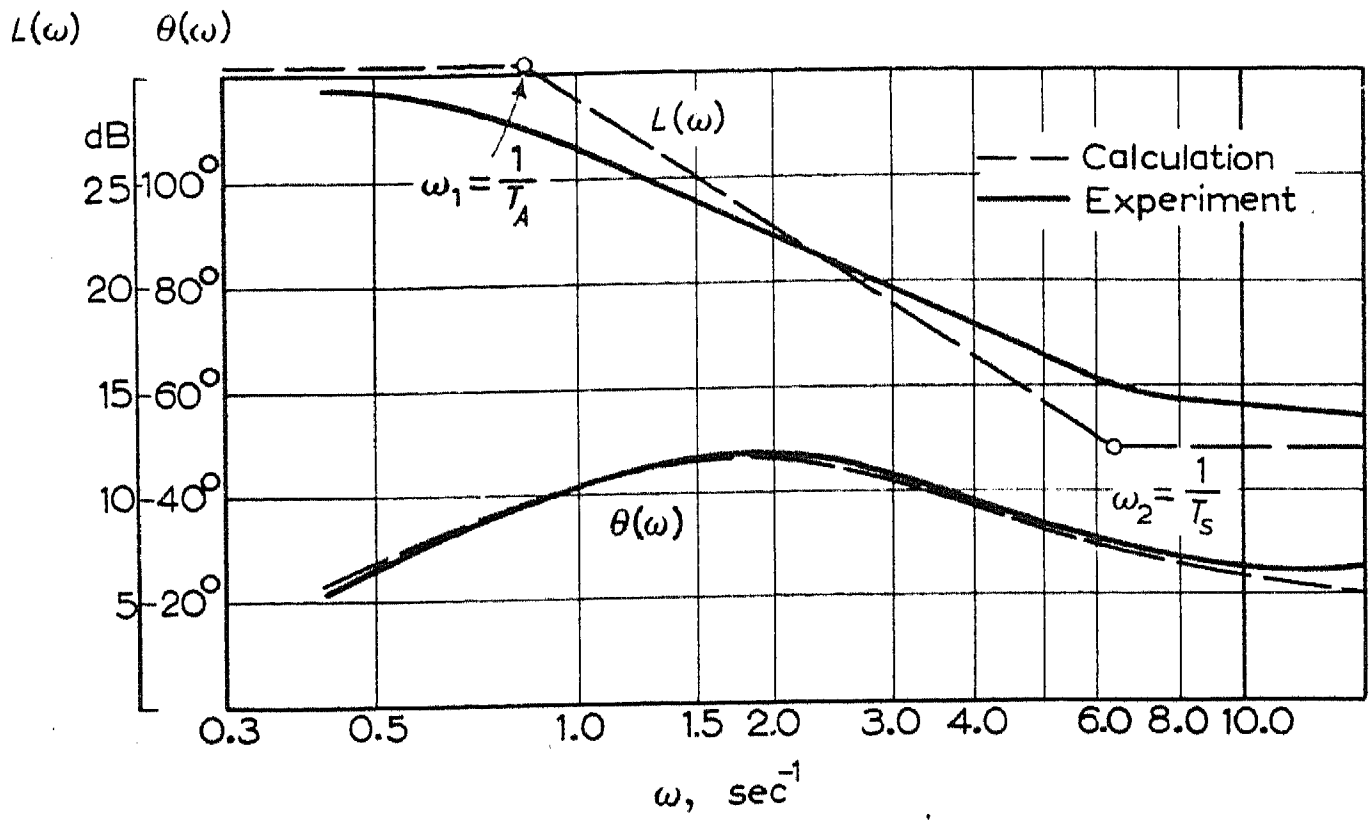

Fig. 3. Log frequency characteristics of an EMU-12A amplidyne plus antihunt transformer (T_s = 0.17 sec, T_A = 1.2 sec).

T_A and T_c, calculated from name-plate data, differ considerably from test values. The data for the EMU–12A plus TS–72/60 may serve as an example. The circuit parameters for Fig. 1 are: $W_1 = W_2 = 900$, $r_1 = r_2 = 145\ \Omega$; $m = 1$.

The name-plate data for the TS–72/60 are $W_{1t} = 4800$; $r_{1t} = 232\ \Omega$; $L_{1t} = 95$ H; $W_{2t} = 1100$; $r_{2t} = 10.3\ \Omega$; $L_{2t} = 5$ H.

These give:

$$T_{1t} = \frac{L_{1t}}{r_{1t}} = \frac{95}{232} = 0.41 \text{ sec};$$

$$T_{2t} = \frac{L_{2t}}{r_{2t} + r_2} = \frac{5}{10.3 + 145} = 0.03 \text{ sec};$$

$$T_s = T_{1t}\ T_{2t} = 0.44 \text{ sec};$$

$$K_s = m\,\frac{w_{2t} w_2 T_{1t}}{W_{1t} R_2 T_s} = 1.21;$$

$$K_s T_s = 1.21 \times 0.44 = 0.52$$

The experimental K_a of the EMU–12A (for the m.m.f.) is 5 V/A for armature voltages within the range 30 – 70 V.

But experiments on an EMU–12A plus TS–72/60 gave T_s = 0.17 sec and T_A = 1.2 sec. The frequency characteristics were taken with minimum transformer air gap using the windings fully without additional resistances. The amplidyne armature voltage varied from 30 to 70 V at low frequencies and the transformer's primary current did not exceed 0.3 A.

Thus the name-plate data gave transformer time-constants 2.7 times larger than did experiment. The calculated results with other types of amplidyne and transformer were also considerably different from experiment.

Better results are obtained when frequency test data are used in the calculations. Fig.3 shows the experimental characteristics for a TS–72/60. The shape of the amplitude characteristic confirms that the transformer operator is actually

$$K_s'(p) = \frac{U_2(p)}{U_1(p)} = \frac{K_s' T_s p}{T_s p + 1}$$

The intersection point on the asymptote gives the conjugate frequency ω_c for the component $L_1(\omega) = 20 \log \sqrt{(T_s{}^2\omega^2 + 1)}$ from which T_s can be determined and the amplitude at 10 – 15 sec^{-1} gives K_s.

When measuring antihunt transformer frequency characteristics it is important to vary the primary voltage over the operating range encountered in circuit with the amplidyne unit. The test then give some effective values of T_s and K_s' which take into account the transformer core saturation. Fig.3 was obtained by using a primary voltage composed of 50 V d.c. and 20 V a.c. The a.c. frequency varied from 0.1 – 2 c/s (ω = 0.68 – 13.6 sec^{-1}). The transformer core had no gap, the windings were used fully and additional resistances were not used.

The data of Fig.4 gave T_s = 0.2 sec; K_s' = 0.2. Then calculation gave

$$K_s = 1.15; \qquad T_A = 1.45 \text{ sec.}$$

These values of T_s and T_A are much closer to the experimental ones.

When T_s and T_A have been determined it is possible to determine the transient performance rapidly with an accuracy sufficient for practical purposes, and hence to check the suitability of the transformer.

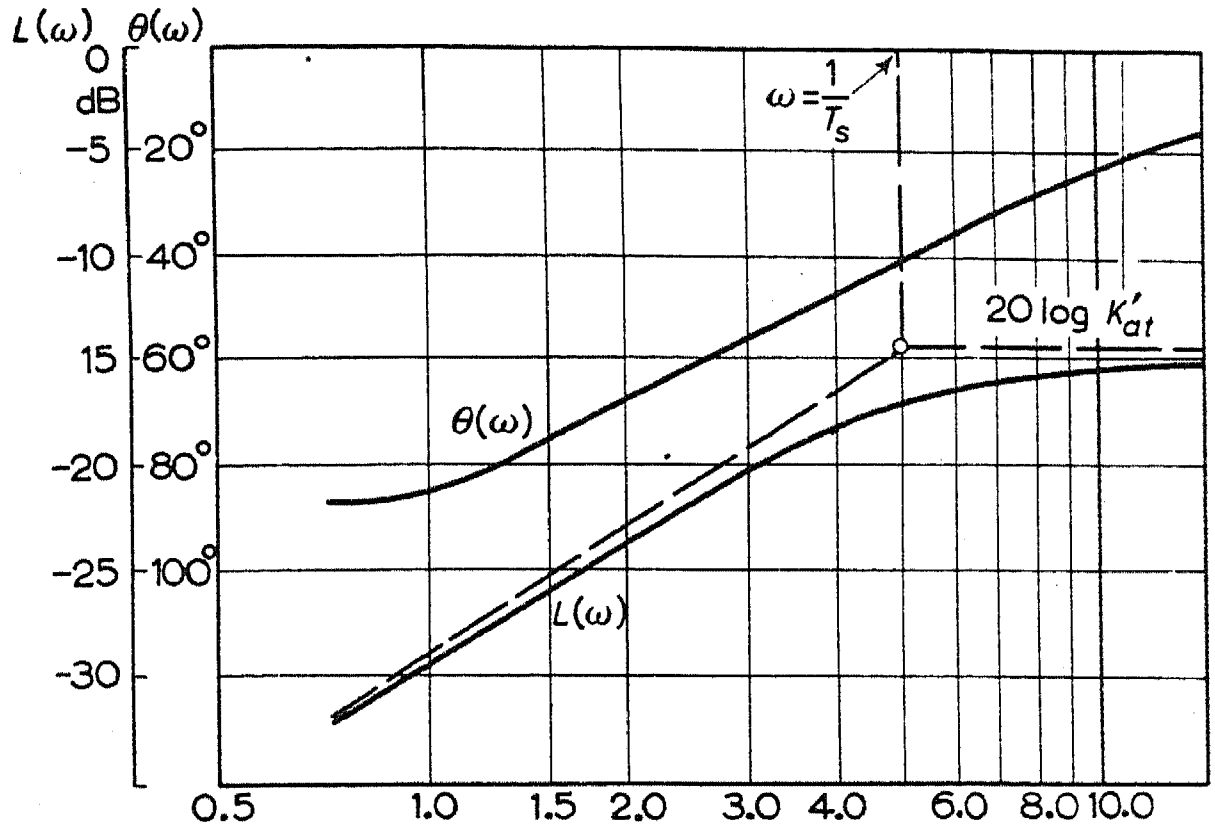

Fig. 4. Log frequency characteristics of TS–72/60 antihunt transformer.

As an example we may consider a 20.5 kW unit with an EMU–12A and a TS–72/60. T_m = 0.1 sec; T_g = 0.5 sec, the armature time-constant T_r is 0.075 sec. K is 23 with 30 – 180 V on the generator; T_s = 0.17 sec and T_A = 1.2 sec.

The characteristic vector of the entire open loop system is equal to the product of those for the amplidyne–transformer and generator–motor units:

$$W(j\omega) = \frac{K(T_s j\omega + 1)}{(T_A j\omega + 1)(T_g j\omega + 1)[T_m j\omega + (1 - T_m T_r \omega^2)]}$$

The log frequency characteristics are:-

Amplitude:

$$L(\omega) = 20 \log K + 20 \log \sqrt{T_s^2\omega^2 + 1} - 20 \log \sqrt{T_A^2\omega^2 + 1} - 20 \log \sqrt{T_g^2\omega^2 + 1)} - 20 \log \sqrt{T_m^2\omega^2 + (1 - T_m T_r \omega^2)^2} \quad (11)$$

Phase:

$$\theta(\omega) = \tan^{-1} T_s\omega - \tan^{-1} T_A\omega - \tan^{-1} T_g\omega - \tan^{-1} \frac{T_m\omega}{1 - T_m T_r \omega^2} \quad (12)$$

Fig.2 shows these characteristics plotted from the above data. The experimental characteristics are also shown. Fig.2 shows that neglect of the armature circuit time constant leads to considerable error in the transient performance because of phase errors.

Tests on several drive units showed that a phase margin of 30^{o} gives entirely satisfactory transient performance.

A STATISTICAL ASSESSMENT OF THE STABILITY OF INDUCTION MOTOR CHARACTERISTICS*

I. P. ISAEV

Moscow Rail Transport Engineering Institute

(Received 14 August 1956)

The problem and essentials of the method

In a number of induction motor applications the stabilities of characteristics dependent on manufacturing tolerances in the parameters have to be assessed.

The actual parameters of identical motors always differ slightly from nominal so the characteristics will also differ from nominal. This shows why motors working in parallel on a single power drive are unequally loaded. Hence follows the practical interest of estimates of divergences in characteristics due to motor parameter differences.

In essence the parameters which determine the motor characteristics are assumed to follow a normal random distribution law, with mathematical expectations and standard deviations for the parameters.

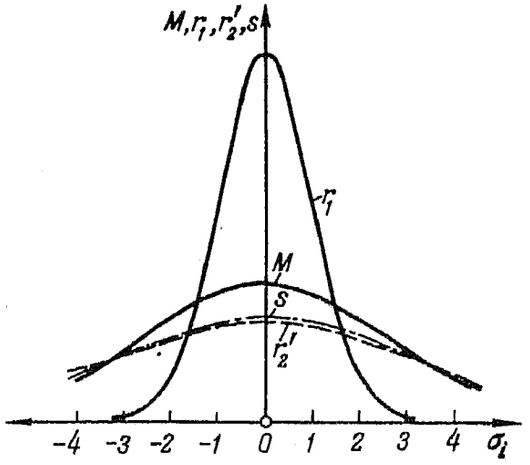

Fig. 1.

Elektrichestvo No. 4, 64–69 (1957). [Reprint Order No. EL. 7]

Statistical analysis of motor tests shows this to be so. By way of example, Table 1 gives the values, and Fig.1 the distribution curves,

TABLE 1

Motor parameters	Theoretical nominal values	Arithmetic means from type tests	Standard deviation, referred to mean value, %
Resistance of stator winding (Ω)	1.385	1.365	2.6
Rotor resistance (assumed) (Ω)	1.440	1.448	10.2
Slip, %	1.67	1.41	10.1
Torque, kg-m	96.0	95.5	7.0

for the stator resistance, rotor resistance (referred), slip and torque of KAMO-133-2 induction motors, as obtained in type tests at the Vladimir Il'ich Works.

Since the graphs are actually normal distribution curves, we may assume that the very general conditions of Lyapunov's theorem for independent variables, or of Bernstein's theorem for weakly dependent variables, are satisfied. According to this some function X of the independent variables x, v, ... z, with mathematical expectations $\bar{x}$, $\bar{v}$, ... $\bar{z}$, and corresponding small deviations k, l, ... q, may be represented accurate to the second order of small quantities, as follows

$$X(x, v, \ldots, z) = X(\bar{x}, \bar{v}, \ldots, \bar{z}) \pm t\sigma \qquad (1)$$

where

$$\sigma^2 = \left(\frac{\partial \bar{X}}{\partial \bar{x}}\right)^2 k^2 + \left(\frac{\partial \bar{X}}{\partial \bar{v}}\right)^2 l^2 + \ldots + \left(\frac{\partial \bar{X}}{\partial \bar{z}}\right)^2 q^2; \qquad (2)$$

t being a certain number.

Considering $X(x, v, \ldots z)$ in (1) as the mathematical expectation of the nominal motor characteristic, we may from equation (2) determine the standard deviation of this characteristic as a function of the deviations in the parameters.

From Lyapunov's theorem it is possible to state that, with a probability $P_t = 1 - Q_t$ the parameters will in practice remain within the bounds $\bar{X} \pm t\sigma_x$.

Stability of characteristics in an induction motor

We will first of all determine the effect of manufacturing tolerances in the resistances on the torque deviations at a given slip.

The torque at the nominal parameter values is

$$M = \frac{mpU_1^2(r_2'/s)}{9.81\omega[(sr_1 + ar_2')^2 + (x_1 + ax_2')^2 s^2]}\,[k_g - m] \qquad (3)$$

The voltage is assumed to be constant at the nominal value and the voltage system to be symmetrical.

Since the parameters are statistically distributed we will assume:

$$r_1 = \bar{r}_1 \pm t\sigma_{r1};\quad r_2' = \bar{r}_2' \pm t\sigma_{r2};\quad x_1 = \bar{x}_1 \pm t\sigma_{x1};$$

$$x_2' = \bar{x}_2' \pm t\sigma_{x2}$$

The bars denote the nominal resistances and reactances, respectively, σ being the standard deviation; t is a certain number.

The incremental torque due to small resistance and reactance increments, accurate to quantities of the second order, is

$$dM = \frac{\partial M}{\partial r_2'}\,dr_2' + \frac{\partial M}{\partial r_1}\,dr_1 + \frac{\partial M}{\partial x_2'}\,dx_1 + \frac{\partial M}{\partial x_2'}\,dx_2'$$

and according to equation (2) the deviation of the motor torque is given by

$$\sigma_m^2 = \left(\frac{\partial \bar{M}}{\partial \bar{r}_2'}\right)^2\sigma_{r2}^2 + \left(\frac{\partial \bar{M}}{\partial \bar{r}_1}\right)^2\sigma_{r1}^2 + \left(\frac{\partial \bar{M}}{\partial \bar{x}_1}\right)^2\sigma_{x1}^2 + \left(\frac{\partial \bar{M}}{\partial x_2'}\right)^2\sigma_{x2}^2$$

Determining the partial differential coefficients from equation (3) and substituting into them the mathematical expectations for the motor parameters, we find that

$$\sigma_m^2 = \frac{c^2}{[(\bar{r}_1\bar{s} + a\bar{r}_2')^2 + (\bar{x}_1 + a\bar{x}_2')^2 s^2]^2} \times$$

$$\times \left\{ \left(1 - \frac{2a\bar{r}_2' \cos^2\bar{\phi}}{\bar{r}_1\bar{s} + a\bar{r}_2'} \right)^2 \sigma_{r2}^2 + 4\bar{r}_2'^2 \left[\frac{\bar{s}^2 \cos^4\bar{\phi}}{(\bar{r}_1\bar{s} + a\bar{r}_2')^2} \sigma_{r1}^2 + \right.\right.$$

$$\left.\left. + \frac{\sin^4\bar{\phi}}{(\bar{x}_1 + a\bar{x}_2)^2} (\sigma_{x1}^2 + a\sigma_{x2}^2) \right] \right\}, \qquad (4)$$

where

$$\cos^2\bar{\phi} = \frac{(\bar{r}_1\bar{s} + a\bar{r}_2')^2}{(\bar{r}_1\bar{s} + a\bar{r}_2')^2 + (\bar{x}_1 + a\bar{x}_2')^2 s^2}$$

$$c = \frac{mp\bar{U}_1^2\bar{s}}{9.81\omega}$$

In practical calculations it is sometimes more convenient to use a per unit basis, relating to operation under the nominal conditions. Using the notation $\sigma_m / \bar{m} = \sigma_{m0}$ (and analogous notations for the partial standard deviations of the other parameters), and dividing the right-hand side of equation (4) by the square of the nominal torque, we get:

$$\sigma_{m0} = \left(1 - \frac{2a\bar{r}_2' \cos^2\bar{\phi}}{\bar{r}_1\bar{s} + a\bar{r}_2'} \right)^2 \bar{r}_2'^2 \sigma_{r20}^2 + 4\bar{r}_2^2 \left[\frac{\bar{s}^2\bar{r}_1^2 \cos^4\bar{\phi}}{(\bar{r}_1\bar{s} + a\bar{r}_2')^2} \sigma_{r10}^2 + \right.$$

$$\left. + \frac{\sin^4\bar{\phi}}{(\bar{x}_1 + a\bar{x}_2')^2} (\bar{x}_1^2 \sigma_{x10}^2 + \bar{x}_2'^2 a^2 \sigma_{x20}^2) \right]. \qquad (5)$$

This relative standard deviation formula for the torque enables us to estimate the effect of changes in the stator and rotor resistances and reactances.

It is clear from equations (4) and (5) that the torque deviation is a variable quantity which depends on the operating conditions to which the deviation is referred.

When the slip is small, i.e. on the stable part of the motor characteristic, we may assume $s^2 \approx 0$ and $\sin^4 \bar{\phi} \approx 0$. Consequently, the torque deviations will be defined by the following equation:

$$\sigma_{m0} = \pm 1 - \frac{2a\bar{r}_2'^2}{\bar{r}_1\bar{s} + a\bar{r}_2'} \cos^2 \bar{\phi}\, \sigma_{r2} \qquad (5a)$$

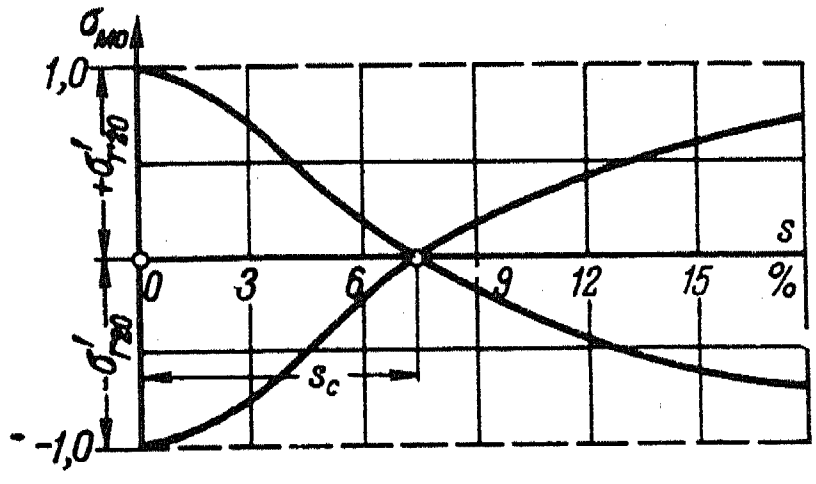

Fig. 2.

As an example, Fig. 2 shows the graph (based on (5a)), for the variation in the standard deviation of the torque of KAMO-133-2 motors with slip, where $r_1 = 1.77$ ohm; $r_2 = 1.565\ \Omega$; $a = 1.03$ and $s_c = 0.075$.

Equation (5a) shows that at small slip the torque deviations are determined, other things remaining equal, by the rotor resistance tolerances. Stability of rotor resistance within reasonable limits is therefore above all else essential if the desired stability is to be obtained.

As methods of stabilising the short-circuit rotor resistances in large induction motors we may recommend the following: (a) selective checking of the rotor bar blank sizes; (b) selective checking of bar material resistivity and (c) use of electric contact welding on the bars instead of autogenous welding, since the latter is liable to leave porosities or cavities at the seams which render the phase resistances unequal.

Equations (4) and (5) show that the torque deviations on starting ($s = 1$) are primarily affected by the tolerances in stator resistance and reactance. In this case the rotor resistance tolerance is of less importance.

The effect of tolerances in any particular type of motor at a given slip may be estimated from equations (4) and (5) for the appropriate mathematically expected parameters.

In general, the standard deviations in the parameters of the various phases may differ. The symmetrical components method, supplemented by statistical considerations, may be used to study the deviations in the characteristics of such an "asymmetric" motor.

However, let us consider the simpler case in which the standard deviations of the phase resistances are assumed to be equal.

Knowing the standard deviations of the parameters, we can determine the standard deviation in the torque. With nominal parameters the maximum torque is given by equation (6), viz.

$$M_m = \frac{C_1}{r_1 + \sqrt{r_1^2 + (x_1 + ax_2')^2}} \tag{6'}$$

where

$$C_1 = \frac{mpU_1^2}{2a \cdot 9.81 \cdot 2\pi f}$$

The increment in the maximum torque due to increments in the resistances and reactances is

$$dM_m = \frac{\partial M_m}{\partial r_1} dr_1 + \frac{\partial M_m}{\partial x_1} dx_1 + \frac{\partial M_m}{\partial x_2'} dx_2'$$

and the standard deviation of the maximum torque is

$$\sigma_{M_m}^2 = \left(\frac{\partial \bar{M}_m}{\partial \bar{r}_1}\right)^2 \sigma_{r1}^2 + \left(\frac{\partial \bar{M}_m}{\partial \bar{x}_1}\right)^2 \sigma_{x1}^2 + \left(\frac{\partial \bar{M}}{\partial \bar{x}_2'}\right)^2 \sigma_{x2}^2$$

where σ_{r1}, σ_{x1}, and σ_{x2} are the standard deviations of the corresponding parameters.

Determining the partial differential coefficients from equation (6) and substituting into them the mathematical expectations for the parameters, we get from equation (2) the standard deviation in the maximum torque, viz.

$$\sigma_{Mm}^2 = \frac{\bar{M}_m^2}{\left[\bar{r}_1 + \sqrt{(\bar{r}_1^2 + (\bar{x}_1 + a\bar{x}_2')^2)}\right]^2} \text{ x}$$

$$\times\left\{\left[1+\frac{\bar{r}_1}{\sqrt{[\bar{r}_1^2+(\bar{x}_1+a\bar{x}_2')^2]}}\right]^2\sigma_{r1}^2+\right.$$

$$\left.+\frac{(\bar{x}_1+a\bar{x}_2')^2}{[\bar{r}_1^2+(\bar{x}_1+a\bar{x}_2')^2]}\,(\sigma_{x1}^2+a^2\sigma_{x2}^2)\right\}. \qquad (7)$$

Analogously, we may also find the standard deviation in the slip corresponding to this maximum torque. For this purpose we use the expression which defines the critical slip, viz.,

$$s_c=\frac{ar_2'}{\sqrt{[r_1^2+(x_1+ax_2')^2}} \qquad (8)$$

from which we get

$$\sigma_{sc}^2=\left(\frac{\partial\bar{s}_c}{\partial\bar{r}_1}\right)^2\sigma_{r1}^2+\left(\frac{\partial\bar{s}_c}{\partial\bar{x}_1}\right)^2\sigma_{x1}^2+\left(\frac{\partial\bar{s}_c}{\partial\bar{x}_1'}\right)^2\sigma_{x2}^2+\left(\frac{\partial\bar{s}_c}{\partial\bar{r}_2'}\right)^2\sigma_{r2}^2$$

Determining the partial differential coefficients from equation (8) and using the mathematical expectations applying to their parameters, we get

$$\sigma_{sc}^2=\bar{s}_c^2\left\{\frac{\sigma_{r2}^2}{\bar{r}_2'^2}+\frac{1}{[\bar{r}_1^2+(\bar{x}_1+a\bar{x}_2')^2]^2}\times\right.$$

$$\left.\times\,[\bar{r}_1^2\sigma_{r1}^2+(\bar{x}_1+a\bar{x}_2')^2(\sigma_{x1}^2+a^2\sigma_{x2}^2)]\right\} \qquad (9)$$

This gives the standard deviation in the slip corresponding to the maximum torque. Comparison with equations (7) and (9) shows that the effect of deviations from nominal in the winding inductances on the critical slip deviation may be neglected in the practice, and that we may consider σ_{sc} as independent of σ_{x1} and σ_{x2}. On the other hand, deviation of the inductances from nominal has a considerable effect on the deviation of the maximum torque.

A lucid representation of the effect of tolerances on the motor characteristic stability is obtained if the origin of a system of orthogonal co-ordinates (s,M) is made to coincide with the point of maximum torque, and the deviations $t\sigma_c$ and $t\sigma_m$ are laid off along the axes (Fig.3). The locus of possible standard deviations in the maximum

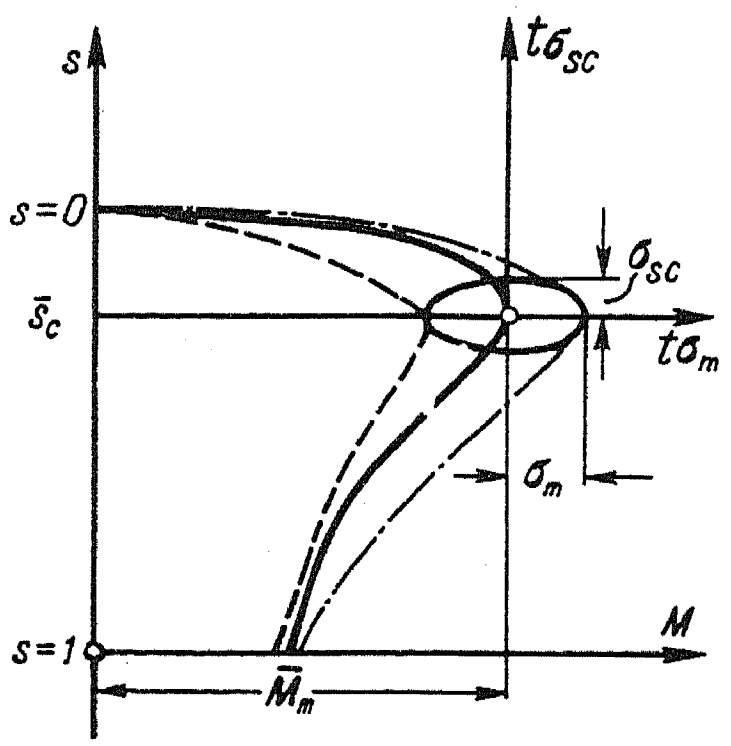

Fig. 3

torque will then in general be represented by the ellipse

$$\left(\frac{s - \bar{s}_c}{\sigma_{sc}}\right)^2 + \left(\frac{M - \bar{M}_m}{\sigma_{Mm}}\right)^2 = 1$$

The locus of the limiting deviations in the maximum torque will also be an ellipse in this system of co-ordinates, being

$$\left(\frac{s - \bar{s}_c}{t\sigma_{sc}}\right)^2 + \left(\frac{M - \bar{M}_m^2}{t\sigma_{Mm}}\right) = 1$$

obtainable from the previous ellipse by a t-fold increase in the semi-axes.

Parallel operation of induction motors

The deviations in the maximum torque and in the corresponding slip due to deviations in the parameters are responsible for variations in the motor characteristics.

Motors with differing characteristics operating in parallel in the same electrically-driven system will have the load non-uniformly distributed between them, which is usually undesirable.

To assess the effect of deviations in the motor parameters on the non-uniformity of load distribution for operation in the range $0 \lesssim s \lesssim s_c$, we use the equation for the mechanical characteristic, viz.,

$$M = M_m \frac{2(1+\epsilon)}{s/s_c + s/s_c + 2\epsilon} \tag{10}$$

We found above that s_c is a function of the parameters and of the tolerances, given in general as $s_c = \bar{s}_c \pm t\sigma_{sc}$, and that $M_m = \bar{M}_m \pm t\sigma_{Mm}$.

To render the results more general, we will assume that under load the motors show a σ_s not dependent on manufacturing tolerances and determined by the operating conditions. In this case the torque increment for small increments m s, s_c and M_m, is determined by

$$dM = \frac{\partial M}{\partial s} ds + \frac{\partial M}{\partial s_c} ds_c + \frac{\partial M}{\partial M_m} dM_m$$

and, according to equation (2), σ_M becomes

$$\sigma_M^2 = \left(\frac{\partial \bar{M}}{\partial \bar{s}}\right)^2 \sigma_s^2 + \left(\frac{\partial \bar{M}}{\partial \bar{s}_c}\right)^2 \sigma_{sc}^2 + \left(\frac{\partial \bar{M}}{\partial \bar{M}_m}\right)^2 \sigma_{Mm}^2$$

Differentiating (10), we find that σ_m under these conditions is

$$\sigma_M^2 = \left[\frac{2\bar{M}_m(1+\epsilon)}{(\bar{s}^2 + \bar{s}_c^2 + 2\epsilon\bar{s}\,\bar{s}_c)^2}\right]^2 \left[\bar{s}^2(\bar{s}^2 - \bar{s}_c^2)^2 \sigma_{sc}^2 + \right.$$

$$+ \frac{\bar{s}^2\bar{s}_c^2(\bar{s}^2 + \bar{s}_c^2 + 2\epsilon\bar{s}\,\bar{s}_c)^2}{\bar{M}_m^2} \sigma_{Mm}^2 + \bar{s}_c^2(\bar{s}_c^2 - \bar{s}^2)\,\sigma_s^2 +$$

$$\left. + \frac{\bar{s}^2\bar{s}_c^2(\bar{s} - \bar{s}_c)^4}{(1+\epsilon)^2}\left(\frac{\bar{r}_1}{\bar{r}_2'}\right)^2 \sigma_{sc}^2\right] \tag{11}$$

or, in relative units,

$$\sigma_{M0}^2 = \sigma_{Mm}^2 + \frac{1}{(\bar{s}^2 + \bar{s}_c^2 + 2\epsilon\bar{s}\,\bar{s}_c)^2}\left\{(\bar{s}_c^2 - \bar{s}^2)^2\sigma_{s0}^2 + \right.$$

$$\left. + \left[(\bar{s}^2 - \bar{s}_c^2)^2 + \frac{\bar{s}_c^2}{(1+\epsilon)^2}(\bar{s}^2 + \bar{s}_c^2 - 2\bar{s}\,\bar{s}_c)^2\left(\frac{\bar{r}_1}{\bar{r}_2'}\right)^2\right]\sigma_{sc}^2\right\} \tag{12}$$

Let us assume that the motors are "ideally" produced, i.e. that their parameters are exactly the nominal ones. In this case we have to put $\sigma_{sc} = \sigma_{Mm} = 0$ in equation (12), derived from equations (7) and (9).

Hence,

$$\sigma_{m0} = \frac{\bar{s}_c^2 - \bar{s}^2}{\bar{s}^2 + \bar{s}_c^2 + 2\epsilon \bar{s}\,\bar{s}_c}\,\sigma_{s0} \qquad (13)$$

Consequently, the load divergence will be determined by the slip divergence which, in turn, is determined by the conditions of operation. Conversely, if such a divergence is impossible, i.e. $\sigma_s = 0$, and the motors are produced with due tolerances, the differences in the loadings will be completely determined by the deviations in their parameters, viz.

$$\sigma_{M0}^2 = \sigma_{Mm0}^2 + \frac{1}{(\bar{s}^2 + \bar{s}_c^2 + 2\epsilon \bar{s}\,\bar{s}_c)^2}\left\{(\bar{s}^2 - \bar{s}_c^2)^2 + \right.$$

$$\left. + \frac{\bar{s}_c^2}{(1+\epsilon)^2}(\bar{s}^2 + \bar{s}_c^2 - 2\bar{s}\,\bar{s}_c)^2\left(\frac{\bar{r}_1}{\bar{r}_2'}\right)^2\right\}\sigma_{sc}^2 \qquad (14)$$

Therefore equations (11) and (12) enable us to solve two practical problems, viz. either by assuming the tolerances as given, to determine the permissible slip divergence from the permissible torque divergence or, conversely, to assume the slip as given and to determine the permissible standard deviations in the parameters from the permissible torque divergence.

By way of example, we shall solve the first of these problems for the induction-type traction motors used in individual-drive a.c. locomotives. We will define the wheel-pair rim tolerances so that the induction motors in the electric locomotive one-hour rated have the same torque divergence as the DPE-400A d.c. motors used in VL-22^{m} electric locomotive under the regulations in force (a divergence in the wheel rims of 15 mm produces a divergence of about ±4 per cent in the DPE-400A loadings when the motors are connected in parallel).

This problem has become very important nowadays since various a.c. locomotives are being developed. We use equation (11) in which we assume that

$$\sigma_s = -n_2/n_1\,\sigma_{D0}$$

The standard deviation in the wheel diameters, as related to the parameters of induction-type traction motors and the locomotive operating conditions, is given in the following general form

$$\sigma_{Do} = \sigma_{Mo} \frac{\bar{M}(\bar{s}^2 + \bar{s}_c^2 + 2\epsilon \bar{s}\,\bar{s}_c)^2}{2\bar{M}_m \bar{s}_c (\bar{s}_c^2 - \bar{s}^2)} \cdot \frac{n_1}{n_2}$$

Table 2 gives the diameter differences given by this equation, for three types of electric locomotive with induction-type traction motors, viz. OT, OD-1, and OD-II, designed by the NEVZ-Works "Budennii".

TABLE 2

Type of electric locomotive	Nominal diameter of rim (shrouding) of wheel pair, (mm)	Permissible wheel diameter deviation (mm)
OT	1200	5.0
	1050	4.5
OD-1	1200	3.8
	1050	3.2
OD-2	1200	3.0
	1050	2.8

Equation (14) shows that the load divergence is a variable quantity, dependent on the operating conditions. Let us determine from (14) the slip at which the load difference in parallel operation is a maximum.

The condition to be satisfied is that

$$\frac{\partial \sigma_M}{\partial s} = 0$$

Hence the roots of

$$\frac{\partial}{\partial s} \sqrt{\sigma_{Mm0}^2 \bar{M}^2 + 4\bar{M}_M^2 s^2 \frac{(1+\epsilon)^2 (\bar{s}^2 - \bar{s}_c^2)^2 \bar{s}^2 + \bar{s}_c^2 (\bar{s} - \bar{s}_c)^4}{(\bar{s}^2 + \bar{s}_c^2 + 2\epsilon \bar{s}\,\bar{s}_c)^4} \sigma_{sc}^2} = 0$$

must be determined.

Carrying out the differentiation and assuming that the terms containing ϵ will involve higher powers of s than the others, we get approximately (subject to the conditions $\sigma_{Mm0} = 0$):

$$s^4 - 2s\bar{s}_c^2 + \bar{s}_c^4 = 0$$

whence under operating conditions the maximum value is $s'_M = 0.412\ \bar{s}_c$, i.e. the maximum torque divergence of parallel motors allowing for manufacturing tolerances in their parameters, occurs at about 40 per cent of the critical slip.

When we know s'_M, we can determine σ_{Mm0} if we substitute $s = s'_m = 0.412\ \bar{s}_c$ into equations (14).

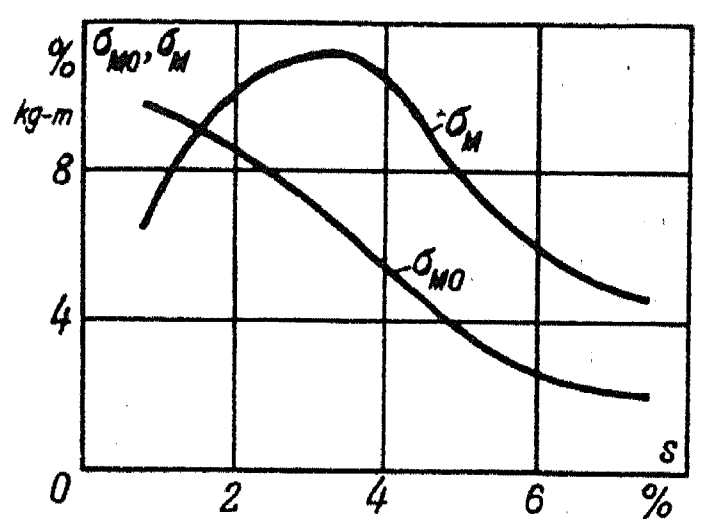

Fig. 4.

Fig. 4 shows by way of example the relative and absolute standard deviations in the torques of type KAMO-133-2 motors, determined from the following data:

$r_1 = 1.77\ \Omega$; $r'_2 = 1.565\ \Omega$; $s_c = 0.075$; $\sigma_{Mm0} = 0.02$; $\sigma_{sc0} = 0.10$.

The above statistical study of the stability in induction motor characteristics enables one to assess the effects of tolerances in various motor parameters scientifically, and to attempt to standardize the tolerances on the basis of the detailed operating conditions and special duties involved.

The statistical method explained above is of general application and may be extended to any other type of motor.

REFERENCES

I.P. Isaev; Effect of manufacturing tolerances on the stability of characteristics in traction motors and electric locomotives. *Elektrichestvo* No.11 (1955).

E.Ya. Kazovskii; Application of probability theory to the design and operation of electric machines. *Trans. LEMI* No.1 (1932).

R. Ruedenberg; Assessment of electrical machines and apparatus by tolerances based on statistical methods. *Z. Angew. Math. Mech.* **9**, No.4 (1929).

THE PROBLEM OF IMPULSE TESTS OF THE TURN INSULATION OF AN H.V. MACHINE*

B.A. ALEKSEEV and V.B. KULAKOLSKII

There is so far no practical method of calculating the impulsive voltages in the windings of electric machines, viz. on the sections and turns in any special part of the winding. Theoretical studies in this field have not yet reached a stage where calculations can be based on them [1]. Experimental investigations give a good idea of the maximum pulse voltages on the first turns of the winding [2], but they do not give adequate data on the voltages across the remaining turns. But a knowledge of the pulse voltages on turns in the centre of the winding, though not necessary for surge protection purposes, is indispensable for turn insulation test purposes.

In recent years two basic methods have been used for testing the turn insulation of assembled windings, viz. travelling-wave tests effected by applying impulses to the ends of the winding [3] and tests based on induced pulse voltages; the latter are carried out by inducing these voltages successively in each pair of winding sections, using a special impulse inductor [4,5].

Basically the travelling-wave test is more convenient, particularly when applied to large slow-running machines, because neither withdrawal of the rotor nor successive testing of all sections of the winding is required. On the other hand, this kind of test is usefully applied only when the turn-voltage pulses in any part of the winding are sufficiently high to test the winding insulation effectively and are obtainable with a pulse amplitude not exceeding the permissible test voltages on the frame insulation. For this reason the turn-voltage distribution over the winding affects the choice of turn insulation test method greatly.

The way various factors influence the turn-voltages in the windings of electric machines must, therefore, also be studied. Pulse tests on

* *Elektrichestvo* No.4, 75–79 (1957). [Reprint Order No. EL.8]

machines of various powers and voltage ratings were, therefore, carried out; the most typical results are tabulated below.

Set-up and test method

The data were measured on the machines with a specially designed portable set-up 10 – 1, consisting of a pulse oscillograph with built-in surge generator.

The generator provides pulses of amplitude up to 350 V, with 0.2 – 5μsec fronts and relatively flat tails at a repetition frequency of 50 c/s. The wave is applied to one end of the winding, the other end being earthed.

The time required for the wave to travel along the winding was determined by measuring the voltage at the open end. The period of the voltage oscillations from the time marks was assumed to be equal to four times the travelling time. The characteristic impedance was assumed to equal the resistance connected to the end of the winding, across which the amplitude of the voltage was half the voltage at the open end.

Minimum impulse voltages on sections

The general pulse voltage distribution on the windings of medium-power motors was investigated in the Central Electrical Research Laboratory between 1950-1952; these investigations have been reported [2,6]. In 1954-1955 the voltages set up on the winding sections of larger electrical machines were determined; these windings differ considerably from motor windings in size, of number turns in the sections, etc. The voltage across a section is determined by two factors, viz. the steepness of the wave front and the electrical length of the section. As the wave penetrates into the winding, the steepness of the front is reduced and so the section voltages decrease. Table 1 and Fig.1 illustrate the relationship between the minimum section voltage and the number of winding sections for several electrical machines.

The second factor which influences the minimum section voltages considerably is the electrical length of the section, as is seen in the table.

Therefore, we may assume that for basket (double-layer) wound machines, the section voltages depend, to a first approximation, on the number of sections per phase or parallel branch, and on the wire length in the sections.

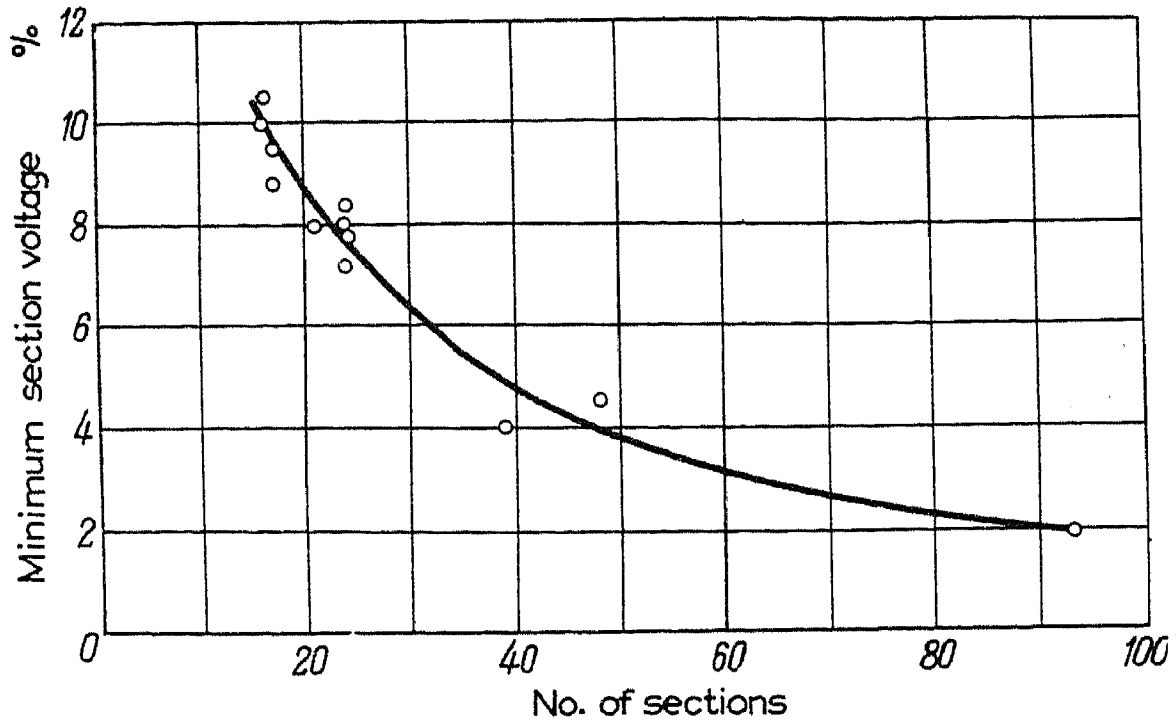

Fig. 1 Relationship between minimum voltage on section and number of sections.

Electric length of section 0.21 – 0.25 μ sec; length of wave front 0.6 μ sec.

The number of turns in the section, length of active steel, etc., do not influence the section voltages directly. But the number of turns in the section is the basic factor determining the turn voltages.

As is well known [2,6,7], pulse voltages are uniformly distributed over the turns of a section. Consequently, the turn voltages are inversely proportional to the number of turns (other things being equal).

Effect of the type of winding

The section voltage distribution in a real machine winding when a pulse is applied differs considerably from that in a circuit consisting of identical *LC* and attenuating elements. The section voltage distribution curve along the winding is not smooth but stepwise, the shape being dependent on the winding circuit and on the spatial disposition of the winding sections.

Inductive coupling between the parts of the winding is the main operative factor.

Tests on a model of part of a medium-power motor stator with inserted winding sections have shown that the sections, and hence the groups, mostly influence one another electromagnetically.

If the section ends are screened electrostatically during the tests, the section voltages are practically unaltered. Sections with sides in the same slot and parallel sections placed in a row interact most strongly. The magnetic couplings are responsible for the way in which the section couplings strongly influence the section voltage distributions. A group of sections round one pole pair has several strongly coupled parallel sections in a row. In impulse winding tests the section voltages appear related in amplitude because the group sections are strongly coupled.

Groups belonging to the various parallel branches of one phase influence one another. Several parallel branches connected to one phase show a certain rise in section voltages relative to a single branch. This is due to the increased number of grouped sections or, which is equivalent, to the stronger magnetic coupling.

When a pulse is applied to two phases, the phases influence one another. This is of great importance because when the turn insulation is tested in a bridge circuit, the pulse is usually applied to the two phases compared. The different current directions in the different phase sections lying close together produces demagnetization while reinforcement takes place when the parallel branches on one phase are used.

Modern machine winding circuits with shortened pitch use different phase sections placed in one slot. Such sections, and also the series and parallel sections of another phase determine the minima of the winding distribution curve. These minima are particularly marked when the ordinal numbers of the sections of the different phases in series are near together. The demagnetization is then caused by current pulses of similar form and amplitude because the windings shape the pulses to the same degree [8].

Fig.2 shows section voltages measured on one phase of a motor when the impulse is applied to one and to two phases. The marked minima correspond to sections placed in the same slot when the second phase sections are in circuit. Fig.2 shows that with two different phase pairs (1–2 and 1–3) the section voltage minima correspond to different phase sections, this being the object of the winding design.

It is possible to avoid section omission due to gaps in the section voltage distribution curve by testing all three phase combinations (1–2, 1–3 and 2–3) successively. In this case, the winding sections (e.g. of phase 2), which are only weakly tested with one phase pair (1–2), will be tested at the normal voltage when the second phase pair (1–3) is used.

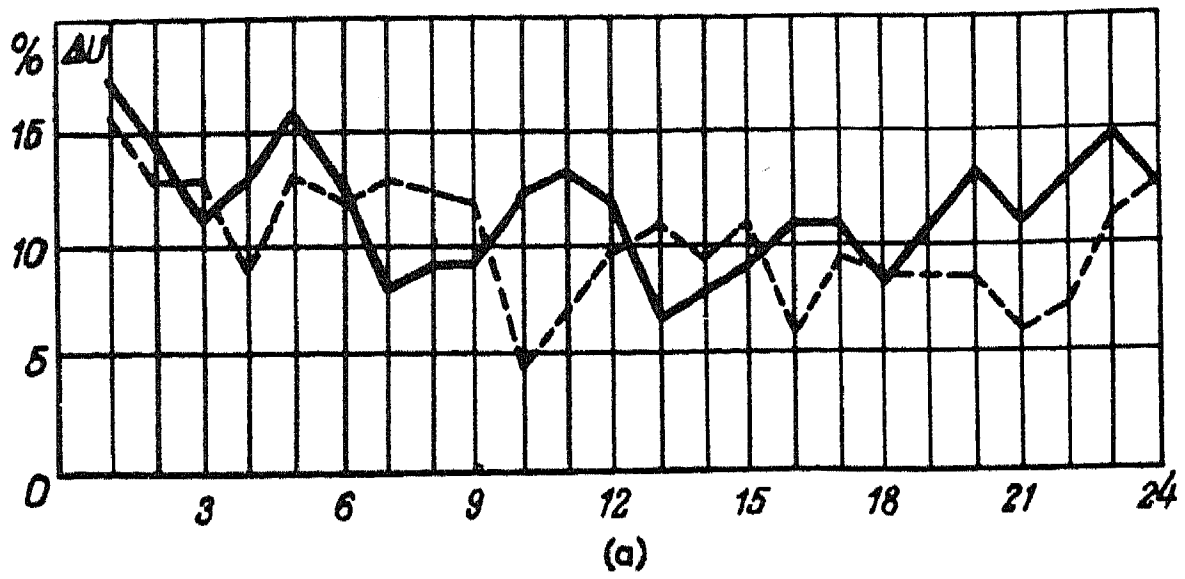

(a)

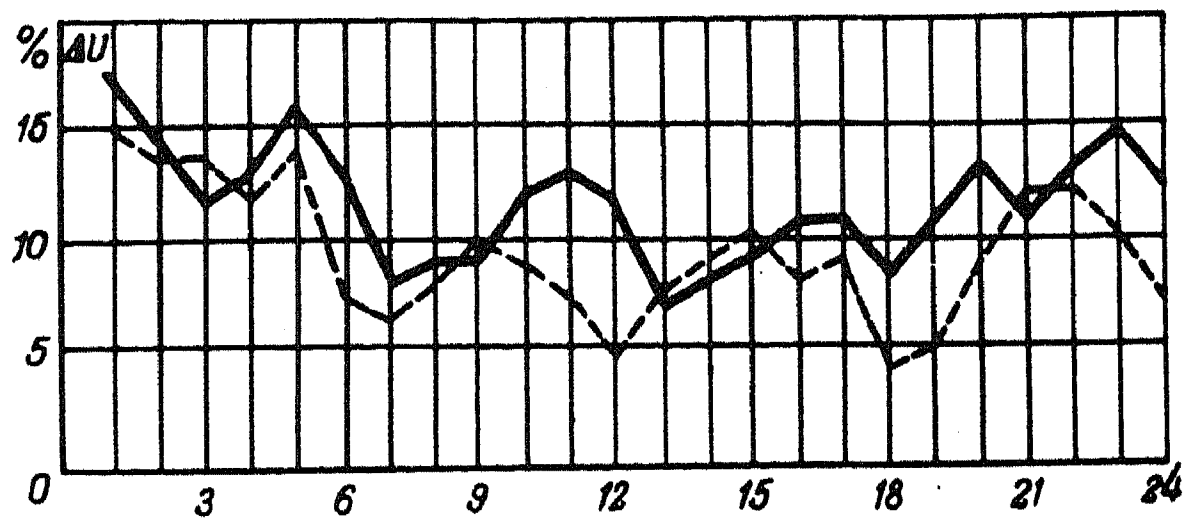

(b)

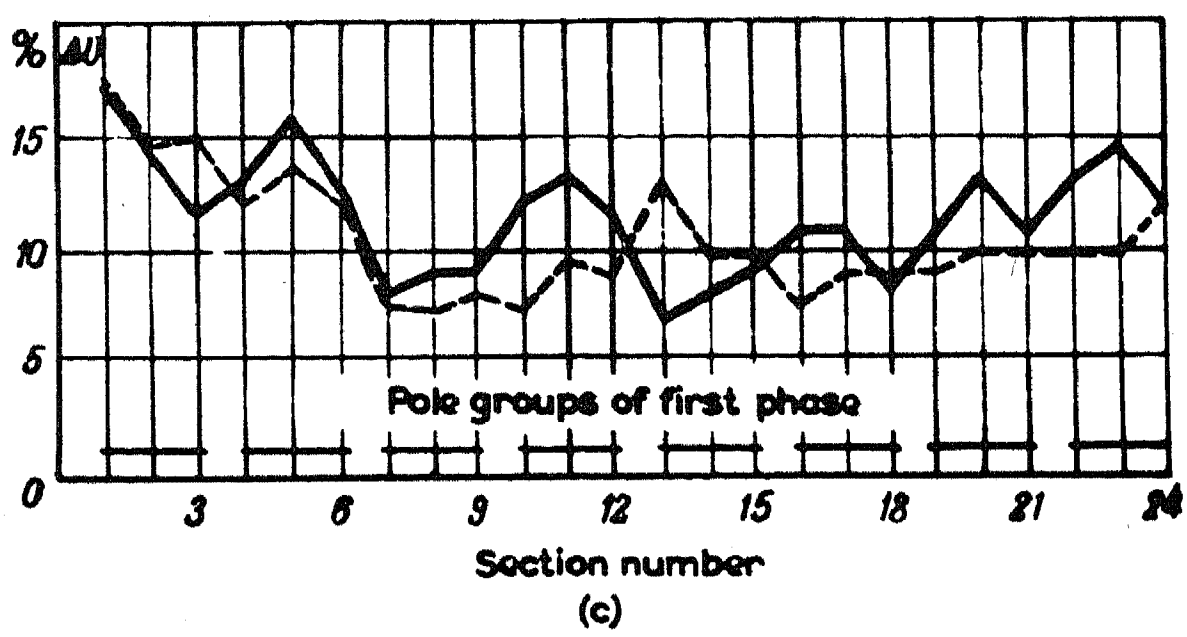

(c)

Fig. 2 Section voltages in a 1st phase branch with different testing circuits.

(a) Simultaneous test of 1st and 2nd phases;

(b) Simultaneous test of 1st and 3rd phases;

(c) Simultaneous test of 1st and 2nd phases connected in opposition.

Full lines: tests on 1st phase alone;

Broken lines: simultaneous test of phases.

There is another method by which gaps in the section voltage curve can be avoided, viz. one phase is tested together with another connected in opposition. In this case the different phase conductors in one slot will reinforce and not demagnetize one another.

The variation of minimum section voltage in a motor winding (6 kV, 200 W, 375 r.p.m.) with the test circuit is illustrated by the following data:

TABLE 1

Test	Minimum section voltage of phase 1 (%)
Phase 1 only	6.5
Phases 1 & 2 (equidirectional connexion)	4
Phases 1 & 3 (equidirectional connexion)	4
Phases 1–2 & 1–3 (general result)	7.5
Phases 1 & 3 (connected in opposition)	7.5

The most informative tests are those using two phase pairs or phases connected in opposition. The minimum section voltage then exceeds that involved in testing a single phase.

Turn insulation test voltages required

Turn insulation tests are obviously of value only if the test voltages on the turns are sufficiently high to reveal insulation defects. The voltages adopted for works tests are usually 50 per cent of the minimum breakdown voltage for new insulation of that particular thickness and structure.

There are no generally accepted recommendations for testing the insulation of machines in service. Hence tests were carried out on insulation with artificial defects, which showed that the breakdown voltage of faulty turn insulation was determined by that across the air gap between turns, and remained sufficiently high whatever the damage type. For example, the turn insulation breakdown voltages of single-layer micafolium sections after a fracture in two directions at right-angles did not fall below 900 V.

In other sections, with the turn insulation completely stripped while the conductor spacing had been maintained at the original insulation thickness, the flash-over voltage between turns remained higher than the works test voltages for section turn insulation on sections not in the same slot. Only when the inter-turn gaps are reduced to ~1/100 mm are the works test voltages sufficient to produce spark-over between turns.

At atmospheric pressure the breakdown voltage of an air gap of practically any width is never less than about 350 V max [9]. Extrapolation of an experimental curve of breakdown voltage vs. distance between two parallel 2.5 x 5.5 mm conductors gave about the same value. The curve was taken from 0.03 to 0.1 mm and extrapolated to zero.

We have therefore to consider 350 V max as the lower limit of turn-insulation test voltages; tests at lower voltages can only detect complete short-circuits.

Insulation defects between conductors at spacings up to 0.1 mm can be detected with test voltages of 350–1000 V max. So, tests at these voltages can only detect a fraction of the winding insulation defects occurring in the practice. When the inter-turn spacings are 0.01 mm (having breakdown voltages of the order of several hundred volts) the gaps may be closed by comparatively small forces. For example, the gap between the bare turns of a synchronous condenser section (6.6 kV, 15,000 kVA, 7500 r.p.m.), which had been brought close together in winding (breakdown voltage at the power frequency 480 V) was closed by applying a force of 11.3 kg, despite the considerable cross-section of the turns (sixteen conductors each of 6 mm^2 section).

It is therefore always necessary to try to raise the test turn voltages to about those used in works tests, which are determined by the turn insulation design and thickness. Lower test voltages (but not below 350 V max) are only justified when sufficiently high voltages cannot be produced by methods acceptable in practice.

Ways of turn insulation testing in electric machines

The tabulated data indicate that it is practically impossible to test the turn insulation of electric machines with travelling waves when the number of turns in the individual sections is great (nine to ten, or more). When the applied surge amplitude does not exceed the standard test voltage (i.e. 7 kV for machines rated 3 kV, 14kV for machines rated 6 kV, and 21 kV for machines rated 10 kV), the turn insulation in the centre of

the winding may receive only about 100–200 V, which is obviously insufficient. With these machines it is at present more expedient to test with induced impulsive voltage [4,5].

However, if the machines have few turns per section, travelling-wave tests are often possible. For example, with a synchronous condenser of 6.6 kV, 15,000 kVA, 750 r.p.m. minimum turn impulse voltages of about 750 V may obtain, with a hydrogenerator of 13.8 kV, 55,000 kW, 62.5 r.p.m., about 550 V; in both cases the test voltage amplitude will not exceed the values permissible for frame-winding insulation tests under service conditions.

When each phase is tested twice (in cyclic combination with each of the other two phases) the minimum turn voltages can be raised slightly, as shown above.

Summarizing, machines for which annual rotor withdrawal is not stipulated (generators, synchronous condensers) and on which turn-insulation test induction is consequently difficult to carry out, it is often possible to test by travelling-wave methods, i.e. by applying impulses to the ends of the phases.

The test turn voltages can be predicted by impulse tests during production or on rewinding. If results of such tests are not available, a decision on the advisability of using an impulse bridge-circuit for testing the turn insulation can be obtained by comparing the winding data with previously derived numerical values. Knowing the number of winding sections and the electric length of a section, the probable turn voltages may be predicted from the curve relating the section voltages to the number of sections (corrected for the electric length of a section) (Fig.1).

The above correction is unnecessary since, with sections with compounded insulation and a total conductor length $\geq$ 20 m, the electric length will usually be below 0.3 μ sec.

Determination of the electric length of a section from the wave propagation data for windings given in "Regulations on Surge Protection" may lead to incorrect results; experience shows that the true speeds may differ considerably from the average values given.

For example, for a 55,000 kW, 13.8 kV hydroelectric generator, the velocity of propagation is given as about 15 m/μ sec, but in reality it approaches 75 m/μ sec; for a 5000 kVA, 6 kV synchronous condenser, it is supposed to be about 25 m/μ sec, but is in fact not more than

14 m/μ sec. This is because the relationships on which the data are based are unrelated to the concrete features of each machine, viz. number of parallel branches, number of turns per slot, method of insulation, winding design, etc.

A method of calculation which would give the basic impulse parameters of the windings and, particularly, the wave propagation velocity from the concrete winding and design data of any machine is much to be desired.

Conclusions

(1) The minimum inter-turn test voltages for a given test surge voltage depend above all on the number of turns in the section, on the number of sections in the branch or phase, on the total wire length in the section and on the surge wave propagation velocity in the winding.

The relationship between the latter velocity and the design parameters has not yet been firmly established; in many cases the data in "Regulations on Protection against Surges" will not be sufficiently close to the measured values.

(2) The impulse voltage distribution over the winding sections depends strongly on the group sequence, which controls the strong electromagnetic coupling between winding sections.

In bridge tests using two phases of the winding, the relative disposition of the tested branch or phase sections (particularly if the pitch is shortened) has a great influence, and the current directions in the tested phases, have a marked influence; the currents in the phases or branches must have opposite directions if its section voltages are to be raised. If this is impossible, all three phase combinations must be tested.

(3) Turn insulation tests are of value only at turn voltages $\leq$ 350 V max. The main point in choosing test methods and circuits is to ensure test turn voltages about equal to those used in works tests.

(4) The preferred method for testing large electric machines, particularly hydroelectric generators with many slots, is to apply a surge voltage to the end of the winding (travelling-wave test), if this assures sufficiently high turn voltages.

(5) The inter-turn voltages expected in travelling-wave tests can be calculated approximately from the machine winding data. As a rule, the test voltages will be sufficiently high in machines with few (two to four) turns per section.

REFERENCES

1. V.A. Karasev and Z.G. Kaganov; Wave propagation in the windings of electrical machines. *Elektrichestvo* No.4 (1949).
2. G.N. Petrov and A.I. Abramov; Inter-turn voltages in the windings of electrical machines during wave processes. *Elektrichestvo* No.7 (1954).
3. A.A. Timofeenko; Set-up for testing the inter-turn insulation of electric motors. *Elektricheskie Stantsii* No.6 (1950).
4. N.V. Smirnov; *Checking and Testing Windings in Electric Machines and Apparatus*. Gosenergoizdat, 1955.
5. N.V. Smirnov; Testing the turn insulation of electric motor windings under service conditions. *Elektrichestvo*, No. 5 (1955).
6. Deckans; Investigation of surges in H.V. motors. A.S.E. – Bull. No.35 (1953).
7. G.G. Shvets and S. Gretskii; Experimental investigation of surges in the windings of electric machines. *Electrical Insulation* No.2 (1938).
8. R.C. Robinson; Distribution of impulse voltages in bar-wound high-speed turbogenerators. *Proc.Instn.Elec. Engrs.* No.77 (1953).
9. A.P. Aleksandrov *et al.* *The Physics of Dielectrics*. G.T.T.I. (1932).

VOLTAGE GRADIENTS IN A LONG-SPARK LEADER CHANNEL*

V.P. LARIONOV

The Lenin All-Union Electrotechnical Institute

(Received 11 June 1956)

Komelkov [1] was the first to show that the leader structure is rather complex in a long-gap spark in air. An extensive ionized region occurs at the tip of the narrow leader channel. This region is composed of separate streamers, i.e. thin, long channels so numerous in the case of a positive discharge that the whole ionized region resembles a cascade of luminous filaments issuing from the tip of the leader. The electrons released at the fronts of the streamers rush along the streamer ducts into the leader channel, leaving positive ions in the ionized region. As the leader penetrates more deeply into the interelectrode space, new streamers appear as the old ones are extinguished, giving an immobile space charge envelope around the narrow leader channel.

The narrow leader channel (the "core") in direct contact with the electrode provides a path along which electrons flow to the electrode in a positive discharge. The voltage gradient along the leader channel determines the ionization conditions at its tip and is therefore the most important parameter. However, this parameter has not yet been fully investigated.

The mean longitudinal gradients were studied at the All-Union Institute of Electrical Engineering by producing an artificial step in the leader channel [2]. The current in the step was first assumed to produce a state of arc-conduction in the channel, the second assumption being that the leader tip potential is unaffected by this, i.e. that the abrupt drop in spark-gap voltage at the instant of producing the step determines the voltage across the channel. Thus, the mean gradients were determined as follows:

$$E_{1m} \approx \frac{U'}{l_1} + E_a \qquad (1)$$

where U' is the abrupt drop in spark-gap voltage.

l_1 is the leader length at the moment of producing the step

E_a is the voltage gradient in the arc channel.

* *Elektrichestvo* No. 4, 80–81 (1957). [Reprint Order No. EL.9]

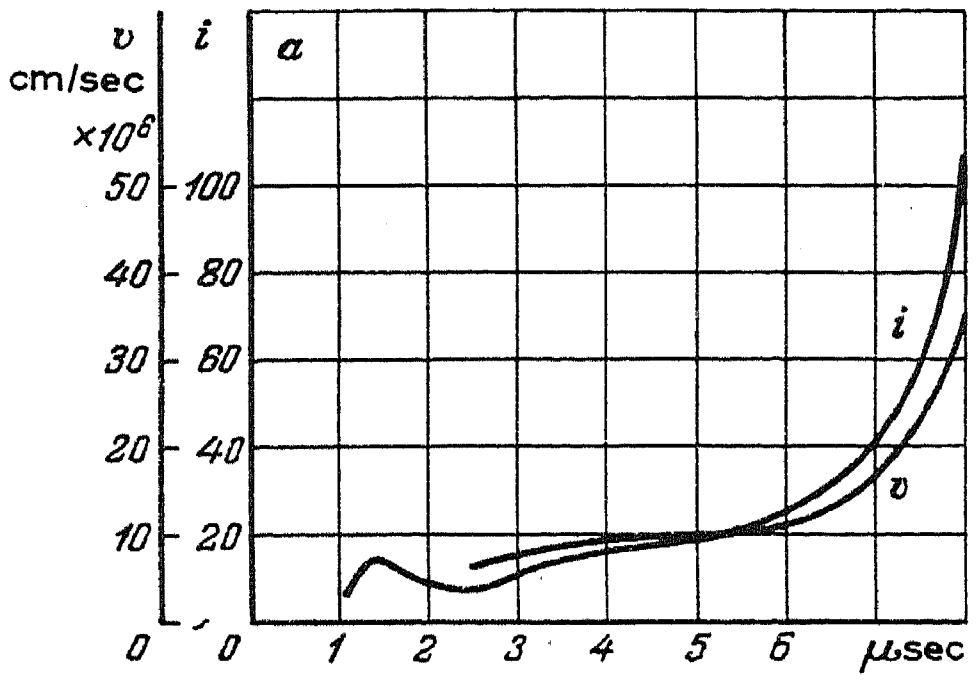

Fig. 1 Leader current and leader tip velocity. Spark gap "rod-plane", 100 cm long. Discharge circuit resistance 2.5 kΩ.

While the first assumption is certainly correct, the second is obviously without foundation. Experience shows that where the step has been formed the current and tip velocity increase considerably; this can only be attributed to an increase in field strength at the tip and therefore to an increased potential on the tip itself. The sudden voltage drop at the instant of step formation does not by any means give the full voltage across the leader channel, so the mean longitudinal voltage gradients calculated from this voltage drop are too low. Using a 200 cm rod-plane gap, the lower values obtained by this method for the mean voltage gradient along the positive leader channel when this was 120 – 140 cm long were found to be between 1200 and 1600 V/cm with discharge circuit resistances of between 140 and 400 kΩ respectively [2]. These figures show that the picture if the developing leader as a highly conducting almost equipotential channel (longitudinal gradients ~ 10 V/cm is not consistent with physical facts.

The longitudinal gradients may be expected to decrease in time owing to the increased current heating the leader channel. It is here of interest to consider the final stages of leader development.

The abrupt drop in spark-gap voltage when the main discharge strikes can be regarded as the sum of the voltage across the leader channel and the potential of its tip immediately before reaching the plane. Thus, assuming that the tip potential is zero near earth, it is possible to obtain a value, which we know to be exaggerated, for the mean longitudinal channel gradient at the instant immediately preceding the main discharge. The gradients obtained under the above test conditions were between 1000 and 1600 V/cm, regardless of the discharge resistance (in 42 tests the drop was between 230 and 370 kV).

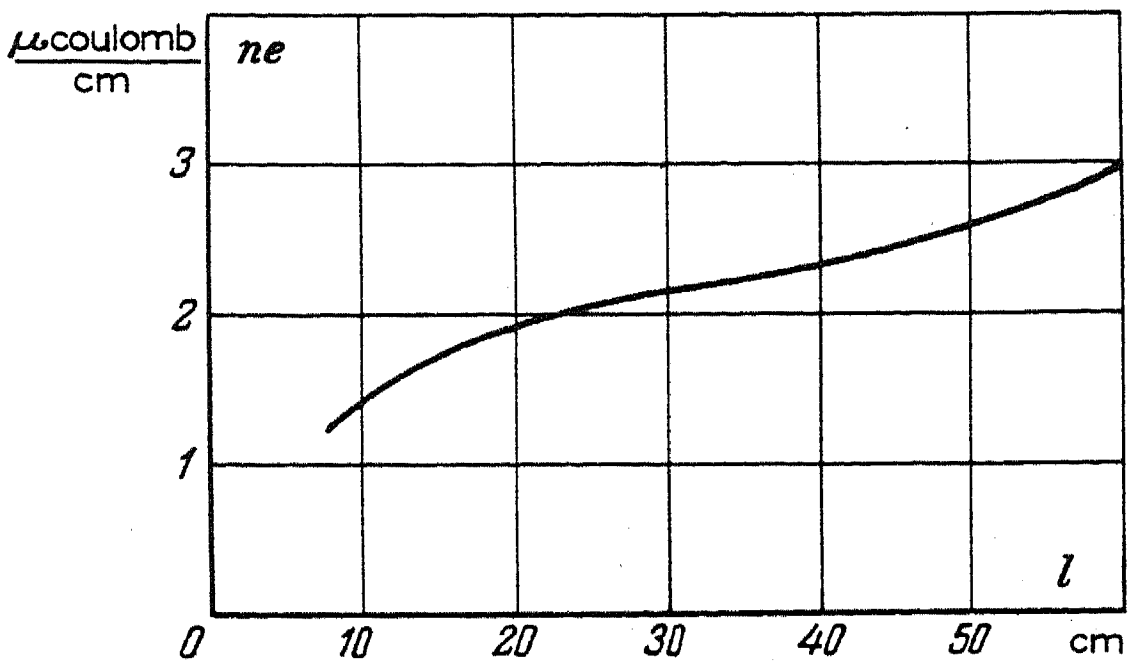

Fig. 2 Distribution of the excess positive charge along the leader (for the discharge of Fig. 1).

Thus, the *lower* limit for the mean channel gradient determined when the leader bridges 60 – 70 per cent of the spark gap is between 1200 and 1600 V/cm, and the *upper* limit, determined immediately before the leader reaches the plane, is between 1000 and 1600 V/cm. This shows that the mean longitudinal gradient decreases considerably during development.

The channel current, i, is given by $i = nev$, where v is the tip velocity, e the electronic charge and n the number of electrons leaving the channel per unit increase in length (ne is numerically equal to the linear excess positive space charge density in the leader envelope). On the other hand, i may be expressed as the number of electrons released during ionization per unit length of the leader, n', and by the electron drift velocity, v' produced by the longitudinal gradients in the channel, viz.

$$i = nev = n'ev', \quad \text{i.e.} \quad nv = n'v' \tag{2}$$

As the tip of the leader approaches the plane, the leader current and the tip velocity increase considerably. Of the two, the current grows more rapidly, which means that the linear density of excess charge increases in the lower part of the leader. The variation in leader current and tip velocity in the rod-plane gap is shown in Fig. 1. In 5 μsec (from 3 μsec to 8 μsec) the current increases ten times, the tip velocity five times, and their ratio $ne = i/v$ two times. The distribution of linear excess charge density along the whole channel for the same discharge is shown in Fig. 2.

v' is less than v [3]. An increase in ne along the leader channel therefore means, in accordance with (2), an increase in n' in the channel plasma.

Let us consider the discharge records for the rod-plane gap shown in Fig.3. The records were obtained with a high-speed rotating camera with a 'Jupiter-3' lens, by the well-known method [1] of photographing simultaneously through a number of slits at different distances from the plane. The records show that at any particular instant (the times are determined by reference to the instant when the main discharge strikes) the channel diameter ("core") is almost constant throughout the length.

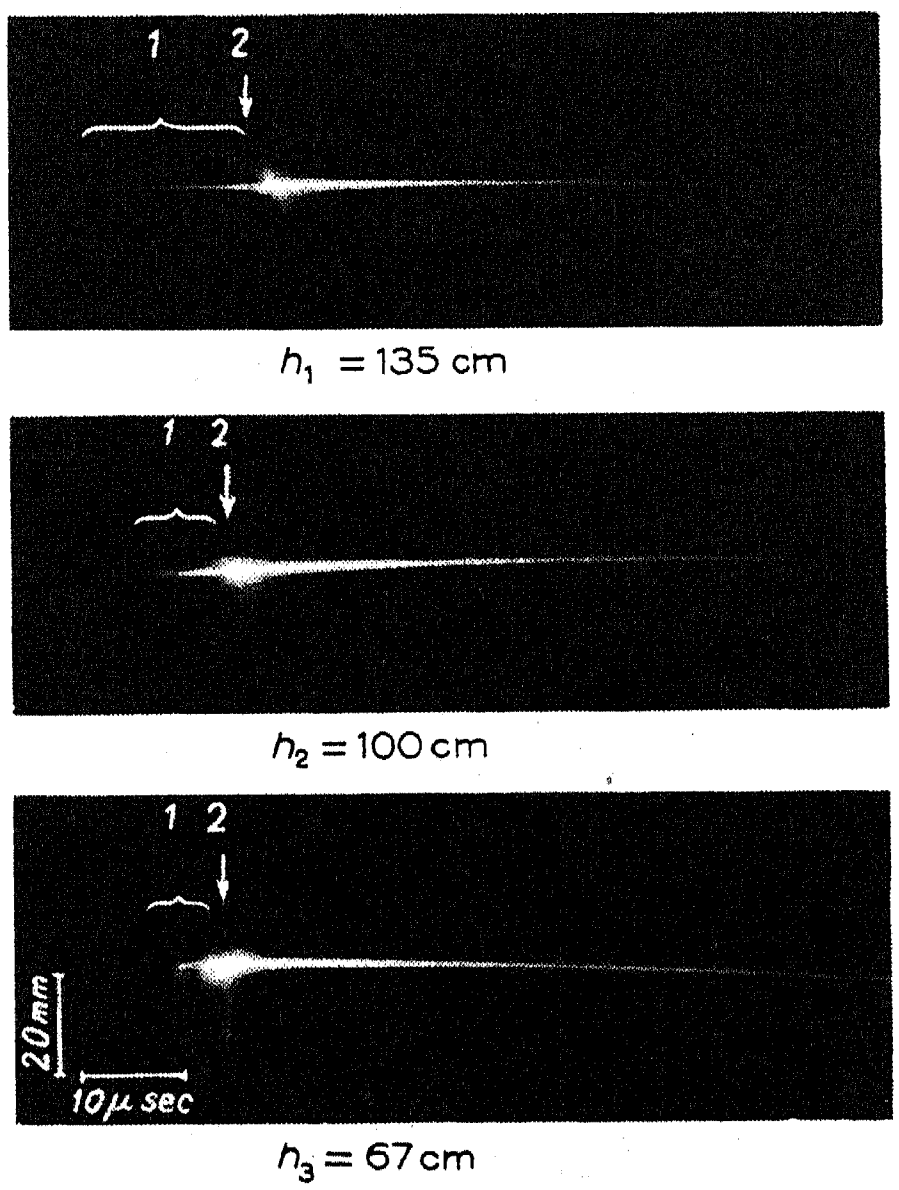

Fig.3 Time-base records for the leader channel. Rod-plane gap, 150 cm long. Discharge circuit resistances 28 kΩ; h = distance, between the leader tip and the plane; 1 - leader stage of the discharge; 2 - main discharge. Side branches round the main channel are visible in the bottom record.

The higher linear electron density in the lower part of the channel (of constant diameter), indicates a higher conductance and a lower longitudinal voltage gradient. The initial voltage gradients therefore vary along the leader channel, being higher at the top, and lower at the bottom. The gradients should fall with time, particularly in the older parts of the channel, owing to thermal ionization.

Since the linear excess positive ion density is constant ($ne = i/v \approx$ const.) Loeb [3] assumes the leader channel homogeneous throughout its length and the voltage gradients constant along the channel.

REFERENCES

1. V.S. Komelkov; The structure and parameters of the leader discharge. *Izv. Akad. Nauk SSSR* (Technical Sciences Section) No.8(1947).
2. V.P. Larionov; The impulse discharge mechanism in a long air gap. *Elektrichestvo* No.7 (1952).
3. L.B. Loeb; Some aspects of breakdown streamers. *Phys. Rev.* **94**, No.2 (1954).

MEASUREMENT OF EARTH RESISTANCES*

A.B. OSLON

Zlatoust

(Received 28 August 1955)

A three-electrode circuit is used to measure the resistances of an earthing system, these being: the earth electrode (earthing circuit), the current electrode and the potential electrode. All quantities referring to the earth electrode are denoted by the K, those referring to the current electrode by subscript T and those referring to the potential electrode by P.

Current is passed through the earth and current electrodes. The potential of the circuit is measured via the potential electrode. The earth resistance equals the measured potential divided by the current passing.

In Fig.1 the voltmeter and ammeter are instruments specially designed for measuring the resistances of earthing systems.

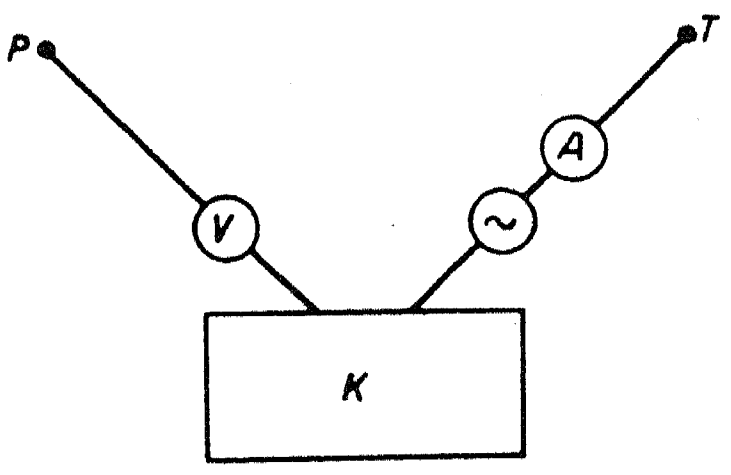

Fig. 1.

It is usually assumed that the current and earth electrodes must be sufficiently far apart not to distort the field and that a sufficiently large zero potential zone remains between them. The potential electrode must be placed in the zero potential zone [1,2].

Let us assume that we already know the earth resistance of the circuit R_K. Is it then possible, having placed the current electrode at an arbitrary point, to so locate the potential electrode that the measured resistance is equal to R_K? If this is possible, how can we determine the 'locus of precise measurements'?

To answer this question we will use the analogy between an electrostatic field and the field due to a current in a conducting medium.

* *Elektrichestvo* No. 2, 56–58 (1957). [Reprint Order No. EL. 10]

Maxwell's equations with potential coefficients for the three electrodes are

$$\phi_K = \alpha_{KK} I_K + \alpha_{KT} I_T + \alpha_{KP} I_P$$

$$\phi_T = \alpha_{TK} I_K + \alpha_{TT} I_T + \alpha_{TP} I_P$$

$$\phi_P = \alpha_{PK} I_K + \alpha_{PT} I_T + \alpha_{PP} I_P$$

Current flow from the electrodes into the ground is taken as positive:

Neglecting the current drawn by the voltmeters we get:

$$I_P = 0, \quad I_T = -I_K$$

The measured resistance is

$$R_{\text{meas}} = \left| \frac{\phi_K - \phi_P}{I_T} \right|$$

Assuming $\alpha_{12} = \alpha_{21}$, we have

$$R_{\text{meas}} = \alpha_{KK} + \alpha_{TP} - \alpha_{KT} - \alpha_{KP} \qquad (1)$$

The actual earth resistance

$$R_K = \alpha_{KK}$$

If $R_{\text{meas}} = R_K$, the following condition must be satisfied:

$$\alpha_{TP} = \alpha_{KT} + \alpha_{KP} \qquad (2)$$

Equation (2) is the answer to our question. From this we can draw the following conclusions:

(a) It is theoretically possible to measure earth resistances accurately when the measuring and earth electrodes are placed arbitrarily close together

(b) When the measuring electrodes have been placed in a certain way, the result of the measurement is independent of which is the current electrode and which the potential electrode.

From (a) it follows that the measurement may be accurate even when the current electrode distorts the field of the earth electrode, and from (b) that the second electrode need not necessarily be placed in a zone of zero potential.

We will demonstrate the usefulness of (b) for any measurement performed by the 'three-point' method used for obtaining potential distributions in the field, measuring the footing-resistances of steel towers connected through earth wires, when the earthing circuit is disconnected from the base of the tower, etc. For this purpose we will represent the measuring circuit as a passive four-terminal network, all elements being linear over the entire current range. In Fig.2, 1′ and 2′ represent the earth electrode, 1 the current electrode and 2 the potential electrode.

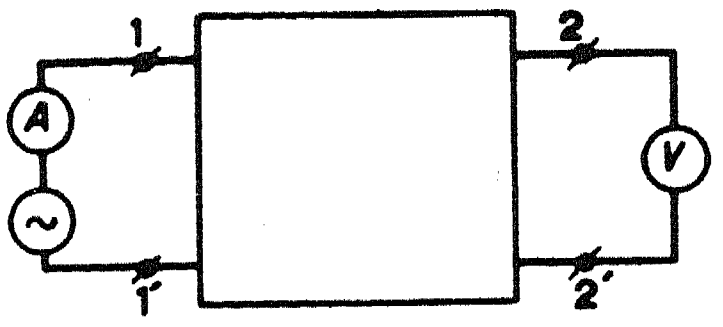

Fig. 2

The following relationships apply to such a four-terminal network:

$$U_1 = AU_2 + BI_2, \quad I_1 = CU_2 + DI_2$$

Assuming $I_2 = 0$, we get

$$R_{\text{meas}} = \frac{U_2}{I_1} = \frac{I}{C}$$

Let us reverse the current and potential electrodes, (Fig.3). We then get

$$U_2 = DU_1 + BI_1, \quad I_2 = CU_1 + AI_1$$

then $I_1 = 0$ and

$$R'_{\text{meas}} = \frac{U_1}{I_2} = \frac{I}{C}$$

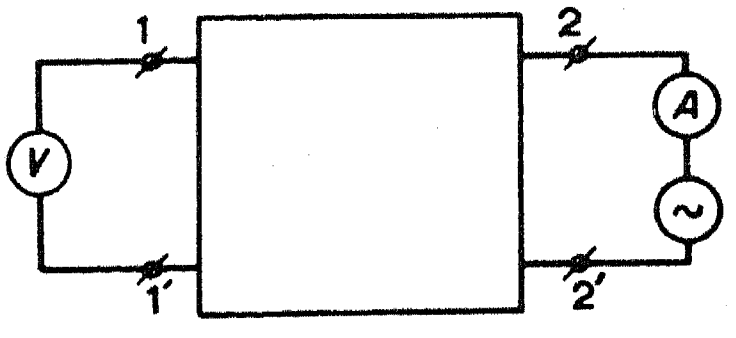

Fig. 3

The identity $R_{\text{meas}} = R'_{\text{meas}}$ is the most general demonstration of (b).

We give below examples of electrode sitings satisfying equation (2). In the examples the soil is assumed to be homogeneous and of resistivity ρ.

A concentrated earth electrode

An earth electrode will be termed concentrated if its field is radial and spherical, at a short distance away (~ a few metres). At this distance (2)

$$\alpha_{KM} = \frac{\rho}{2\pi r_{KM}}$$

where r_{KM} is the distance (subscript M denoting any measuring electrode).

Since the measuring electrodes are concentrated electrodes, we always have

$$\alpha_{KP} = \frac{\rho}{2\pi r_{KP}}$$

These expressions and equation (2) show that for the earth resistance measurement to be accurate we must have

$$\frac{1}{r_{TP}} = \frac{1}{r_{KT}} + \frac{1}{r_{KP}} \qquad (3)$$

or

$$r_{TP} = \frac{r_{KT}\, r_{KP}}{r_{KT} + r_{KP}}$$

In practice it is desirable that the total lead length to the measuring instrument ($r_{KT} + r_{KP}$) should be a minimum, this being the case when $r_{KT} = r_{KP}$.

If r_{KT} must not be less than a certain value for some reason, the same condition must be imposed on r_{KP}, since the conditions applying to both electrodes are similar. In this case

$$r_{TP} = \frac{r_{KM}}{2} \qquad (4)$$

The relative positions of the electrodes are indicated in Fig.4.

A radial earth electrode

The equipotential lines of a radial earth electrode on the surface of the ground are ellipses, so

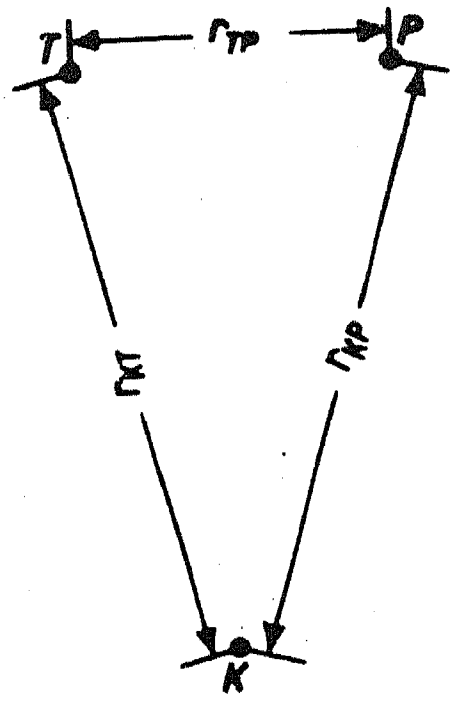

$$\phi = \frac{I\rho}{4\pi c} \ln \frac{a + c}{a - c}$$

where a is the semi-major axis, and "c" the focal distance, equal to the length of the earth electrode l; instead of 8π we took 4π, because the ground represents a half-space.

Hence,

$$\alpha_{KM} = \frac{\rho}{2\pi l} \ln \frac{2a + l}{2a - l}$$

Fig. 4. Recommended positions for the measuring of electrodes when testing a small earth electrode $r_{TP} = r_{KP}/2 = r_{KT}/2$.

where $2a$ is the sum of the distances from the measuring electrode to the ends of the radial earth electrode.

We will measure r_{KM} from the mid-point of the earth electrode.

When $r_{KT} = r_{KP}$ (Fig. 5)

$$\alpha_{KM} = \frac{\alpha_{TP}}{2} = \frac{\rho}{4\pi r_{TP}} = \frac{\rho}{8\pi x} = \frac{\rho}{2\pi l} \ln \frac{2a + l}{2a - l}$$

where x and y are the co-ordinates of the measuring electrode in the first quadrant.

Hence,

$$x = \frac{i}{4 \ln \frac{a2a + l}{2a - l}}$$

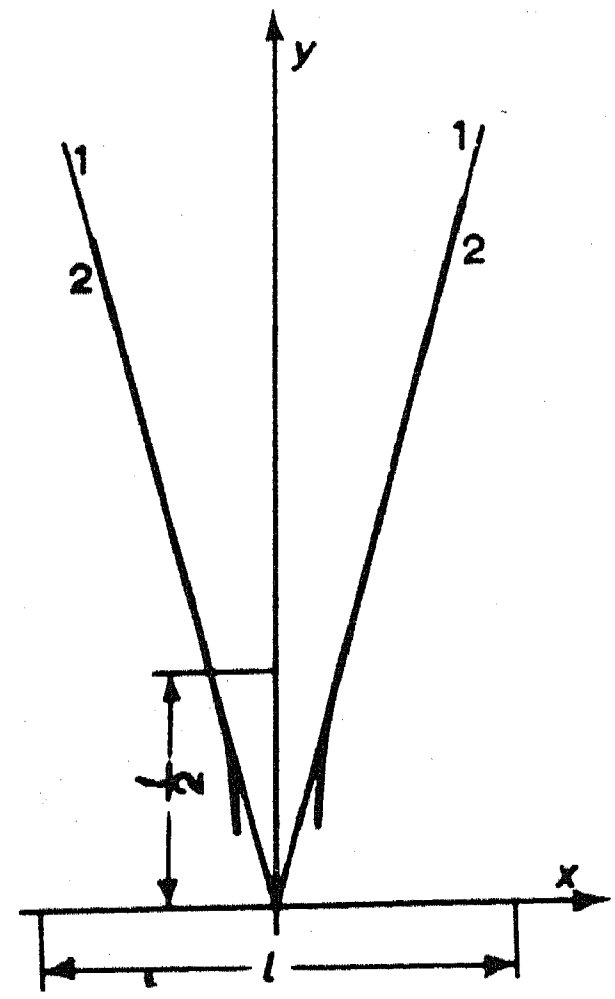

Fig. 5. Resistance measurement for a radial earth electrode. 1. Lines along which equation (4) is satisfied for symmetrically disposed electrodes. For these, $x' = y'\sqrt{15}$; 2. Lines of accurate measurement (columns 3 and 4 of table).

We will find the relation between x and y which assures accurate measurements. From the equation of an ellipse

$$\frac{x^2}{a^2} + \frac{y^2}{b^2} = 1$$

we have

$$y = \sqrt{\frac{b^2(a^2 - x^2)}{a^2}}$$

We have, therefore, obtained a single-valued solution applicable to measuring electrodes disposed symmetrically about the y-axis.

The measured data are given in the first six columns of the following table. As fundamental datum we took the semi-minor axis b of the ellipse.

All distances are in metres.

α/ρ emphasises that the result is independent of the character of the soil (ρ is measured in ohm-metres).

TABLE 1

b	a	x	y	$\frac{\alpha_{PT}}{\rho}$	$\frac{\alpha_{KM}}{\rho}$	x'	$\frac{\alpha'_{PT}}{\rho}$	$\Delta R_K'\%$
2.5	10.6	1.41	2.47	0.00564	0.0282	0.63	0.126	77.4
5	11.2	1.73	4.94	0.0460	0.0230	1.27	0.0625	18.3
10	14.1	2.8	9.8	0.0284	0.0142	2.53	0.0315	3.44
20	22.4	5.2	19.4	0.0154	0.0077	5.0	0.0158	0.45
30	31.6	7.6	29	0.0104	0.0052	7.47	0.0106	0.22

Let us assume that $l = 20$ m, the earth electrode diameter to be $d = 1$ cm, sunk to a depth $t = 50$ cm.

For a radial earth electrode (1)

$$R_K = \frac{\rho}{2\pi l} \ln \frac{l^2}{dt}$$

In our case $R_K = 0.09\rho$.

The table shows that when x has the values given in column 3, we get, with the values of y in column 4, $\alpha_{BT} = 2\alpha_{KM}$ and $\Delta R_K = 0$.

The last three columns show the error of measurements when the electrodes are placed to correspond with equation (4), i.e. on the lines 1 (Fig.5). y' is assumed equal to y, in which case we get practically $\alpha'_{KM} = \alpha_{KM}$.

The table shows that when the electrodes are arranged to correspond with equation (4), distances of $l/2$ from the mid-point of the radial earth electrode to the measuring electrodes are sufficient to assure an accuracy of 5 per cent.

Circuit consisting of linear horizontal segments (polygon, star, etc.)

Each linear segment i sets up a potential

$$\phi_i = \frac{I_i \rho}{2\pi l_i} \ln \frac{2a_i + l_i}{2a_i - l_i}$$

the measuring electrode where $2a_i$ is the sum of the distances from the measuring electrode to the ends of segment i;

l_i being the length of segment i;
I_i the current flowing from it into the ground.

The potential set up at the measuring electrode by the whole circuit becomes

$$\phi_{KM} = \sum \phi_i = \frac{\rho}{2\pi} \sum \frac{I_i}{l_i} \ln \frac{2a_i + l_i}{2a_i - l_i}$$

Let us assume $I_i/l_i = I_K/L$, where $L = \Sigma l_i$. Then,

$$\alpha_{KM} = \frac{\phi_{KM}}{I_K} = \frac{\rho}{2\pi L} \ln \Pi_i \frac{2a_i + l_i}{2a_i - l_i}$$

Where Π is the product sign.

We use a rectangular circuit to show that a correct choice of distance from the circuit will give a satisfactory accuracy when the electrodes are placed in accordance with equation (4). Distances are measured from the centre of the circuit.

Fig.6 shows a rectangular earthing system and also two possible locations for the measuring electrodes. We know [3] that for such a system

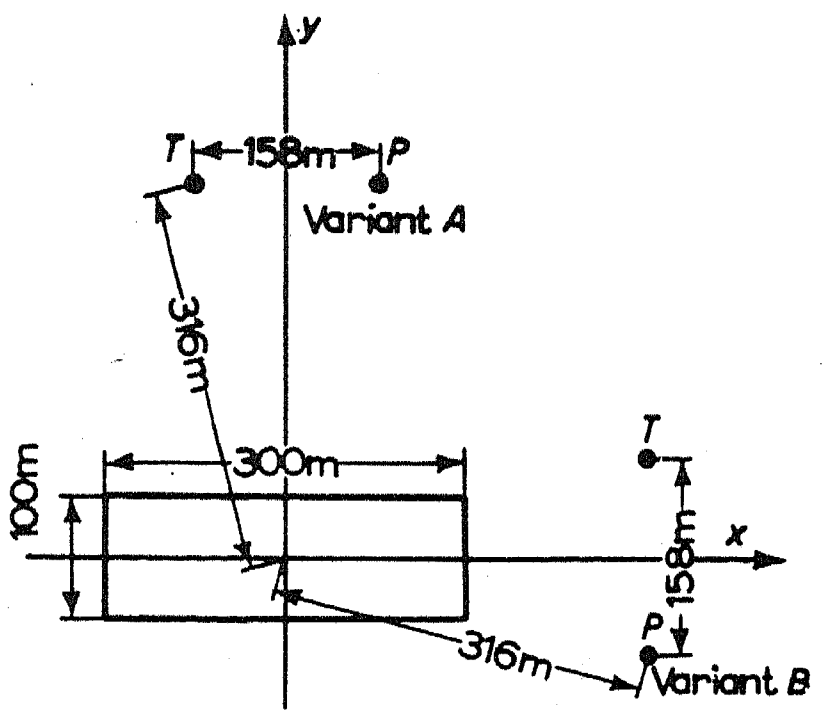

Fig.6. Earth resistance measurement on a rectangular earthing system.

$$R_K = \frac{\rho}{2\pi L} \ln \frac{8L^2}{\pi b t}$$

where L is the perimeter of the circuit;
b the width of the earthing strip; t the depth to which it is sunk in the earth.

In our case L = 800 m, b = 50 mm, t = 50 cm. With these parameters, $R_K = 3.58 \times 10^{-3}\rho$.

The above formulae give

	α_{KM}/ρ	α_{TP}/ρ	ΔR_K '
Variant A	0.050×10^{-3}	1.06×10^{-3}	1.7
Variant B	0.574×10^{-3}	1.06×10^{-3}	2.5

By using additional internal strips, vertical earth electrodes, etc. the earth resistances may be reduced, but it cannot be less than the resistance of a hemisphere of diameter equal to the circuit diagonal D = 316 m, for which

$$R_K = \frac{\rho}{\pi D} = 10^{-3}\rho$$

In this extreme case the error reaches 8.8 per cent for B. In general an error of 10 per cent is regarded as acceptable [1,3,4].

In the literature [2–4] recommended for use, when measuring the resistance of the earthing of large objects

$$r_{KP} \geqslant 5D; \quad r_{TP} = 40 \text{ m}; \quad r_{KT} \geqslant (5D + 40) \text{ m}$$

These cause exceptionally large errors. Indeed, we would get in our case

$$r_{KP} = 1580 \text{ m}, \quad \alpha_{KP} = \frac{\rho}{2\pi r_{KP}} = 0.1 \times 10^{-3}\rho; \quad r_{TP} = 40 \text{ m}, \quad \alpha_{TP} =$$

$$= \frac{\rho}{2\pi r_{TP}} = 4 \times 10^{-3}\rho$$

$$r_{KT} = 1620 \text{ m}, \quad \alpha_{KT} = \frac{\rho}{2\pi r_{KT}} \approx 0.1 \times 10^{-3}\rho; \quad \Delta R_K = \alpha_{TP} - \alpha_{KP} - 3_{KT} =$$

$$= 3.8 \times 10^{-3}\rho$$

$$\Delta R_K{}' = \frac{\Delta R_K}{R_K} 100 = 3.8 \times 10^{-3}\rho / 3.58 \times 10^{-3}\rho \times 100 = 106\%$$

and in the extreme case for $R_K = 1 \times 10^{-3}\rho$

$$\Delta 3_K = 380 \text{ per cent}$$

So in measuring the earth resistances of large objects the distance between the measuring electrodes and the centre of the system must not be shorter than the diagonal of the earth contact, and the interelectrode distance not less than half this.

REFERENCES

1. K.I. Lur'e; *Testing the Earth Connections of Electrical Plant.* Gosenergoizdat (1950).
2. K.A. Krug; *Fundamentals of Electrical Engineering.* Gosenergoizdat (1946).
3. L.N. Baptiddnov and V.I. Tarasov; *The Electrical Equipment of Power Stations and Sub-stations* Vol.II, Gosenergoizdat, (1948).
4. *Protection of Industrial Plants and Buildings against Lightning* (Edited by I.S. Stekol'nikov) Akad. Nauk SSSR (1951).

AUTOMATION OF ELECTRIC DRIVES FOR BUCKET-CHAIN DREDGERS*

L.F. SHKLIARSKII

Bauman Higher Technical College, Moscow.

Automatic load drive and manoeuvring winch control is a current problem in ensuring maximum dredger productivity.

Attempts† had earlier been made to render the drive control automatic, e.g. in 1937 in the "Primorzoloto" trust [1]. They were based on the use of fluid flywheels with servomotors actuated by current relays in the stator circuit of the bucket chain drive motor. Such a stepwise control could not be widely used in practice††.

Therefore the output control required by the soil variations is performed manually in most induction-motor dredgers, viz. by altering the lateral feed rate. Rheostats are used in the manoeuvring winch rotor circuit, the bucket drive motor speed being constant.

The automatic control system described below is based on the manual one, viz. that the lateral feed rate must change with the soil properties, the bucket drive speed being kept practically constant to ensure maximum productivity.

---

* *Elektrichestvo* No.1, pp.22-25, (1957).

† Only a.c. driven dredgers are considered.

†† A design for 0.23 m^3 bucket (1949: "Sibelektromontazh" trust) for both d.c. (generator + motor) and a.c. systems. Provided for automatic rheostat control of the maneouvring winches. But the IZTM works adopted the d.c. drive system for industrial production.

[Reprint Order No. EL.11]

Field tests by the author in 1951, 1954 and 1955 on excavators in the Northern and Southern Urals gave approximate relationships between power, current and torque for bucket- and manoeuvring-winch drives, from which the winch motor characteristics could be more accurately defined. These requirements are specified below.

When, for example the buckets are incompletely filled during excavation and therefore the bucket motor load is lower, the bucket load must be increased by increasing the pressure on the ground, i.e. by increasing the latersl feed rate. On the other hand when the buckets become too full the lateral feed rate must be reduced.

Moreover, the desirability of limiting the bucket and manoeuvring winch drive overloads on encountering obstacles in the ground also calls for a reduction in lateral feed. The manoeuvring winch drives must therefore have flexible characteristics.

This can be checked from the field tests characteristics, one of which is shown in Fig.1.

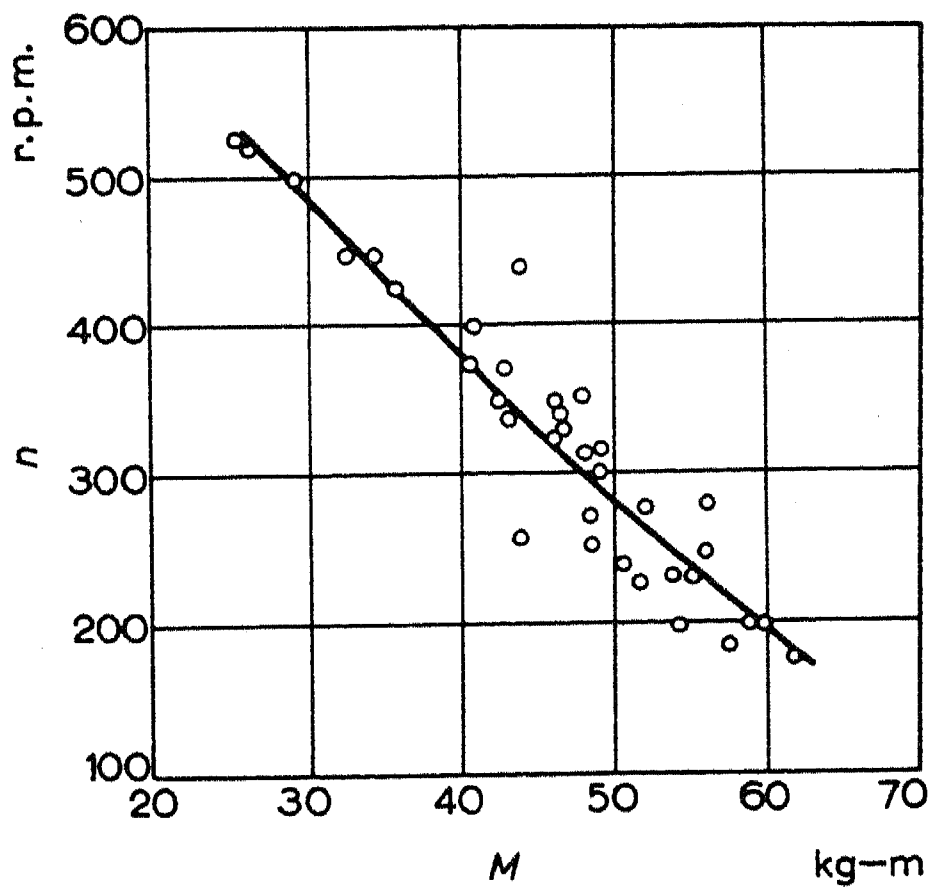

Fig.1. Mechanical characteristics of a manually controlled winch motor on a dredger with 0.38 m^3 buckets. Motor ratings P_n = 25.8 kW, n_n = 575 rev/min, M_n = 44 kg m.

The maximum winch motor torque must not exceed the value permitted by the winch rope strength. This means it must stall at $M_{max} = 1.5\ M_n$.

Thus the characteristic must approximate to hyperbolic, the stalling torque being M_{max} (at $n = 0$).

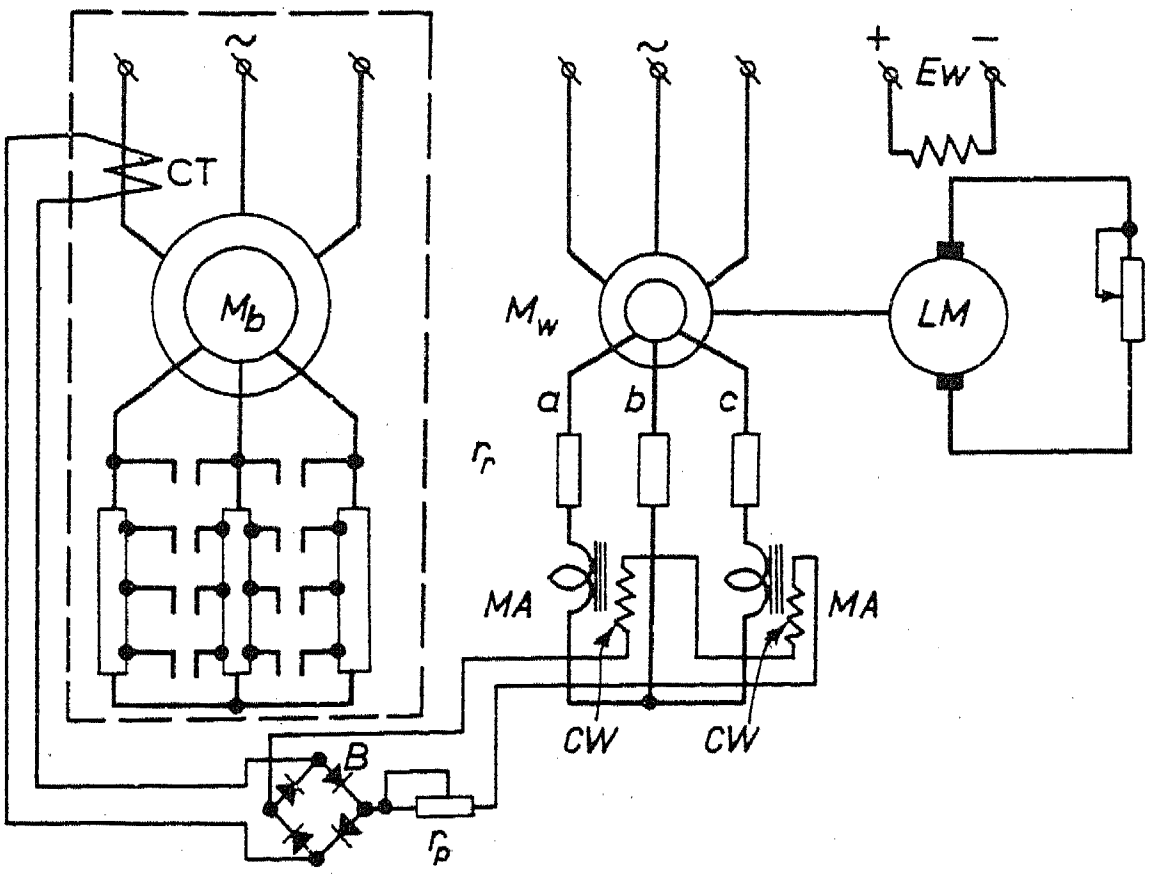

Fig. 2. Basic circuit diagram of the laboratory test set-up.
M_w: winch motor; *LM*: loading machine;
M_b: bucket drive motor replaced by a rheostat in the laboratory.

Control of the winch drive motor with a resistor r_r in series with the rotor and magnetic amplifiers (MA, Fig. 2) is the most suitable as regards motor temperature rise and automatic control of characteristics as a function of bucket drive motor load assuming that slipring-type induction motors are used for driving the manoeuvring winch.

The magnetic amplifier control windings *CW* are fed via a metal rectifier *B* from the current transformer *CT* in the bucket drive stator circuit. The manoeuvring winch motor M_w is controlled automatically by the bucket drive stator current.

This system does not require the existing electrical equipment to be rearranged, and is not very expensive. A number of alternative reactor-controlled slipring motors with different saturable reactors in the rotor circuit have been studied to determine the minimum capital outlay, weight and space requirements. This work led to the two-phase saturable reactor system (two single-phase a.c. windings on a common core, (Fig. 2) being adopted. The curves for M_w at different control currents i_c are shown in Fig. 3.*

---

* The induction motor used in the laboratory tests was a type AK-51-6, P_n = 1.7 kW, n_n = 905 rev/min, U_n = 220/380 V, I_1 = 8.5/3.8 A, η = 0.725, p.f.== 0.72, I_2 = 20.2 A, E_2 = 57 V, stalling torque/normal torque = 2, x_s = 11.3 Ω, r_1 = 5.5 Ω, r_2 = 6 Ω. Ratings of the loading machine: Type PN 28.5, P_n = 2.8 kW, U_n = 220 V, I_n = 15.8 A, n_n = 1500 rev/min.

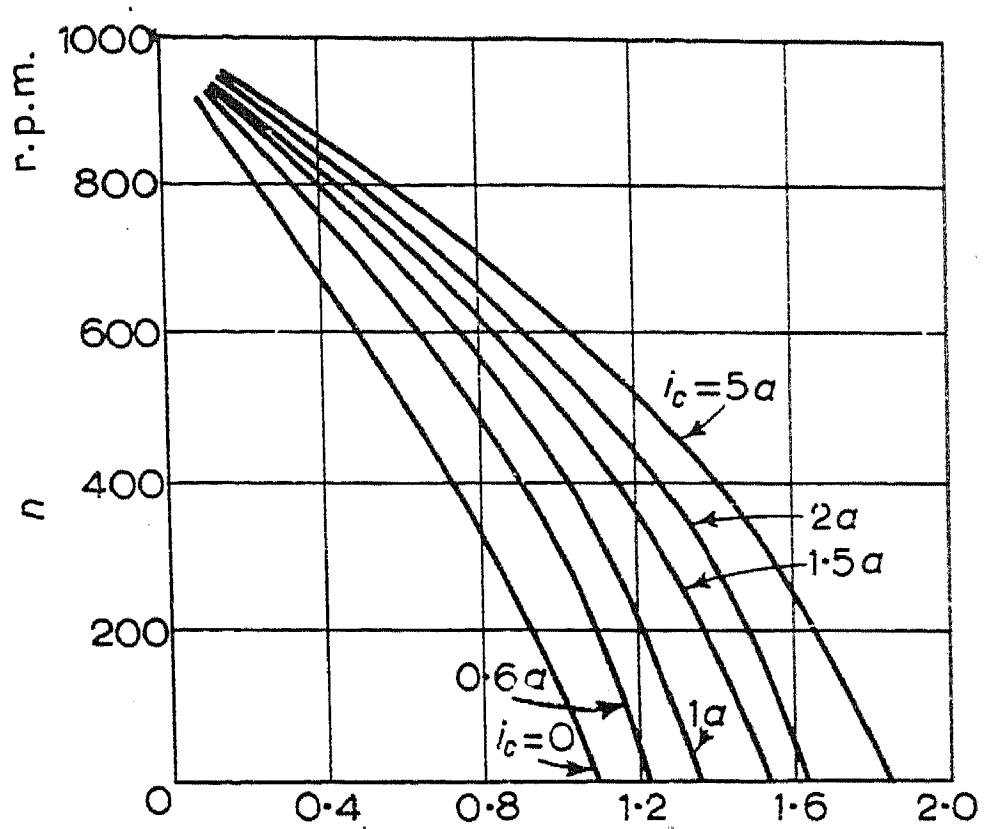

Fig. 3. Experimental mechanical characteristic of M_w in the circuit of Fig. 2 for different control currents, i_c.

The system with asymmetric (two-phase) control reactances (MA) in the rotor circuit may be analysed via the symmetrical components method [2]. Although the general theory of induction motor operation with asymmetry in the secondary circuit has been fully treated in the literature [3–6], no expression for the torque applicable to this case and convenient for practical use has yet been given. Therefore we derive below an expression for the torque as a function of slip, based on the equivalent circuit for a forward rotating field (positive phase-sequence), Fig. 4(a), and for a reverse rotating field (negative phase sequence), Fig. 4(b).

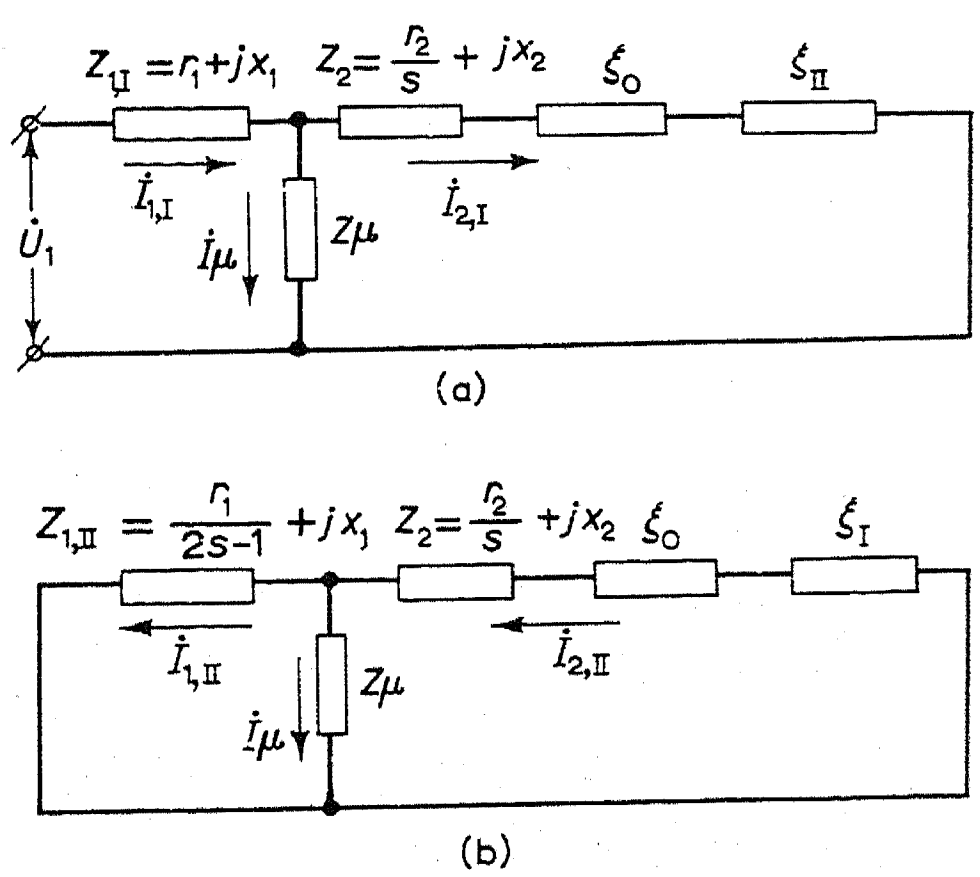

Fig. 4. Equivalent circuit of the induction motor for the direct (a) and the inverse field (b).

The equivalent impedances of the zero, positive and negative phase sequences ξ_0, ξ_I, ξ_{II}, respectively, which are determined by the magnetic amplifier reactances x_a and x_c in the two rotor phases, can be written as follows:*

$$\xi_0 = j\,\frac{x_a + x_c}{3} \tag{1}$$

$$\xi_I = j\,\frac{x_a + a^2 x_c}{3} \tag{2}$$

$$\xi_{II} = j\,\frac{x_a + x_c}{3} \tag{3}$$

From the equivalent circuits of Fig.4, neglecting the magnetizing current ($I_\mu = 0$), some simple steps give the torque as:

from the direct field

$$M_I = K\,\frac{(r_2/2)(c^2 + b^2)}{(a_c - b^2 + d)^2 + b^2(a + c)^2}\;; \tag{4}$$

from the inverse field

$$M_{II} = K\,\frac{\dfrac{r_1}{(2_s - 1)d}}{(a_c - b^2 + d)^2 + b^2(a + c)^2}\;; \tag{5}$$

where

$$K = \frac{mV_1^2}{9.81\omega}\;; \qquad a = r_1 + \frac{r_2}{s}\;;\dagger \qquad b = x_s + \frac{1}{3}(x_a + x_c)\;;$$

$$c = \frac{r_1}{2s - 1} + \frac{r_2}{s}\;; \qquad d = \frac{1}{9}\left[(x_a - x_c)^2 + w_a w_c\right]$$

---

* The resistances of the a.c. windings on the magnetic amplifier are neglected.

† r_2 includes the internal resistance of the rotor phase as well as the external series resistances r_r.

The total torque is the algebraic sum of the forward and reverse torques, i.e.

$$M = M_{\mathrm{I}} + M_{\mathrm{II}} \tag{6}$$

equations (4),(5) and (6) therefore enable us to derive the mechanical characteristics for different signals at the magnetic amplifier inputs which determine the corresponding reactances x_a and x_c.

The experimental curves (Fig.3) show that there is practically no undesirable torque drop due to core saturation [7-8] in the half-synchronous speed range. The torque drop can therefore be neglected in calculating the mechanical characteristics.

This system (Fig.2) makes it possible to obtain the desired winch motor characteristic automatically, (e.g. similar to that shown in Fig.1) and to satisfy the requirements laid down at the beginning of the article.

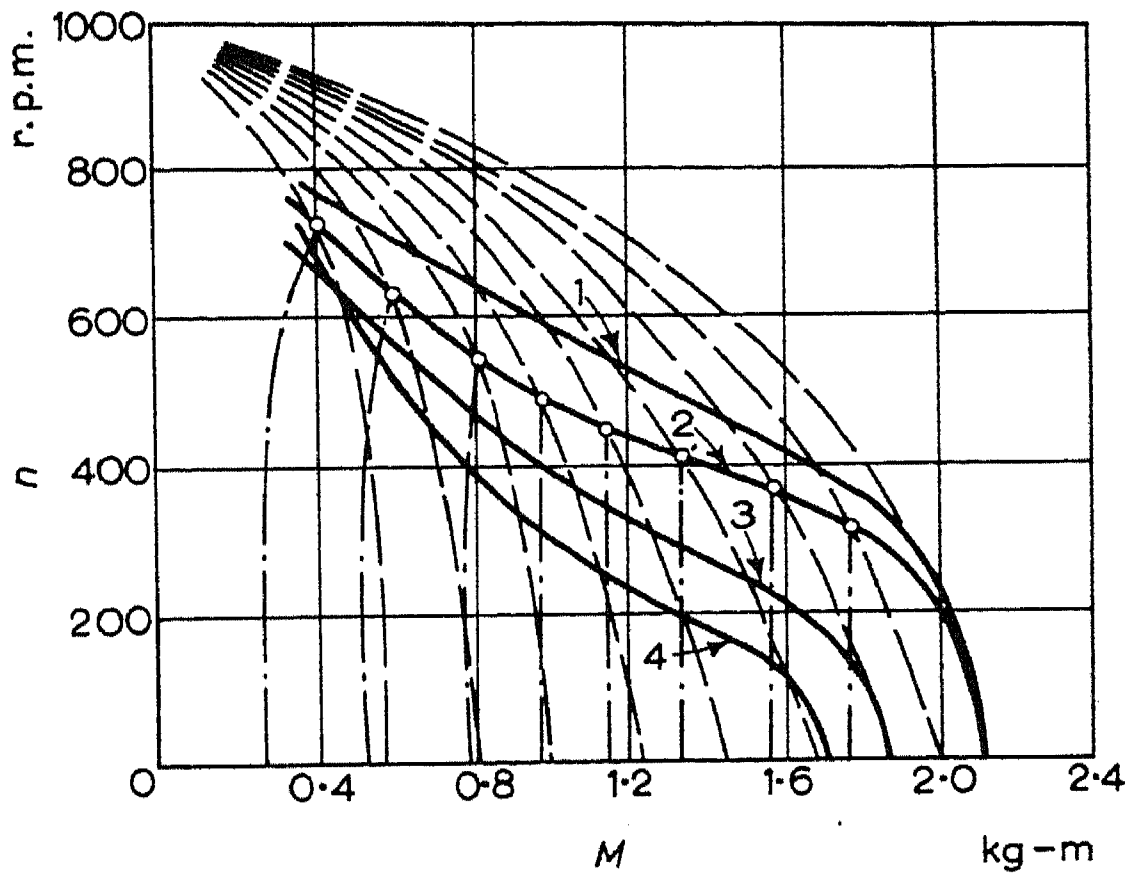

Fig.5. Characteristics of M_w in the circuit of Fig.2 obtained under laboratory conditions. —— . —— . —— static torque.

Fig.5 shows several such laboratory test curves obtained with various m.m.f. increments in the magnetic amplifier control circuits. 1 and 2 were obtained with two single-phase amplifiers and 3 and 4 with one two-phase amplifier.

The asymmetric impedances in the rotor give rise to direct and inverse fields, the stator current contains a component of normal frequency f_1 and another of reduced frequency $f_3 = f_1(1 - 2s)$, which cause beating. But Fig.6 shows that this beat remains slight even at minimum signals

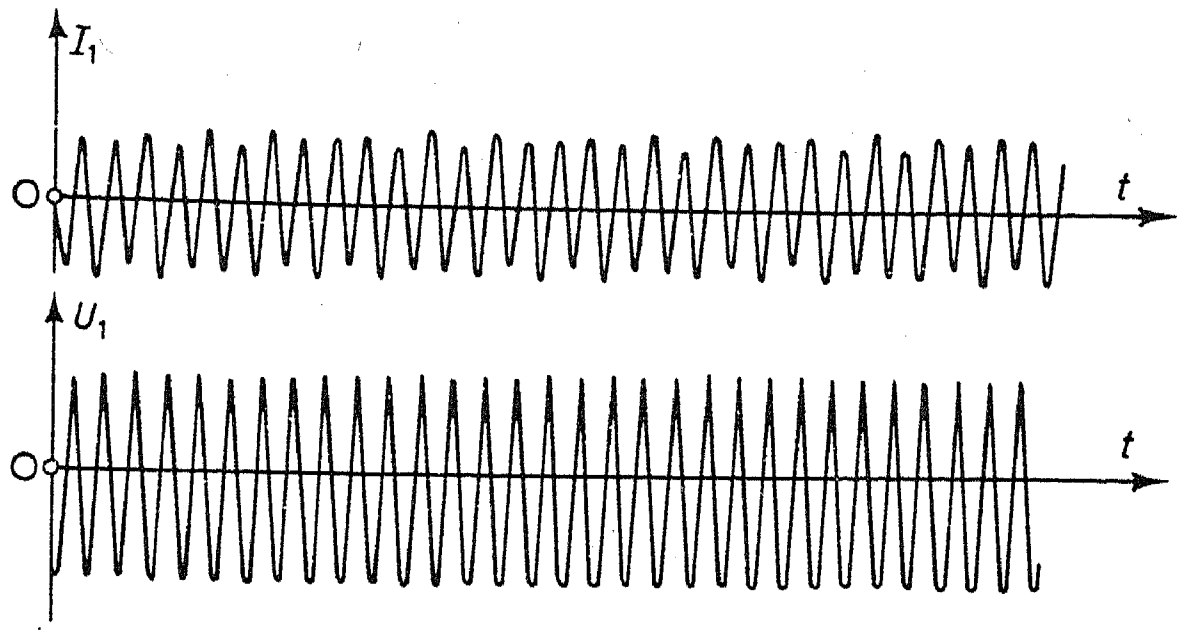

Fig. 6. Oscillograms for I_1 and U_1 in the stator.

($i_c = 0$) when the asymmetry is maximal.* The additional winding temperature rise due to the reduced frequency currents is also very small. The stator terminal voltage is practically unchanged.

The reduced p.f. typical of inductor control systems cannot be considered as hindering the use of this system on dredgers since the winch drives on those with 0.155, 0.21 and 0.38 m^3 buckets are of relatively low ratings (18 – 26 kW). Static capacitors connected to the stator terminals will improve the p.f.

Conclusions

(1) Laboratory and theoretical work has shown that the magnetic amplifier system provides the required winch motor characteristics automatically.

(2) The system is simple. The main electrical equipment need not be rearranged or changed in order to introduce it. The capital cost is low.

(3) The automatic control system would reduce the strain on the operator and increase his productivity.

List of symbols

x and x_c — magnetic amplifier inductive reactances in the a and c rotor phases;

α — operator rotating vectors through 120^p;

* When $i_c = 0$ the modulus of the coefficient of current unbalance ($\gamma = \dot{I}_{II}/\dot{I}_I$), which specifies the degree of asymmetry in the rotor circuit, was 0.68.

$Z_{1,I}$ positive-sequence impedance of one stator phase;

$Z_{1,II}$ negative-sequence impedance of one stator phase;

Z_2 impedance of one rotor phase;

r_1 and x_1 resistance and inductive reactance of one stator phase;

r_2 and x_2 referred resistance and inductive reactance of a rotor phase;

x_k inductive reactance of one motor phase;

U_1 phase voltage on the stator;

$\dot{I}_{1,I}$ positive-sequence stator current;

$\dot{I}_{1,II}$ negative-sequence stator current;

$\dot{I}_{2,I}$ positive-sequence rotor current;

$\dot{I}_{2,II}$ negative-sequence rotor current;

$m_1 = m_2 = m$ = number of phases in stator and rotor;

ω_0 = synchronous angular velocity of the motor;

s = slip;

w_c and r_c are the number of turns and resistance of the magnetic amplifier control winding respectively.

REFERENCES

1. A.G. Vecheslov and P.K. Shindel'man; Automatic Control of the manoeuvring Winch on a 210 litre Electric Dredger. *Sovetskaya Zolotopromyshlennost'* No.4 (1937).
2. K.A. Krug; *Fundamentals of Electrical Engineering*. Gosénergoizdat (1952).
3. K.F. Wagner and R.D. Evans; *Symmetrical Components*. (1933).
4. G.I. Shturman; *Asymmetry of the Secondary Circuits in Induction Motors*. ONTI (1935).
5. G.B. Merkin and E.D. Nesgovorova; *Induction Motor Operation with Rotor Asymmetry*. Trudy Leningradskogo Industrial'nogo Institute, No.2 (1938).

6. M.P. Kostenko; *Electrical Machines (Special Part).* Gosénergoizdat (1949).
7. S.N. Veshenevskii; *Calculation of Characteristics and Impedances in Electric Motors.* Gosénergoizdat *(1955).*
8. T.H. Barton and B.C. Doxey; Operation of Three-phase Induction Motors with Asymmetric Rotor Circuit Impedances. *Proc. Inst. Elect. Engrs.* A **102,** No.1 (1955).

DIFFERENTIAL PROTECTION CIRCUITS WITH MAGNETIC RESTRAINT*

A.D. DROZDOV

Ordzhonikidze Polytechnical Institute, Novockerkassk

(Received 19 October 1955)

The simple principle of magnetic restraint, known since 1930, has now also been applied to differential protection. We are now well acquainted with the theory of this principle and have evolved methods of eliminating the dependence of relay response on the phase relations of the individual phases; also rational relay designs using one or more restraining windings exist [1 - 4].

The present communication presents methods of synthesizing, transforming and designing differential protection circuits.

Fig. 1(a) shows a symmetrical circuit containing a balance coil and split restraining or premagnetizing coils connected into the arms of the protection circuit. One three-limb core could be used instead of the two two-limb cores shown in Fig.1: tests show that the results obtained with this arrangement are quite similar to those with two-limb cores.

By applying the law of conservation of current the circuit of Fig.1(a) can be simplified without appreciably altering its characteristics. Two coils with different numbers of turns could be used instead of the three coils in series on the outer and central limbs.

Let us remove the coil $w_{na}/2$ on the right-hand limb, and reduce the turns on the working winding by $w_{na}/2$, thus retaining the nett ampere turns, and increase the turns on the left-hand premagnetizing coil by the same number, or, which amounts to the same, let us transfer $w_{na}/2$ turns from the right-hand to the central and left-hand limbs. The new working winding then has $w_w = w'_w - w_{na}/2$ turns.

To maintain the ampere-turns produced in the central limb by I_b we have to increase the balance winding turns by $w_{na}/2$.

* *Elektrichestvo* No. 2, 33–36 (1957).

[Reprint Order No. EL. 12]

Furthermore, we will remove $w_{nb}/2$ turns from the left-hand limb a correspondingly reduce the balance turns and increase the right-hand premagnetizing turns. The new number of turns on the balance windin is

$$w_{bl} = w'_{bl} + w_{na}/2 - w_{nb}/2$$

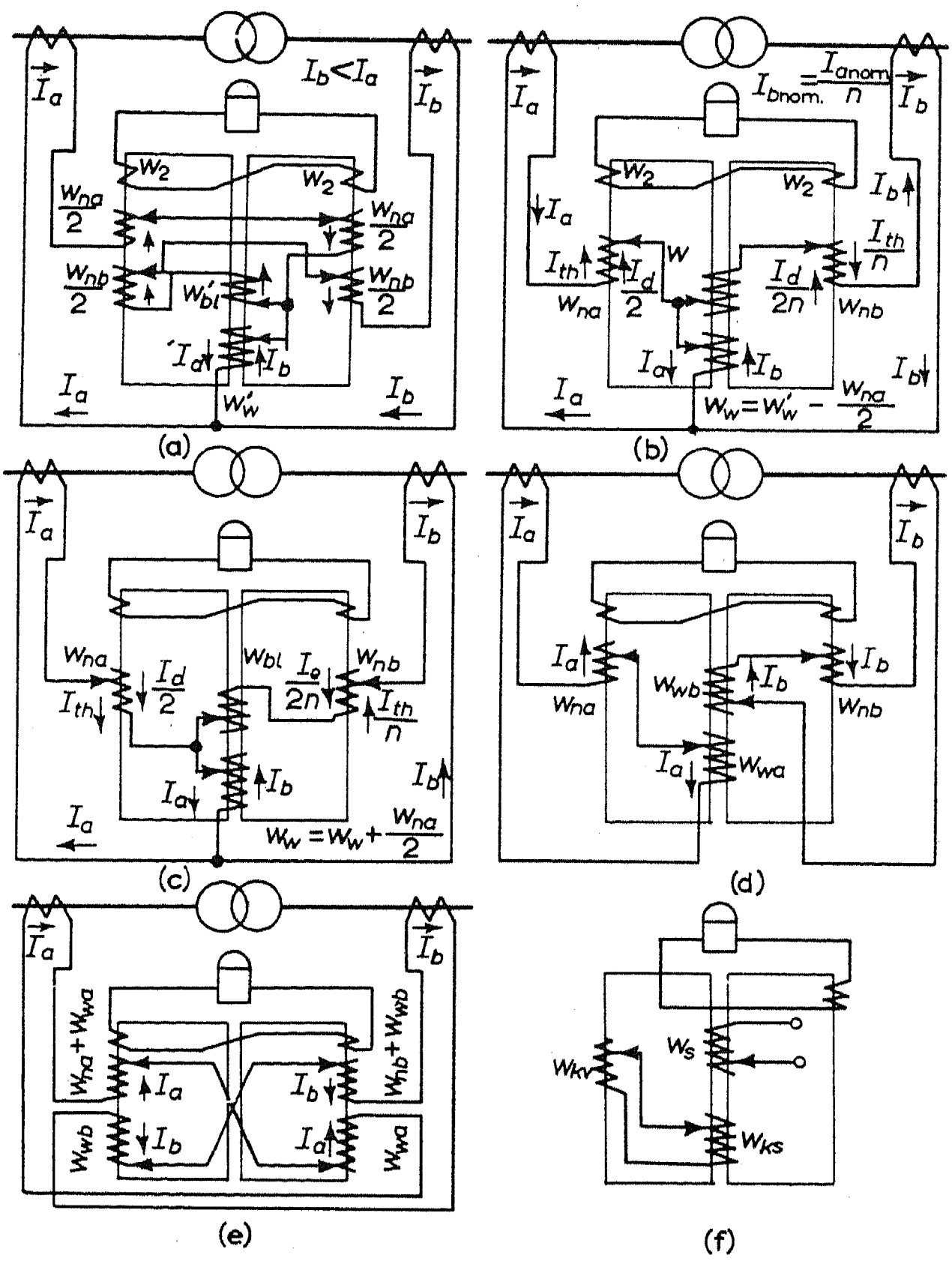

Fig. 1 Differential protection circuits with equal total numbers of ampere-turns.

(a) with separate working and premagnetizing windings;
(b) equivalent circuit with premagnetizing windings partly acting as working coil;
(c) the same, but with reversed senses of the premagnetizing coils;
(d) and (e) with separate circuits.
(f) saturable transformers with short-circuited turns.

Fig.1(b) shows the circuit so obtained. The premagnetizing coils act partly as the working winding. Therefore we may add the turns on the working and balance windings and determine them from the following formulae:

$$w'_w = w_w + w_{na}/2; \quad w'_{bl} = w_{bl} - w_{na}/2 + w_{nb}/2$$

The total may be fractional. We derive below the formulae and give an example of winding calculation for the circuit of Fig.1(b).

The total turns are determined from the ampere-turns found experimentally via the response of an unrestrained relay, viz. F = 70 A:

$$w'_w = cF/I_{sa} = 1.05 \text{ x } 70/5 = 14.7$$

where I_{sa} = 5 A is the operate current on the side of the winding a; $c = I_{sa}/I_{so}$ is a factor allowing for the increase in operate current with a unilateral internal fault over the current occurring with a symmetrical bilateral supply. The well-known formula for c for mechanical relays gives

$$c = \frac{2}{\sqrt{4 - k_r^2}}$$

The restraining factor k_r is assumed as 0.6 when c = 1.05. We can determine c for magnetically restrained relays similarly because their characteristics at low currents are similar to those of mechanical relays. w_{na} then is (1, 2)

$$w_{na} = k_r w'_w = 0.6 \text{ x } 14.7 = 9$$

The effective k_r will be greater at high currents as may be established experimentally or from the curves of double magnetization (2).

If the ratio of the nominal currents $n = I_a/I_b$ is assumed as 1.46, w_{nb} for the second premagnetizing coil becomes

$$w_{nb} = nw_a = 1.46 \text{ x } 9 = 13$$

and w_w is

$$w_w = w'_w - \frac{w_{na}}{2} = 14.7 - 4.5 \approx 10$$

The current in the arms of the protection circuit may be divided into the through-current I_{th} and the differential current I_d. Since I_d flows from the current transformer secondary to the differential circuit from both sides, we get

$$I_a = I_{th} + \frac{I_d}{2}; \quad I_b = \frac{I_{th}}{n} - \frac{I_d}{2n}$$

The magnetizing forces in the right-hand and left-hand circuits due to I_{th} must be equal and opposite, i.e.

$$n(w_w + w_{na}) - w_w - w_{bl} = w_w + w_{bl} + w_{nb} - w_w \qquad (1)$$

from which we can determine w_b

$$w_{bl} = (n-1)w_w + 0.5(nw_{na} - w_{nb}) =$$

$$= 0.46 \text{ x } 10 + 0.5(1.46 \text{ x } 9 - 13) = 4.67 \approx 5 \qquad (2)$$

The second term 5 on the right-hand side of equation (2) allows for imperfect agreement between the ratios of rounded-off turns and currents for the premagnetizing windings.

Since w_{bl} has been rounded off equation (1) will be satisfied at some current ratio other than nominal, corresponding to the winding parameters adopted and determined from equation (1), viz.

$$\Delta n_{wd} = \frac{w_w + w_{bl} + w_{nb} \text{ x } 0.5}{w_w + w_{na} \text{ x } 0.5} = \frac{10 + 5 + 6.5}{10 + 4.5} = 1.482 \qquad (3)$$

Hence I_{th} will cause an additional flux unbalance in the two cores, which is equivalent to the unbalance-current increasing by

$$\Delta i_{ub} = \frac{n - n_{wd}}{n_{wd}} 100 = \frac{1.46 - 1.482}{1.482} 100 = -1.5 \text{ per cent}$$

If we assume $w_{bl} = 4$, $n_{wd} = 1.414$; $\Delta i_{ub} = 3.25$ per cent. For an operate current $I = 10$ A, $w_w = 5$; $w_{bl} = 2.22 \approx 2$; $\Delta i_{ub} = 2.1$ per cent; and when $w_{bl} = 3$, so $\Delta i_{ub} = -7.0$ per cent. Even when the choice of w_{bl} is not correct, as in the latter example, the effect of the i_{ub} is fully compensated by the restraint (7 per cent $\ll$ 60 per cent).

For compensation to be obtained we must have

$$i_{ub} + \Delta i_{ub} < k_r$$

If the restraint is strong enough there is no need for the ratios of the current transformers to be exactly equal.

Fig.1(a) may be modified in yet another way, viz. by transferring $w_{na}/2$ from the left-hand to the centre and right-hand limbs. w_w is then increased, viz.

$$w_w = w'_w + 0.5\, w_{na} = 14.7 + 4.5 \approx 19$$

This gives the circuit of Fig.1(c) which differs from the original in the sense of the premagnetizing windings, which have the same turns as in Fig.1(a).

Equations (1 – 3) may also be applied to Fig.1(c) if the signs of w_{na} and w_{nb} are reversed, viz.

$$w_{bl} = (n-1)w_w - 0.5(nw_{na} - w_{nb}) = 8.7 \approx 9:$$

$$n_{wd} = \frac{w_w + w_{bl} - 0.5w_{nb}}{w_w - 0.5w_{na}} = 1.482$$

$$\Delta i_{ub} = -1.5 \text{ per cent}$$

If we assume $w_{bl} = 8$, $n_{wd} = 1.414$ and $\Delta i_{ub} = 3.25$ per cent. Consequently the figures are unchanged, from which we conclude that Fig.1(b) and (c) are equivalent as regards balancing the secondary currents, although Fig.1(c) would appear to have advantages owing to the greater number of turns.

When other protection circuits are connected to one of this type the secondary circuits may have sometimes to be split. Fig.1(b) may then take the form shown in Fig.1(d). Fig.1(e), obtained by separating the common coils in Fig.1(d) will also serve.

The restraining characteristics of the circuits must be identical if leakage is disregarded. But they actually differ in curvature (2). If the restraining and secondary windings are placed on the same limbs, and the working windings on the opposite limbs (Fig.1,a) the characteristic will become concave and k_r will increase for large currents due to

additional premagnetization in one part of the magnetic circuit. In Fig.1(b) the premagnetizing coils act as working coils so its characteristics will be less concave than those of Fig.1(a). The characteristics of Fig.1(d) and (b) are similar. The concavity for Fig.1(c) is much greater than that for Fig.1(a). Fig.1(e) has approximately linear characteristics because all windings are on the same limbs.

Fig.1(b) is preferable owing to its simplicity, universal usefulness, smaller number of turns and symmetrical characteristics. The premagnetizing coil connections can here be reversed (Fig.1 c) or the circuits may be separated (Fig.1,d). No alterations to the design are required.

Fig.1(b) can be made to give a saturable transformer with short-circuited turns with a lower sensitivity to aperiodic currents. One such circuit is shown in Fig.1(f). Here the right-hand core with its windings is the transformer proper. In the short-circuited circuit of the left-hand core a current partly compensating the effect of the primary (alternating) current on the right-hand core is set up which reduces the number of primary turns, as it were. However, the effect of the constant current is not reduced, which results in a reduced sensitivity. Saturable transformers are more fully treated in (4).

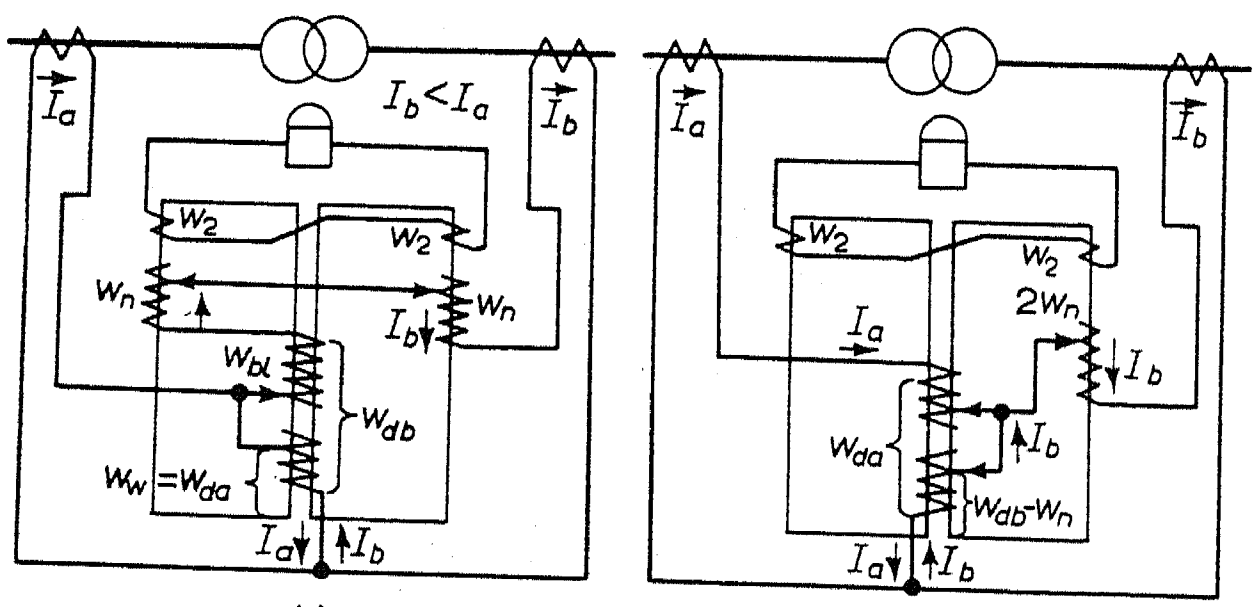

Fig. 2 Differential protection circuits with premagnetizing windings in one arm.
(a) with separate working and premagnetizing windings;
(b) simplified equivalent circuit.

The circuit is simplified if the premagnetizing coils are placed asymmetrically, i.e. in one arm only (Fig.2,a). The circuit is further simplified by transferring the left premagnetizing coil to the central and right-hand limbs, as shown in Fig.2(b). A disadvantage of Fig.2(b) is that the leakage flux is asymmetric when only I_{th} flows. If i_{ub} and

I_{th} are in phase in the premagnetizing windings ($nI_b > I_a$), both the circuits of Fig.2 are under great restraint, as illustrated by curves 2

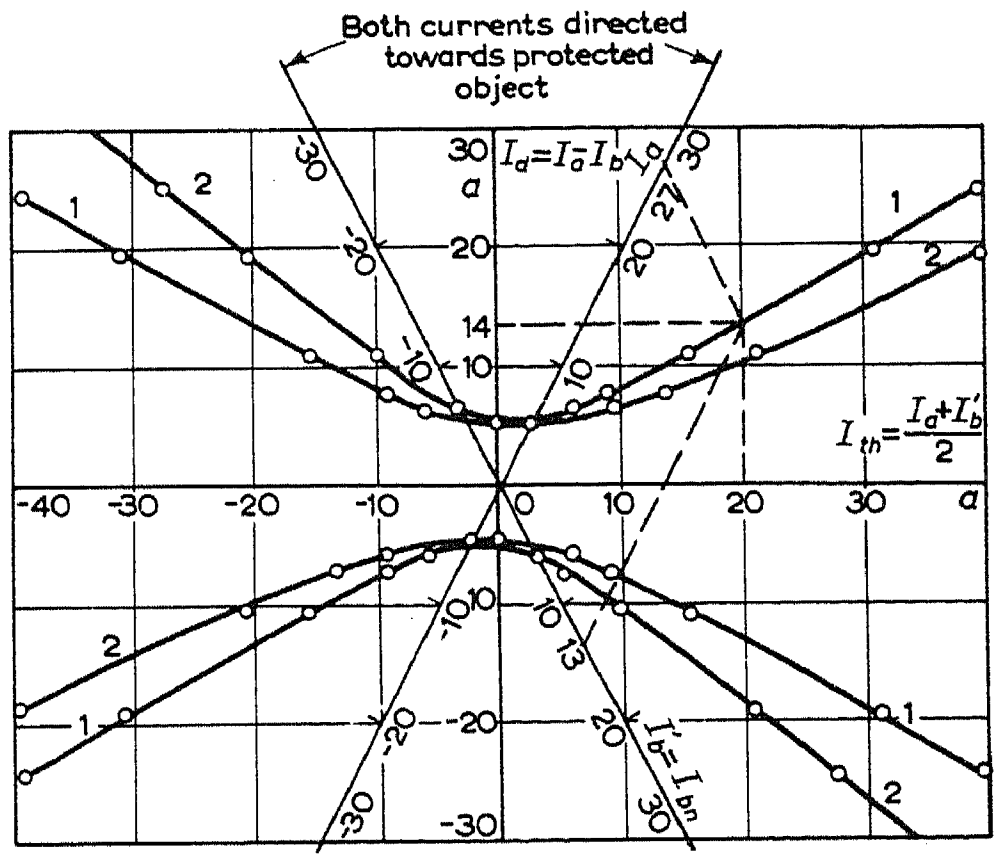

Fig.3 Experimental characteristics of differential protection circuits.

(a) symmetric circuit;

(b) asymmetric circuit.

in Fig.3, which refer to Fig.2(a). Symmetric circuits have symmetric characteristics (curve 1). The curves of Fig.3 are universal and give the currents in the protection circuit arms in terms of the oblique coordinates I_a and nI_b. Curves 2 may be made more symmetric by increasing w_{bl} (Fig.2), but this will normally introduce a flux which is difficult to control.

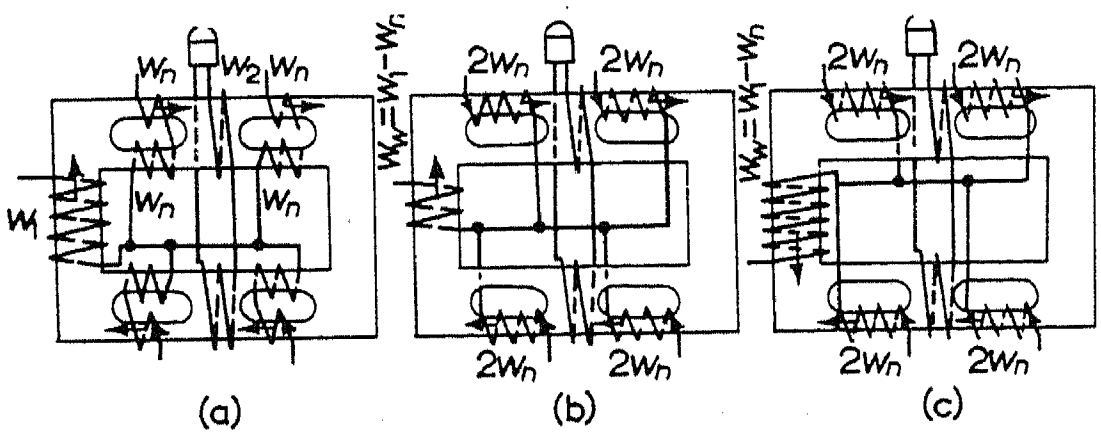

Fig.4 Differential protection circuits of multiply wound transformers with equal total numbers of ampere-turns.

(a) with separate primary and premagnetizing windings windings;

(b) with premagnetizing windings partly acting as primary coil;

(c) with reversed connections to the premagnetizing windings.

The circuits of Fig.2 are simpler than those of Fig.1 but restraints depend on the direction of I_{ub} which is difficult to predict. The location of the restraining coils is also of some importance. Fig.1(b) can easily be converted into the assymetric circuits of Fig.2.

A differential protection circuit with several restraining coils can be designed round a transformer with slots in the magnetic circuits (Fig.4,a). The four premagnetizing coils act here independently. Fig.4(a) may be simplified as above, the equivalent circuit Fig.4(b) in which the premagnetizing windings act partly as primary coils being then obtained. The circuit can also be used with reversed premagnetizer connections (Fig.4,c); the curve is then strongly convex. But Fig.4(b) is preferable because it is simpler and has less turns.

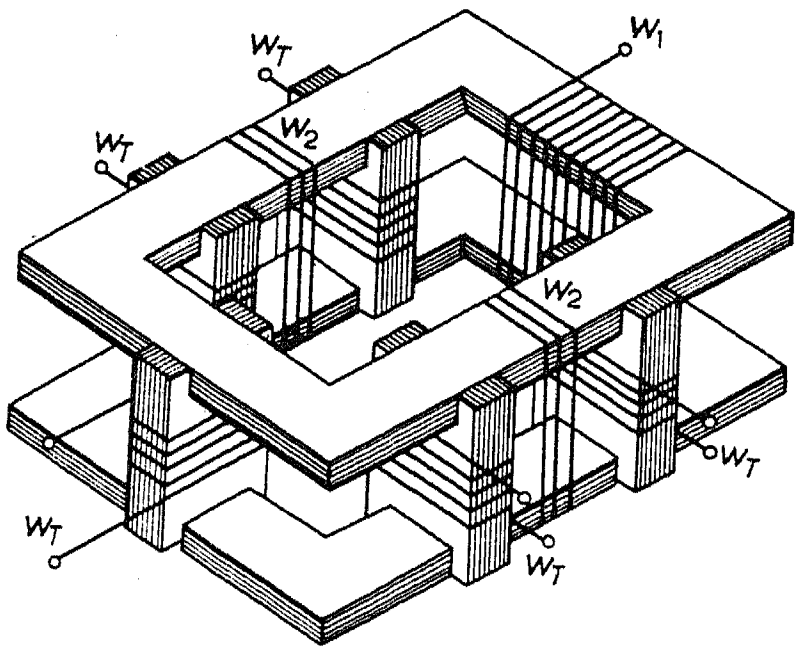

Fig.5 Saturable transformer with 5 premagnetizing coils on the cross-members.

The premagnetizing coils may also be formed by cross-connections (Fig.4), i.e. by threading the turns first through one, and then through the other opening. It is then convenient to use a different core design with cross-members (Fig.5). This has the advantage of simplifying coil winding and facilitating alterations. There is no restraining effect with an internal symmetrically fed fault, this making for reliability of operation. The damping characteristics of this arrangement are effected by a certain dispersion owing to the different arrangement of the coils. The construction of working coil and magnetic system is simpler with the longitudinally slotted magnetic circuit, the whole unit being more rigid and compact. This design may therefore be regarded as more satisfactory.

REFERENCES

1. V.I. Ivanov; *Relays and Relay Protection.* Gosenergoizdat (1932).
2. A.D. Drozdov; Fundamental equations of saturable differential current transformers for relay protection. *Elektrichestvo* No.6 (1954).
3. M.B. Tsfasman; Design of differential protection with magnetic restraint for transformers. *Elekt. Stantsii* No.3 (1955).
4. A.D. Drozdov; Saturable current transformers with short-circuited turns for relay protection. *Elektrichestvo* No.10 (1953).

THE STABILITIES OF MEASURING INSTRUMENTS USING MAGNICO AND ALNICO*

E.G. SHRAMKOV, A.V. MITKEVICH and N.B. KOVALEV

Although permanent magnets made from alloys of iron, nickel and aluminium are extensively used in modern devices, the stabilities of such systems have not been fully studied nor have they been exhaustively treated in the literature. The measuring apparatus used previously has been of low sensitivity and the methods of measurement have not been sufficiently accurate to detect small flux variations and hence prevented a sound appraisal of the way the systems behave.

Some experimental data on Alni and Alnico permanent magnets have been published [1 – 3], which state that flux variations of several per cent were observed. Other papers [4 – 6] mainly give general information with no experimental data. One paper [7] describes a sensitive balance method in which balance is obtained by varying the current through a coil in the air gap of the magnet, though data are only given for a few magnets. Ballistic null-methods for measuring accurately the flux densities in the air gaps of permanent magnets have also been described [8 – 10]. Kronenberg [10] gives data also on the stabilities of Alni and Alnico magnets.

Measuring instruments and magnetic systems investigated

A special type of measuring apparatus based on null-principles was developed to measure relative flux changes of about 10^{-2} per cent. These new instruments were used to study the stability of one kind of magnet system with Alnico and Magnico magnets. Rectangular magnets with pole pieces held together in a silumina diecasting were held in rings of magnetically soft material to complete the flux path. The system differed from those used in electromagnetic instruments only by having a somewhat longer core which was pressed into a brass bush with an external thread to secure the system during the flux measurements. One of the

* *Elektrichestvo* No. 3, 62–67 (1957). [Reprint Order No. EL.13]

measuring instruments developed consists of a balance with arms having different masses (similar to that described in [7]). The balance beam rests with its knife edges on jewel bearings. One arm bears a pointer which is observed with a telescope. A gear transmission train actuated by a handle is used for positioning the system and balancing is achieved by varying the current through a coil in the air gap. At balance the current in the coil is inversely proportional to the flux density.

The other measuring instrument was developed by N.B. Kovalev. Here two opposing torques acting on a moving system are balanced; one torque is produced by an astatic electrodynamic measuring system and the other by the current in a test coil and the flux of the system. The stationary and the moving coils of the electrodynamic system and the test coil are all connected in series. The moving system is suspended, and carries a mirror. A fixed mirror is placed below the first one so that two images (from the two mirrors) of a scale placed near the telescope can be seen. When the two torques are equal, or when no current flows in the coils, the instrument reads zero, and the two images coincide. When the two torques balance the current in the coils is proportional to the flux density in the air gap. A handle is used to position the magnetic system.

In both measuring instruments the coil current was measured potentiometrically accurate to ~ 0.005 per cent. Since the instruments were designed for making extensive measurements provision was made to ensure accurate resetting of the magnetic systems. The temperature of the instrument room was maintained constant at $22^{\circ} \pm 0.1^{\circ}C$. All readings were made from another room which contained the potentiometer. The reproducibility was estimated to be ~ 0.03 per cent for each instrument. The results given below were obtained mainly with the first instrument; the second instrument was primarily used to verify the readings of the first.

Altogether we investigated 94 systems; 50 were fitted with Magnico magnets (40 were produced in August, 1952 and 10 in February, 1955) and 44 of Alnico (produced in May – September, 1953 and in November, 1954). Only the most typical results will be described.

All 94 systems were magnetized practically up to saturation with a d.c. electromagnet having special pole pieces embracing the system. Magnetic stabilization, i.e. partial demagnetization, was carried out mainly by applying a 50 c/s field which was gradually reduced to zero. For this purpose another electromagnet with laminated sheet steel yoke and pole pieces was used; the pole pieces were arranged as in the d.c. magnetizing electromagnet.

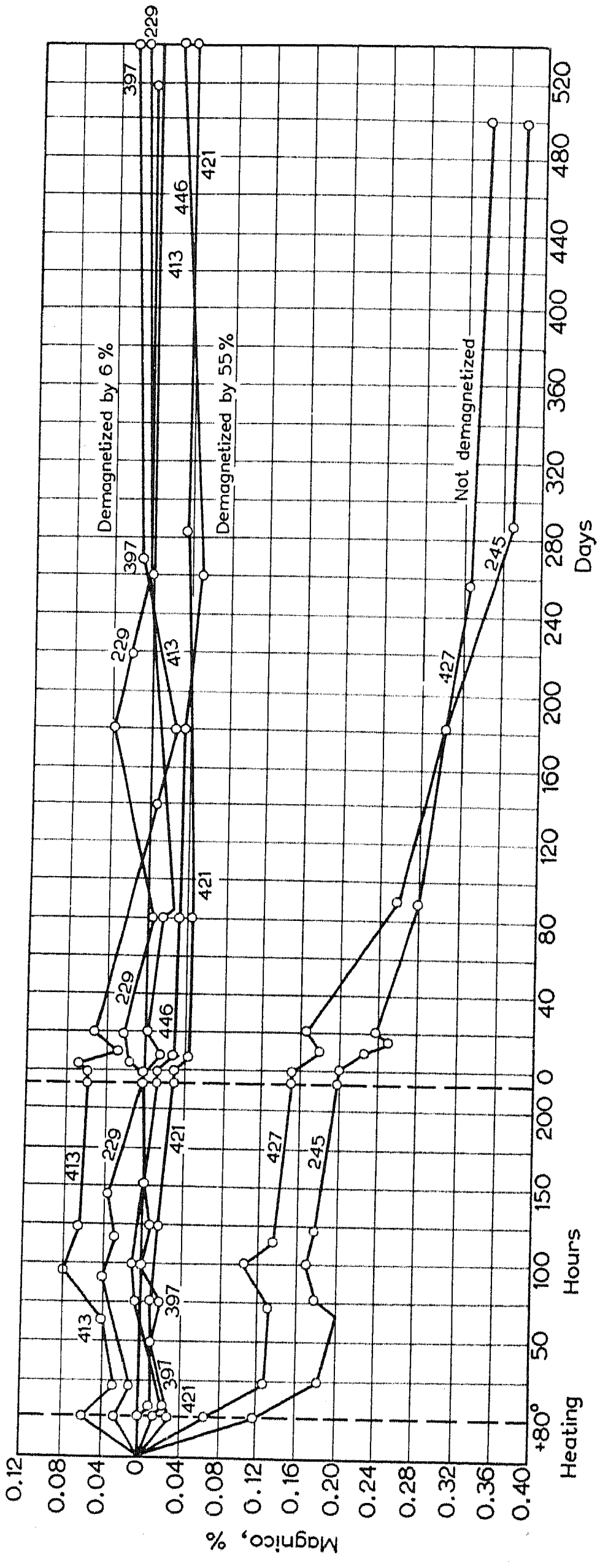
Demagnetized by 6 %
Demagnetized by 55 %
Not demagnetized
229
397
413
421
446
427
245
Days
Hours
Heating
+80°
Magnico, %
0.12
0.08
0.04
0
0.04
0.08
0.12
0.16
0.20
0.24
0.28
0.32
0.36
0.40
0
40
80
120
160
200
240
280
320
360
400
440
480
520
50
100
150
200

Fig. 1.

Magnetic systems with Magnico alloy magnets

Heat treatment effects following magnetization and stabilization, and the effect of the degree of stabilizing demagnetization on the consequent behaviour were studied on Magnico alloy systems for periods of up to 1½ years.

Fig.1 shows the results obtained on seven systems six months after manufacture (the system numbers are shown against the curves on this and the following figures). The ordinate indicates the percentage flux density variation in the working gap, the abscissae indicating the annealing temperatures and time in hours and days.

All seven systems were magnetized: two were not subsequently demagnetized (lower curves), two others (nos. 446 and 421) were 55 per cent demagnetized using an a.c. electromagnet and the remaining three (nos. 229, 397 and 413) were 6 per cent demagnetized, using the same method. Next, six were treated at +80°C for 1 hr and cooled down to room temperature. (The heating time of about 30 min is not included). One (no. 397) which was 6 per cent demagnetized was not subjected to heat treatment (the curve starts from the vertical dashed line marked "anneal").

The six treated systems were first measured 2 – 3 hr after heating and the unannealed one was first measured approximately 30 min after demagnetization. Fig.1 shows that heating at +80°C led to a flux increase of 0.03 – 0.06 per cent in 6 per cent demagnetized systems, whereas in 55 per cent demagnetized systems a slight weakening of 0.02 – 0.03 per cent resulted. In the systems which were not demagnetized the flux drop was 0.07 to 0.12 per cent. The flux drop was greater following annealing at +80°C; for example, a drop of 0.9 per cent was observed for one non-demagnetized system.

The flux changes were most pronounced during the first few days after heat treatment for the non-stabilized systems. Stabilized systems were stable to within a few hundredths of one per cent.

Systems 6 – 10 per cent demagnetized and given a second heat treatment at +80°C showed flux increases of sometimes up to 0.16 per cent. Treatments subsequent to the second or third were found to have comparatively little effect and the annealing time if > 1 hr, was unimportant; annealing for 1 or 4 hr produced approximately the same effect.

Investigations on systems immediately after manufacture, and some time afterwards showed that annealing at +80°C has more effect on the flux when carried out immediately after manufacture. This is quite possibly due to structural changes in the magnet or to some other changes in the system as a whole.

The stabilities of measuring instruments using Magnico and Alni

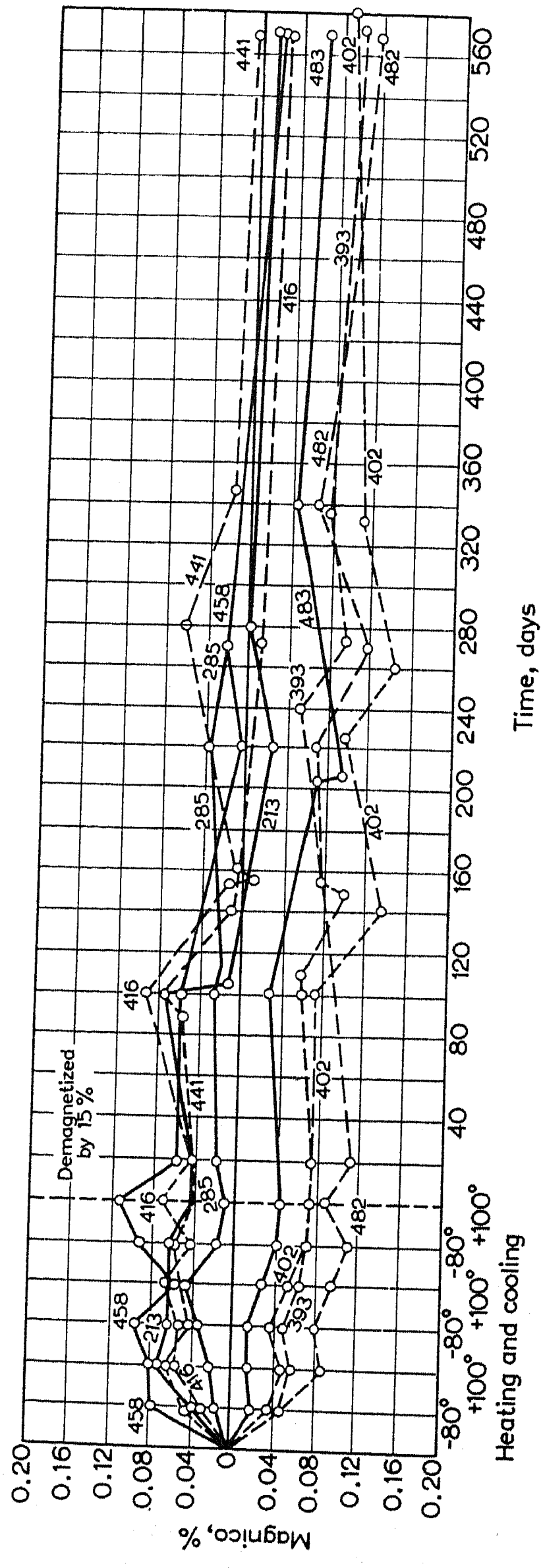

Fig. 2.

In practice magnetic systems are sometimes conditioned by thermal cycling prior to magnetization. It was desired to elucidate how this treatment would influence subsequent behaviour of the system. Fig.2 gives data for nine systems, five of which (broken lines) were given 10 cycles from $-80^{o}C$ to $+100^{o}C$ before magnetization; each temperature being maintained for 4 hr. The remaining four systems (full lines) did not undergo this treatment. Next, all the nine systems were magnetized and partly demagnetized using an a.c. electromagnet. Five systems were demagnetized 12 – 15 per cent (upper curves in Fig.2) and four 60 – 70 per cent (lower curves). After this all the systems were given 3 cycles from $-80^{o}C$ to $+100^{o}C$, temperature being maintained for 2 hr; the treatment being started with cooling.

The curves show that thermal conditioning produces slight flux increases in 12 – 15 per cent demagnetized systems whereas the flux decreases slightly in systems demagnetized 60 – 70 per cent. Whether the magnet was cooled before or after being annealed made no difference to its subsequent behaviour.

Similar systems, 20 and 45 per cent demagnetized, gave curves which lie between the upper and lower groups in Fig.2.

The data show that preliminary thermal treatment does not affect the subsequent behaviour to any noticeable extent, i.e., this treatment is not essential. All the nine systems studied were about equally stable. A rather important fact is that even those 60 – 70 per cent demagnetized were satisfactorily stable.

Magnetic shunts were applied before magnetization in some cases and, after demagnetization and a few cycles to $+80^{o}C$ the shunts were moved from one limiting position to the other. The stabilities of these systems did not differ from those of systems without shunts.

Systems with Alnico magnets

Fig.3 shows the effects of post-magnetization heat treatment followed by stabilization, and of the degree of stabilizing demagnetization on Alnico systems. Six systems were magnetized and then demagnetized 6 – 10 per cent using an a.c. electromagnet. All these were then subjected to six heat treatments at $+80^{o}C$, each heating being followed by cooling to room temperature. The higher temperature of $+80^{o}C$ was maintained for 1 hr with three specimens (full curves) and 4 hr with the other three (broken curves). As before, the time required to reach $+80^{o}C$ (30 min) is not included in the duration of the heat treatment.

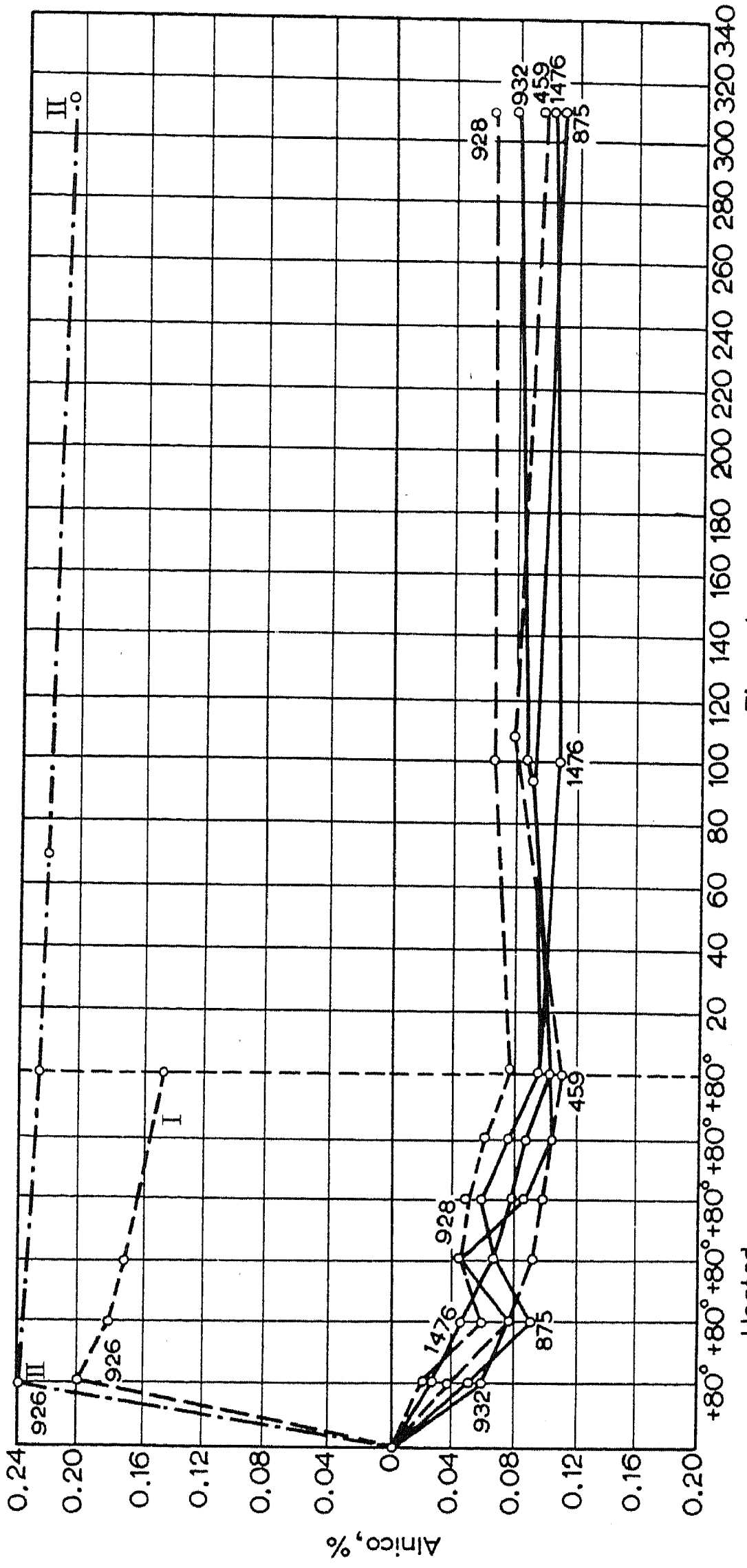
II
928
932
459
1476
875
I
926
III
926
1476
459
928
1476
875
932
0.24
0.20
0.16
0.12
0.08
0.04
0
0.04
0.08
0.12
0.16
0.20
Alnico, %
0
20
40
60
80
100
120
140
160
180
200
220
240
260
280
300
320
340
Time, days
+80°
+80°+80°
+80°+80°+80°
Heated

Fig. 3.

The curves show that 1 and 4 hr annealing have approximately the same effects. Further treatments beyond the second also have comparatively little effect. One system (top curve, I) stands out from the others. An unusually large flux change was found after the first heat treatment, and therefore the system was subjected to a new series of heat treatments two weeks later (curve II, Fig.3). This confirmed that there was a genuine difference between this system and the others, which did not disappear after the subsequent heat treatments. During the work on Alnico magnets yet another system was discovered which reacted to heating in the same manner as no. 926 (Fig.3). These two which reacted quite strongly to annealing had originally the same flux densities as all the others. So some definitely undesirable irregularity requiring separate investigation occurred here.

Two systems were annealed at +300°C for 4 hr, which caused little change in their subsequent reactions.

A number of systems demagnetized by varying percentages (between 4 and 20 per cent), and one system not demagnetized at all, were subjected to several cycles between +80°C and −80°C. With two exceptions the resulting flux reductions were less than 0.06 per cent. The exceptions were one demagnetized 4 per cent which had its flux reduced by approximately 0.18 per cent and the non-demagnetized system which dropped by approximately 0.7 per cent.

All the partially demagnetized systems were found to be about equally stable and the variations during a year did not much exceed 0.01 per cent (within the limits of experimental error).

The systems were normally magnetized in groups placed between the poles of an electromagnet. Partial demagnetization was carried out using a 50 c/s a.c. electromagnet. The magnets were therefore magnetized and demagnetized under conditions differing from their normal working conditions. A magnet in a 50 c/s field is also more strongly demagnetized near the surface. Consequently various demagnetization methods were studied at the same time as the premagnetization heat treatment.

Five of the eleven systems were given 11 cycles from −80°C to +120°C, each temperature being maintained for 2 hr before magnetization (dashed curves, Fig.4). The remaining six systems were not so treated (full curves, Fig.4). All eleven were magnetized and then demagnetized by 6 – 10 per cent by various methods. Heat treatment at +80°C for 4 hr followed. Three systems were demagnetized using the field of a d.c. electromagnet with pole pieces sufficiently large to enclose the systems.

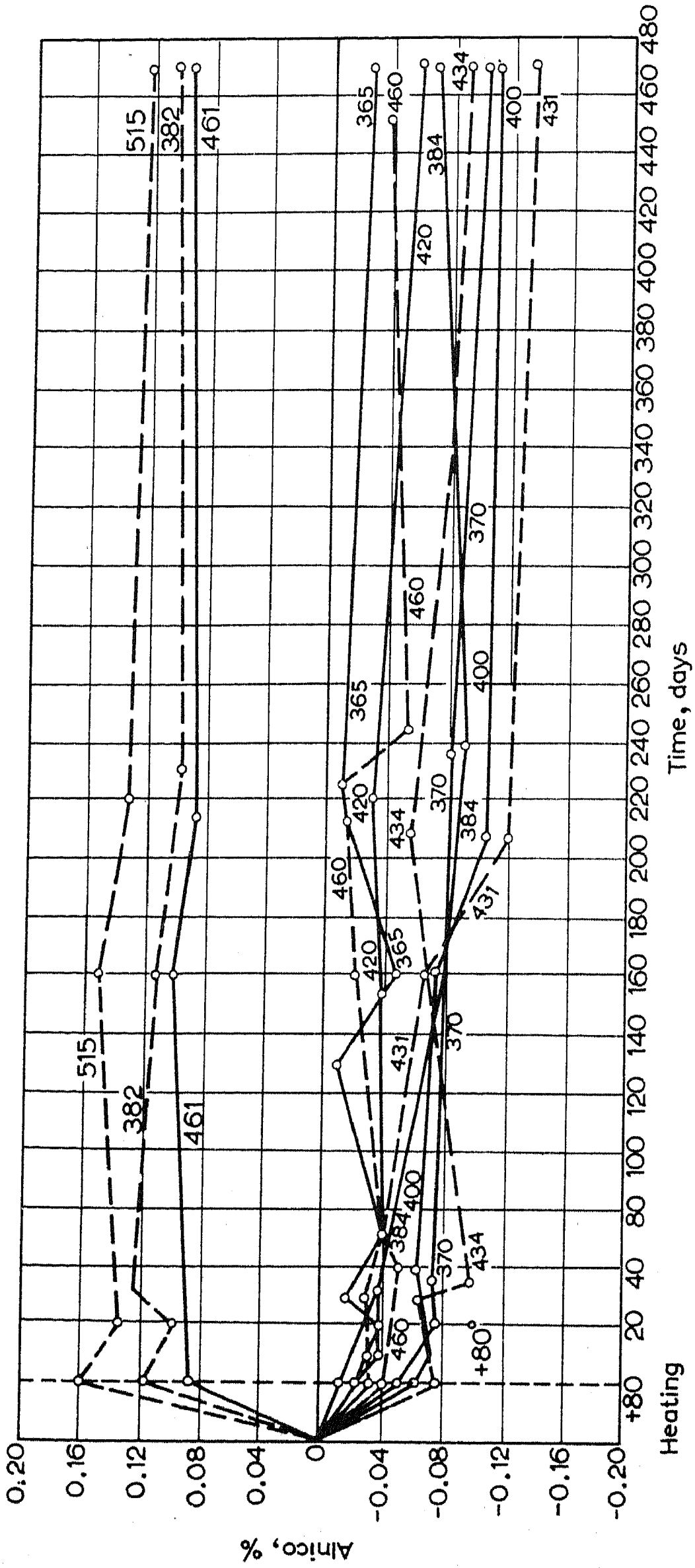
Alnico, %
0.20
0.16
0.12
0.08
0.04
0
-0.04
-0.08
-0.12
-0.16
-0.20
Heating
+80
+80°
20
40
80
100
120
140
160
180
200
220
240
260
280
300
320
340
360
380
400
420
440
460
480
Time, days
515
382
461
365
460
420
384
434
400
431
370

Fig. 4.

The exciting current was smoothly reduced to zero and reversed 1 to 2 times/sec. The curves obtained lie in the upper part of Fig.4. Two systems were demagnetized by d.c. coils placed directly on the magnets. The direction and magnitude of the direct currents in these coils were altered as with the electromagnet. Two other systems were a.c. demagnetized using the same coils. The remaining four systems were demagnetized in the usual way using an a.c. electromagnet. The curves for the last eight systems (lower curves in Fig.4) are more or less similar, the spread in the points being within the limits of experimental error (0.03 per cent). The systems demagnetized with d.c. and a.c. electromagnets were interchanged to check that a different type of curve resulted from demagnetization with the d.c. electromagnet. It was found that the type of curve obtained depended on the method of demagnetization, not on the particular system considered.

Fig.4 shows that the systems demagnetized by means of the coils wound directly on the magnets, i.e. those magnetically stabilized under conditions similar to their working conditions, are affected by subsequent heat treatment and time in approximately the same manner as the systems demagnetized with the a.c. electromagnet; their fluxes show a slight drop. A.C. electromagnet demagnetization is therefore sufficiently reliable. But systems demagnetized with the d.c. electromagnet reacted quite differently to heat treatment; their fluxes increased by up to 0.2 per cent. It would seem that large pole pieces make demagnetization with d.c. electromagnets more difficult than with a.c. electromagnets. The latter method is more similar to the way in which magnets are normally demagnetized during use.

Fig.4 also shows that premagnetization heat treatment has little effect on the subsequent behaviour of Alnico magnet systems and so is not essential. The same conclusion had also been reached for Magnico systems.

The present work also included some tests of the effects of magnetic shunts. Magnetic shunts were fitted to six of the above eleven systems before magnetization, and after demagnetization and heat treatment at $+80^{o}C$ these shunts were transferred between extreme positions. Nos. 365, 400, 461, 515 and 420 had shunts fitted after annealing, i.e. moved to have maximum shunting effect, while no. 431 had its shunt removed. Fig.4 shows that the stabilities are approximately the same with or without shunts. Only in no. 431 did the flux decrease by ~ 0.09 per cent during the first six months after the de-shunting, and this has remained stable for the last nine months.

Effects of temperatures, vibration and external magnetic field

These effects were studied mainly on magnetically and thermally stabilized Alnico and Magnico magnets, .i.e. ones which had undergone temperature cycle conditioning after magnetization and demagnetization.

The systems were demagnetized by varying percentages (5 – 10 per cent) and after demagnetization were thermally cycled a number of times (+80°C to +20°C) and subsequently annealed at either +50°C or –50°C for 5 hr. The flux changes after this treatment were within the limits of experimental error.

Magnico magnets heat-treated after stabilization, but only annealed at 50°C retained their fluxes practically unchanged for one year after stabilization.

Vibration at 30 c/s and accelerations of 7g produced no effect on Magnico and Alnico magnets demagnetized by 6 – 10 per cent.

These systems were subjected to an external uniform d.c. field of 4 ampere/turns/cm and also to a 50 c/s a.c. field of 4 ampere-turns/cm peak. No changes were produced by this test.

A flux increase of up to 0.09 per cent was observed in some cases when a 50 c/s field of amplitude 40 ampere-turns/cm had acted on Alnico magnets demagnetized by 6 – 10 per cent by an a.c. electromagnet. Those demagnetized 6 – 10 per cent by a d.c. electromagnet showed even greater flux increases, namely 0.1 – 0.4 per cent.

The causes of the flux increases found in the Alnico systems used in the earlier tests were investigated by demagnetizing them in a weak 50 c/s field from coils wound direct on the magnets. The fluxes decreased.

In a second test the systems were demagnetized in the same type of field but with the coil wound on the ring completing the magnetic circuit. In this case the flux in the air gap was increased.

It seems possible that in the first case only the actual magnets become demagnetized, causing flux reduction in the air gap, whereas in the second the comparatively weak alternating field affects the properties of the ring completing the circuit more than the actual magnets. It is also possible that applying the demagnetizing coil to the ring (which was originally magnetized in the opposite sense to the magnets) improves the properties of the magnetic circuit and thus increases the air gap flux.

It is suggested that the flux increase found when the system has been subjected to a comparatively weak external field (40 ampere-turns/cm), is associated with the way this field affects the magnet keeper ring.

Conclusions

The work on Magnico and Alnico magnets largely solved a number of problems relating to their stabilities against various external factors and indicated rational technical means of stabilizing them satisfactorily.

The results apply to a considerable extent to other such items. But as the shape of the circuit and the material influence the stability to some degree more general deductions can only come from further work with various designs.

REFERENCES

1. A.S. Zaimovskii, P.I. Denisov, E.S. Berkovich and N. Ia. Drozdov; Improving the magnetic properties of iron–nickel–aluminium alloys. *Elektrichestvo* No.20, 22 (1937).
2. A.A. Kuznetsov, A.S. Naimovskii and V.V. Usov; *Metals and Alloys in Electrical Engineering* p.280. Gosenergoizdat (1949).
3. L.M. L'vova, A.S. Zaimovskii and V.V. Usov; *Ibid.* p.282.
4. K. Hoselitz; Modern hard magnetic materials. *J. Sci.Instrum.* **23**, 65 (1946).
5. J.H. Goss; Permanent magnet materials. *Mech.Engng., N.Y.* **70**, 671 (1948).
6. A.J. Tyrrell; The performance and stability of permanent magnets. *J. Brit.Instn.Radio Engrs.* **10**, 182 (1950).
7. S.F.Knight; A sensitive balance for stability tests on permanent magnets. *Proc.Inst.Elec.Engrs.* **96**, 635 (1949).
8. R.K. Tenzer; A contribution to the ballistic null-method for precise measurement of magnetic flux densities. *Arch.Elektrotech.* **40**, No.7, 406 (1952).
9. R.K. Tenzer; A precision measuring circuit for research on the ageing of permanent magnets. *Arch.Tech.Messen* No.239, 285 (1955).
10. K.J. Kronenberg; An investigation of ageing in permanent magnets. *Z. Angew.Phys.* **9**,321 (1953).

EFFECT OF EXCITER SATURATION ON TRANSIENTS IN SYNCHRONOUS MACHINES*

L.Z. SHENKMAN

It has been repeatedly stated [1,2] that the exciter affects transients in synchronous machines. Short-circuit and voltage recovery tests with the exciter connected to the generator rotor winding give a time constant T_d' somewhat smaller than that obtained by field-switching tests with the exciter disconnected. Exciter effects must therefore be allowed for when a more accurate knowledge of transients in synchronous machines is required.

Analytical solution of the differential equations for transients in a synchronous machine plus those for exciter transients is rather complicated and is possible only if the equations are linearized by neglecting exciter saturation [2]. This linearization causes considerable errors and vitiates the results. We have analysed transients in a system of synchronous machine plus exciter (allowing also for saturation) by integrating the equations numerically using the no-load exciter characteristic.

Theoretical formulae

As is usual when setting up the equations [2] we neglect the stator transient and stator resistance, the speed changes and also the effect of damper windings. The differential equation for the transient can then be written [3 - 4]:

$$E_{\text{det}} = E_d + T_d' \frac{dE_d}{dt} \qquad (1)$$

where

E_{det} is the steady-state e.m.f. determined by the excitation current corresponding to the exciter terminal voltage;

* *Elektrichestvo* No.1, 35–38 (1957). [Reprint Order No. EL.14]

E_d is the e.m.f. determined by the excitation current;

T'_d is the transient time constant

$$T'_d = T_{d0} \frac{x'_d}{x_d}$$

The stator current equation for a three-phase stator short circuit is the same form:

$$I_{det} = I_d + T'_d \frac{dI_d}{dt} \qquad (2)$$

I_d being related to E_d on a per unit basis by the following obvious relation:

$$I_d = \frac{E_d}{x_d}$$

The exciter transient differential equation can be representated with satisfactory degree of accuracy by that for e.m.f. equilibrium in the exciter winding [5 – 6]:

$$U_e = i_e r_e + 2pw\sigma \frac{\Phi_n}{E_{en}} \cdot \frac{dE_e}{dt} \qquad (3)$$

here

E_e and U_e are the e.m.f. and terminal voltage of the exciter,

i_e is the current in the exciter winding,

$2p$ is the number of exciter poles,

w is the number of turns per pole in the field winding

Φ_n and E_{en} are the rated effective magnetic flux and corresponding rated e.m.f.

σ is the magnetic flux leakage coefficient for the main exciter poles, equal to the ratio of total to effective flux ($\sigma > 1$)

To integrate nonlinear equations numerically we write them in finite difference form. The synchronous machine transient equation is

$$E_{d2} = \frac{2\Delta t}{2T'_d + \Delta t} E_{\text{det}} + \frac{2T'_d - \Delta t}{2T'_d + \Delta t} E_{d1} \tag{4}$$

Neglecting saturation we can write on a per unit basis:

$$E_{*d} = I_{*r}$$

where

I_{*r} is the ratio of the rotor current to the no-load value.

Then

$$I_{r2} = \frac{2\Delta t}{2T'_d + A_t} I_{\text{ret}} + \frac{2T'_d - \Delta t}{2T'_d + \Delta t} I_{r1} \tag{5}$$

The equation for the exciter transient is:

$$\frac{U_{e1} + U_{e2}}{2} = \frac{i_{e1} + i_{e2}}{2} r_e + k \frac{E_{e2} - E_{e1}}{\Delta t} \tag{6}$$

where

$$k = \frac{2pw\sigma\Phi_n}{E_n}$$

Exciter armature reaction is allowed for by subtracting γI_r from i_e (2)

$$\delta E_{\text{arm.react.}} = c\sigma I_r \gamma \tag{7}$$

where

γ is the armature reaction coefficient

c is the gradient of the exciter no-load characteristic, $c = f(E_e)$ (Fig.1).

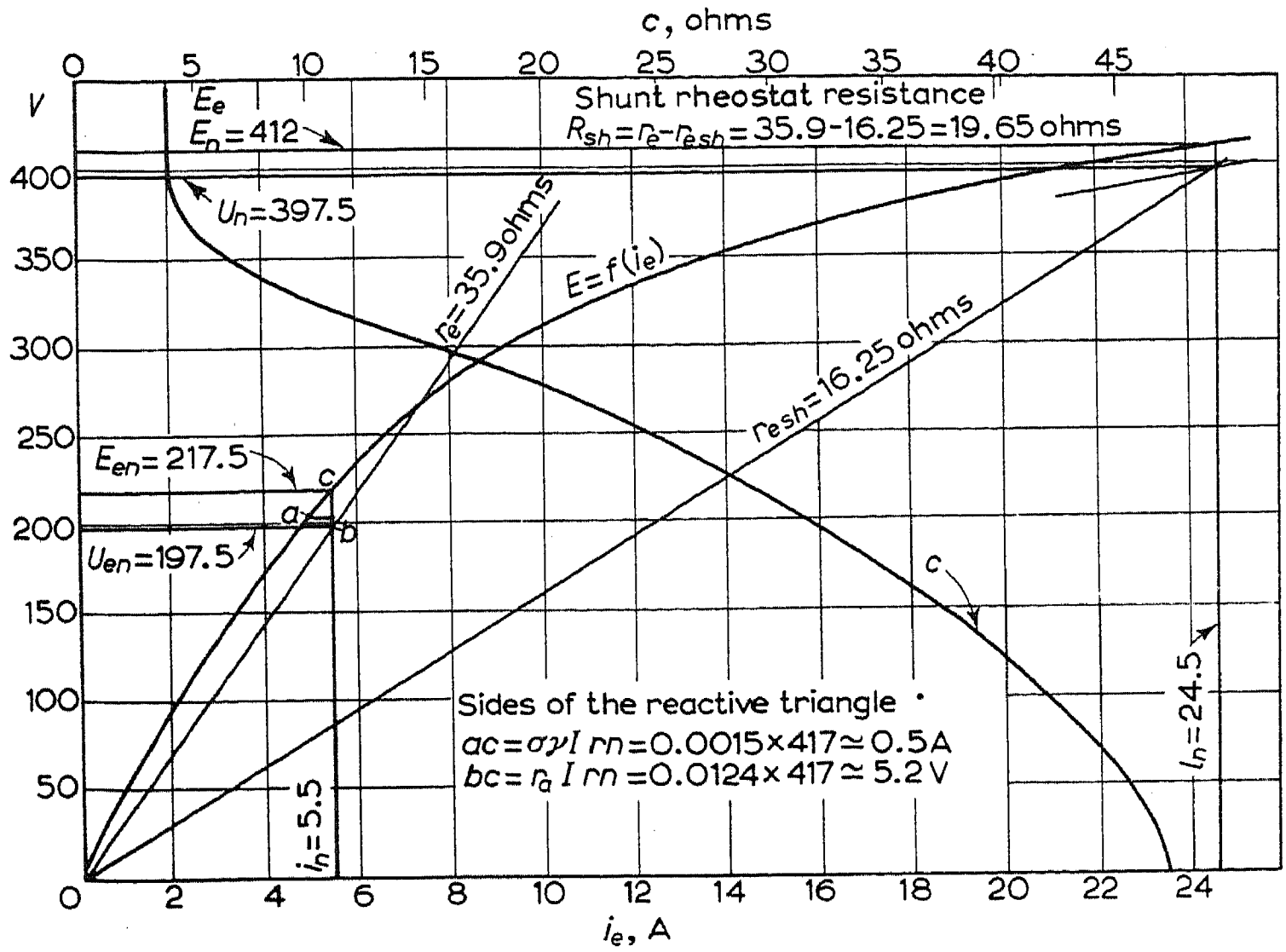

Fig. 1

The relation between exciter terminal voltage and e.m.f. can be rom equation (7) expressed simply as

$$U_e = E_e - (c\sigma\gamma + r_a)\, I_r \tag{8}$$

here

r_a = resistance of the exciter armature, made up of the armature, compoles and compensating winding resistances and the equivalent brush contact resistance.

Introducing (8), (6) becomes:

$$\frac{E_{e1} + E_{e2}}{2} - (c\sigma\gamma + r_a)\frac{I_{r1} + I_{r2}}{2} =$$

$$= \frac{i_{e1} + i_{e2}}{2} r_e + k\frac{E_{e2} - E_{e1}}{\Delta t} \tag{9}$$

So the exciter e.m.f. and current can be expressed in terms of their previous values as:

$$E_{e2} + i_{e2} r_e \frac{\Delta t}{2k - \Delta t} = E_{e1} \frac{2k + \Delta t}{2k - \Delta t} - i_{e1} r_e \frac{\Delta t}{2k - \Delta t} - (I_{r1} + I_{r2})\, r_e \frac{\Delta t}{2k - \Delta t} \qquad (10)$$

where

$r_e = c\sigma\gamma + r_a$ is the equivalent exciter resistance.

When field-forcing is automatic we assume that the whole or part of the exciter field rheostat is cut out from the beginning of the transient.

$$(r_e = r_{e.sh} - \Delta R_{sh})$$

When compounding is used a term proportional to the stator current is introduced on the right-hand side of (9):

$$c\, k_i\, I_d$$

where k_i is the compounding coefficient [2].

Thus the problem is reduced to the simultaneous numerical solution of equations (5) and (10) with the exciter no-load characteristic $E_e = f(i_e)$, (Fig.1), whereby

$$\underset{*ret}{I} = \frac{U_e}{R_r I_{e0}} \qquad (11)$$

where

R_r is the rotor resistance,

I_{e0} is the rotor current at no-load, and $U_e = E_e - (c\sigma\gamma + r_a)\, I_r$

Transient calculation

Consider a three-phase short-circuit at the stator terminals of a T-2-25-2 turboalternator with a model B 4-120-3000 exciter.

The T-2-25-2 turboalternator parameters are* [7]

P_n	= 25 MW	x_d''	= 12.9%	Rotor currents	
U_n	= 10.5 kV	x_d'	= 23.3%	I_{r0}	= 164 A
I_n	= 1720 A	x_d	= 199%	I_{rn}	= 417 A
$\cos\phi$	= 0.8	R_r	= 0.473 Ω	I_{1r}	= 267 A
T_{d0}	= 9.9 sec	r_a	= 0.19%	T_d'	$= 9.9\,\frac{0.233}{1.99} = 1.16$ sec.

The parameters of the model B4-120-3000 exciter are: P = 120 kW, U = 230 V, I_a = 520 A.

$2p$ = 4, number of parallel field windings,

a = 1, number of turns per pole of this winding,

w = 600, number of turns per pole of the armature winding,

w_a = 23.

Exciter resistance r_e = 16.25 Ω, compoles, r_c = 0.0021 Ω, armature, r_a = 0.0053 Ω.

Flux at the rated load, $\Phi_n = 2.58\text{x}10^6$ maxwell.

E.m.f. at rated load, E_n = 238 V. Resistance of the armature circuit† $r_a(75^\circ\text{C})$= 0.0124 Ω.

Leakage coefficient σ = 1.15 [6]. Coefficient of armature reaction γ = 0.001 [2].

The no-load exciter characteristic $E_e = f(i_e)$ is shown in Fig.1. The shunt rheostat resistance determined from the no-load characteristic (Fig.1) is R_{sh} = 19.65 Ω.

---

* The resistances are given at 75°C, except those for compoles and armature, which are given at 15°C.

† We assume a brush contact drop of 1.5 V.

On introducing the numerical values (5), (8), (10) and (11) become:

$$\underset{*}{I}_{r2} = \frac{2\Delta t}{2.32 + \Delta t}\,\underset{*}{I}_{\mathrm{ret}} + \frac{2.32 - \Delta t}{2.32 + \Delta t}\,I_{r1} \tag{5a}$$

$$U_e = E_e - (0.0015\ c + 0.0124)\ I_r \tag{8a}$$

$$\left.\begin{aligned} E_{e2} + i_{e2}\,\frac{35.9\Delta t}{0.598 - \Delta t} &= \\ = E_{e1}\,\frac{0.598 + \Delta t}{0.598 - \Delta t} - i_{e1}\,\frac{35.9\Delta t}{0.598 - \Delta t} &- \\ - (I_{r1} + I_{r2})\,\frac{(0.0015c + 0.0124)\Delta t}{0.598 - \Delta t} & \end{aligned}\right\} \tag{10a}$$

$$\underset{*}{I}_{\mathrm{ret}} = U_e/77.5 \tag{11a}$$

The compounding coefficient was estimated to be $k_1 = 0.00278$ [2]. The calculation can proceed when Δt is assigned a value. The tabulated form of calculation is most convenient. The results, viz. curves of stator and rotor currents as functions of time, are shown in Fig.2.

Conclusions

(1) Comparison of the stator and rotor current during generator transients found when exciter saturation is allowed for (Fig.2) with those obtained from the linearized differential equations (cf [2], Fig.5) shows that exciter saturation has a considerable effect on the transient especially in its final stages. For example, the exciter effect becomes apparent from the fact that after 10 sec the rotor current with compounding falls by $\Delta I_r = 0.24\ I_{r0}$ is the no-load rotor current.

The linearized system gives $\Delta I_r = 1.2 I_{r0}$ (cf.2, Fig.5).

The large discrepancy (a factor 5) is explained by the armature reaction being assumed to remain constant at its initial value throughout the transient (linearized no-load characteristic) in the linearized system.

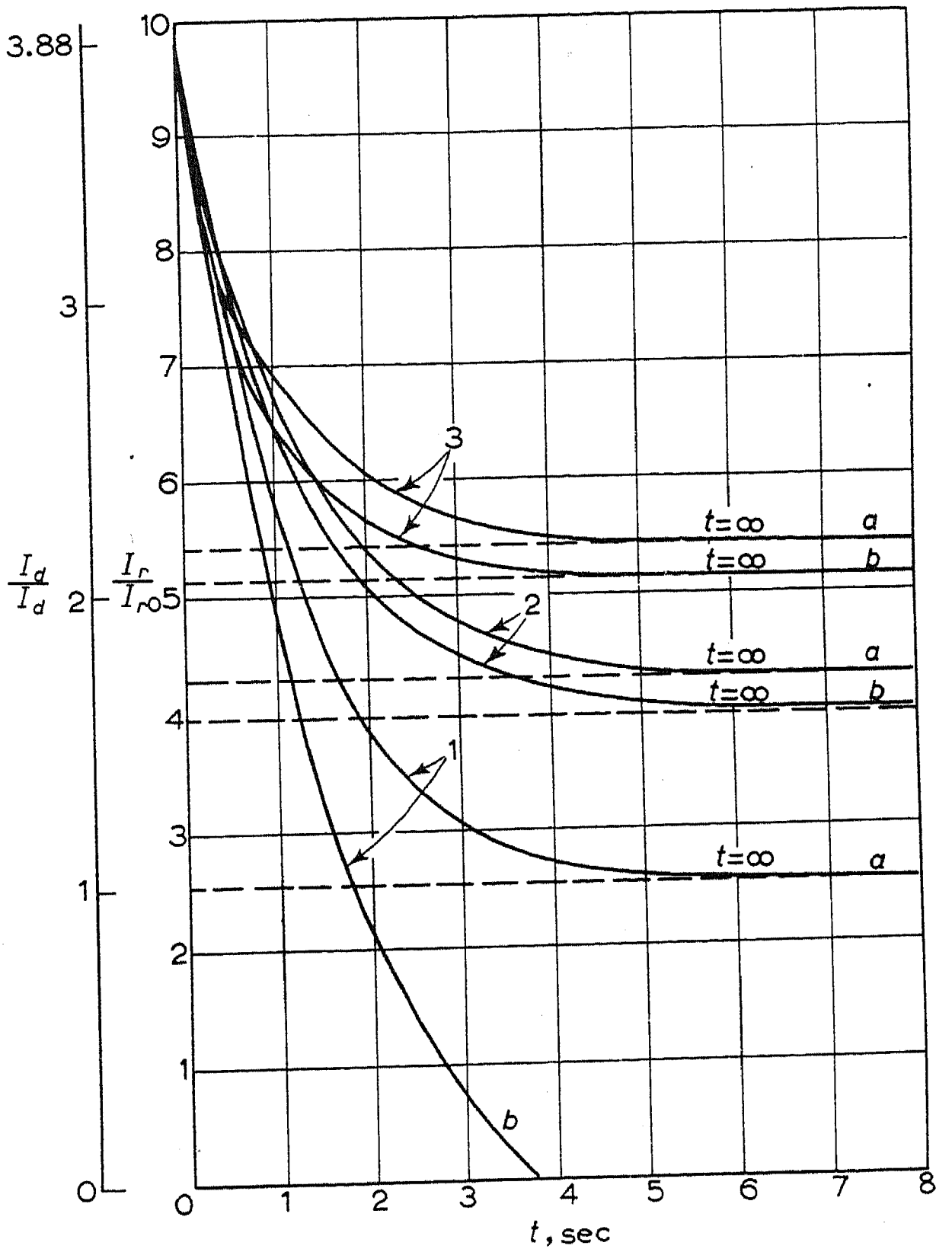

Fig. 2. (a) Neglecting the effect of the exciter

(b) Including the effect of the exciter

1 – without additional measures on the exciter,

2 – with compounding,

3 – with automatic field forcing.

The equivalent armature circuit resistance is here large $r_e = 0.2\, R_r$, [2]. This causes a large drop in exciter terminal voltage and therefore a large fall in the rotor current.

Neglect of exciter saturation thus makes its apparent effect on the transient considerably greater than the real one.

(2) The greatest distortions of the transient picture due to neglect of exciter saturation occur when automatic field-forcing or compounding is used. In this case the exciter voltage rapidly approaches its limiting value (within 0.5 – 0.7 sec), complete exciter saturation

occurs and armature reaction becomes very small. The effect of the exciter on the transient is then noticeable only during the initial stage when the exciter voltage has not yet risen to its limiting value. The exciter affects the steady-state rotor-current only via the voltage drop in r_a, which is 15 per cent of $r_{e\ \max}$.

Again we notice the beneficial effect of compounding on the whole transient process.

(3) No great differences are introduced when non-linearity is allowed for in the absence of automatic field-forcing and compounding. For example, under the conditions obtaining when T'_d is determined experimentally, the exciter works on the unsaturated part of its characteristic and appears to be highly effective. As has been stated [2] considerable demagnetization or remagnetization can then occur. This can be observed if for some reason the exciter armature resistance or the armature reaction are increased.

The author is indebted to L.G. Mamikoniants Cand.Tekh.Nauk for valuable advice and suggestions during the preparation of this article.

REFERENCES

1. L.G. Mamikoniants; Improving the accuracy of synchronous machine parameters. *Elekt. Stantsii* No.11 (1949).
2. L.V. Tsukernik; Transients systems in synchronous machine + exciter systems. *Elektrichestvo* No.10 (1954).
3. S.A. Ul'yanov; *Short-Circuits in Power Systems*. Gosenergoizdat (1952).
4. P.S. Zhdanov; *Power System Stability*. Gosenergoizdat (1948).
5. V.T. Kas'yanov; Theoretical calculation of exciter voltage rise rates. *Elektrosila* No.9 (1951).
6. V.T. Kas'yanov; *Design of Salient-Pole Synchronous Generators*. (1951).
7. *Electrical Engineering Reference Book*. Gosenergoizdat (1952).

THE BEHAVIOUR OF RELAY PROTECTION ON UNSYNCHRONIZED RECLOSING*

TSZO KHU

Molotov Power Engineering Institute, Moscow

(Received 14 March 1956)

Unsynchronized automatic reclosing of individual transmission lines of power systems has lately assumed increasing importance on account of its simplicity and effectiveness. However, this must not be taken as meaning that all the problems associated with this use of automatic reclosing have been sufficiently studied and solved. In particular, one of these problems is the behaviour of relay protection and prevention of its incorrect operation during unsynchronized reconnexion [1]. We will consider this problem below with reference to systems having large earth-fault currents.

It is well-known that unsynchronized closing of a transmission line may result in a synchronous operation and power swings and, consequently, (owing to the varying power angles between e.m.f. vectors of the generators) variations of the phase currents, voltages and other electrical quantities may occur, similar to those occurring in the case of power swings caused by disturbances to the static or dynamic stability of the system.

Immediately after unsynchronized reconnexion negative and zero phase-sequence components may appear for a short time due to partial reclosures resulting from the sequential making of the circuit-breaker contacts.

We will assume equal positive and negative sequence impedances and also that the station e.m.f's NM (Fig.1a) have the same magnitude. Referring to the equivalent circuits (Fig.1d), the negative and zero-sequence currents will be: when a single phase is closed:

$$I_2^{(I)} = I_0^{(I)} = 2 \sin \frac{\delta}{2} \frac{1}{2z_{1t} + z_{0t}} \qquad (1)$$

* *Elektrichestvo* No. 1, 42–51 (1957). [Reprint Order No. EL. 15]

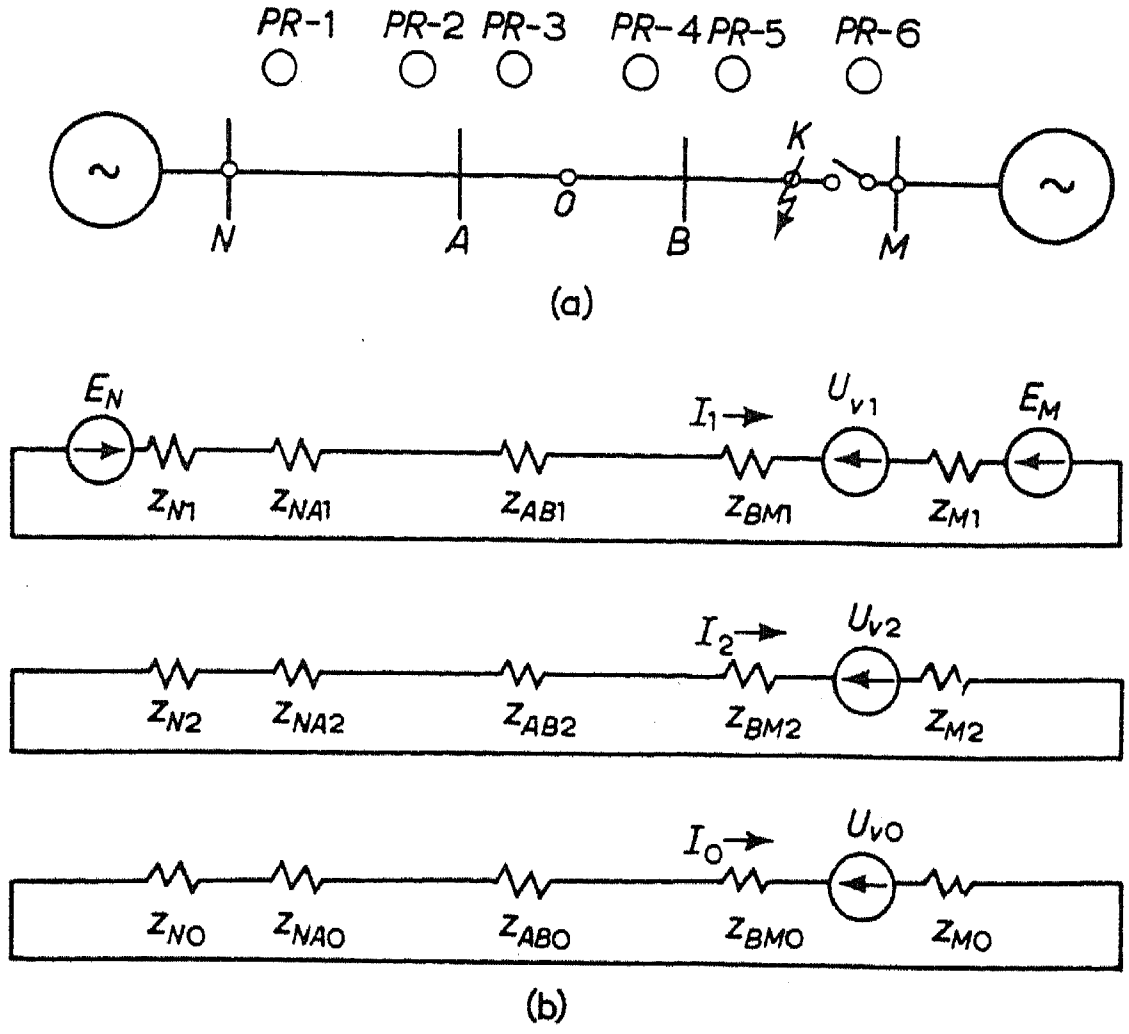

Fig. 1. Actual circuit and equivalent circuits of various phase-sequences during unsynchronized automatic reclosing.

when two phases are closed

$$I_2^{(II)} = 2 \sin \frac{\delta}{2} \frac{z_{0t}}{z_{1c}(2z_{0t} + z_{1t})} \tag{2}$$

$$I_0^{(II)} = 2 \sin \frac{\delta}{2} \frac{1}{2z_{0t} + z_{1t}} \tag{3}$$

where

z_{1t} and z_{0t} are the total impedances of the positive and zero sequences of the whole system;

δ is the difference of the e.m.f. vector angles of the generators in partially reclosed operation. If we assume that δ can reach 180^o during unsynchronized reconnexion the maximum negative and zero sequence currents will, according to equations (1), (2) and (3) be determined in the following way:

When $z_{1t}/z_{0t} > 1$

$$I_{2max} = \frac{2}{2z_{1t} + z_{0t}} \tag{4}$$

$$I_{0max} = \frac{2}{2z_{0t} + z_{1t}} \tag{5}$$

When $z_{1t}/z_{0t} < 1$

$$I_{2max} = \frac{2z_{0t}}{z_{1t}(2z_{0t} + z_{1t})} \tag{6}$$

$$I_{0max} = \frac{2}{2z_{1t} + z_{0t}} \tag{7}$$

The above expressions for electrical quantities as functions of δ after unsynchronized reconnexion are the same equations as in the case of power swings or loss of stability when the oscillations are initiated by a short-circuit. The only difference between unsynchronized reconnexion and power swings following short-circuit is that δ may take values up to 180^{o} (in the first case) whereas in the second case δ, being initially the angle under the operating conditions preceding the short-circuit, cannot change discontinuously and will become large only a certain time after the oscillation starts.

Incorrect operation of relay systems during oscillations is due to the fact that unsynchronized automatic reclosing may occur at large values of δ and, after reclosing, asynchronous operation and oscillations may take place.

The behaviour of distance relays on a line, the circuit of which is indicated in Fig. 1(a), is considered as an example of the behaviour of such protective systems after unsynchronized reclosing. We analysed the response of the relay units RZ-4, RZ-5 of this system. The analysis was carried out in the complex impedance plan (Fig. 2). The results of the analysis may be summarized as follows.

The distance protection operating with an impedance relay and a directional power relay, may operate incorrectly on unsynchronized reclosing if the electrical centre of the system is situated inside the protected zone or in its immediate neighbourhood. In cases in which the electric centre of the system during the unsynchronized

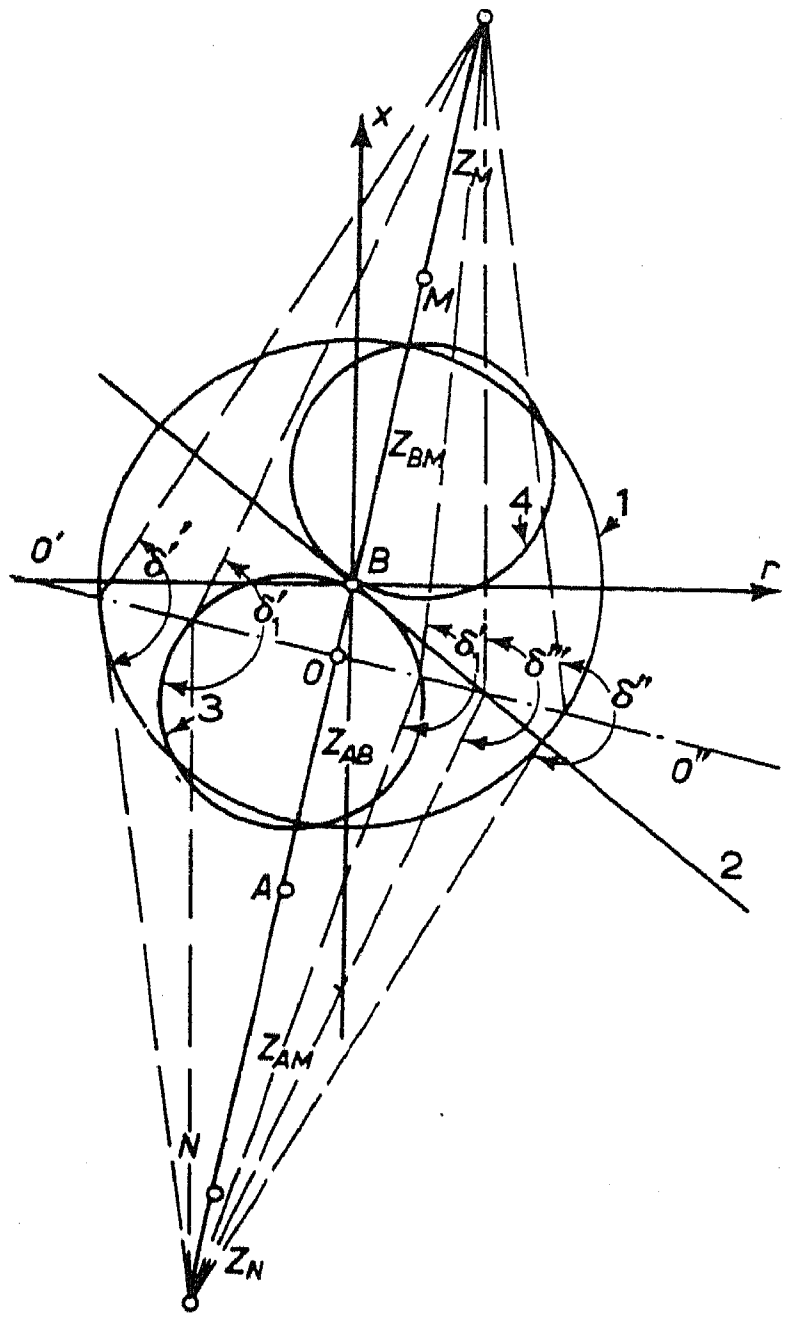

Fig. 2. Analysis of the behaviour of distance protection during unsynchronized reclosing, represented in the complex resistance-impedance plane.

(1) Characteristic of the impedance relays of the protection units PR–4 and PR–5 (Fig. 1);

(2) Characteristic of the directional power relays PR–4 and PR–5;

(3) and (4) Characteristics of the directional impedance relays of PR–4 and PR–5. The straight line $0'\ 0''$ is the locus of the impedance vectors at the terminals of the relays PR–4 and PR–5.

reclosing is behind the busbars of the sub-station in which the protection is installed, the possibility of an incorrect operation may be eliminated by using, for example, for a protection relay PR–5 (Fig. 2) an impedance relay having a directional distance element.

It follows that we arrive at the same conclusions as resulted from the analysis of the behaviour of distance protection under power swings [2].

Protection systems responding to negative and zero-sequence components and acting without time-lag may also operate incorrectly on unsynchronized reconnexion.

An instantaneous zero-sequence relay may operate if its setting current is smaller than the maximum zero-sequence current at unsynchronized reconnexion (cf. expressions (5) and (7)). The behaviour of a directional instantaneous zero-sequence relay during unsynchronized reconnexion depends on the behaviour of its directional power element. If, on unsynchronized reconnexion the zero-sequence current at the location of the relay set for the direction towards the busbars leads the voltage of the same phase-sequence, the directional power element will not respond and, consequently, neither will the directional zero-sequence relay. This, for example, corresponds to the behaviour during unsynchronized reconnexion of the protective equipment PR–4 in the section BM (Fig.1a). The zero-sequence relay can be rendered insensitive to the effects of partially reclosed operation by the use of an auxiliary relay with delayed action, having a time-lag slightly greater than the time required for closing the contacts of all three phases of the circuit breaker.

During unsynchronized reconnexion it is also possible for incorrect operation to occur in directional protection with carrier-current, lock-out, for example, a protection of type RZ–164. At the inception of the asymmetric conditions the protection is started, and when the asymmetry disappears, the directional elements of the protection are switched over to phase current and line voltage; the protection can then operate just as in the case of symmetric short-circuits on the protected element. The protection located in the section reclosed out of synchronism may operate also before the disappearance of the asymmetry if the voltage transformers are connected to the busbars, and the unsynchronized automatic reclosing is carried out by a circuit-breaker requiring a comparatively long time for closing the contacts of all three phases (e.g. a circuit-breaker with individual drives for each phase).

Differential current protective systems of all types, including phase comparison systems, should in principle never operate incorrectly on unsynchronized reconnexion.

Most of the devices, nowadays widely used, for lock-in protection systems in the case of power swings are based on two principles, viz. (1) on the use of the different character of variation of the electrical quantities in the case of short-circuits and power swings respectively and (2) on the principle of starting the protection at

the appearance of negative or zero-sequence components for a time sufficient for its operation. The devices based on the first principle prepare the relay circuit for tripping in the case of a sudden discontinuous variation of the phase or line currents and/or voltages. The devices based on the second principle prepare the relay circuit for tripping when asymmetrical conditions arise. Both types of device terminate the operation of the protection before the angular phase difference, δ, between the generators rises to a dangerous value (i.e. from the viewpoint of a possible incorrect operation of the protection).

Since in the case of unsynchronized reconnexion a sudden discontinuous variation of the currents and voltages of all phases, as well as negative and zero-sequence components may occur, the lock-in devices mentioned above may be activated just as in the case of short-circuits. Consequently, the protection may operate in the case of unsynchronized reconnexion until its operation is terminated by the lock-in devices. However, we should not conclude from this fact that it is impossible to use lock-in devices for preventing incorrect operation of the protection during unsynchronized automatic reclosing.

Let us consider the possibility of using for this purpose lock-in devices based on the principle of having the protection started by negative-sequence components of the voltage and current (U_2, I_2).

Lock-in devices used for preventing a response of the protection to power swings may also be used for preventing such an incorrect operation in the case of unsynchronized automatic reclosing. For this purpose the voltage or current setting of the starting element of such a device must be greater than the negative-sequence voltage or current associated with unsynchronized reconnexion at the location of the device.

This method of selection is conditional on

$$U_{2\ \mathrm{sh.c.min}}/U_{\mathrm{set}} > k_{\mathrm{sen}} \qquad (8)$$

where

$U_{2\ \mathrm{sh.c.min}}$ is the minimum negative-sequence voltage at the location of the protection in the case of a short-circuit in the protected zone; k_{sen} the required coefficient of sensitivity.

It should be noted that this condition is more easily satisfied in cases where the relays are located at points remote from the enclosed section.

Lock-in devices with time-controlled lock-out may be used to prevent incorrect operation of the protection of any section of the system, except the one reconnected, if unsynchronized automatic reclosing is carried out after the clearance of a short-circuit, i.e. after the operation of the relay protection.

It is well-known that in a system equipped with automatic reclosing gear the resetting time of the lock-in devices with time-controlled lock-out is selected after consideration of the time required for clearing a persisting short-circuit after unsuccessful reclosing. Consequently, the lock-out device started at the inception of a short-circuit and terminating the operation of the protection after a short time, may lock it in the case of unsynchronized reconnexion. If this principle is used it is advisable to use more sensitive starting elements.

For reliable locking, for example, of the protection RZ-3 at unsynchronized reconnexion of the line section BM (Fig.1), the following condition must be satisfied

$$U_{2A\ \text{sh.c.min}} > k_{\text{rel}}\, U_{\text{set}} \tag{9}$$

where $U_{2A\ \text{sh.c.min}}$ is the minimum negative-sequence voltage at the location of PR-3, set-up by a short-circuit in section BM; k_{rel} is the coefficient of reliability ($k_{\text{rel}} > 1$).

A lock-out device with time-controlled lock-out may be used to prevent incorrect operation of a protection in the case that the protection is located not far from the reconnected section.

The use of a combination of negative and zero-sequence components for starting the lock-out devices may in some cases slightly improve the reliability of locking the protection in the case of unsynchronized reconnexion.

To prevent incorrect operation of the protection on unsynchronized reconnexion it is desirable to desensitize the starting elements of the lock-out device where possible. It will then be possible to use lock-out devices with time-controlled, as well as with high-speed, lock-out and also to use a circuit for automatic asynchronous reclosing started by a "discrepancy circuit".

Let us consider the lock-out characteristics of the protection for line sections which may be reconnected unsynchronized.

It is well known that in cases in which the lines are equipped with automatic reclosing gear the lock-in circuits must be designed so that the protection is rapidly reset after a clearance of a short-circuit in the protected zone. The protection reset after the clearance of a short-circuit may respond to asynchronous reclosing in the same way as in the case of unsuccessful reclosing. For this reason lock-in devices with time-controlled lock-out of the conventional type cannot in this case prevent incorrect operation of the protection. Desensitization of the starting elements of the lock-out devices may in this case find only very limited application. The minimum negative sequence voltage or current at the location of the protection will frequently be smaller during short-circuits in the protected section than during unsynchronized reconnexion of this section. This can be partly explained by the fact that on unsynchronized reconnexion the whole negative-sequence current passes through the reclosed section, whereas in the case of a short-circuit the current is divided into two parts. If it is impossible to render the protection insensitive to the effect of unsynchronized reclosing by desensitization of the starting elements of the lock-out device, the reclosing must be carried out in the following way.

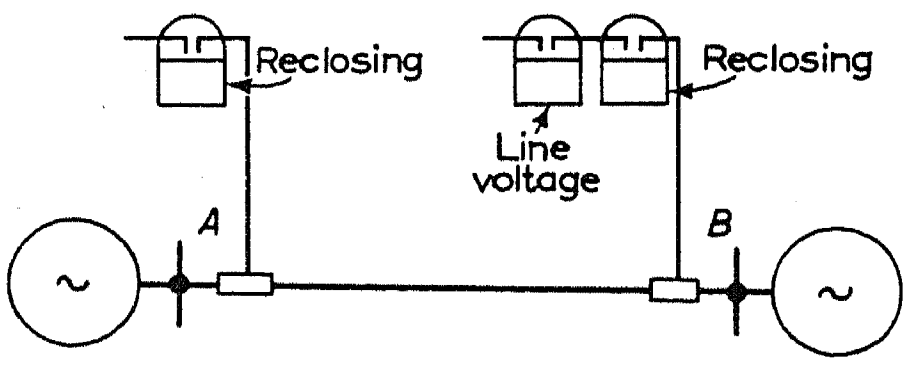

Fig. 3 Sequence of the unsynchronized reclosing of the line section *AB*. The contact of the line voltage relay is closed when the line is live.

The line is first reclosed from end *A* (Fig.3) in the absence of an opposing voltage. Reclosing from end *B* is carried out only when the closing from the end *A* is successful, i.e. if there is no sustained fault on the line. After successful reclosing from end *A*, the protection is made inoperative and reclosing from the end *B* is carried out after the protection has been made inoperative. To render the use of this method possible it is necessary in addition to making ineffective the protection at the end *A*, to use at the end *B* the lock-out device operating in the case of power swings with time-controlled deblocking and prevention of rapid resetting of the protection after the clearance of the short-circuit.

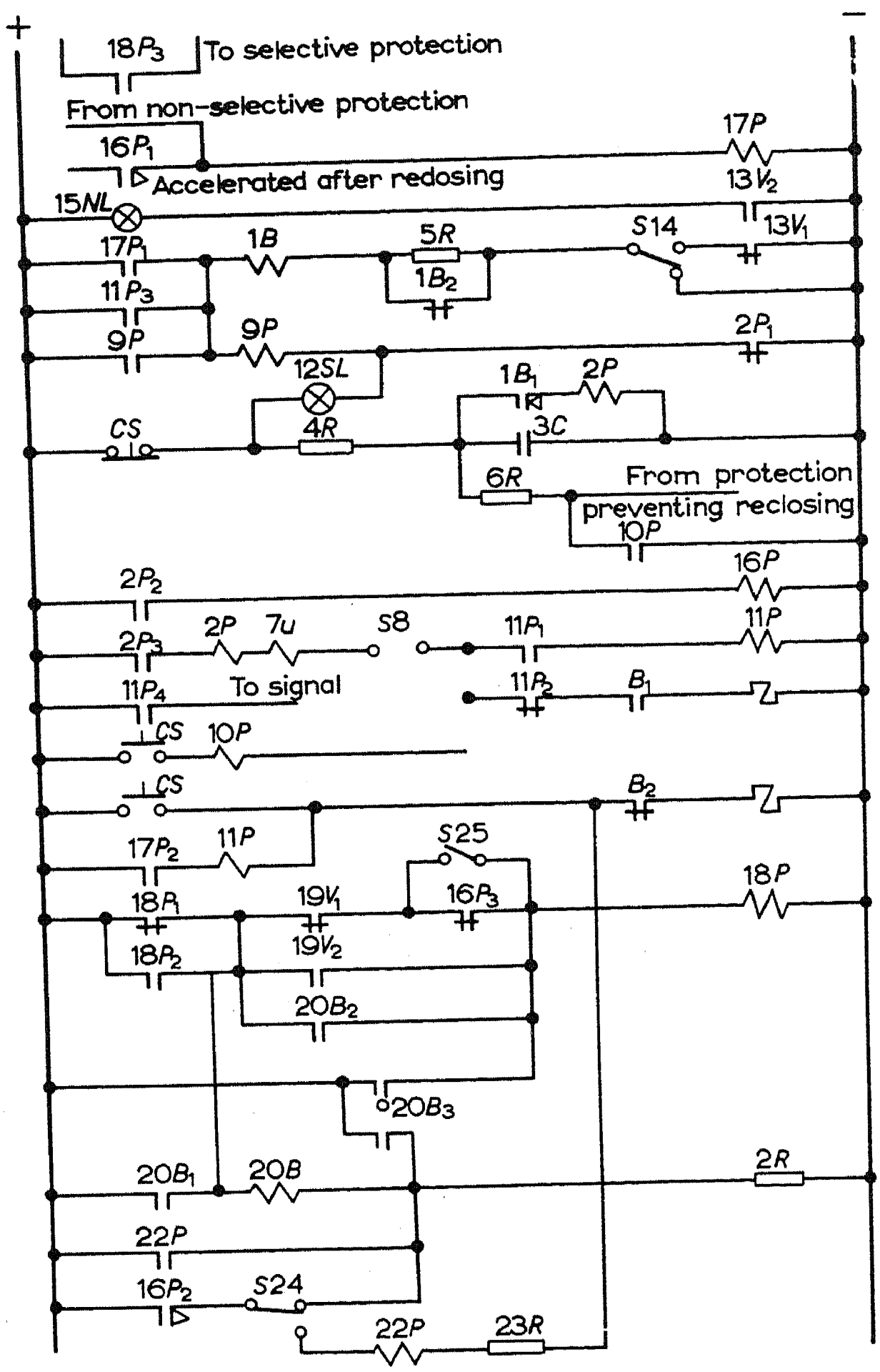

Fig. 4 A possible modification of the circuit for unsynchronized automatic reclosing.

1B, 2P, 3C, 4R, 5R, 6R, elements of relay EVP. 285;

7U signalling relay;

12SL incandescent lamp;

15NL neon lamp;

S8, S14, S24, S25 change-over switches;

18P, 19N, 20V, 21R, Lock-out devices with time-controlled deblocking;

13V voltage relay type EN. 529;

CS control switches;

9P, 17P, 22P intermediate relay type EP. 101;

11P intermediate relay type EP. 131;

10P intermediate relay with series winding;

16N intermediate relay, Type EP. 106;

23R series resistance.

The contacts as shown in the positions occupied by them when the line is closed and the circuit ready for operation.

A possible modification of the automatic reclosing gear, satisfying the conditions discussed is shown in Fig.4. This circuit is based on the commercial circuit APV-2, but is started by the relay protection. It contains change-over arrangements enabling the line to be tested from either end.* The change-over arrangements in the circuit of Fig.4 are shown in the position for testing the line. Relay 13H is designed for carrying out the detection of an opposing voltage, rendering the protection ineffective at end *A* after successful test of the line is carried out in the following way.

Simultaneously with the despatch of a closing signal to the circuit breaker, relay 16P starts operating. Its normally open contact $16P_2$ is closed and shunts the time relay 20V, whereas its normally closed contact $16P_3$ opens and interrupts the circuit of relay 18P. The relay 20B returns then into its initial position and cannot operate until the contact $16P_2$ of relay 16P drops off, and relay 18P biases the protection circuits and the windings of relay 20 EV. When the circuit-breaker contacts have closed, the armature of relay 16P drops off with a certain time lag. Owing to this, relay 20V will operate once more and the protection will become ineffective after its contact $20V_3$ has closed. In this way the lock-out device blocking the protection in the case of power-swings may be used for the same purpose during unsynchronized automatic reclosing.

The circuit contains further an intermediate relay 22P, for rapid deblocking of the protection when the circuit is used for reclosing from end *B*. This ensures rapid isolation of the line in the case of asymmetric short-circuits, when owing to an irregularity in the automatic reclosing circuit reclosing from end *B* takes place earlier than that from end *A*.

Conclusions

(1) Protection systems having to operate under the asymmetrical conditions produced for a short while during unsynchronized reclosing, can be neutralized against these effects by the use of an auxiliary relay with slightly delayed action.

(2) The lock-out devices neutralizing the protection against the effects of power swings may also be used to prevent incorrect operation of the protection on unsynchronized automatic reclosing.

---

* Testing is to be taken as meaning automatic reclosing of the line from one end in the absence of an opposing voltage.

In some cases this is obtained by desensitizing the starting elements of the lock-out devices and in others by using more sensitive starting elements and providing them with time-control deblocking devices.

(3) Incorrect operation of the protection of an unsynchronized reclosed section may be prevented in all cases.

REFERENCES

1. L.G. Mamikonyats; Use of asynchronous operation of generators for improved reliability of the power supply. *Elektrichestvo* No. 8 (1955).
2. A.M. Fedoseev; *Relay Protection of Power Systems*. Gosenergoizdat (1952).

GENERATORS FOR ELECTRIC SPARK-MACHINING OF METALS*

A.L. LIVSHITS AND I.S. ROGACHEV

In electric methods of machining metals the metal is cut or its structure and durface finish altered thermally or chemically by an electric current supplied direct to the tool or work. Electro-erosion is a special type of electrical machining based on joule heating.

Three fundamental conditions must be satisfied if electrical erosion is to give true-scale machining and if the blank is to reproduce the tool electrode shape faithfully.

(1) The current pulses supplied must be sufficiently short, the "feed rate" being determined by the distance between the elementary portions of the electrodes. The maximum pulse durations $t_1 < 10^{-4}$ sec [1] and $t_1 < 10^{-3}$ sec [2] recommended in the literature cannot be confirmed. The precision of the tool-shape reproduction and the cutting rate are increased, and the tool wear and power consumption reduced, if the pulse duration is between 10^{-3} and 10^{-2} sec. Only under "soft" operating conditions, in machining hard alloys and for delicate work should the pulse duration be reduced to 0.15×10^{-3}sec [3,4], or less.

(2) The area between electrode and work to which the pulse is supplied must be fairly small to obtain the required energy concentration together with acceptable finished maximum surface-roughnesses.

The area varies with the working cond tions from 10^{-4} mm^2 to several mm^2 and the maximum surface roughness from 10^{-3} to 0.5 mm.

(3) The pulses must be supplied continuously at the requisite frequency and space-mark ratio.

* *Elektrichestvo* No. 3, pp. 19–23, (1957). [Reprint Order No. EL.17]

The pulse repetition frequency in electro-erosion lies within the audio range. The pause space mark ratio varies from 1.1 to $10–10^2$.

The above conditions are satisfied by supplying the electrodes through a discharge channel (making arc or spark) or through a contact between micro-roughnesses of the electrodes moving relatively to one another (breaking arc or spark) [3]. In the first case a special voltage pulse source is required, viz. an impulse generator; in the second case, a mechanical device which produces a relative electrode displacement (rotation, vibration, etc. is required, the electrodes being connected into a d.c. or a.c. circuit. Combined electrical and mechanical generation systems are also possible.

The load on the impulse generator is the erosion gap, i.e. a short arc or sparking and arcing discharge between the electrodes. The distances between the electrode sections, the volume and surface concentrations of the erosion products in the working zone, the conditions of particle and gas removal, etc., may all vary during the operation. Different types of generators will react differently to such variations. If the amplitude, duration and frequency of the impulses supplied by the generator do not depend on the physical conditions in the erosion gap, they are termed *independent*. If this is not so, they are referred to as *dependent*. Certain generators have some parameters (e.g. polarity, mark–space ratio) which depend on the conditions in the erosion gap, whereas others (e.g. the frequency) do not.

The method of generation, the type of generator, type of current, working fluid, polarity, tool material, etc., imply certain differences between electro-erosion methods. For example, the spark-cutting method uses electrical generation, a *dependent* (relaxation) generator, asymmetric pulses of alternating polarity, an insulating fluid, direct polarity (tool–cathode, work–anode). The new electric– impulse method [3] also uses electrical generation, an insulating liquid, but an *independent* generator, *unipolar* current pulses, and reversed polarity (in working steel). The mechanical–anodic method uses mechanical generation via a dependent generator, unipolar current pulses, an electrolyte (waterglass) and direct polarity. The electric-contact method differs from the mechanical–anodic method in the preferred use of pulses of alternating polarity and in the working medium (air, water, less frequently oil). Because the two latter methods involve relative motion the chances of reproducing the shape of the tool electrode are restricted.

Electrical erosion is polar in nature, i.e. with given electrode materials, working medium and pulse parameters, there is a definite pulse polarity which gives the maximum rate of removal of metal from the work and the minimum from the tool. Also if an unsuitable polarity is used solid pyrolytic residues from the liquid medium deposit on the electrodes, which disrupts the steady erosion process and spoils the surface of the work. So electro-erosion should employ unipolar impulses.

Machining by unipolar impulses of considerable duration increases the rate of removal of material by a factor 10, reduces the relative wear by factors of 5 – 20, and the energy consumption by factors of 3 – 5 relative to alternating-polarity impulses produced by a dependent relaxation generator [3].

Hence a new branch of electrical engineering had to be developed, viz. the production of *strong unipolar impulse currents at low voltages at audio-frequencies*. It is very difficult to generate such currents because there are no suitable generators. This led to a number of compromise solutions, taking the form of dependent relaxation generators of asymmetrical alternating current and voltage impulses (of types RC, RCL, RCLL, etc.) used to supply spark-machining units [3], and of rotary generators for asymmetrically alternating impulse voltages [5].

In principle, sources of unipolar voltage pulses can be based on:

(a) current interruption; (b) rectification of sinusoidal or pulse-type alternating voltages; (c) superposition of direct and alternating e.m.f.'s of different wave-forms; (d) direct generation; (e) various combinations of the foregoing principles.

Two types of unipolar pulse generator using current interruption exist: (a) with turbo-type mercury-jet interrupters, first realized in the Odessa Polytechnical Institute in 1951, similar to the well-known systems used in radio engineering [6] and (b) with electrolytic interrupters [7], designed specially for electro-impulse machining. Both types of interrupters can produce currents of some 10 A at frequencies up to 100 pulses/sec. Their use is limited to "soft" operating conditions.

Independent pulse generators, based on half-wave rectification of sinusoidal voltages at power or higher frequencies using semi-conductor (selenium) rectifiers were produced between 1950 and 1955 for frequencies of 50 – 500 pulses/sec. and currents up to 100 A at mean voltages of up to 50 V. The advantages of such systems are their

simplicity and reliability and the possibility of supplying several independent circuits simultaneously by using both half-waves. Drawbacks of selenium rectifier generators are the inverse current half-wave due to the inverse conductivity of the barrier layer and its considerable capacitance, furthermore the need for special voltage supply at frequencies above 50 pulses/sec. (frequency converter, or for mark-space ratios exceeding 2, a generator of alternating pulses).

When selenium is replaced by new semi-conductor rectifiers (germanium, silicon, etc.) considerable current densities can be used, the capacitances being also small and the back-resistances high; this extends the useful frequency and current ranges considerably, and has added advantages of high efficiency and small dimensions. Electronic systems could give any frequency but are out of the question because of the small attainable currents. Ionic rectifier systems (thyratrons without grid-control) could furnish frequencies up to 3 - 5 kc/s [4], but only at low efficiencies, and would also be unduly bulky, even if only required to supply currents of around 0.1 A. The use of mercury power rectifiers is limited by their frequency range (500 - 700 pulses/sec) and low efficiency at the low voltages required.

The simplest way of obtaining unipolar pulses by superposing direct and alternating e.m.f.'s of different forms is to use a sinusoidal alternating e.m.f. In this case the direct component must equal the peak alternating voltage; however, the relative pulse duration obtained by interrupting an arc discharge at 20 - 30 V will be very large, this being undesirable for work in an erosion gap. To obtain a pulse of shorter relative duration we require an asymmetrical pulse voltage source, obtained from special rotary generators or electronic or ionic apparatus. A drawback of superposed voltages is the need to use two supplies of specially chosen and matched characteristics. The limiting frequencies and currents are determined by the characteristics of the voltage sources.

Unipolar pulses can be generated directly by using ionic or electronic apparatus and rotary generators.

Ionic generators are preferable owing to their relatively simple construction when powerful unipolar pulses of low frequency (up to 150 pulses/sec) of controllable amplitude, relative duration and frequency are required. The power from ionic generators is practically unlimited, so the rate of removal of the metal is also unlimited. For example, with the ionic generators developed in 1950-1951 in the Ministry of the Machine Tool Industry [3], a rate of removal of material was ~ 6000 mm^3/min, this being 8-10 times higher than the limiting rate of removal in spark-machining. Disadvantages of independent ionic generators are their much

more complicated circuits for obtaining high frequencies, their low p.f.s and efficiencies, high transformer ratings and non-sinusoidal mains load currents.

Pulse generators using valves can provide low currents and high frequencies. This is because there are no hard valves designed for currents around 10-100 A (RMS) at voltages around 10 V. The development of controllable germanium or silicon power rectifiers will greatly improve this type of generator. Combined electronic and ionic unipolar pulse generators may also be considered [4].

The rotary pulse generators form a new branch of electrical engineering opened up only since 1951. We can distinguish machines for generating unipolar pulses directly and machines generating alternating pulse voltages, subsequently rectified either within or outside the machine.

Commutatorless d.c. machines must involve the circuit being altered in time by continuously introducing new circuit elements via sliding contacts. This is the principle on which a unipolar commutatorless d.c. machine is based. One of the authors [8] has suggested that this principle could also be used for producing unipolar pulses.

Let us imagine that the air gap in a unipolar d.c. machine varies periodically in width around the armature periphery, due to the arrangement of stator teeth (Fig.1). The flux density in the air gap will then

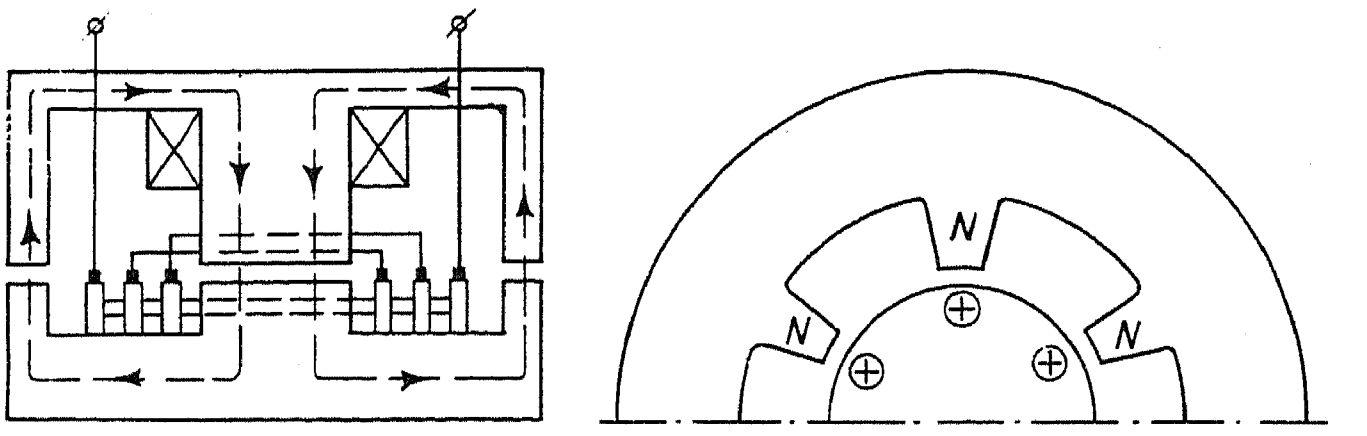

Fig. 1. General system of the unipolar generator.

also vary periodically. When the armature rotates at constant speed, e.m.f.'s will be induced in the bars of that armature winding, the instantaneous values of which will be proportional to the flux densities under the bars. If the ends of the bars are connected to slip rings running under brushes, the e.m.f. between the brushes will always have the same direction. By appropriate choice of air gap and stator slot dimensions, the minimum e.m.f. can be kept sufficiently small and the pulses will be practically unipolar and of a quite satisfactory form.

The frequency of the unipolar impulses is

$$f = zn/60 \qquad (1)$$

where z is the number of stator teeth; n the rotor speed in rev/min.

The maximum e.m.f. is

$$E_{max} = kB_{max}lv \qquad (2)$$

where k is the number of series-connected bars in the winding (no. of pairs of slip rings);

B_{max} = maximum flux density in the air gap,

l = active length of a bar, m;

v = peripheral speed of the armature, m/sec.

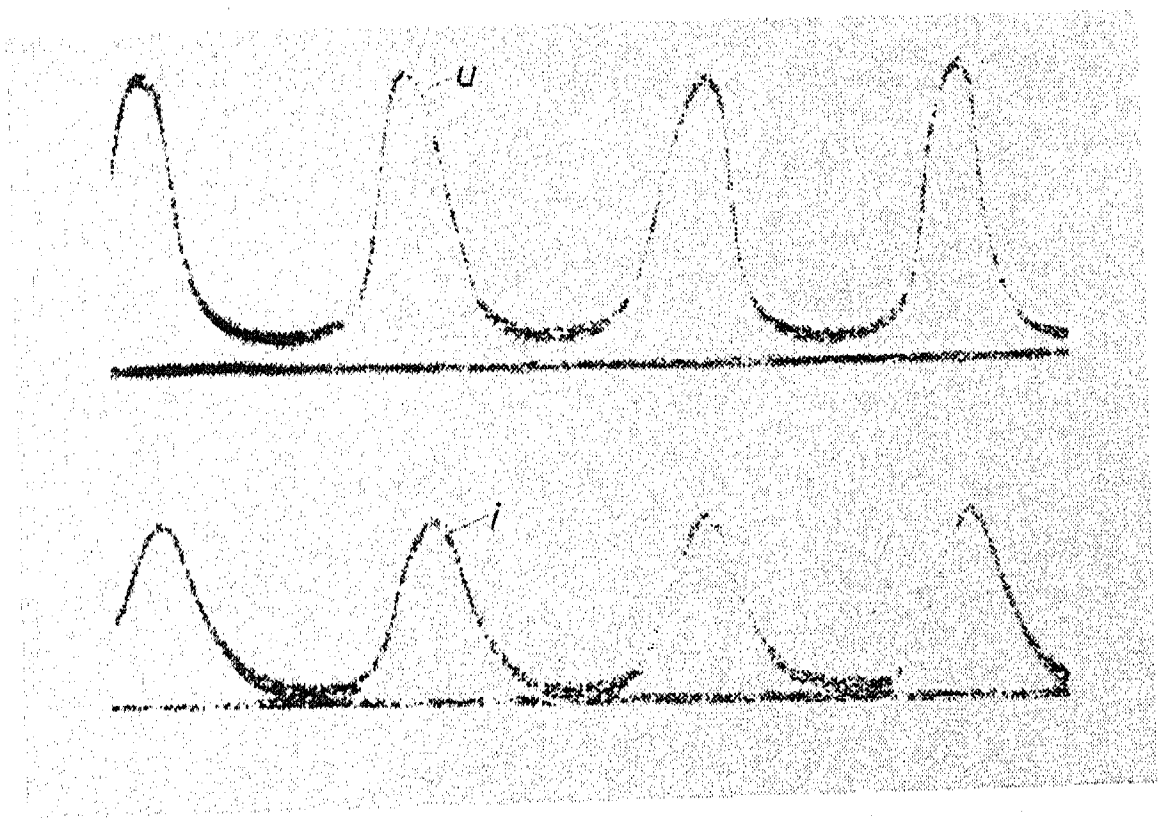

Fig. 2. General view of a unipolar pulse generator.

The Department of Electrical Machinery at Kharkov Polytechnical Institute carried out the design and testing of an experimental unipolar generator for a mean current of 150 A, mean voltage of 15 - 20 V and a frequency of 800 pulses/sec on behalf of the Ministry of the Machine Tool Industry in 1953–55; it was produced by the Kharkov Electrical Machine Works [9]. Fig.2 is a view of this generator, Fig.3 showing oscillograms of the voltage and current.

The second group of rotary pulse generators are those which generate alternating pulse voltages, subsequently rectified.

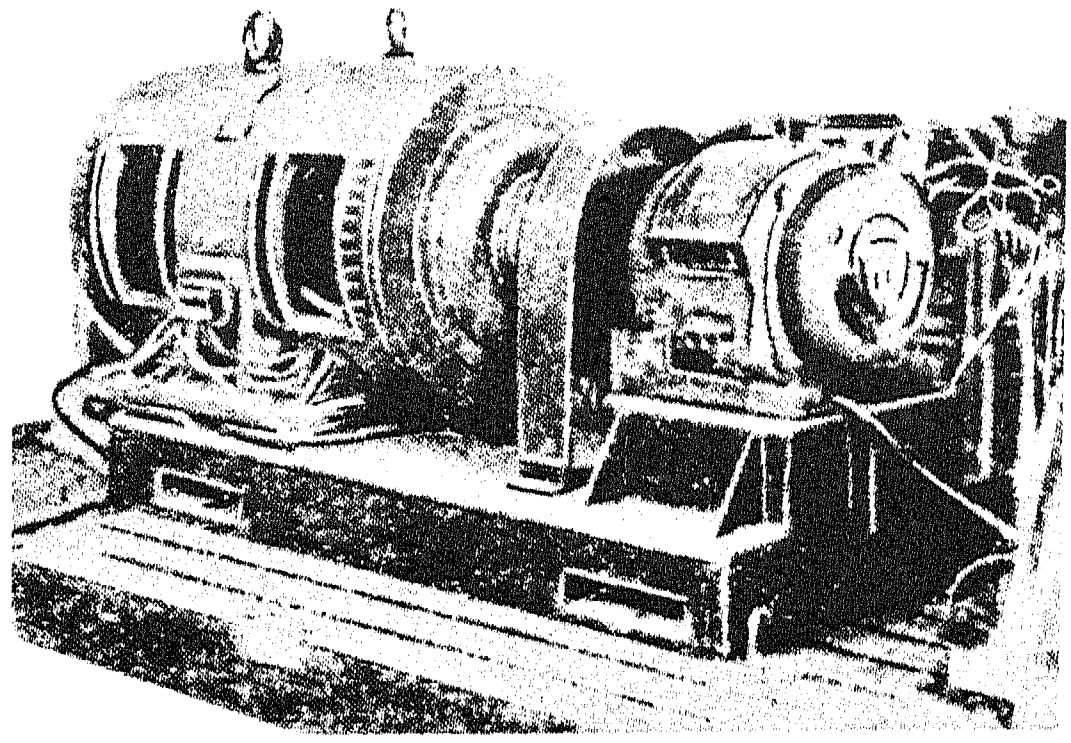

Fig. 3. Voltage (u) and current (i) oscillograms for the unipolar pulse generator.

One style of self-rectifying pulse generator was suggested by the authors jointly with Perchik and Borisenko [10,11], and designed by the Department of Electrical Machinery at the Kharkov Polytechnical Institute. This consists of a pole-changing magnetic system and poles formed on the stator or rotor, and an armature winding, situated, correspondingly, on the rotor or stator. The ends of the armature winding are led out to the commutator consisting of two systems of bars arranged alternately and insulated from one another. The number of bars equals the number of poles. The bars of each system are electrically interconnected, and each system is connected to one end of the winding. Two systems of brushes run on the commutator, so arranged that the brushes of either polarity are simultaneously only on one system of bars and have a relative displacement corresponding to the width of a bar. The pole arc/pitch ratio is chosen much smaller than normal (lower than 0.5), and the armature winding is arranged under the poles in narrow segments. This design produces an e.m.f. of very marked pulse character. Fig.4 shows diagrammatically

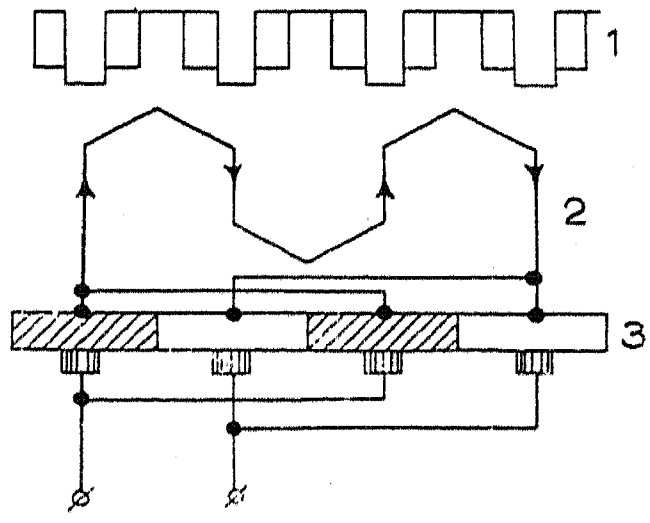

Fig. 4. Theoretical circuit of commutator-type pulse generator.
1)- Stationary poles with field winding;
2 - Rotating armature winding;
3 - Commutator.

a generator with a four-pole stationary magnetic system 1 and rotating armature coil 2, placed in four slots. The ends of the winding are led out to the commutator 3, consisting of four bars on which the brushes run. It is easy to design this generator for the desired voltage which, with given dimensions and speed, is determined by the number of armature conductors connected in series.

The frequency is

$$f = pn/30 \tag{3}$$

where p is the number of pole pairs, n being the rev/min.

Since the armature winding occupies only a small part of the periphery, two or more independent windings can be used, each having its own commutator which can be connected to separate loads.

Experimental generators of this type were produced in the Kharkov Polytechnical Institute and in the Experimental Machine Tool Research Institute and were found to work very satisfactorily with an erosion-machining load. The Kharkov Polytechnical Institute designed and investigated a number of generators of a type suggested by the Experimental Machine Tool Research Institute and built by the Kharkov Electrical Machine factory, for frequencies up to 1000 pulses/sec, mean currents up to 300 A, mean voltages up to 40 V, and also designed a batch of experimental generators producing 400 pulses/sec, mean currents of 80 A and mean voltages of 30 V [12] from tests carried out

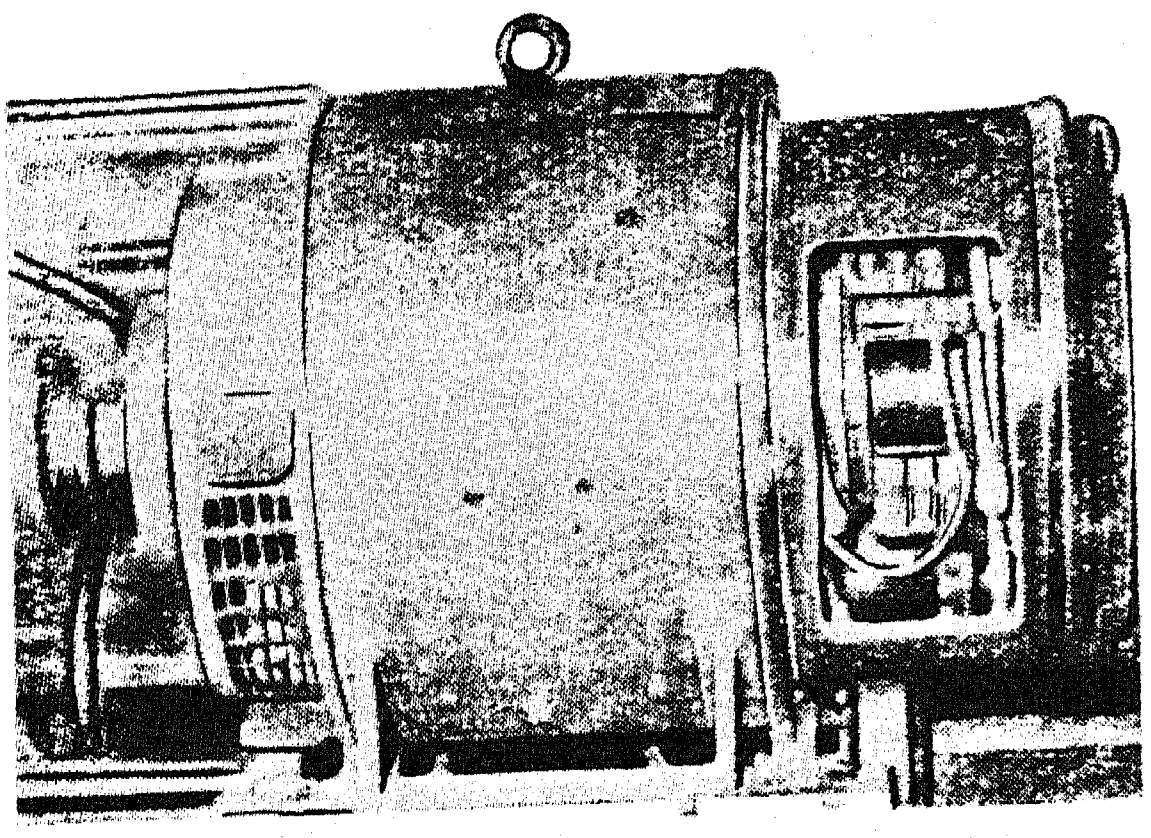

Fig. 5. General view of commutator-type pulse generator.

at the Experimental Machine Tool Research Institute. Fig.5 is a general view of such a machine, Fig.6 showing current and voltage oscillograms of one of the generators.

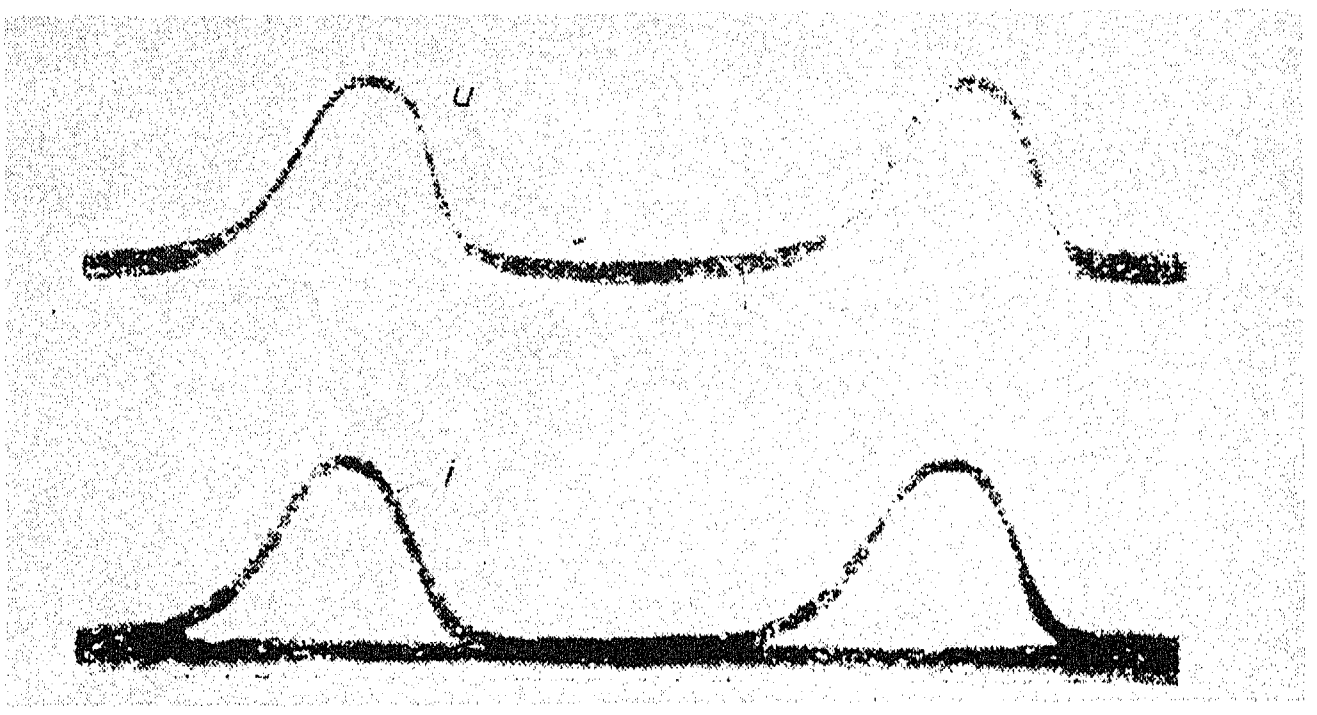

Fig. 6. Voltage (u) and current (i) oscillograms for the commutator-type pulse generator.

The commutator-generator is most suitable for currents from 10 – 20 to 500 – 600 A and for frequencies from 150 to 1000 pulses/sec.

The generator may alternatively be connected to a rectifier inside or outside the machine.

This type of commutator-generator with full-wave rectifier may also be provided with a half-wave rectifier. For this purpose the ends of the windings are also brought out to slip-rings. The load is connected between the ring and the commutator. This halves the pulse frequency and the relative duration is considerably reduced. Two independent loads can then also be supplied simultaneously. This kind of operation was investigated with one of the generators and proved to be quite reliable, apart from the increased stability of the operation in the gap, due to the smaller relative pulse duration.

Comparison of these rotary generators with other types of independent generator indicates that in the ranges 10 – 600 A and range 150 – 1000 pulses/sec they exhibit considerable advantages, viz. the conversion from mains a.c. to unipolar current impulses is shortened from three stages to two, the efficiency is increased by a factor 1.5 – 2, the p.f. being also increased; the number of units is reduced by a factor 1.5 – 2, the working conditions are considerably simplified and the reliability improved.

Rotary unipolar impulse generators are at present the best source of supply for electric pulse-machining installations. The Ministry

of the Electrical Industry has now released the first series of generators for electric-impulse broaching and copying machines.

REFERENCES

1. B.R. Lazarenko and N.I. Lazarenko; *Electric Spark-Machining of Metals*. Gosenergoizdat (1950).
2. B.R. Lazarenko and N.I. Lazarenko; Electric spark-machining of metals. *Elektrichestvo* No.8 (1955).
3. A.L. Livshits and V. Ya. Rassokhin; Present state and development prospects in electric methods of metal shaping and working. *Stanki i Instrument* No.11 (1954); No.1 (1955).
4. A.L. Livshits, N.I. Blitshtein *et al;* Improvement of the productivity of electric-erosion-machining of metals in soft operating conditions. *Technical Report ENIMS-KB*. MSiIP (1955).
5. Yu. V. Mordvinov; Inductor-type impulse generator. Author's affidavit No.95245 (1952); No.97622 and No. 97623 (1953).
6. *Technical Encyclopedia* Vol.26, pp.484-492. OGIZ RSFSR (1934).
7. L.A. Goncharski; Rotating electrolytic contact-breaker, *Elektrichestvo* No.4 (1954).
8. A.L. Livshits; Commutatorless unipolar pulse generator. Author's affidavit No. 880 MSiIP (1951).
9. I.S. Rogachev, L.D. Perchik *et al; Unipolar pulse generator.* Technical Report of the Kharkov Polytechnical Institute "V.I. Lenin" (1955).
10. I.S. Rogachev and A.L. Livshits and L.D. Perchik; A rotary generator for unipolar current pulses. Author's affidavit No. 101332, (1952).
11. I.S. Rogachev, A.L. Livshits, L.D. Perchik and N.I. Borisenko; Synchronous generator with mechanical rectifier. Author's affidavit No. 98751, (1953).
12. I.S. Rogachev, L.D. Perchik *et al;* Development and investigation of rotary pulse generators. Technical Reports of the Kharkov Polytechnical Institute "V.I. Lenin" (1953–1955).

INTERNATIONAL SERIES OF MONOGRAPHS ON ELECTRONICS AND INSTRUMENTATION

Editors: **D. W. Fry** (*Harwell*) *and* **W. Higinbotham** (*Brookhaven*)

WITH the applications of electronics and instrumentation expanding more rapidly every year the need increases for authoritative up-to-date accounts of recent advances. It is to meet such a need that the Pergamon International Series of Monographs on Electronics and Instrumentation was started a few years ago. The authors who contribute are all specialists actively engaged in research and in close touch with the most recent developments in their respective fields.

Of the monographs already published Dr. J. B. Birks' *Scintillation Counters*, Mr. A. B. Gillespie's *Signal, Noise and Resolution in Nuclear Counter Amplifiers* and the one by Mr. I. A. D. Lewis and Mr. F. H. Wells on *Millimicrosecond Pulse Techniques* will be of particular interest to everyone interested in nucleonics. The physics of secondary electron emission and its applications in many electronic devices is discussed in the monograph *Physics and Applications of Secondary Electron Emission* by Dr. H. Bruining; whilst the theory of probability as applied to electronics, communication and radar has been dealt with elegantly by Mr. P. M. Woodward in *Probability and Information Theory with Applications to Radar*.

Others in the series are Professor J. R. Mentzer's *Scattering and Diffraction of Radio Waves* and *An Introduction to Electronic Anologue Computers* by Mr. C. A. A. Wass. With the rapidly increasing use of electronic calculating machines in many branches of applied science, Mr. Wass's monograph is likely to be of considerable interest to everyone with problems in dynamics and kinematics.

A further addition to the series to be published shortly is Mr. A. H. W. Beck's monograph entitled *Space Charge Waves*. A strong need exists for a book which reviews the many advances made in microwave valves using distributed circuits during the last few years; Mr. Beck's book does this.

The ready sale which these monographs have is convincing evidence of the wide interest with which they are received. It is the intention of the editors and publishers to maintain in the future the high standard which has already been set, both in merit and quality of production.

Titles in this series:

Vol. 1. **Signal Noise and Resolution in Nuclear Counter Amplifiers** by A. B. GILLESPIE. *Price 25s.* ($4.50)

Vol. 2. **Scintillation Counters** by J. B. BIRKS. *Price 25s.* ($4.50)

Vol. 3. **Probability and Information Theory With Applications to Radar** by P. M. WOODWARD. *Price 25s.* ($5.00)

Vol. 4. **Physics and Applications of Secondary Electron Emission** by H. BRUINING. *Price 25s.* ($5.50)

Vol. 5. **Millimicrosecond Pulse Techniques** by I. A. D. LEWIS and F. H. WELLS. *Price 50s.* ($7.50)

Vol. 6. **Introduction to Electronic Analogue Computers** by C. A. A. WASS. *Price 40s.* ($6.50)

Vol. 7. **Scattering and Diffraction of Radio Waves** by J. R. MENTZER. *Price 30s.* ($4.50)

Vol. 8. **Space-charge Waves** by A. H. W. BECK. *Price 90s.* ($15.00)

PERGAMON PRESS

LONDON NEW YORK PARIS LOS ANGELES

4 & 5 Fitzroy Square, London, W. 1

122 East 55th Street, New York 22, N.Y.

PERGAMON INSTITUTE

NEW YORK AND LONDON

122 E. 55th STREET
NEW YORK 22

4 & 5 FITZROY SQUARE
LONDON W.1

Aims and Purpose of the Institute

I. To establish a Translation Panel of competent and highly qualified translators from Russian and other Slavonic languages into English; and to make available the services of the Institute and its Translation Panel to scientists, learned societies, government agencies and industry throughout the world on a non-profit-making basis. The Institute shall charge its customers for these services on a co-operative cost-sharing plan.

II. To encourage, co-ordinate and foster (by the holding of Symposia, for instance) the teaching of Russian at higher seats of learning; and to provide the teaching institutions with the necessary textbooks and tools of learning which will enable non-Russian-speaking scientists to acquire quickly a working knowledge of Russian sufficient for them to read Russian scientific literature.

III. To translate and disseminate such of the scientific, technical and medical literature printed in Russian and other Slavonic languages as, in the opinion of competent scientific advisers, will be of definite benefit and value to scientists not speaking these languages.

IV. To establish and publish, with the assistance of the appropriate scientific institutions in the U.S.S.R., a series of monographs in the English language reviewing progress in broad areas of Soviet scientific activity.

V. A. To publish a journal devoted to reporting translation work done anywhere in the world from Russian and other Slavonic languages into English in the fields of science, technology and medicine, in order to prevent duplication.

B. To serve as a forum in which Soviet and non-Russian-speaking scientists will be able to discuss problems of common concern—both scientific and administrative.

C. To be a place where people engaged in the teaching of Russian to non-Russian-speaking scientists can report on their experience and exchange information which will be of assistance to persons working in this field.

VI. To compile and publish specialized dictionaries from and into Russian and the principal Slavonic languages for subjects where such dictionaries are lacking.

VII. To sponsor and foster research into the organization of scientific information, mechanical systems for storing and retrieving information, and mechanical translation.

VIII. To assist and advise learned societies and professional bodies on their publication problems with a view to reducing the cost of printing and distribution of their publications in the interests of the wider and more efficient dissemination of scientific information.

Pergamon Institute Services and Projects

The following are the projects which have already been started or are being planned, and some of the services which are available:

It is planned to hold a Symposium in 1958 either in Washington or in London, sponsored by the Institute and several interested Universities, to examine the following problems:

(a) How to assist with the establishment of extra-curricular courses for the teaching of Russian in the science, medical and engineering faculties at higher seats of learning in the English-speaking world.

(b) How to teach the reading of Russian scientific and technical texts to scientists and technologists in the minimum amount of time.

(c) What tools of learning are required.

Discussions are taking place with the relevant authorities in the U.S.S.R. on the commissioning of a series of review volumes, with complete bibliographies, covering broad areas of Russian scientific, medical and technical progress for the period 1920–1956.

The Institute now publishes a number of selected Russian journals in complete translation:

* * Problems of Virology
* * Problems of Hematology and Blood Transfusion
* * Journal of Microbiology, Epidemiology and Immunobiology
* * Biophysics
* * Problems of Oncology
* * Sechenov Physiological Journal of the U.S.S.R.
* † Bulletin of the Academy of Sciences of the U.S.S.R.: Geophysics Series
* ‡ Radio Engineering and Electronics
* ‡ Telecommunications
* § The Physics of Metals and Metallography
* § Abstracts of Metallurgy
* ¶ Applied Mathematics and Mechanics

Selected papers from the following are also published:
Atomnaya Energiya (Atomic Energy) Electric Technology, U.S.S.R.

* Published by the Institute on the initiative and with the financial support of the United States Department of Health, Education and Welfare, Public Health Service, The National Institutes of Health.

† Published in association with the American Geophysical Union with the financial support of the National Science Foundation.

‡ Published with the support of the National Science Foundation, in collaboration with the Massachusetts Institute of Technology.

§ Published under the auspices of the Board of Governors of Acta Metallurgica with financial assistance from the National Science Foundation and the United States Atomic Energy Commission.

¶ Published with the support of the National Science Foundation, in collaboration with the American Society of Mechanical Engineers.

The Institute now provides a selection of significant papers from Russian medical and biological literature (other than those listed above) which are available to those interested, under a co-operative cost-sharing plan.

A number of important Russian monographs and books are to be published in English in 1958, including the work of Academician A. N. Semenov, who recently shared the Nobel Award for chemistry with Sir Cyril Hinshelwood, and the classic course of theoretical physics by Academician Landau and his colleague, Professor Lifshitz.

The Institute will supply on request, free of charge, a monthly contents list in English of all the significant articles and books being currently published in the U.S.S.R. and other countries in the Soviet orbit. Persons interested in any article mentioned in these contents lists may order from the Institute a full English translation which will be supplied with a minimum of delay.

The Institute will undertake to supply, on request, bibliographical information on work published in the U.S.S.R. and other Soviet orbit countries on all subjects in the field of science, technology and medicine, and to provide abstracts and résumés of such publications; to provide, with the co-operation of the respective National Academies of Sciences in these countries, to learned societies, Government departments and industrial organizations only, for the purpose of research and reference, books and journals published in the U.S.S.R. and the Soviet orbit countries, including micro-cards and micro-films when available of books and articles published over the past twenty years, including material published during the 1939–1945 war as far as available; to supply the complete translation of selected journals and books if suitably recommended by learned societies, Government departments or trade associations; to supply, with the aid of its expert panel of translators, resident all over the world, translation work in all branches of science, technology and medicine from and into any language.

ELEKTRICHESTVO

ELECTRIC TECHNOLOGY, U.S.S.R.

1958 VOLUME 1 MAY

CONTENTS

Made and printed in Great Britain by The Campfield Press, St. Albans